Design of new molecular folded topologies and of a photoswitchable foldamer host

Chenhao Yao

université de BORDEAUX

THÈSE PRÉSENTÉE

POUR OBTENIR LE GRADE DE

DOCTEUR DE

L'UNIVERSITÉ DE BORDEAUX

ÉCOLE DOCTORALE DES SCIENCES CHIMIQUES

SPÉCIALITÉ CHIMIE ORGANIQUE

Par Chenhao Yao

Conception de nouvelles topologies moléculaires repliées et d'un hôte foldamère photocommutable

Sous la direction de : Yann FERRAND

Soutenue le 18/11/2021

Membres du jury :

Mme. FAURE, Sophie	Directeur de Recherche, CNRS, Clermont-Ferrand	Rapporteur
M. BARDELANG, David	Chargé de Recherche, CNRS, Aix Marseille	Rapporteur
M. DUROLA, Fabien	Chargé de Recherche, CNRS, Bordeaux	Examinateur
M. HUC, Ivan	Professeur, Ludwig Maximilians Universität, Munich	Examinateur
M. FERRAND, Yann	Directeur de Recherche, CNRS, Bordeaux	Examinateur

Conception de nouvelles topologies moléculaires repliées et d'un hôte foldamère photocommutable

La chimie des foldamères est un domaine de recherche en développement rapide où les scientifiques étudient la construction de diverses architectures artificielles inspirées des conformations repliées des biopolymères. Cette thèse porte sur la conception et la construction de topologies moléculaires complexes et de mouvements moléculaires commutables. Dans la première partie, avec la stratégie du disrupteur hélicoïdal, des macrocycles de tailles variables ont été construits (de 4 unités à 12 unités) à base de dérivés de quinoléinecarboxamides (Q^F). Les macrocycles formés adoptent de nouvelles conformations totalement différentes des conformations hélicoïdales de leurs précurseurs respectifs. Ces nouvelles structures ont été confirmées par RMN et études cristallographiques. Dans la deuxième partie, un foldamère hélice-feuillet-hélice symétrique, capable d'accueillir une molécule invitée en forme de T, a été préparé. L'irradiation lumineuse des feuillets aromatiques modifient l'architecture du foldamère ce qui provoquent la dissociation du complexe et libèrent la molécule en forme de T. Un traitement thermique permet la reformation du complexe hôte-invité. Dans la troisième partie de cette thèse, la conception d'un nœud Prusik moléculaire, basée sur un foldamère de type hélice-feuillet-hélice, est discutée. Les conformations des architectures hélice-feuillet-hélice, telles que la forme conique, l'hélice multiple et le précurseur du nœud Prusik, ont été étudiées.

Mots clés: Foldamère, Macrocycle, Photocommutable, Topologie, Noeud moléculaire, Matériau intelligent, Auto-assemblage, Cristallographie, RMN

Design of new molecular folded topologies and of a photoswitchable foldamer host

Foldamer chemistry is a rapidly developing research area where scientists study the construction of various artificial architectures that inspired from the folded conformations of biopolymers found in nature. This thesis focuses on the design and construction of complex molecular topologies and switchable molecular motions. In the first part, with the helical disruptor strategy, variable sizes of macrocycles were built up (from 4 units to 12 units) based on quinolinecarboxamides derivatives (Q^F). Macrocycles adopted novel conformations which were totally different with the helical conformations of their own foldamer precursors. Those novel structures were confirmed by NMR and crystallographic studies. In the second part, a symmetrical helix-sheet-helix foldamer was prepared which has a bind with T-shape rod. The photoreactions within aromatic sheets change the architectures of foldamer that cause dissociation of complex and release the rod. A thermal treatment would recover foldamer back to initial conformation and lead to the re-formation of host-guest complex. In the third part, to build up the molecular Prusik knot, different turn units were incorporated with helix segments to form helix-turn-helix foldamers. The conformations of helix-turn-helix architectures were well investigated, they adopted several kinds of conformations, such as cone-shape, multiple-helix and precursor of Prusik knot.

Keywords: Foldamer, Macrocycle, Photo-switch, Topology, Molecular knot, Smart material, Self-assembly, Crystallography, NMR

UMR 5248 Chimie et Biologie des Membranes et Nanoobjets (CBMN)
Institut Européen de Chimie et Biologie (IECB)
2 rue Robert Escarpit 33607 PESSAC CEDEX

Acknowledgements

First of all, I want to thank my supervisor, Dr. Yann Ferrand for giving me a chance to join his group and start my study in France. As a supervisor, his guidance and support encouraged me in past four years. He put great amount of attention to lead me to solve the problems of living in France. I also want to thank Dr. Ivan Huc for his insightful discussion and helpful suggestions. It is impossible for me to finish my study and this thesis without their effort. These years I spent in our lab will be valuable experience during in my future life. I appreciate Dr. Victor Maurizot, Dr. Lucile Fischer and Eric Merlet for their kind help and friendliness. Due to these lovely leaders in our lab, my study and life in France are cheerful and colorful. I want to send my appreciation to my collaborators Dr. Mcclenaghan Nathan and Dr. Anh Thy Bui for their help in my photoreaction experiments.

I thank Dr. Brice Kauffmann who solved all X-ray crystal structures in my project. Many appreciations to Axelle Grélard and Estelle Morvan for their assistance with NMR measurements. I also thank Dr. Frédéric Rosu and Loïc Klinger for their kind help with mass measurements.

I want to thank all the members in Bise Group and IECB, previous and present, I will always remember the nice time we spent together in our lab and group events: Xiaobo, Arthur, Sunbum, Siyuan, Pedro, Ko, Sai Reddy, Bappadittya, Floriane, Krishnendu, Harsha, Mathieu, Alice, Victor K., Vincent, Suprahash, Mathilde, Xavier, Camille, Jinqi, Lianjin, Gabrielle and many others. Furthermore, I thank many friends I met here: Jinhua, Jie, Jiaming, Peizhao, Qilei, Wenzhi, Hongwei. Because of all of them, I spent a happy life in Bordeaux.

Last but not least, no words can express my appreciation to my parents and family, they support me in everything and stand in my side. Their encouragements and support keep me going further during my study and whole life.

List of Abbreviations

P : 2,6-diaminopyridine and 2,6-pyridinedicarboxylic acid
Q^F : 7-amino-8-fluoro-2-quinolinecarboxylic acid
A^F : 1,8-diaza-9-fluoro-2,7-anthracene-dicaboxylic acid
A^H : 1,8-diaza-2,7-anthracene-dicaboxylic acid
Boc: *tert*-butyloxycarbonyl
CD: circular dichroism
$CHCl_3$: chloroform
$CDCl_3$: deuterated chloroform
DCM: dichloromethane
DIPEA: diisopropylethylamine
Ghosez reagent: 1-chloro-*N*,*N*,2-trimethyl propenylamine
GPC: gel permeation chromatography
***i*BuOH**: isobutanol
M.W.: molecular weight
MMFFs : Merck Molecular Force Field static
NMR : nuclear magnetic resonance
ppm : parts per million
PyBOP: benzotriazol-1-yl-oxytripyrrolidinophosphonium hexafluorophosphate
TFA: trifluoroacetic acid
THF: tetrahydrofuran
TLC: thin layer chromatography

Content

General introduction

Foldamers, defined as "artificial folded molecular architectures",[1] are inspired by the structures and functions of biopolymers. The main motifs existing in biopolymers (helices, linear strands, turns and sheets) are commonly in most foldamer families. Those artificial secondary structures rely both on the contribution of weak non-covalent bond (such as hydrogen bonds, electrostatic forces, π-π stacking and metal-ligand coordination) and strong covalent bonds.

To mimic the structure and biological properties of biopolymers, many peptides nucleic acids (PNAs)[2] and peptoids[3] have already been successfully designed and prepared. In 1996, Seebach and Gellman et al. reported that the helical structures formed by β-peptides are more stable than those of α-peptides.[4] Followed their research, various β-peptides (Figure **1**) with different side chains, γ-peptides and δ-peptides were studied.[5] The amide bond replaced by, for example, ureas, hydrazide or hydroxyamide groups can also achieve folded structures. These foldamers are based on the analogy to biological systems which are also called "biotic".

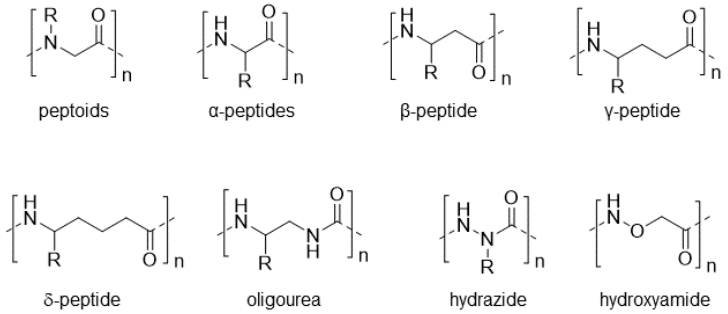

Figure **1.** Examples of biotic foldamer backbones.

In contrast, "abiotic" foldamers possess backbones and folding segments that are different from those of biotic foldamers. Many of them (Figure **2**) were built up with aromatic sequences: oligo-phenylene-ethynylenes,[6] aza-heterocycles,[7] aromatic urea oligomers and aromatic

1 For a book, see: S. Hecht, and I. Huc, editors. *Foldamers: structure, properties and applications*. John Wiley & Sons, **2007**.
2 Nielsen, P. E.; Egholm, M.; Berg, R. H.; Buchardt, O. *Science* **1991**, *254*, 1497.
3 Simon, R. J.; Kania, R. S.; Zuckermann, R. N.; Huebner, V. D.; Jewell, D. A.; Banville, S.; Ng, S.; Wang, L.; Rosenberg, S.; Marlowe, C. K. *Proc. Natl. Acad. Sci. USA* **1992**, *89*, 9367.
4 Appella, D. H.; Christianson, L. A.; Karle, I. L.; Powell, D. R.; Gellman, S. H. *J. Am. Chem. Soc.* **1996**, *118*, 13071-13072.
5 Semetey, V.; Rognan, D.; Hemmerlin, C.; Graff, R.; Briand, J.-P.; Marraud, M.; Guichard, G. *Angew. Chem. Int. Ed.* **2002**, *41*, 1893-1895; Li, X.; Yang, D. *Chem. Commun.* **2006**, 3367-3379.
6 Nelson, J. C.; Saven, J. G.; Moore, J. S.; Wolynes, P. G. *Science* **1997**, *277*, 1793.
7 Bassani, D. M.; Lehn, J.-M.; Baum, G.; Fenske, D. *Angew. Chem. Int. Ed.* **1997**, *36*, 1845-1847.

oligoamides.[8] Hydrogen bonding and hydrophobic interactions contribute to the folding of both aliphatic and aromatic foldamers. Meanwhile, structure of aromatic foldamer can also be supported by aromatic stacking.

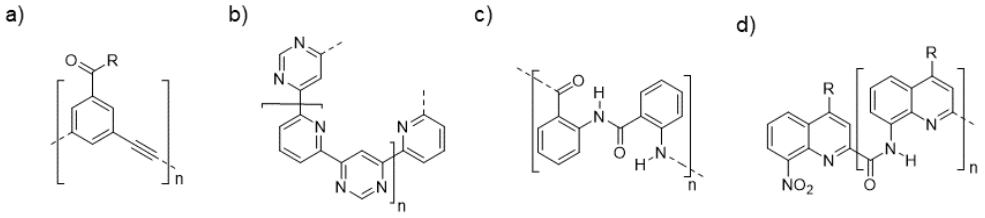

Figure **2.** Representative backbones used in aromatic foldamer chemistry: a) oligo-phenylene-ethynylenes; b) aza-heterocycle oligomer; c) aromatic oligoamides and d) quinoline-based oligoamides.

In our group, aromatic oligoamide-based foldamers have been constantly studied. Various monomers with different curvatures coding for different diameters have been developed to evolve the structures of foldamers. Both side chains and main chains can be tuned for the purpose requirements. Hydrophobic, hydrophilic, anionic or cationic side chains are all subjected of choices. Conformations of the foldamers are modulated by the choice of the monomers. Depending on the monomers used, single, double or even quadruple helix can be formed.[9] Assemblies of helical foldamers either by covalent bonding or non-covalent interactions have been demonstrated.[10]

Aromatic oligoamides can fold into stable and well-defined helical structure. Through the development of these foldamers in last two decades, some novel properties have been explored: a) multiple helical structure;[11] b) helix-sheet-helix super secondary structure;[12] c) molecular capsules with high selectivity for different molecules.[13] In this thesis, we will discuss some molecular topological structures built up with aromatic oligoamides.

8 Hamuro, Y.; Geib, S. J.; Hamilton, A. D. *J. Am. Chem. Soc.* **1996**, *118*, 7529-7541; Berl, V.; Huc, I.; Khoury, R. G.; Krische, M. J.; Lehn, J.-M. *Nature* **2000**, *407*, 720-723; Jiang, H.; Léger, J.-M.; Huc, I. *J. Am. Chem. Soc.* **2003**, *125*, 3448-3449.

9 Ferrand, Y.; Gan, Q.; Kauffmann, B.; Jiang, H.; Huc, I. *Angew. Chem. Int. Ed.* **2011**, *50*, 7572-7575; Gan, Q.; Bao, C.; Kauffmann, B.; Grélard, A.; Xiang, J.; Liu, S.; Huc, I.; Jiang, H. *Angew. Chem. Int. Ed.* **2008**, *47*, 1715-1718.

10 Gole, B.; Kauffmann, B.; Maurizot, V.; Huc, I.; Ferrand, Y. *Angew. Chem. Int. Ed.* **2019**, *58*, 8063-8067; De, S.; Chi, B.; Granier, T.; Qi, T.; Maurizot, V.; Huc, I. *Nat. Chem.* **2018**, *10*, 51-57; Ferrand, Y.; Huc, I. *Acc. Chem. Res.* **2018**, *51*, 970-977.

11 Gan, Q.; Ferrand, Y.; Bao, C.; Kauffmann, B.; Grélard, A.; Jiang, H.; Huc, I. *Science* **2011**, *331*, 1172; Ferrand, Y.; Gan, Q.; Kauffmann, B.; Jiang, H.; Huc, I. *Angew. Chem. Int. Ed.* **2011**, *50*, 7572-7575.

12 De, S.; Chi, B.; Granier, T.; Qi, T.; Maurizot, V.; Huc, I. *Nat. Chem.* **2018**, *10*, 51-57; Sebaoun, L.; Maurizot, V.; Granier, T.; Kauffmann, B.; Huc, I. *J. Am. Chem. Soc.* **2014**, *136*, 2168-2174; Lamouroux, A.; Sebaoun, L.; Wicher, B.; Kauffmann, B.; Ferrand, Y.; Maurizot, V.; Huc, I. *J. Am. Chem. Soc.* **2017**, *139*, 14668-14675.

13 Horeau, M.; Lautrette, G.; Wicher, B.; Blot, V.; Lebreton, J.; Pipelier, M.; Dubreuil, D.; Ferrand, Y.; Huc, I. *Angew. Chem. Int. Ed.* **2017**, *56*, 6823-6827; Mateus, P.; Chandramouli, N.; Mackereth, C. D.; Kauffmann, B.; Ferrand, Y.; Huc, I. *Angew. Chem. Int. Ed.* **2020**, *59*, 5797-5805.

In chapter 1, the helical conformation of foldamer was disrupted by the removable disruptor groups, to provide the possibility of foldamer to be cyclized. Using this strategy, macrocycles with different sizes were prepared and characterized. Different with their analogous helices, those macrocycles showed restricted backbones. Macrocycles also adopted novel conformations which were totally different with the initial helical conformations.

In chapter 2, we will show that a symmetrical helix-sheet-helix foldamer can bind a T shape guests. The quantitative photoreaction within aromatic sheets changes the shape of the foldamers that causes dissociation of guest from the foldamer. A thermal treatment would recover the initial conformation and the re-formation of the host-guest complex. A highly efficient photo-switchable host-guest system was established with aromatic foldamers.

In chapter 3, to build up a molecular Prusik knot, different turn units were incorporated with helical segments to form helix-turn-helix foldamers. Different conformations of those foldamers were thoroughly investigated. Rods with diverse sizes were also prepared for assessing the binding properties the knot precursor.

Chapter I: Frustrated helicity: from stable aromatic amide helix to macrocycle

1. Introduction

Macrocyclic structures are common employed in drug discovery and biology,[1] interest and application in those fields make macrocyclic chemistry to be one of the most dynamic and promising frontiers to be developed. In past decades, innumerable macrocyclic molecules with novel conformation and properties have been reported,[2] while crucial challenges still remain in the superior construction of valuable macrocycles with total control over the shape and functions.

Macrocyclization is intimately linked to the stabilization of molecular shape.[3] There are traditional examples that demonstrate macrocycles may show restrict conformational flexibility[4] and stability. Macrocycles are commonly observed in nature as around 20% of natural product molecules possess cyclic structures.[5] Thus the preparation of macrocyclic structures is a very active area of research nowadays.[6] Macrocyclization can give rise to stable molecular shapes giving access to many applications. In flexible backbones, macrocycles reduce the conformational spaces available and improve the conformations which are possible for the noncyclic precursors but that may be disfavored for entropic reasons, as a result rigid conformation is always performed. Disulfide bridge formation in protein structures and stapling of α-helical peptides or proteins are typically examples in Nature. In rigid conformations, final macrocycles generally have a similar structure with their corresponding precursors.

1.1 Preorganization of macrocycles

1 Góngora-Benítez, M.; Tulla-Puche, J.; Albericio, F. *Chem. Rev.* **2014**, *114*, 901-926.
2 Gradillas, A.; Pérez-Castells, J. *Angew. Chem., Int. Ed.* **2006**, *45*, 6086-6101; Parenty, A.; Moreau, X.; Campagne, J. M. *Chem. Rev.* **2006**, *106*, 911-939.
3 Martí-Centelles, V.; Pandey, M. D.; Burguete, M. I.; Luis, S. V. *Chem. Rev.* **2015**, *115*, 8736-8834.
4 Marsault, E.; Peterson, M. L. *J. Med. Chem.* **2011**, *54*, 1961-2004.
5 Frank, A. T.; Farina, N. S.; Sawwan, N.; Wauchope, O. R.; Qi, M.; Brzostowska, E. M.; Chan, W.; Grasso, F. W.; Haberfield, P.; Greer, A. *Mol. Divers.* **2007**, *11*, 115-118.
6 Kopp, F.; Marahiel, M. A. *Nat. Prod. Rep.* **2007**, *24*, 735-749.

The specific properties of macrocycles are more often associated with the preorganization of their building blocks or precursors,[7] providing macrocycles with some significant applications in chemistry, materials science, medicine and biology.[8]

Preorganization of open-chain precursors gives rise to appropriate conformations, and this constitutes a key factor that determines their ability to cyclize.[9] As cyclization reactions are always the last step in the synthetic strategy,[10] an appropriate structure of the precursors will lead to high yielding ring-closure reactions, otherwise the compounds with an unfavorable conformation usually cannot be cyclized at all.[11] Usually entropy and enthalpy changes are the key for the formation of the desired product or the unwanted oligomeric byproducts.

It is commonly admitted that enforced propinquity often leads to higher reactivity.[12] The proximity of reactive centers enhances the process of reactive interaction,[13] so the activation energy for a macrocyclization reaction can be much lower if the two active groups are closer (preorganization) before the cyclization reaction to happen. The energy required to mix the reaction centers together and to re-strain their motion in order to facilitate the formation of the ring-bond has to be paid for the preorganization step.

One of the most famous macrocycles are the crown ethers. Nucleophilic substitution reactions have been used to prepare them, in which one heteroatom (oxygen, sulfur or nitrogen) acts as the nucleophile for the ring-closing step. This strategy was first approach for the discovery of crown ethers by Pedersen[14] and the same for the synthesis of polyaza macrocycle and cryptands by Lehn (Figure **1**).[15]

7 Fu, H.; Liu, Y.; Zeng, H. *Chem. Commun*. **2013**, *49*, 4127-4144; Iyoda, M.; Yamakawa, J.; Rahman, M. J. *Angew. Chem., Int. Ed*. **2011**, *50*, 10522-10553; Gong, B. *Acc. Chem. Res.* **2008**, *41*, 1376-1386.
8 Höger, S. *Chem.—Eur. J*. **2004**, *10*, 1320-1329; Yamaguchi, Y.; Yoshida, Z.-i. *Chem.—Eur. J*. **2003**, *9*, 5430-5440.
9 Lafontaine, J. A.; Provencal, D. P.; Gardelli, C.; Leahy, J. W. *J. Org. Chem.* **2003**, *68*, 4215-4234.
10 Casadei, M. A.; Galli, C.; Mandolini, L. *J. Am. Chem. Soc*. **1984**, *106*, 1051-1056.
11 Hoffmann, R. W. *Angew. Chem., Int. Ed*. **2000**, *39*, 2054-2070.
12 Blankenstein, J.; Zhu, J. *Eur. J. Org. Chem.* **2005**, *2005*, 1949-1964.
13 Sierra, M. A.; de la Torre, M. C. *Angew. Chem., Int. Ed*. **2000**, *39*, 1538-1559.
14 Pedersen, C. J. *J. Am. Chem. Soc*. **1967**, *89*, 7017-7036; Pedersen, C. J. *J. Am. Chem. Soc*. **1967**, *89*, 2495-2496.
15 Lehn, J. M. *Acc. Chem. Res.* **1978**, *11*, 49-57.

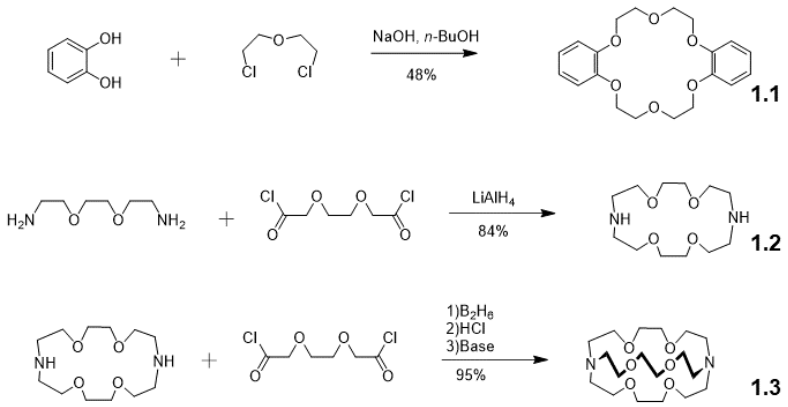

Figure 1. Synthesis of crow ether and cryptands.

1.2 shape-persistent macrocycles

In some special cases of rigid building block macrocycle, the geometry of the blocks will determine the probability of the macrocyclization reaction. The so-called shape-persistent macrocycles consist of rigid subunits and generally have structures close to those of their related noncyclic precursors.[16] Generally, their synthesis is high yielding, even when it entails the oligomerization of multiple units. The key feature of the shape-persistent macrocycle is the use of a multiple-center H-bonding system to keep an intramolecular folding (Figure 2), which was carried out by Hamilton and co-workers in 1994.[17] The construction of helical structure is in Figure 2. The intramolecular H-bonds of between five-donor types existence in the 2,6-pyridinedicarboxamide motif would be weak, while the electrostatic repulsion between the pyridine N-atom and adjacent amide O-atom twist a 180° rotation of the amide bond. The positive cooperativity of H-bonds and electrostatic repulsion will form the multiple-center H-bonding system, which will keep the structure stable. Gong and co-workers explored the concept to include the H-bonded oligomeric carboxyamides based on aromatic methoxybenzene and pyridine motifs. [18] The intermolecular H-bonding system also bring the advantage in the process of synthesis, highly efficient one-pot macrocyclization process is

16 Li, Z.-T.; Hou, J.-L.; Li, C.; Yi, H.-P. *Chem. Asian J.* **2006**, *1*, 766-778; Zhang, W.; Moore, J. S. *Angew. Chem., Int. Ed.* **2006**, *45*, 4416-4439; Yamato, K.; Kline, M.; Gong, B. *Chem. Commun.* **2012**, *48*, 12142-12158; Moore, J. S. *Acc. Chem. Res.* **1997**, *30*, 402-413; Zhao, D.; Moore, J. S. *Chem. Commun.* **2003**, 807-818; Grave, C.; Schlüter, A. D. *Eur. J. Org. Chem.* **2002**, *2002*, 3075-3098.

17 Hamuro, Y.; Geib, S. J.; Hamilton, A. D. *Angew. Chem., Int. Ed.* **1994**, *33*, 446-448.

18 Zhu, J.; Parra, R. D.; Zeng, H.; Skrzypczak-Jankun, E.; Zeng, X. C.; Gong, B. *J. Am. Chem. Soc.* **2000**, *122*, 4219-4220; Berl, V.; Huc, I.; Khoury, R. G.; Krische, M. J.; Lehn, J.-M. *Nature* **2000**, *407*, 720-723.

always be carried out during the preparation.[19] During the one-pot synthesis, monomers are used as starting materials and under the reaction condition, the chain of monomers keeps growing until the length of the oligomeric precursor is enough to be cyclized. As a result of one-pot synthesis, the favorable product is determined by the very nature of monomers. With the process of reaction, the precursor chains react with monomers to form amide bond and grow longer and longer, the angle of each amide bond also rise to the curvature of noncyclic precursor. The ring close reaction only occur after noncyclic oligomers reached on cycle. Based on this mechanism, macrocycles with backbone of reduced curvature would obtain enlarged cavities.

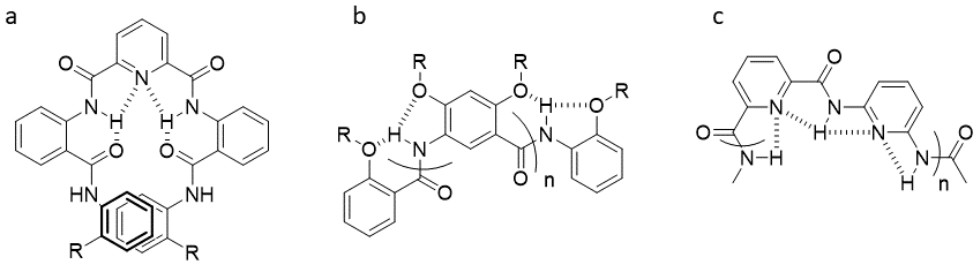

Figure 2. Structures of a) helically folded pyridine-based oligomer; b) helically folded methoxybenzene-based foldamers and c) pyridine-based foldamers assemble into a double helix structure.

Gong and co-workers have studied the structure of macrocycles **1.5** which showed a folded conformation.[20] The structure can be prepared from precursor **1.4**. During the reaction, macrocyclic products can be obtained with 20-57% yield. They found that a strategy based on the rigid shape of starting material **1.4** can be used to prepare macrocycles **1.5** which folded as a double-decked crescent (Figure 3). Two tris(phenylene ethynylene) moieties in macrocycle **1.5** are parallel to each other, the folded conformation is supported by the π-π stacking interaction.

19 Feng, W.; Yamato, K.; Yang, L.; Ferguson, J. S.; Zhong, L.; Zou, S.; Yuan, L.; Zeng, X. C.; Gong, B. *J. Am. Chem. Soc.* **2009**, *131*, 2629-2637.
20 Lin, L.; Zhang, J.; Wu, X.; Liang, G.; He, L.; Gong, B. *Chem. Commun.* **2010**, *46*, 7361-7363.

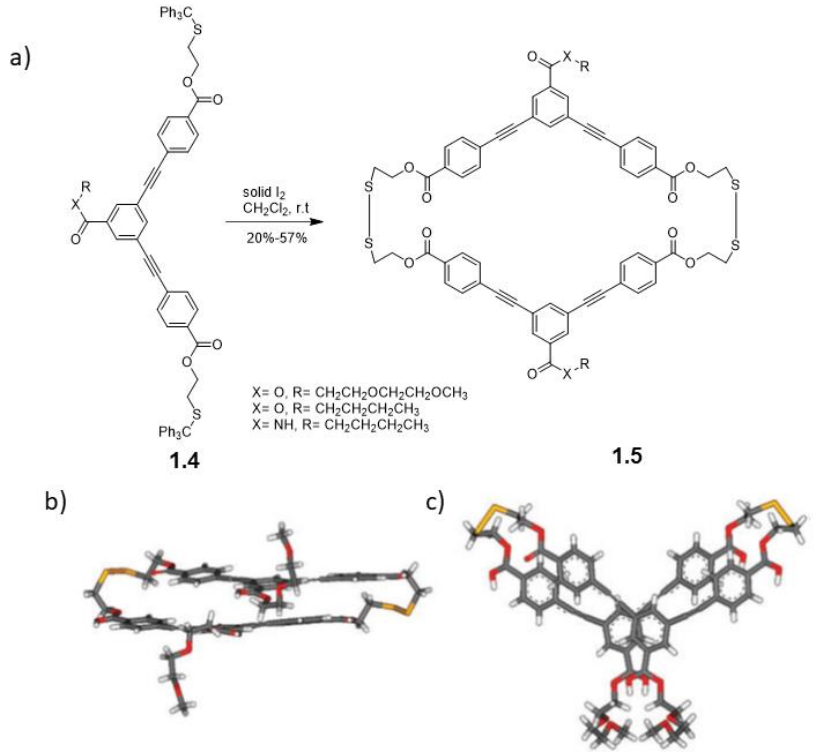

Figure 3. a) Synthesis of rigid macrocycles containing a folded pattern; b) side view and top view of X-ray structure of **1.5**.

Bertozzi and co-workers reported the first synthesis of varying sizes cycloparaphenylenes (CPPs).[21] They prepared compounds **1.8** using a nonselective macrocyclization reaction to obtain [1+1], [2+2], [3+3] macrocycles (Figure 4). After aromatization of **1.8**, macrocycle **1.9** was obtained. As these structures correspond to the shortest-possible segment of an armchair carbon nanotube, they refer to those structures as "carbon nanohoops". The building blocks **1.6** and **1.7** folded conformations favor the macrocyclization reaction, and the conformations were supported by the *syn* dimethoxy functional groups.

21 Jasti, R.; Bhattacharjee, J.; Neaton, J. B.; Bertozzi, C. R. *J. Am. Chem. Soc.* **2008**, *130*, 17646-17647.

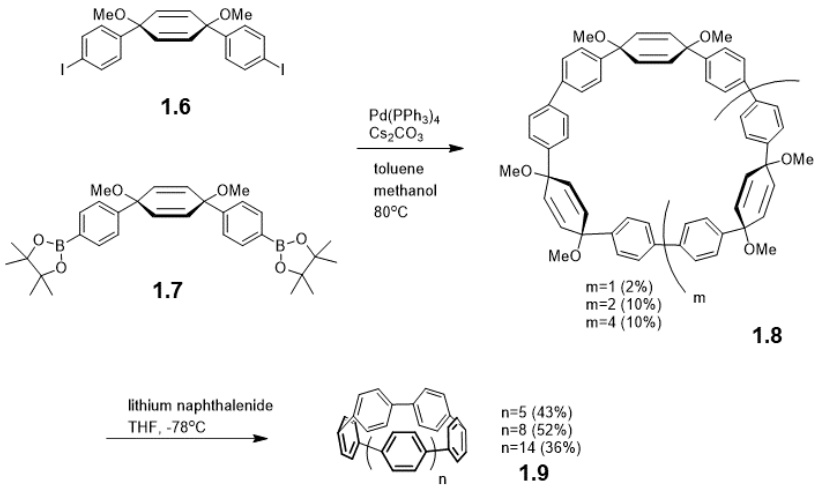

Figure 4. Synthesis of [9]-, [12]-, and [18] CPP.

Macrocycles can also be prepared by more than two building blocks based on rigid aromatic components. The Li and co-works has studied the synthesis of the rigid macrocycle **1.13**, which is obtained from short-chain precursor **1.10** and two small units **1.11** and **1.12** (Figure 5). Multicomponent assembly between three build blocks is directed by intramolecular hydrogen bonding, favoring the macrocyclization.[22] They prepared various macrocyclic structures starting from different starting materials, and theirs results showed that the less strained structure is preferentially formed.

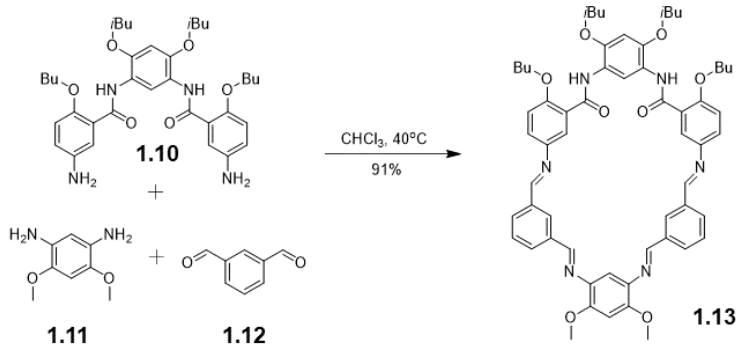

Figure 5. Macrocyclization reaction between three starting materials.

Another strategy is to use one-pot macrocyclization of small building blocks, allowing a chain to elongate until it proved long enough to cyclize. The recently reported shape-persistent cavity-containing aromatic macrocycles can be classified in three general categories, porphyrin

22 Lin, J.-B.; Xu, X.-N.; Jiang, X.-K.; Li, Z.-T. *J. Org. Chem.* **2008**, *73*, 9403-9410.

derivatives,[23] arylene ethynylene macrocycles and macrocyclic Schiff bases,[24] with properties such as guest binding, sensing and medicine.

Gong and co-workers have thoroughly studied the cyclization of rigid oligoamides.[25] In the example showed in Figure 6 one large macrocycle **1.17** was prepared from mixing aromatic diamine **1.11** and a functional aromatic diacid chloride **1.14** in a one-pot synthesis. The reaction starts from short units and shows good yields. The open chain precursor has a rigid crescent shape conformation, which can help to overcome the entropy barrier of the macrocyclization reaction. The folded conformation of the precursors will continue to grow until it can position two reactive ends close enough to form the final macrocycle. As the conformation of precursors showed a key role, different temperature will affect the outcome of the reaction. For example, 6-mer macrocycle **1.17** is the main product when the macrocyclization was carried out at low temperature, while the 8-mer macrocycle is favored at high temperature.

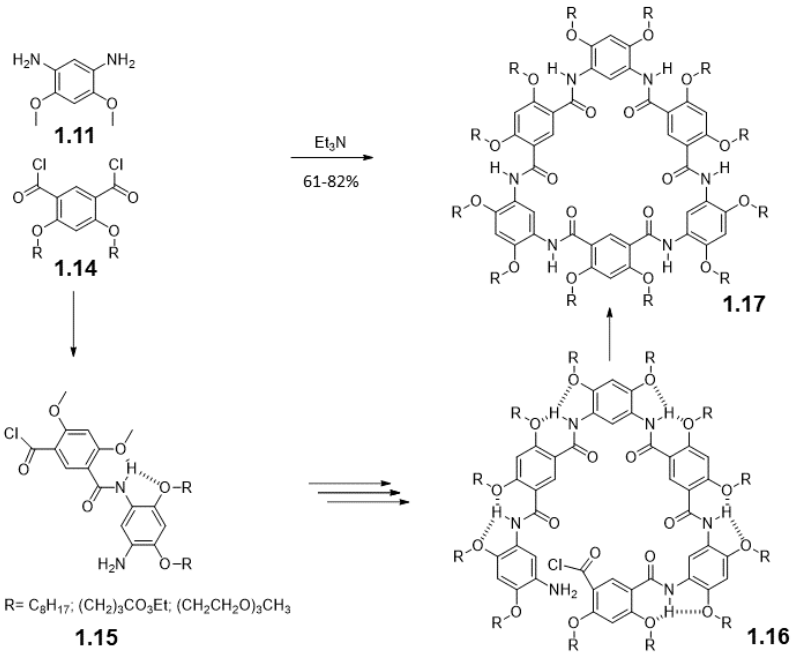

Figure 6. Synthesis of 6-mer macrocycle by a [3+3] process.

23 Sessler, J. L.; Seidel, D. *Angew. Chem., Int. Ed.* **2003**, *42*, 5134-5175; Misra, R.; Chandrashekar, T. K. *Acc. Chem. Res.* **2008**, *41*, 265-279.

24 Brooker, S. *Coord. Chem. Rev.* **2001**, *222*, 33-56; Borisova, N. E.; Reshetova, M. D.; Ustynyuk, Y. A. *Chem. Rev.* **2007**, *107*, 46-79.

25 Sanford, A. R.; Yuan, L.; Feng, W.; Yamato, K.; Flowers, R. A.; Gong, B. *Chem. Commun.* **2005**, 4720-4722; Yuan, L.; Feng, W.; Yamato, K.; Sanford, A. R.; Xu, D.; Guo, H.; Gong, B. *J. Am. Chem. Soc.* **2004**, *126*, 11120-11121; Yamato, K.; Kline, M.; Gong, B. *Chem. Commun.* **2012**, *48*, 12142-12158.

The efficiency of the macrocyclization reactions depends of the rigid structures of the open chain which rely on the formation of stable three-center hydrogen bonds among the amide N-H and one OR group at each of the adjacent building blocks.[26] As a result, if one alkyloxy is removed in the precursor thus removing a hydrogen bond, it will affect the macrocyclization reaction and bring a significant difference in the properties of the final cyclized product. Figure 7 is an example provided by Gong and co-worker. The reaction between alkyloxy substituted monomeric acid chloride **1.14** and monomeric diamines **1.11** did not lead to the designed macrocycles and the cyclization reaction was processed from the corresponding trimeric diamine **1.19** and diacid **1.18** (left way) to obtain **1.22a** (46%). This kind of [1+1] macrocyclization process has been used in the preparation of some macrocycles with highly constrained backbones. While in some design, the solubility of the intermediates precluded the use of this strategy and it was necessary to change the starting material. For example for **1.22b**, they need to perform the macrocyclization from starting material **1.20** and **1.21**.

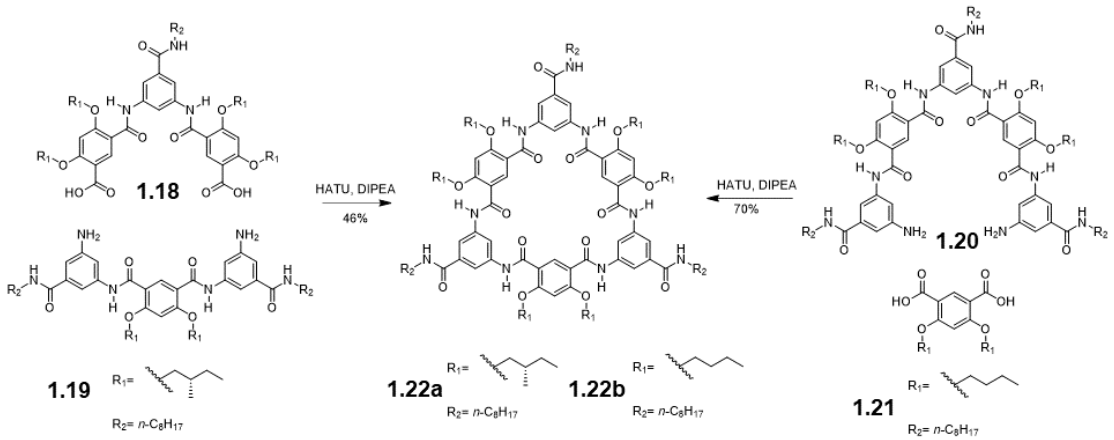

Figure 7. Synthesis of a constrained backbone macrocycle from different starting materials.

1.3 Porphyrin based macrocycles

Because one-pot synthetic strategy is relatively straightforward Osuka et al prepared a series of expanded porphyrins using the oxidative coupling reaction of *meso*-pentafluorophenyl

26 Yang, L.; Zhong, L.; Yamato, K.; Zhang, X.; Feng, W.; Deng, P.; Yuan, L.; Zeng, X. C.; Gong, B. *New J. Chem.* **2009**, *33*, 729-733; Wu, X.; Liang, G.; Ji, G.; Fun, H.-K.; He, L.; Gong, B. *Chem. Commun*. **2012**, *48*, 2228-2230; Kline, M.; Wei, X.; Gong, B. *Org. Lett*. **2013**, *15*, 4762-4765.

substituted tripyrrane (Figure 8). One can note that expanded porphyrins having more than six pyrrole rings have distorted structures.[27]

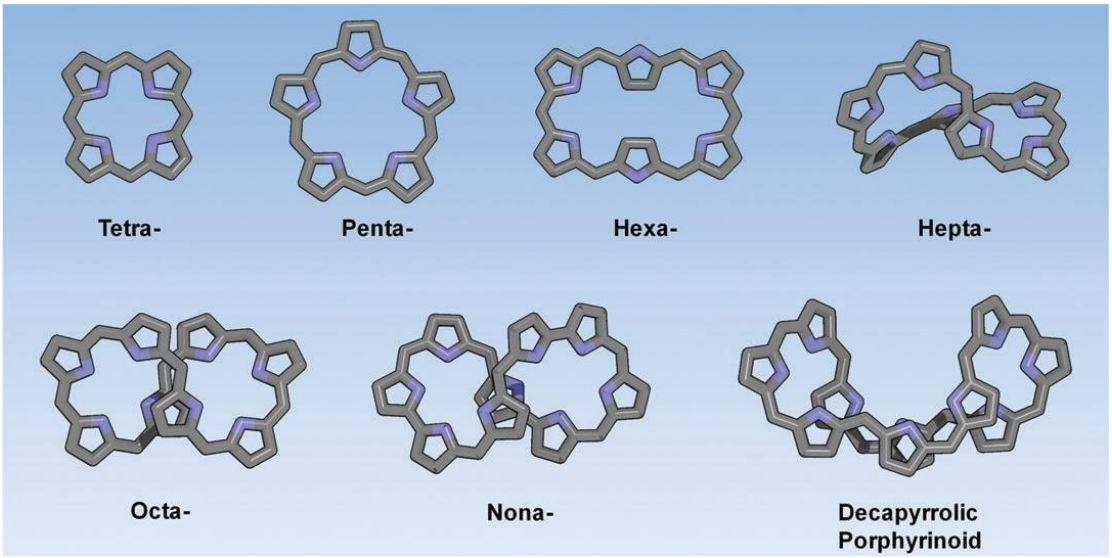

Figure 8. Structure of various porphyrinoids.

Osuka developed a ring-size selective synthesis of expanded porphyrins by using dipyrromethane as starting material. Methanesulfonic acid was used as catalysts for ring size selective synthesis of *meso*-aryl expanded porphyrins including porphyrin **1.24** (9%), hexaphyrin **1.25** (19%), octaphyrin **1.26** (38%) (Figure 9).[28] In this case different products were isolated, providing for example an easy synthetic access to octaphyrin **1.26**.

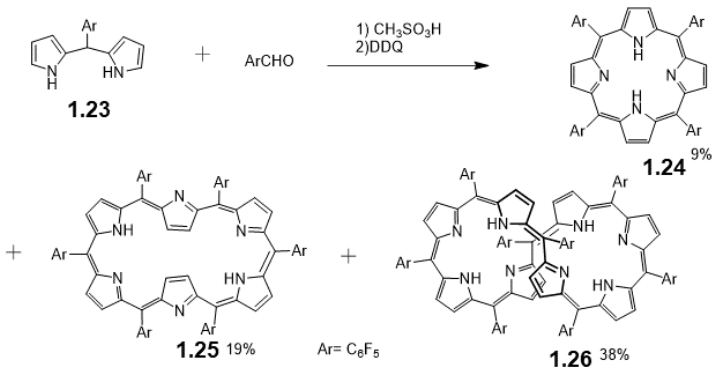

Figure 9. Synthesis of porphyrin, hexaphyrin and octaphyrin.

27 Shin, J.-Y.; Kim, K. S.; Yoon, M.-C.; Lim, J. M.; Yoon, Z. S.; Osuka, A.; Kim, D. *Chem. Soc. Rev.* **2010**, *39*, 2751-2767; Shin, J.-Y.; Furuta, H.; Yoza, K.; Igarashi, S.; Osuka, A. *J. Am. Chem. Soc.* **2001**, *123*, 7190-7191.
28 Taniguchi, R.; Shimizu, S.; Suzuki, M.; Shin, J.-Y.; Furuta, H.; Osuka, A. *Tetrahedron Lett.* **2003**, *44*, 2505-2507.

Following these seminal results, Osuka and co-workers changed the starting materials to tripyrrane. They also tested the oxidative coupling reaction of functional tripyrrane under TFA catalysis followed by a chloranil oxidation. After purification they were able to isolate the hexaphyrin **1.28** in 24% yield (Figure 10). They also isolated nonaphyrin **1.29** in 9% and dodecaphyrin **1.30** in 2.7%.[29]

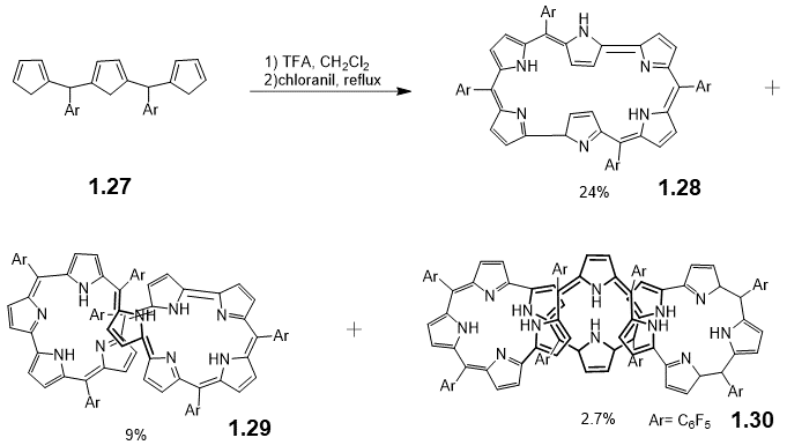

Figure 10. Synthesis of hexaphyrin, octaphyrin and dodecaphyrin.

The structure of the resulting product was assessed by X-ray diffraction analysis (Figure 11). The dodecaphyrin is a symmetric helical conformation consisting of two inward-direct tripyrrane units (pyrroles L, A, and B, and F, G, and H) and two flapped-direct tripyrrane units (pyrroles C, D, and E, and I, J, and K). They also showed the intermolecular hydrogen bonding interactions between adjacent pyrrole NH protons and close unprotonated nitrogen atoms. These hydrogen bonds also help stabilizing the constrained conformation of dodecaphyrin.

29 Shimizu, S.; Taniguchi, R.; Osuka, A. *Angew. Chem., Int. Ed.* **2005**, *44*, 2225-2229; Shimizu, S.; Cho, W.-S.; Sessler, J. L.; Shinokubo, H.; Osuka, A. *Chem.—Eur. J.* **2008**, *14*, 2668-2678.

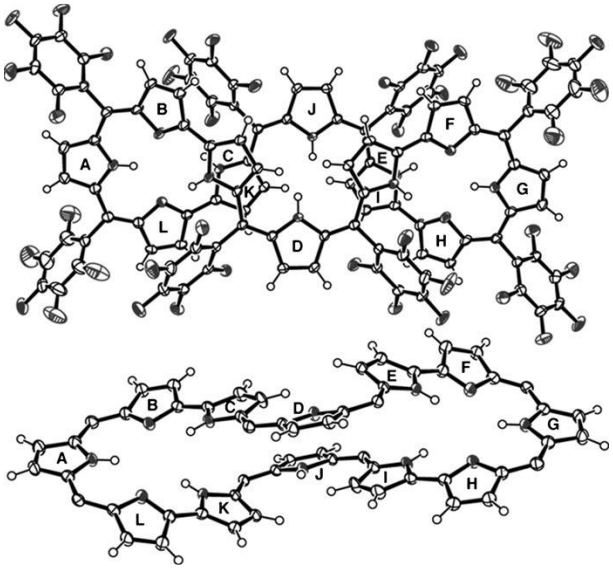

Figure 11. Crystal structure of dodecaphyrin **1.30**.

Then, they mix the dodecaphyrin with an excess amount of an oxidative agent 2,3-dichloro-5,6-dicyano-1,4-benzoquinone (DDQ) and the solution color changed from blue to dark green and they obtained the product **1.31**. They tried a further oxidation by treating the solution with an excess amount of MnO_2 and the color of solution immediately turns from dark green to yellow green, to yield product **1.32**.[30]

Fortunately, they can detect the change of conformation by X-ray crystallography (Figure 12). As mentioned above **1.30** proved to be a symmetric helical conformation consisting of two kinds of tripyrrane units, while the first oxidized form **1.31** is a simple cyclic conformation with *Ci* molecular symmetry, the second oxidized form **1.32** showed a doubly twisted figure-eight conformation with C_2 symmetry.

Dodecaphyrins **1.30**, **1.31**, and **1.32**, with three different oxidation states, are all chemically stable molecules and the oxidation states can be converted back by reduction using $NaBH_4$.

30 Soya, T.; Kim, W.; Kim, D.; Osuka, A. *Chem.—Eur. J.* **2015**, *21*, 8341-8346; Yoneda, T.; Soya, T.; Neya, S.; Osuka, A. *Chem.—Eur. J.* **2016**, *22*, 14518-14522.

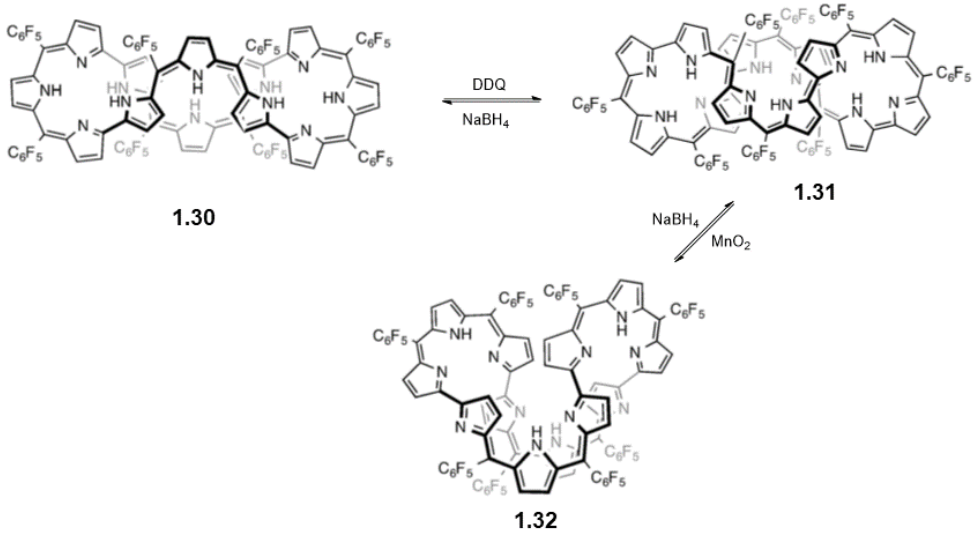

Figure 12. Redox behavior of dodecaphyrin **1.30**.

2. Introduction to foldameric architecture

A foldamer is defined as "any oligomer that folds into a conformationally ordered state in solution, the structures of which are stabilized by a collection of noncovalent interactions between nonadjacent monomer units",[31] that means foldamers can fold for example into a stable helical conformation. Due to the stable folding in crescent structures, foldamer can be used as precursors of shape-persistent macrocycles.

In our group various family of aromatic amino acid monomers have been produced over the years for the design of foldamer architectures.[32] As shown in Figure 13a conjugation, hydrogen bonds (dotted lines), and electrostatic repulsions (red arrows) all keep the stabilization of folded conformation at each aryl-amide bond. In a long sequence, the resulting curvature generate a helix. Aromatic stacks within the helix also benefit to its stability which is particularly increased in protic media. Multiple-center hydrogen bond system (red dotted lines) in all monomers contribute to stable conformation of resulted foldamer (Figure 13b).

31 Hill, D. J.; Mio, M. J.; Prince, R. B.; Hughes, T. S.; Moore, J. S. *Chem. Rev.* **2001**, *101*, 3893-4012.

32 Ferrand, Y.; Huc, I. *Acc. Chem. Res.* **2018**, *51*, 970-977; Gan, Q.; Ferrand, Y.; Bao, C.; Kauffmann, B.; Grélard, A.; Jiang, H.; Huc, I. *Science* **2011**, *331*, 1172; Ferrand, Y.; Gan, Q.; Kauffmann, B.; Jiang, H.; Huc, I. *Angew. Chem. Int. Ed.* **2011**, *50*, 7572-7575; Wang, X.; Wicher, B.; Ferrand, Y.; Huc, I. *J. Am. Chem. Soc.* **2017**, *139*, 9350-9358; Wang, X.; Gan, Q.; Wicher, B.; Ferrand, Y.; Huc, I. *Angew. Chem., Int. Ed.* **2019**, *58*, 4205-4209; Gan, Q.; Wang, X.; Kauffmann, B.; Rosu, F.; Ferrand, Y.; Huc, I. *Nat. Nanotechnol.* **2017**, *12*, 447-452; Bao, C.; Kauffmann, B.; Gan, Q.; Srinivas, K.; Jiang, H.; Huc, I. *Angew. Chem., Int. Ed.* **2008**, *47*, 4153-4156.

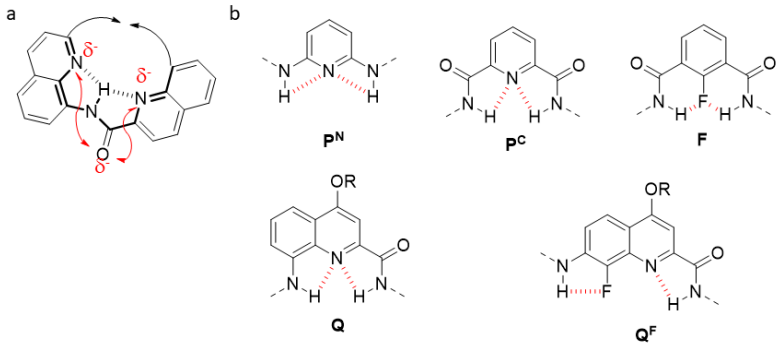

Figure 13. a) Local interactions that govern aromatic oligoamide folding. b) Formula of main chain units. 2,6-diaminopyridine (P^N), 2,6-pyridinedicarboxylic acid (P^C), 2-fluoro-1,3-benzenedicarboxylic acid (F), 7-amino-8-fluoro-2-quinolinecarboxylic acid (Q^F), 8-amino-2-quinolinecarboxylic acid (Q). "R" groups diverge from the folded objects and determine their solubility.

Helices display a special space conformation, in which the two ends of the strand diverge and are not preorganized to undergo macrocyclization (Figure 14). To generate a macrocycle from a helix, we need to overcome this structural issue. The temporary introduction of disruptors of helicity disturb the proper folding of the helix and thus give a chance to the strand to be cyclized. After the cyclisation, a deprotection step can be performed to get rid of the disruptor and recover a certain form of the helicity.

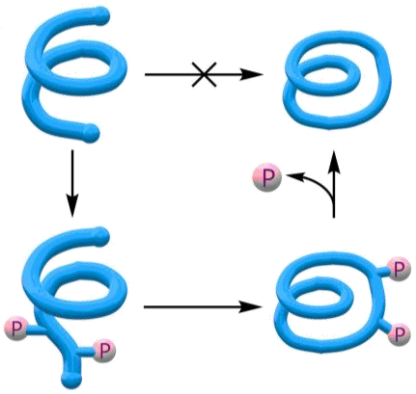

Figure 14. The ends of a long helix may not meet, yet the introduction of disruptors of helicity (P groups) allows cyclization. A constrained macrocycle is obtained after removal of the P groups.

The macrocyclization of a short trimer of quinoline oligoamide spanning slightly more than one turn was reported in 2004.[33] Noncyclic precursors which was prepared from the 8-amino-2-quinolinecarboxylic acid (Q) keep a particularly stable helical conformation in essentially any solvent. The stability of the helical conformation is supported by the

33 Jiang, H.; Léger, J.-M.; Guionneau, P.; Huc, I. *Org. Lett.* **2004**, *6*, 2985-2988.

electrostatic repulsions between amide oxygen atoms and neighboring quinoline endocyclic nitrogen atoms, and by bifurcated hydrogen bonds between amide NH and adjacent quinoline nitrogen atoms, as a result, the favorable value of curvature is 2.5 units per turn. With a minimal distortion of bending angles, shape-persistent trimeric macrocycle **QC$_3$** can be obtained (Figure 15a,c).

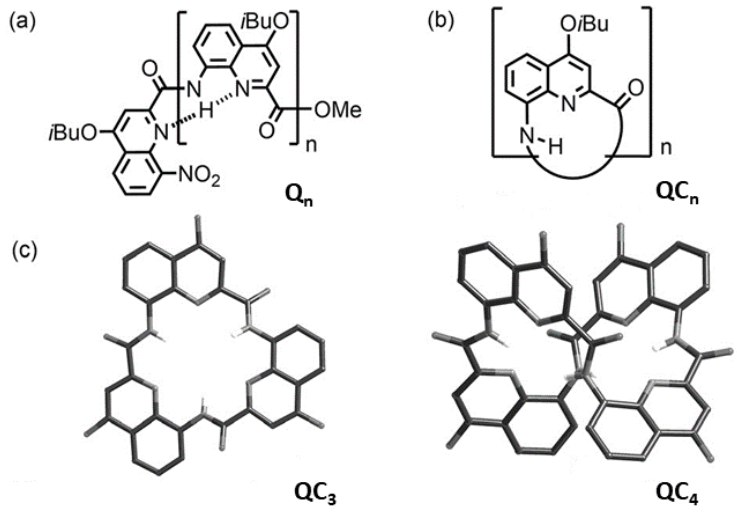

Figure 15. Chemical structures of: a) noncyclic 8-amino-2-quinolinecarboxylic acid oligoamides, and b) the corresponding macrocycles **QC$_n$**. c) crystal structures of **QC$_3$** and **QC$_4$**

Helical tetramer **Q$_4$** spans around 1.5 turns. Macrocyclization can be carried out under conditions that destabilize the folded helix, for example, heat and high concentrated LiCl. The cyclic structure can be achieved by reducing the stability of the noncyclic helix. If we compare the macrocyclization conditions for **QC$_3$** and **QC$_4$**, it is easy to figure out that **QC$_4$** needs more energy to cyclize because of its diverging ends.

As far longer sequences are concerned, for example pentamer of Q, their folding into helices is even more pronounced (e.g. two-turns for the Q$_5$) and consequently the extremity of the helix will be separated by two layers of aromatic rings, that means macrocyclization will never be able to proceed. The macrocyclization of a stable two-turn helical aromatic pentamide was reported.[34] As shown in Figure 16, the alkylation of some secondary amide by a dimethoxybenzyl (DMB) group in oligomers of Q destabilizes the favored helical

34 Urushibara, K.; Ferrand, Y.; Liu, Z.; Masu, H.; Pophristic, V.; Tanatani, A.; Huc, I. *Angew. Chem., Int. Ed.* **2018**, *57*, 7888-7892.

conformations, and allows the cyclization to carry on. The deprotection of DMB group using TFA at 60°C can lead to the macrocycle **QC$_5$**. This strategy will be described in details in the following.

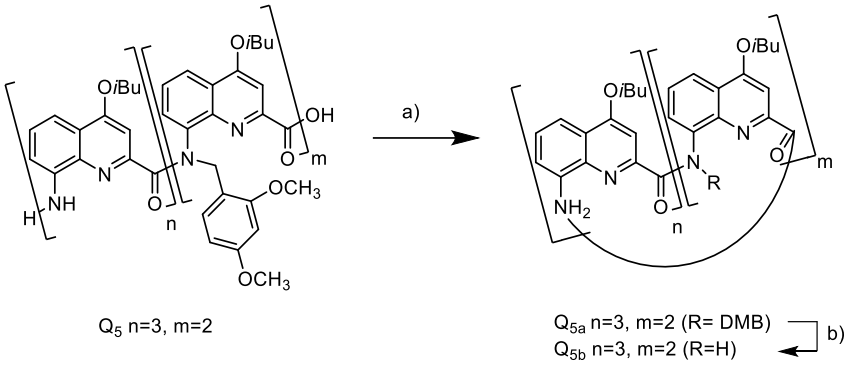

Figure 16. Macrocyclization of **Q$_5$**. Condition: a) PPh_3, trichloroacetonitrile, DIPEA, $CHCl_3$, 45%; b) TFA, 60 °C, quant. DMB=2,4- dimethoxybenzyl.

3. Building block: Q^F unit

Beside the monomer 8-amino-2-quinolinecarboxylic acid (Q), our group also reported previously that 7-amino-8-fluoro-2-quinolinecarboxylic acid (Q^F) based sequences can fold into helical shape that can further self-assemble in multiple helices. Like for Q oligomers, Q^F helical conformation is provided by electrostatic repulsions between carbonyl group and hetero atoms of the aromatic group (Figure 17a), intramolecular hydrogen bonding (Figure 17b) and interaction between aromatic groups. Moreover, the fluoroquinoline based foldamers span 4 monomers per turn defining a cavity large enough to accommodate an alkyl chain as a guest. The structure of single helix of Q^F was observed in the solid state. In the solid state, Q^F tetramer (Q$^F_4$) spans just about one turn and due to the steric hindrance,[35] two ends of the sequence deviate from planarity and overlap into a single helix with a pitch of approximately 3.5 Å (Figure 18).

In this chapter, we will see how we adapted the strategy based on the helicity disruptors (dimethoxy benzyl) to prepare a series of macrocycle based on 7-amino-8-fluoro-2-quinolinecarboxylic acid monomers.

35 Gan, Q.; Bao, C.; Kauffmann, B.; Grélard, A.; Xiang, J.; Liu, S.; Huc, I.; Jiang, H. *Angew. Chem. Int. Ed.* **2008**, *47*, 1715-1718.

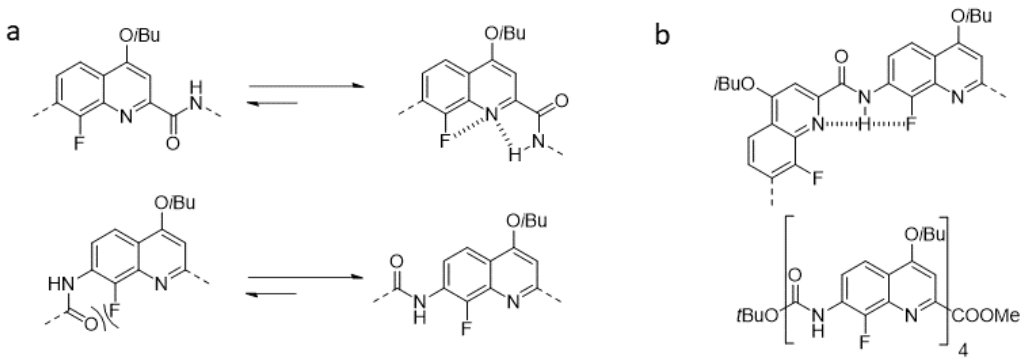

Figure 17. a) Electrostatic repulsion between carbonyl and hetero atoms of aromatic ring. b) Multiple-center H-bonding system between two Q^F monomer.

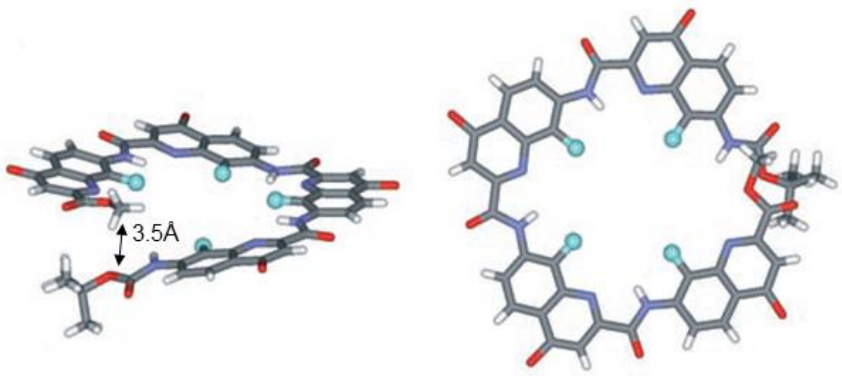

Figure 18. $\mathbf{Q^F_4}$ as a single helix; the fluorine atoms converging towards the helix hollow space is shown as spheres.

4. Result and discussion

4.1 Dimer

4.1.1 Synthesis

The monomer 7-amino-8-fluoro-2-quinolinecarboxylic acid (Q^F) protected with Boc on N terminus and methoxy on C terminus has been reported,[36] our objective is thus to produce the secondary amine using a reductive amination reaction to further obtain DMB protected dimer after coupling with an activated acid. The secondary amine was obtained with a reductive amination reaction. 2,4-dimethoxybenzaldehyde will react with the amine of Q^F to form a Schiff base, followed by the reduction of the latter using sodium triacetoxyborohydride to obtain the

36 Bao, C.; Kauffmann, B.; Gan, Q.; Srinivas, K.; Jiang, H.; Huc, I. *Angew. Chem., Int. Ed.* **2008**, *47*, 4153-4156.

secondary amine in good yield. The DMB protected dimer **4** was obtained from the coupling reaction between the secondary amine **2** and the acid chloride of **3** as shown in Scheme **1**. 1-chloro-N,N,2-trimethyl-1-propenylamine (Ghosez's reagent) was used to convert **3** to its corresponding acid chloride, because oxalyl chloride would generate HCl during the acid chloride conversion which may affect the Boc group. The active acid chloride was coupled with the amine **2** and dimer **4** was obtained after column purification in high yield. To obtain the amine Q^F dimer **5**, Boc deprotection of dimer **4** was achieved using HCl (4N in dioxane solution). What should be mentioned is that the TFA conditions usually used for deprotection reaction, cannot be used to avoid cleaving the DMB groups. The saponification of the methyl ester of dimer **5** is performed using NaOH dissolved in a THF/water mixture.

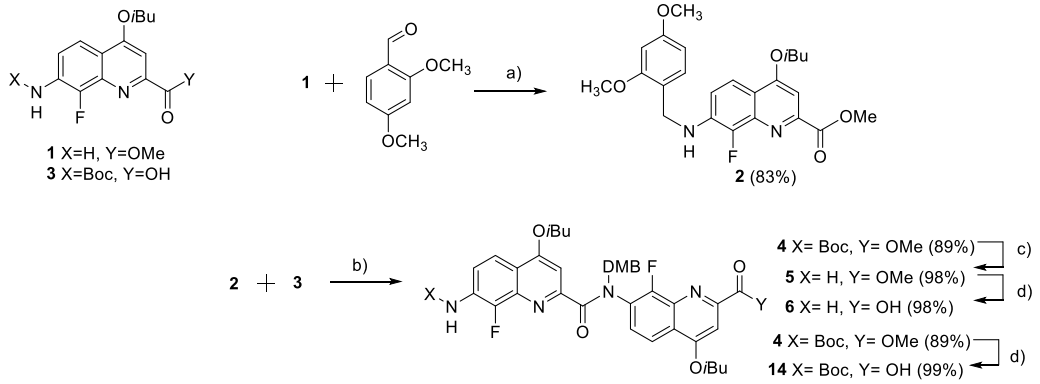

Scheme 1. Synthesis of DMB protected Q^F dimer **5** : a) sodium triacetoxyborohydride, 1,2-Dichloroethane, room temperature, 16h; b) i) 1-chloro-N,N,2-trimethyl-1-propenylamine, $CHCl_3$, room temperature, 3 h ; ii) DIEA, $CHCl_3$, room temperature, 12 h; c) HCl 4N in dioxane, room temperature, 4h; d) LiOH, THF, H_2O, room temperature, 4 h.

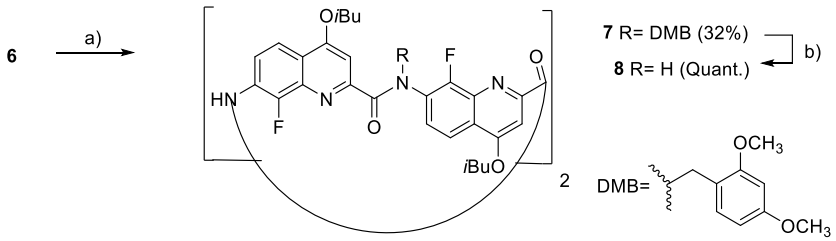

Scheme 2. Synthesis of Q^F tetramer macrocycle **8** : a) triphenylphosphine, trichloroacetonitrile, DIPEA, $CHCl_3$, room temperature, 48 h; b) trifluoroacetic acid, $CHCl_3$, 60°C, 2 h.

Macrocyclization of the amino acid dimer **6** is carried out as a one-pot reaction. Dimer **6** was dissolved in chloroform with triphenylphosphine (PPh_3), trichloroacetonitrile (CCl_3CN) and DIPEA. The PPh_3 and CCl_3CN will activate the acid smoothly to give the corresponding

acid chloride which can react subsequently with the amine group of another dimer to afford DMB protected macrocycle **7** in good yield. The reaction time should not be too short, as usual we let it undergo 2 days. The purification of the macrocycle consisted first, in a silica gel chromatography to remove the amino-acid that cannot be eluted using cyclohexane and ethyl acetate (50:50) as the eluent. It is then followed with a purification using recycling Gel Permeation Chromatography (GPC). GPC can separate molecules according to their sizes. The GPC chromatogram are shown in Figure 19, and as can be observed, after 3 cycles we can obtain the main peak as the product **7**. The interesting fact is that a series of peaks can also be found in the chromatogram, they are obviously larger than macrocycle **7,** yet they could not be identified. After purification by GPC, compound **7** is obtained pure with no trace of larger macrocycles. The product was supported by mass spectrometry, a mass $[M+H]^+$ = 1341.5396 which corresponding to macrocycle **7** (calcd for $[M+H]^+$:1341.5312) was found. DMB free macrocycle **8** was obtained by treating **7** with TFA.

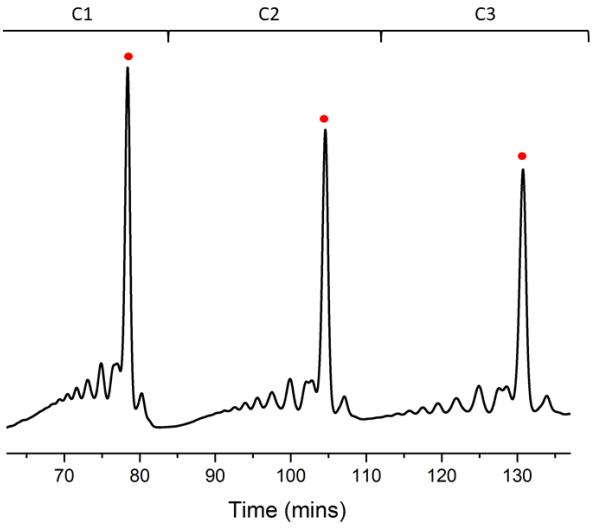

Figure 19. Chromatogram of recycling GPC of **7**. The peaks marked with red circle stand for **7.**

4.1.2 Structure of macrocycles

NMR analysis was employed to study the conformation of macrocycle **7**. A set of sharp resonances was observed in chloroform which indicates a well-defined species in the solution at room temperature. As shown in figure 20, the ^{1}H NMR spectra of **7** revealed a well defined amide region (beyond 10 ppm), an aromatic region (9-6 ppm) and an aliphatic region (below

4.5 ppm). A single amide resonance was identified and is marked with red dots. The macrocycle is constituted of four Q^Fs and two DMB protected groups, leaving two secondary amides. As expected, the single amide signal confirm the symmetric conformation of **7**. Other regions in the NMR spectra can also be used to assess this conclusion: the two methoxy groups in *ortho* and *para* of the DMB group are marked with green and brown color and are found as singlet around 3.80 ppm and 3.38 ppm. Two doublets with a chemical shift of 5.37 and 5.06 ppm (blue) correspond to the diastereotopic methylene groups of the DMB. The symmetric quartet shows AB spin system, two sets of double peaks share the same *J* value (14.1 Hz) and different δ values, which indicated the two diastereotopic CH_2 groups in DMB are symmetrical.

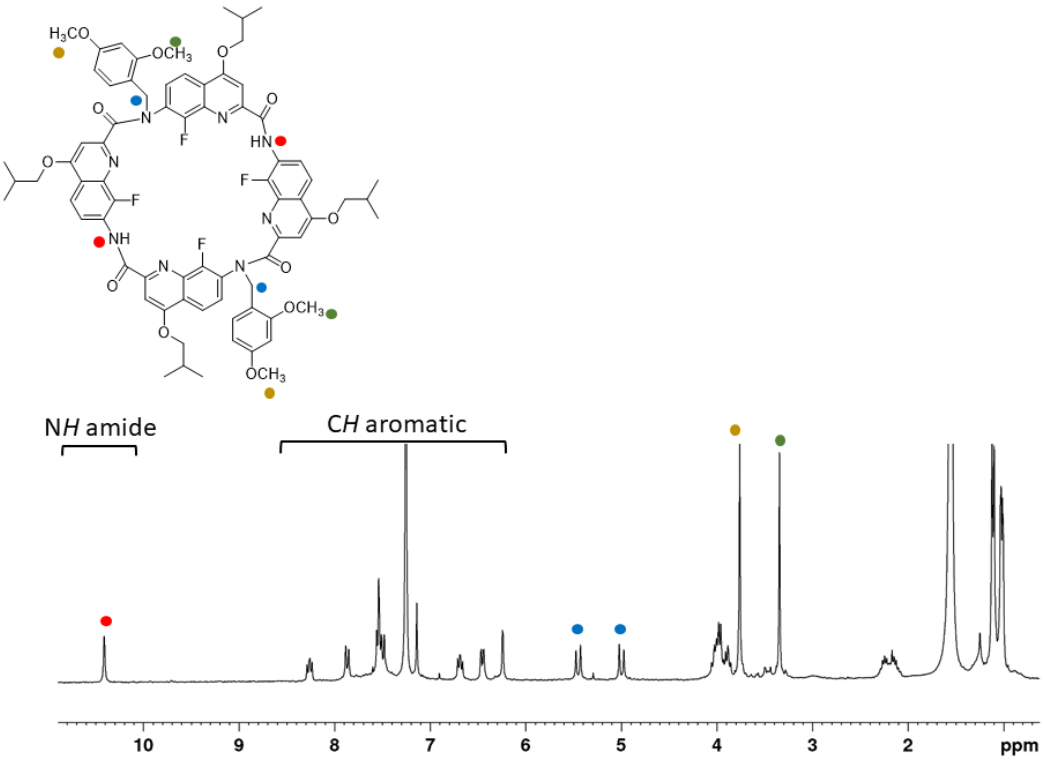

Figure 20. ^{1}H NMR spectrum (300 MHz) of the tetramer macrocycle **7** (0.1 mM) in $CDCl_3$ at 298 K, signals of the macrocycles 7 were marked with different color circles. -NH- was marked with red, -CH_2- was marked with blue, ortho-OCH_3- was marked with green and para-OCH_3- was marked with brown. The zone of aromatic protons from DMB and Q^F can also be divided in the spectra.

The macrocycles are composed of Q^F monomers which bear each a fluorine atom in position 8 that can be used as probe. As shown in Figure 21, two singlets were observed that is

another clear evidence of the symmetrical structure of **7**. The signal at -140 ppm corresponds to the Q^F distant from the DMB group, and that is involved in hydrogen bonds. The other one is close to the DMB protected amide. The effect of hydrogen bonds and DMB groups can also be observed in the chemical shifts of Q^F oligomers before macrocyclization.

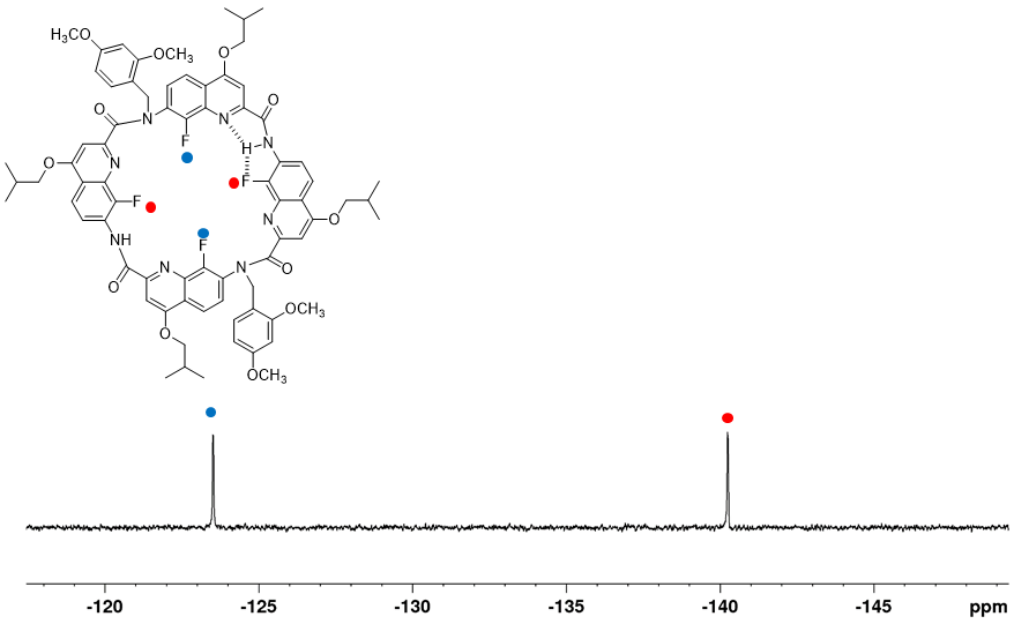

Figure 21. ^{19}F NMR spectrum (300 MHz) of the macrocycle **7** (0.1 mM) in $CDCl_3$ at 298 K. Signals of fluorine are marked with red and blue color.

The conformation of **7** was confirmed by X-ray crystallography. Fortunately, we obtained single crystals suitable for X-ray analysis for **7**. The single crystal was obtained by slow diffusion of hexane into a chlorobenzene solution and the structure was resolved in the *P*-1 space group. As shown in Figure 22, the macrocycle **7** has a classical saddle shape conformation. It can be noted the strong impact of the DMB groups on the conformation of the macrocycle. In the top view (Figure 22a), a *trans* amide group can be observed, this bond configuration proved efficient for hydrogen bonding and stabilizing helical conformation. In the side view of the crystal (Figure 22b), we can observe the DMB protected amides, that reveal a *cis* conformation. The *cis* conformation destabilized the flat structure, and impose a saddle shape conformation.

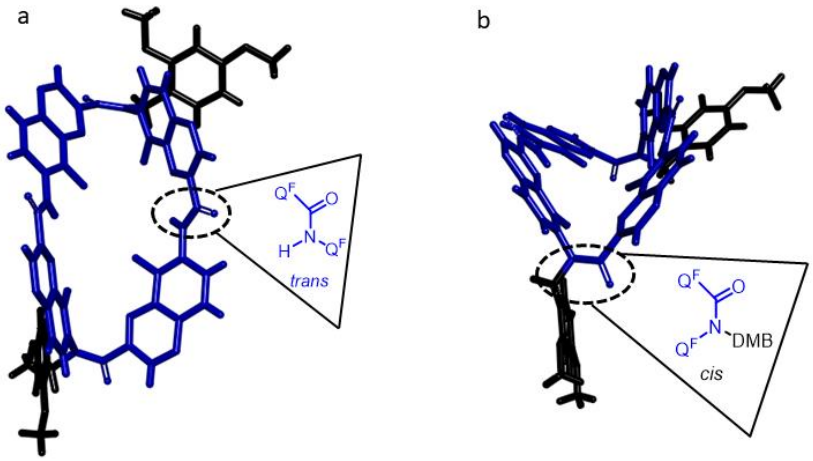

Figure 22. X-ray structure of **7**, DMB groups are colored in black and Q^F units are colored in blue. a) Top view of the crystal structure of macrocycle **7**, the *trans* amide group are shown in the black dot cycle. B) Side view of the crystal structure of macrocycle **7**, the *cis* amide group is marked within the black dot cycle. Side chains (O*i*Bu groups) and included solvent molecules have been removed for clarity.

DMB free macrocycles **8** can be obtained from TFA deprotection of **7**, yet although the reaction proceeded well, product **8** proved insoluble in all the common solvents (chloroform, DCM, DMSO, pyridine, acetone, acetonitrile, hexane, THF …). Thus analysis of the compound by NMR in solution, or in the solid state was not possible.

Energy minimized models were built for the macrocycle **8** as presented in Figure 23. After removal of DMB, the macrocycles **8** showed a flat and symmetric conformation in the space. In the top view (Figure 23a), different from **7**, all the amide were oriented to *trans* isomers and four units of Q^F give a symmetric directions. The macrocycles **8** also has a prefect curvature of 4 units per turn, which is consistent with our previous works. The side view was presented in CPK style (Figure 23b), macrocycle **8** has a completely flat structure which is beneficial to molecular stack and could be the main reason for poor solubility.

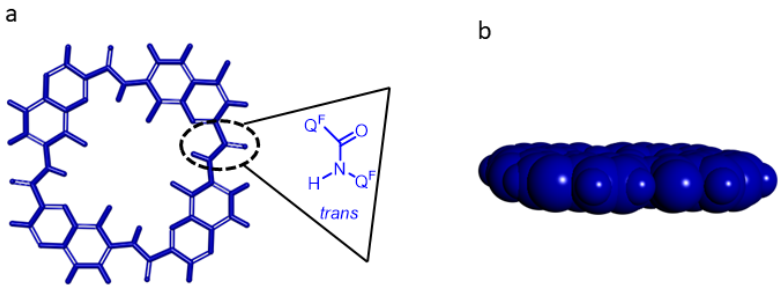

Figure 23. Energy minimized molecular models of the macrocycle **8**. a) Top view of the molecular models of macrocycle **8** in tube representation, note that all amide groups had *trans* conformation. b) Side view of macrocycle **8** in CPK representation. The models were produced with Maestro software package, using MFFS force field, chloroform as solvent and TNCG as minimization method.

In conclusion, the study of macrocycles **7** and **8** validated the DMB strategy to synthesize Q^F macrocycles. The crystal structure and modelling indicate that the DMB can prevent a proper folding and allow the cyclisation. Those results motivated us to challenge the preparation of longer sequences.

4.2 DMB functionalized tetramer

4.2.1 Synthesis

The DMB functionalized tetramer **10** could also be prepared with an alternative strategy (Scheme 3). Ghosez's reagent was used to convert dimer acid **9** (devoted from DMB) to its corresponding acid chloride which was coupled to the DMB containing dimer **5** affording mono DMB tetramer **10**. Deprotection of the Boc group and saponification of the methylester were performed using HCl (4M in dioxane) and LiOH, respectively. Macrocyclization of the tetramer was performed using excess PPh_3 and CCl_3CN to convert **12** to acid chloride *in situ*. This method allows continuous activation of the acid to push the cyclization reaction despite hydrolysis of the acid chloride. After purifying **10** with silica gel chromatography and recycling GPC, DMB groups were removed using TFA at 60°C to afford the macrocycle. GPC was also used to purify the final compound.

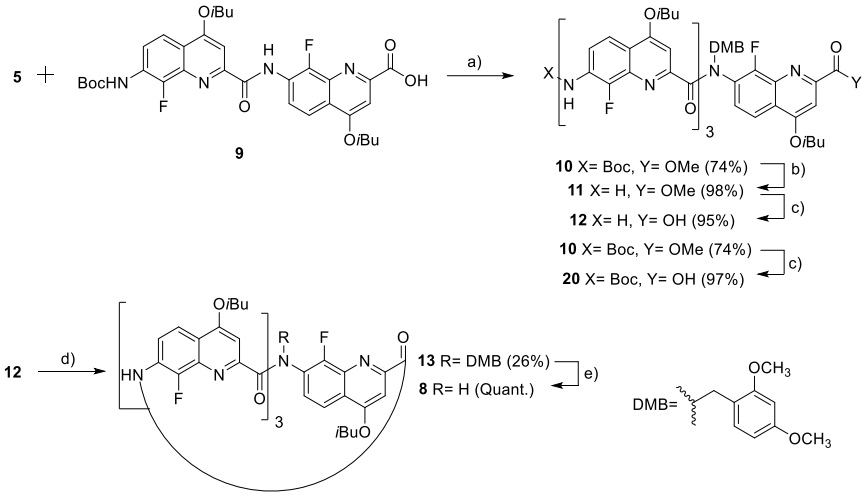

Scheme 3. Synthesis of Q^F tetramer **13**: a) i)1-chloro-N,N,2-trimethyl-1-propenylamine, $CHCl_3$, room temperature, 3 h; ii) DIEA, $CHCl_3$, room temperature, 12 h; b) HCl 4N in dioxane, room temperature, 4 h. c) LiOH, THF, H_2O, room temperature, 4 h; d) triphenylphosphine, trichloroacetonitrile, DIPEA, $CHCl_3$, room temperature, 48 h; e) trifluoroacetic acid, $CHCl_3$, 60°C, 2 h.

Mass analysis revealed a product with $[M+H]^+$ = 1191.4616, which corresponds to the macrocycle **13** (calcd for $[M+H]^+$ = 1191.4598). Surprisingly, here the main reaction is the intramolecular cyclisation and not the intermolecular cyclisation that would have yielded the cyclic octamer. Yet, the GPC chromatogram (Figure 24) revealed products with higher MW that could result from [1+1] cyclization of the tetramer. GPC is a very useful tool to analyze and purify compound of different MW. For example, macrocycle **13** (M.W: 1191.2506 g/mol) takes 26.86 min for a cycle whereas macrocycle **7** (M.W: 1341.4276 g/mol) elutes in 26.19 mins for a cycle (Figure 19).

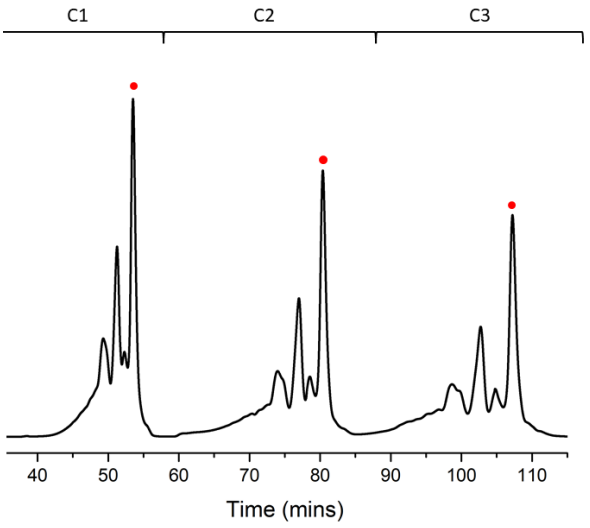

Figure 24. Chromatogram of recycling GPC of **13** purification. The peaks marked with red circle stand for the appearance of **13**. The residual time can be calculated as the time between two cycles of same peaks.

4.2.2 NMR of the tetramer macrocycles

The ^{1}H NMR spectra of tetramer **13** shows a set of sharp resonances (Figure 25) in chloroform at room temperature. Three sharp signals at 12 ppm correspond to the NH amides and are marked with red circles. Around the aromatic region, three doublet of doublet signals corresponding to the aromatic protons of the fluorobenzene ring can be identified and are marked with blue circles. The ^{19}F NMR spectrum shows one set of three signals at -141 ppm (Figure 26), whereas as one signal is found at -127 ppm (red circles). The latter corresponds to the fluorine close to the DMB group. Unfortunately, we were not able to grow X-ray suitable crystals of **13**. However, NMR, allows us to prove the unsymmetrical nature of macrocycles **13**.

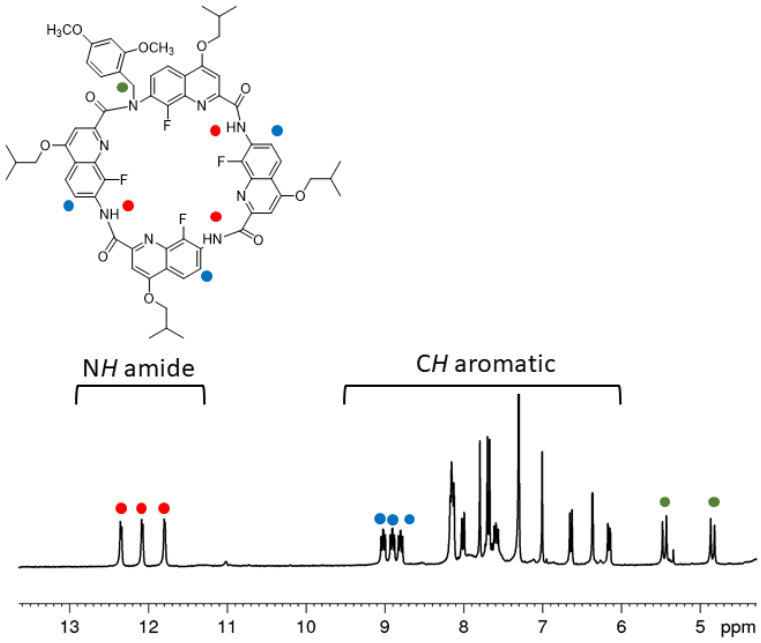

Figure 25. ^{1}H NMR spectrum (300 MHz) of the tetramer macrocycle **13** (0.8 mM) in $CDCl_3$ at 298K, NH- amide are marked with red circles, whereas isolated aromatic protons of Q^F are marked as blue circles. The diastereotopic methylene of the DMB group are marked with green circles.

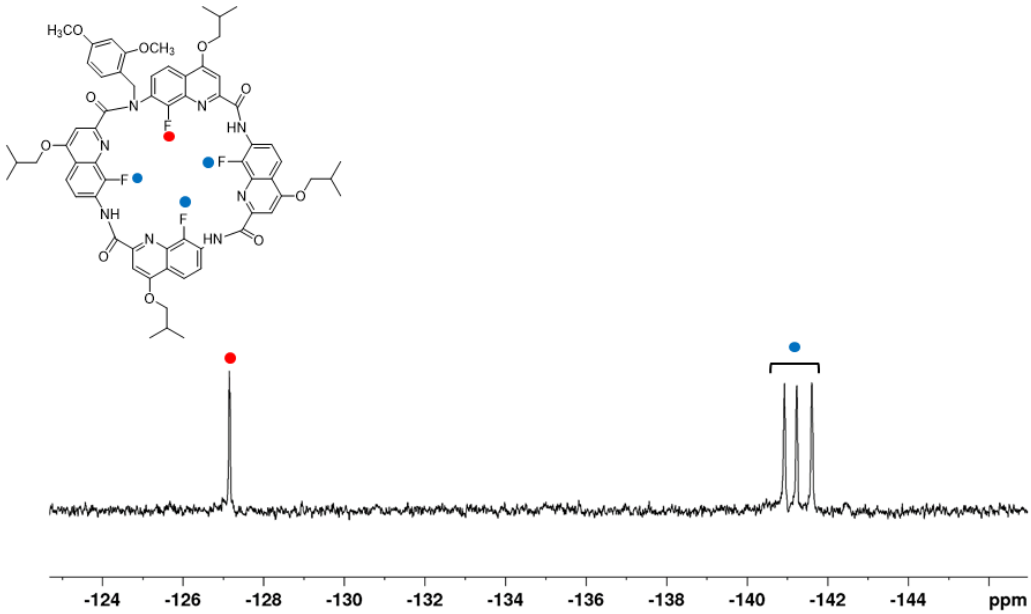

Figure 26. ^{19}F NMR spectrum (300 MHz) of the macrocycle **13** (0.8 mM) in $CDCl_3$ at 298 K, signals of fluorine in the macrocycles **13** were marked with two different color circles. Resonances of DMB protected Q^F is marked with red cycles, hydrogen bond donner Q^F is marked with blue cycles.

We also investigated the DMB deprotection reaction of **13** to afford the free DMB Q^F sequence macrocycles. With the product, we face the same solubility problem with the product **8** from macrocycle **7**. The poor solubility stopped the NMR study and crystallization of the final macrocycle **8**.

4.3 Hexamer

4.3.1 Synthesis of hexameric macrocycle

DMB functionalized hexamer macrocycle **18** was prepared using the same strategy as presented above (Scheme 4). Hexamer **15** was obtained from the coupling reaction between the acid chloride of dimer acid **14** and the tetramer amine **11** which after Boc deprotection and saponification of the ester yielded to the noncyclic hexamer **17**. The macrocyclization reaction was processed using the *in situ* activation of the acid in acid chloride using PPh_3 and trichloroacetonitrile to afford the DMB functionalized macrocycle **18**. The DMB groups were then cleaved using a TFA treatment to afford macrocycle **19**.

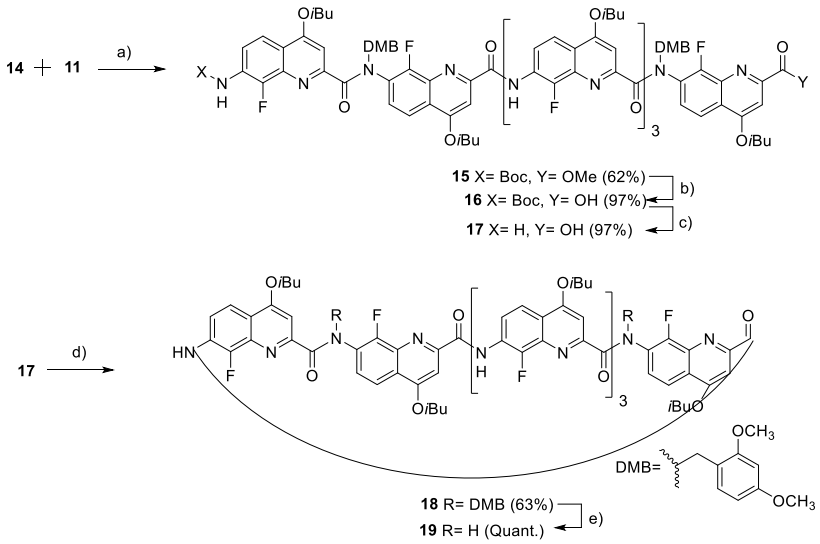

Scheme 4. Synthesis of Q^F hexamer macrocycle **19**: a) i)1-chloro-N,N,2-trimethyl-1-propenylamine, $CHCl_3$, room temperature, 3 h ; ii) DIEA, $CHCl_3$, room temperature, 12 h; b) LiOH, THF, H_2O, room temperature, 4 h; c) HCl 4N in dioxane, room temperature, 4 h; d) triphenylphosphine, trichloroacetonitrile, DIPEA, $CHCl_3$, room temperature, 48 h. e) trifluoroacetic acid, $CHCl_3$, 60°C, 2 h.

^{1}H NMR was used to check all the compounds. However, upon elongating the oligomers, the NMR revealed complex and broad spectra in chloroform at room temperature (Figure 27). This can come from several reasons: i) longer oligomers aggregate more easily, ii) to avoid steric hindrance, DMB groups generate zigzagged undefined conformation, instead of being well folded in helices.

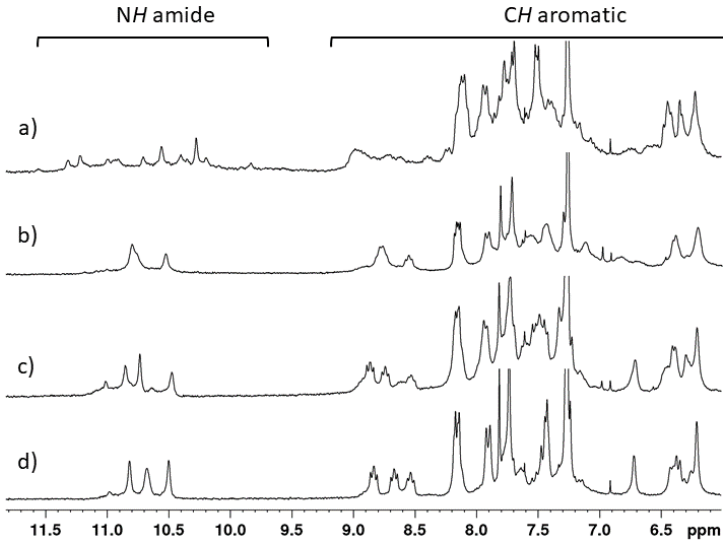

Figure 27. Part of ^{1}H NMR spectra (300 MHz) of: a) macrocycle **18,** b) hexamer amine acid **17**, c) hexamer acid **16**, d) oligomer **15.**

After silica gel chromatography, GPC was used to purify **18**. The main peak (red circle) was collected after 8 cycles (Figure 28). The cycling time for **18** is 25.63 mins, which is shorter than for tetramer macrocycle **7** (26.19 mins). The product was also checked by mass spectrometry, a mass $[M+H]^+$ = 1861.7244 which corresponds to macrocycle **18** (calcd for $[M+H]^+$:1861.7201) was found.

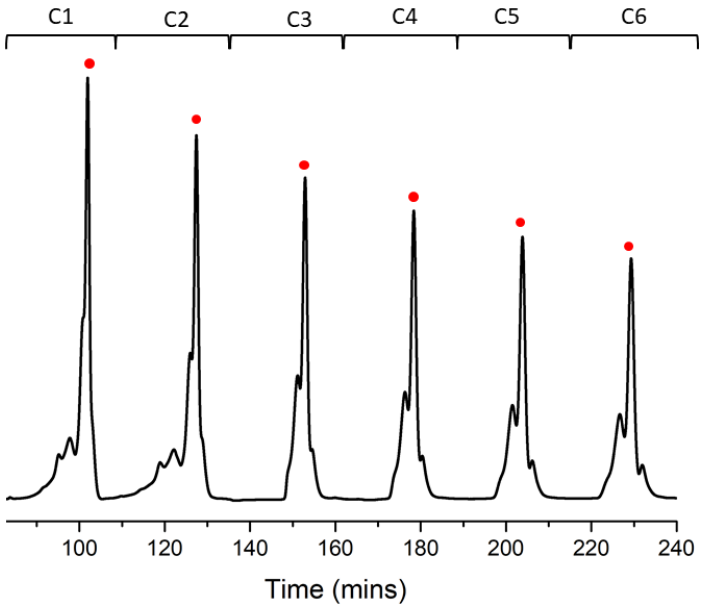

Figure 28. Chromatogram of recycling GPC of **18**. The peaks marked with red circle stand **18**.

4.3.2 Structure of macrocycles

Energy minimized models were built for hexamer **18** as presented in Figure 29. In the model, the two DMB groups (black, Figure 29) force the amide bond to adopt a *cis* configuration, meanwhile the other Q^F monomers can fold regularly as their hydrogen bonding patterns were preserved (blue, Figure 29). Overall $Q^F{}_6$ hexamer helix (i.e. without DMB) is long enough to span 1.5 turns with its ends groups completely diverging (Figure 29c). It was demonstrated that such oligomers can form double helices (Figure 29d). The introduction of DMB disfavored the self-assembly and simultaneously favored the position of the end amine and acid group close enough to achieve an intramolecular cyclization.

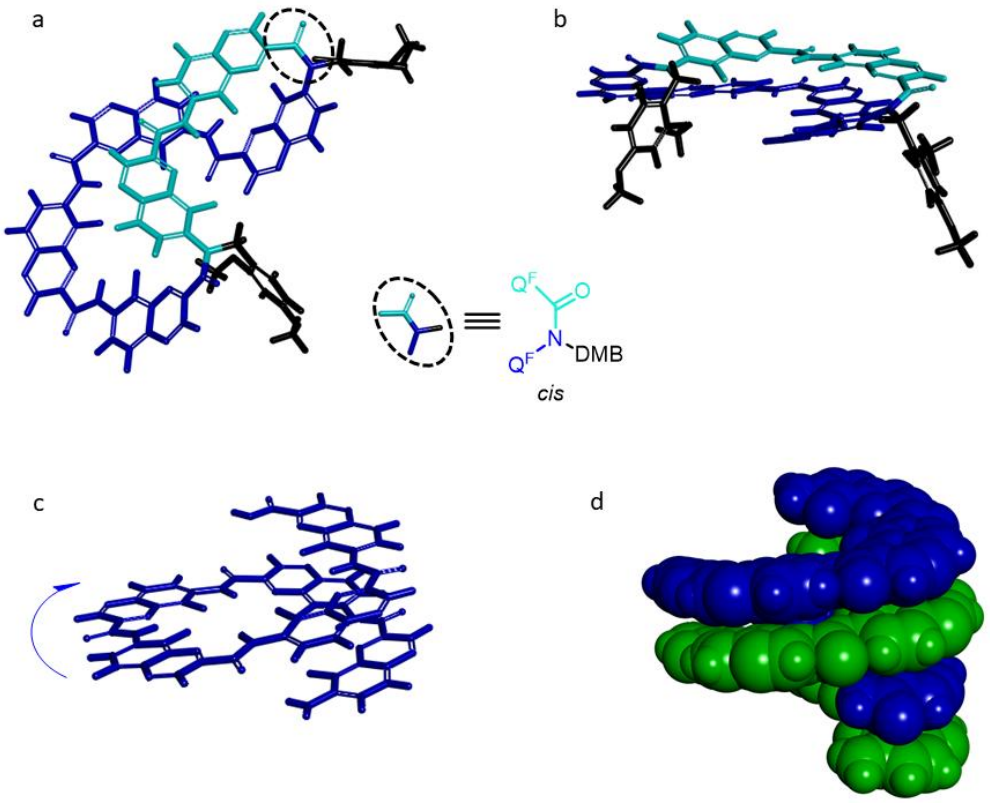

Figure 29. Energy minimized models of macrocycle **18**, a) Top view of **18**, two flipped Q^F units are marked in light blue, Q^F residues are marked as blue, DMB groups are marked as black and the *cis* amide groups are marked within the black dot cycle; b) Side view of the molecular models of macrocycle **18**; side view of Q^F_6 hexamer c) single helix and d) double helices. The models were produced with Maestro software package, using MMFFs force filed, chloroform as solvent and TNCG as minimization method.

During the preparation of macrocycle **18**, a serendipitous discovery was made. Interestingly, a side product with a mass of $[M+H]^+$ = 1785.6663 was found. This mass corresponds to the loss of a fluorine atom and an isobutyl group. Single crystals of the side product **18a** were obtained and the structure was resolved in the *P*-1 space group (Figure 30). The structure revealed that a *cis* amide bond between two adjacent Q^F monomers, that impose a favorable conformation for cyclisation (Figure 30d), associated with the loss of an isobutyl side chain, favored the substitution of the fluorine by the nucleophilic nitrogen of the neighbored quinolone. This cyclization led to the formation of a so called "azahelicene segment". The putative mechanism of the intermolecular cyclisation is described in Scheme 5.

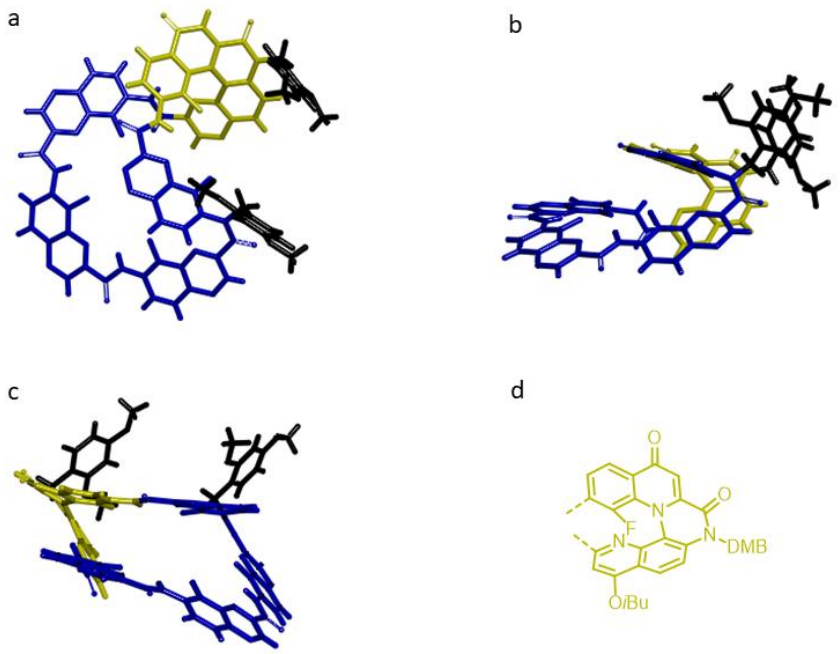

Figure 30. The X-ray structure of **18a**, a) Top view of the macrocycle **18a**, Q^F residues were marked as blue, DMB groups were marked as black and the cyclized group was marked as yellow. b) Side view of the macrocycle **18a**, c) Front view of the macrocycle **18a**, d) Chemical structure of the cyclized group. Side chains (O*i*Bu groups) and included solvent molecules have been removed for clarity.

The formation of the azahelicene proceeds in two steps, first is the cleavage of the isobutoxy side chain to obtain the quinolone (the mesomeric form is the phenol), then a cyclization reaction between the endocyclic amine of the quinolone that substitute the fluorine of the Q^F monomer and that afford a piperazine ring. The study of the azahelicene was not pushed further.

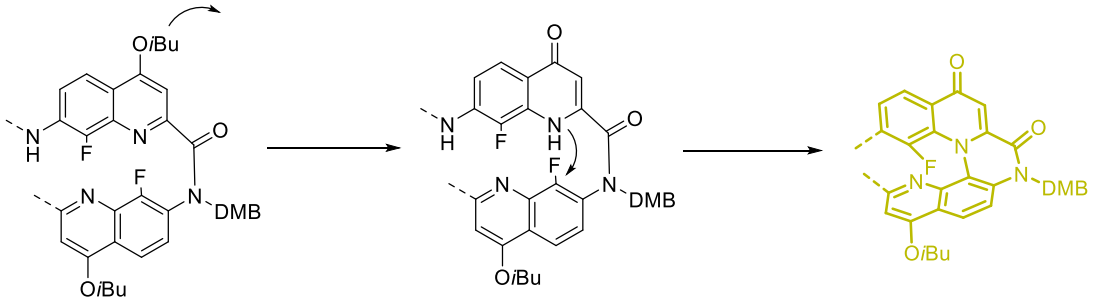

Scheme 5. Cyclization between Q^F units to form azahelicene**.**

Variable temperature NMR experiments were performed to study the dynamic behavior of the DMB free macrocycle **19** (Figure 31). In $C_2D_2Cl_4$, when the temperature was raised from

268 K to 353 K, we can only observe a single set of proton resonances and a single fluorine signal. Upon cooling, broadening of the signal was observed but the coalescence could not be reached. This result reflects the fact that the six Q^F monomers exchange is fast on the NMR time scale. It can be surmised, that upon cooling to lower temperature, the fast exchange would be limited, and we would observe a desymmetrization of the macrocycle and a different environment for each monomer.

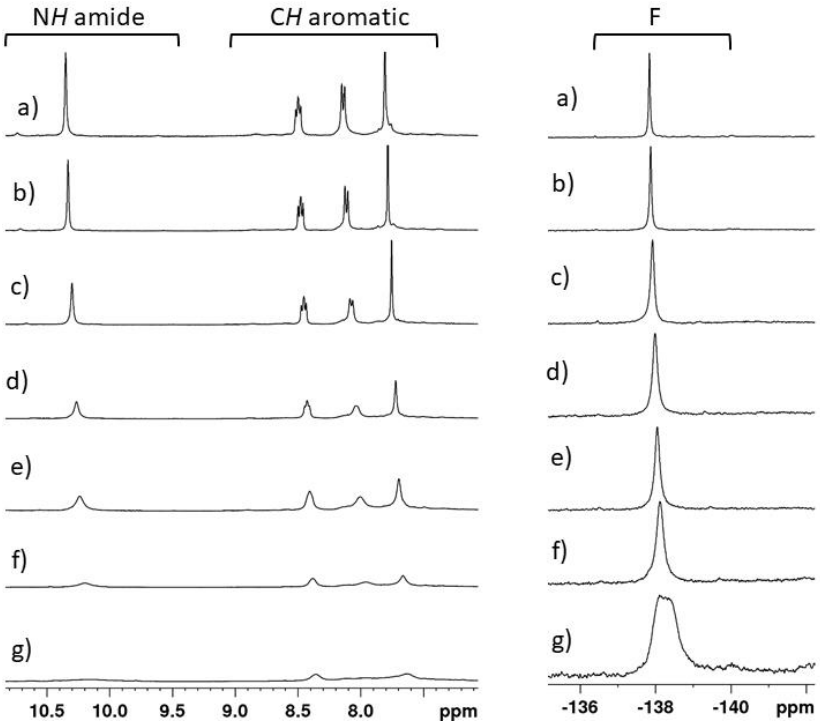

Figure 31. Part of ^{1}H and ^{19}F NMR spectra (400 MHz, $C_2D_2Cl_4$) for variable temperature hexamer **19**, a) 353 K, b) 338 K, c) 323 K, d) 308 K, e) 298 K, f) 283 K, g) 268 K.

Energy minimizations were carried out to decipher the structure of hexamer **19** as presented in Figure 32. The macrocycle shows a "saddle" shape conformation. Whereas macrocycle **8** possess a flat and rigid structure due to the curvature of Q^F which favor 4 units per turn. On the contrary six units cannot accommodate a cycle, as a result, the hexamer macrocycles may adopt a "saddle" shape.

Out of the six Q^F units, five Q^F units worked as a center of multiple hydrogen bond and backbone of macrocycles, only one was exception (marked as light blue in Figure 32a). In the dotted circle (Figure 32a), the amide group showed a *trans* configuration which is similar to the

other amide groups in the macrocycle, yet the amide is flipped with the carbonyl pointing towards the fluorine atom despite the electronic repulsion (H purple, F light blue and O blue). The multiple-center hydrogen bond is broken then the adjacent Q^F unit is flipped.

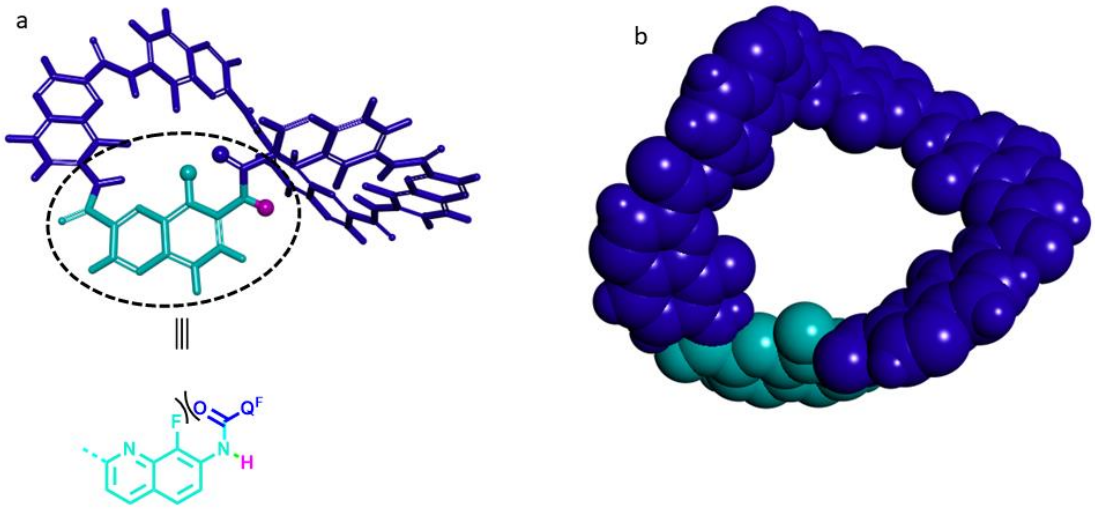

Figure 32. Energy minimized molecular model of macrocycle **19**: a) side view of **19**, Q^F residues involved in multiple H-bonds are marked in blue, Q^F without multiple H-bond is marked as light blue. The flipped *trans* amide group is shown in the dotted circle, F atom was marked as light blue ball, H atom was marked as purple ball and O atom was marked as blue ball; b) top view of **19** in CPK representation. The models were produced using Maestro software package, using MMFFs force field, chloroform as solvent and TNCG as minimization method. Side chains (O*i*Bu groups) have been removed for clarity.

4.4 Octamer

4.4.1 Synthesis

Macrocycle **25** was prepared according to the strategy shown in Scheme 6. Octamer **21** was obtained from the coupling reaction between tetramer DMB acid **20** and tetramer DMB amine **11**, and after the deprotection of Boc and saponification of the methyl ester, octamer **23** was obtained. A macrocyclization reaction was processed using *in situ* activation of the acid to giving the corresponding acid chloride with PPh_3 and trichloroacetonitrile to afford DMB functionalized macrocycles **24**. After the cleavage of the DMB group by TFA treatment, the macrocycle **25** was obtained.

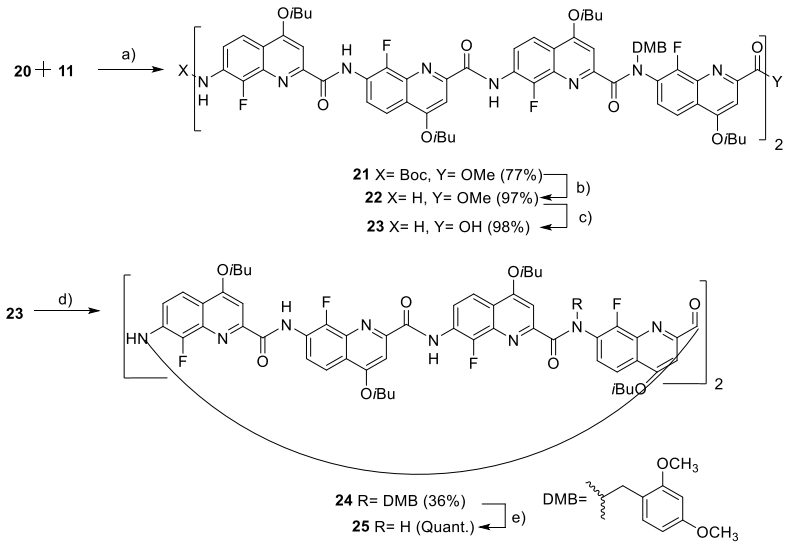

Scheme 6. Synthesis of Q^F octamer macrocycle **25**: a) i)1-chloro-N,N,2-trimethyl-1-propenylamine, $CHCl_3$, room temperature, 3 h ; ii) DIEA, $CHCl_3$, room temperature, 12 h; b) HCl 4N in dioxane, room temperature, 4 h; c) LiOH, THF, H_2O, room temperature, 4 h; d) triphenylphosphine, trichloroacetonitrile, DIPEA, $CHCl_3$, room temperature, 48 h; e) trifluoroacetic acid, $CHCl_3$, 60°C, 2 h.

^{1}H NMR was used to check all sequences. Upon elongating the oligomers, the ^{1}H NMR revealed broad spectra in chloroform at room temperature (Figure 33). This can come from several reasons: i) longer oligomers aggregate more easily despite DMB groups; ii) to avoid steric hindrance, DMB groups lead to zigzagged undefined conformation, instead of well folded helices. Fortunately, after the cleavage of DMB groups, free macrocycle **25** can be dissolved in chloroform at a maximum of 1 mM concentration thus it is possible for us to analyze its structure in solution.

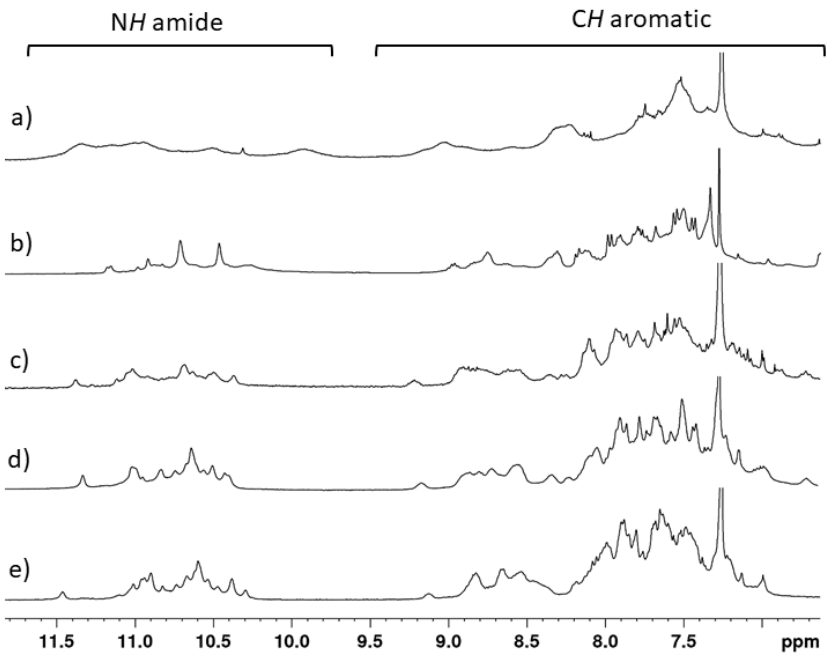

Figure 33. Part of ^{1}H NMR spectra (300 MHz, $CDCl_3$) of synthesis of octamer macrocycle **25**: a) **25**, b) DMB functionalized macrocycles **24**, c) octamer amine acid **23**, d) octamer amine **22**, e) octamer **21**.

GPC chromatogram is shown in Figure 34, and after four cycles, macrocycle **24** was collected as the major product. The residual time of **24** is 25.01 mins, which is shorter than macrocycle **18** (25.63 mins) indicated that **24** has a larger molecular weight than hexamer **18**.

Mass analysis was also performed with **24** and **25**, a mass with $[M+Na]^+$ = 2403.84 was found, which corresponds to the macrocycle **24** (calcd for $[M+Na]^+$:2403.89), the mass of **25** (calcd for $[3M+3H]^{3+}$: 2082.4450) was found with $[3M+3H]^{3+}$ = 2082.4993.

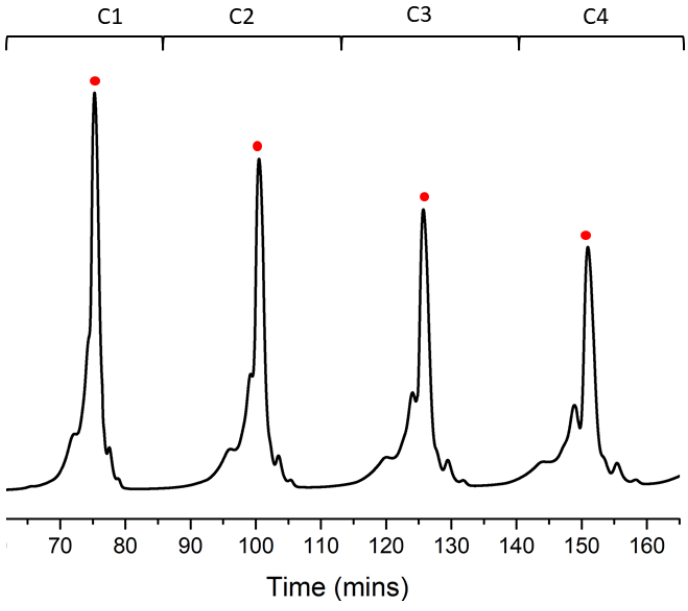

Figure 34. Chromatogram of recycling GPC of **24** purification. The peaks marked with red circle stand for the DMB functionalized macrocycle **24**.

4.4.2 Structure of the octamer macrocycle

Variable temperature NMR study was carried out with the DMB free macrocycle **25** in $C_2D_2Cl_4$. The temperature was raised from 278K to 353K. At 278K, a large number of amide signals can be obtained, many more than the eight that can be expected for a single stable conformation of the macrocycle. Many conformations are in slow exchange at the NMR time scale. At 353K we are close to the coalescence temperature and all the signal almost disappeared, this means that the conformations are exchanging faster.

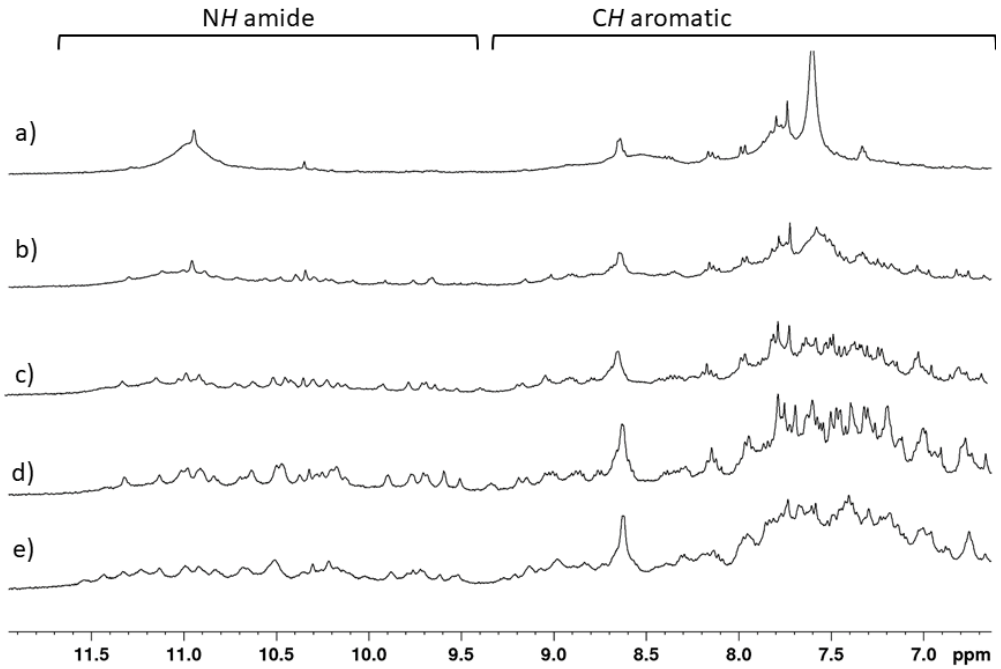

Figure 35. Part of ^{1}H NMR spectra (400 MHz, $C_2D_2Cl_4$) for octamer macrocycle **25** at variable temperature, a) 353 K, b) 333 K, c) 313 K, d) 298 K, e) 278 K.

The length of Q^F_8 octamer helix is enough to allow a two turn fold as shown previously,[37] so it is reasonable to expect that octamer macrocycle **25** will try to adopt a close conformation. Inspired by the literature,[38] we made some hypothesis about the conformation of **25** that are

37 Gan, Q.; Wang, X.; Kauffmann, B.; Rosu, F.; Ferrand, Y.; Huc, I. *Nat. Nanotechnol.* **2017**, *12*, 447-452.
38 Soya, T.; Kim, W.; Kim, D.; Osuka, A. *Chem.—Eur. J.* **2015**, *21*, 8341-8346; Stępień, M.; Sprutta, N.; Latos-Grażyński, L. *Angew. Chem., Int. Ed.* **2011**, *50*, 4288-4340.

represented in figure 36. We surmised that as the oligomer cannot adopt a helical conformation it can take a figure of eight shape (or lemniscate). It exists different handedness combinations between two cycles for such type of folds. There are three possibilities: (P, P) or (M,M) and (P, M).

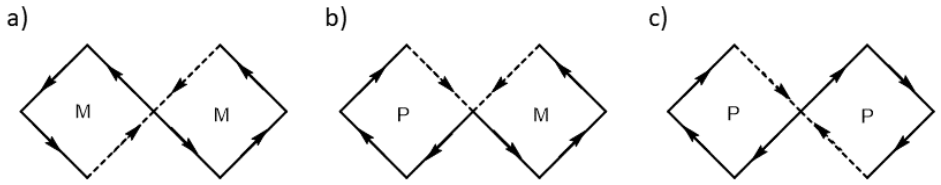

Figure 36. Schematic representations of theoretical macrocycles **25** folding. Straight line represent a Q^F unit, the solid line is in the front and dot line is in the back. Arrows represent handedness P or M. Two ends of cycles connected with each other and stayed in the same layer.

Further characterizations of octamer macrocycle **25** were performed by X-ray crystallography. The X-ray single crystals were grown by slow diffusion of methanol into a chlorobenzene solution and the structure was resolved in the $P2_1/c$ space group. As presented in Figure 37a, **25** has a "figure of 8" shape. The two rings of **25** have the same helicity either *P* or *M*, so we named the conformation as (P,P)-**25** or (M,M)-**25**. Only one enantiomer is shown in Figure 37.

The helical cycles despite having the same handedness display an opposite polarity N→C or C→N, this can also be observed on the position of the F atoms (Figure 37, blue and light blue). Interestingly, observation of the crystal packing revealed a dimer of macrocycles with similar handedness, either all P or all M. This dimer shows a triangular shape. The dimer [(P,P)-**25**]$_2$ that is shown in Figure 37 that the 8 shape macrocycle are arranged in an anti-parallel manner (head-to-tail). The three angles of the triangle were measured to be 69.6°, 54.7° and 55.7°. The dimerisation of Q^F oligomer is a property that is reminiscent of Q^F_8 octamer helix (i.e. non-macrocyclic) and that can form single and double helix. [39]

39 Gan, Q.; Bao, C.; Kauffmann, B.; Grélard, A.; Xiang, J.; Liu, S.; Huc, I.; Jiang, H. *Angew. Chem. Int. Ed.* **2008**, *47*, 1715-1718.

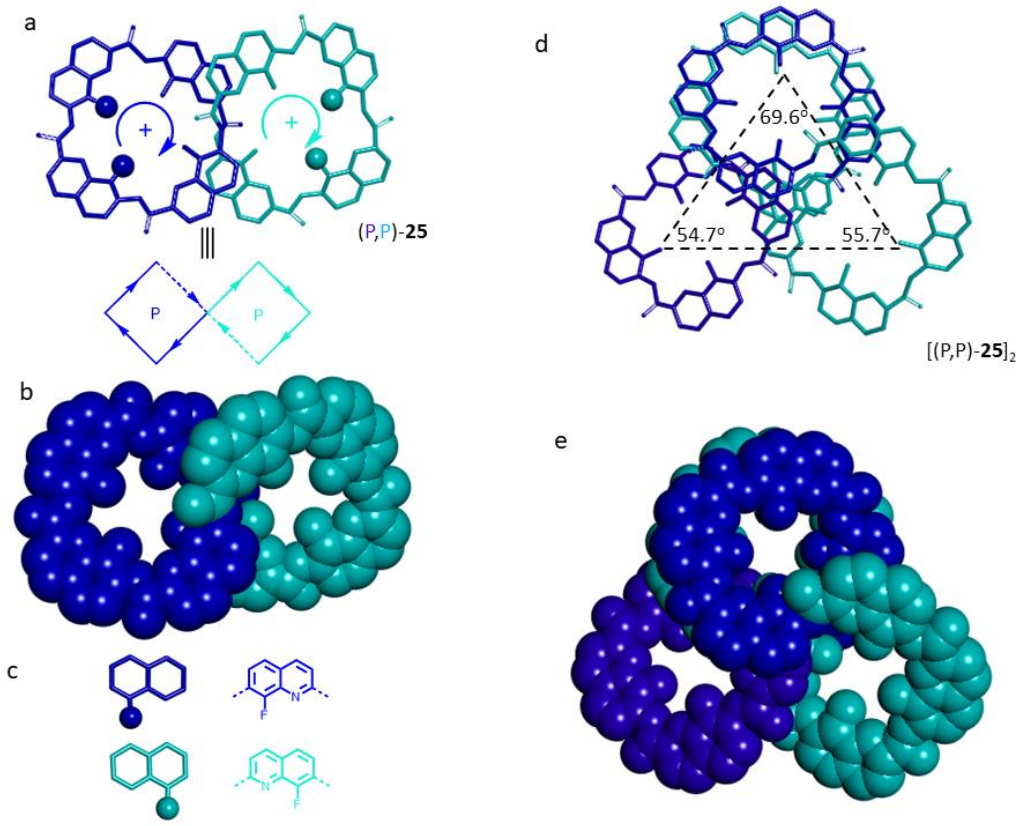

Figure 37. X-ray structure of octamer macrocycle **25**, a, b) Top view of (P, P)-**25**, both cycles have P helicity; c) Q^F monomers in (P, P)-**25**, the orientation of Q^F units are opposite (blue balls and light blue ball). d, e) top view of crystal packing showing a dimeric architecture [(P, P)-**25**]$_2$. Side chains (O*i*Bu groups) and included solvent molecules have been removed for clarity.

The position of F atoms in Q^F units could be used to assess the orientation of the macrocycles and to indicate the symmetry. The macrocycle (P,P)-**25** as an overall C_2 symmetry as for example two F atoms in each cycle marked as green and red balls are equivalent after a 180° rotation of (P,P)-**25** around a horizontal axis (Figure 38 a, b). The overall position of F atoms in macrocycle did not change and the handedness of two cycles is kept similar as (P, P). In the dimer [(P, P)-**25**]$_2$, one can also observe a symmetry (Figure 38 c) through a 180° horizontal rotation (Figure 38d).

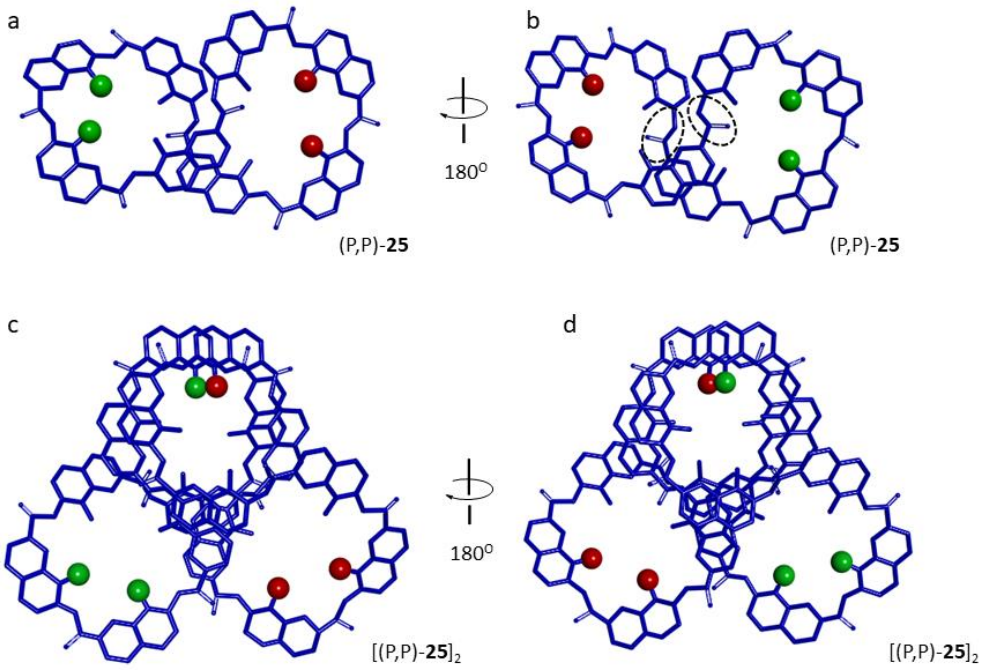

Figure 38. X-ray structure of **25**, a) top view of (P, P)-**25**, two side F atoms were marked as green and red balls; b) (P, P)-**25**, rotated 180° horizontal from a); c) top view of [(P, P)-**25**]$_2$, picked F atoms were marked as green and red; d) [(P, P)-**25**]$_2$, rotated 180° horizontal from c). Side chains (O*i*Bu groups) and included solvent molecules have been removed for clarity.

As for **25**, all eight amide groups revealed a *trans* configuration, while two of them are not involved in a classical hydrogen bond pattern (dotted circle, Figure 38b). In these two amides, the carbonyl group of the amide is flipped towards the F atom of the adjacent Q^F unit whereas the NH is oriented opposite of the F atom, which broke the hydrogen bond pattern. The adjacent Q^F unit was free to flip to the side without changing the handedness of the helix. As a result, cyclic octamer **25** adopted a figure of eight shape.

4.5 Dodecamer

4.5.1 Synthesis

Dodecameric macrocycle **30** was prepared with the same strategy as for the shorter macrocycles (Scheme 7). The triple DMB protected dodecamer **26** was obtained from the

coupling reaction between tetramer acid **20** and octamer amine **22**, which after Boc deprotection and methyl ester saponification, yield the hexamer **28**. The macrocyclization reaction was performed using the *in situ* activation of the acid in acid chloride using PPh_3 and trichloroacetonitrile to afford DMB functionalized macrocycle **29**. The DMB groups were then cleaved using a TFA treatment to afford macrocycle **30**.

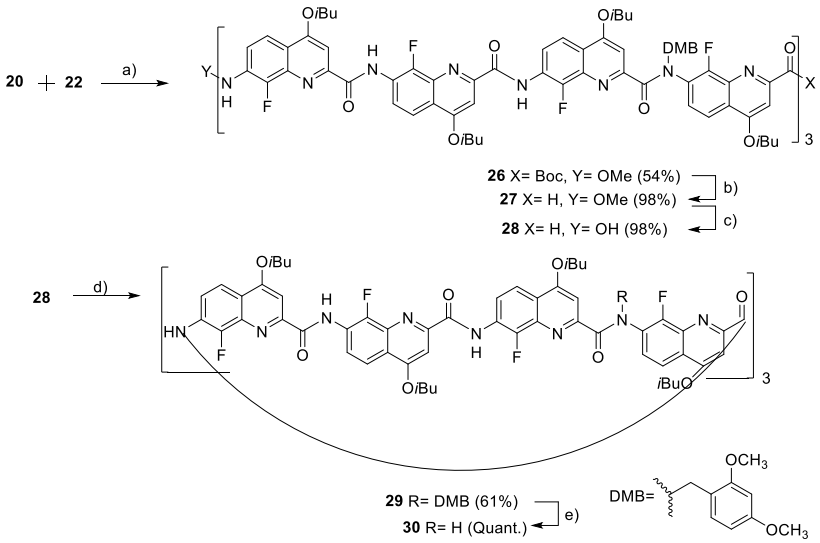

Scheme 7. Synthesis of Q^F dodecamer macrocycle **30**: a) i)1-chloro-N,N,2-trimethyl-1-propenylamine, $CHCl_3$, room temperature, 3 h ; ii) DIEA, $CHCl_3$, room temperature, 12 h; b) HCl 4N in dioxane, room temperature, 4 h; c) sodium hydroxide, THF, H_2O, room temperature, 4 h; d) triphenylphosphine, trichloroacetonitrile, DIPEA, $CHCl_3$, room temperature, 48 h; e) trifluoroacetic acid, $CHCl_3$, 60°C, 2 h.

^1H NMR was used to check all the compounds. However, upon elongating the oligomers the NMR revealed complex and broad spectra in chloroform at room temperature (Figure 39). This can come from several reasons: i) longer oligomers aggregate more easily, ii) to avoid steric hindrance, DMB groups lead to zigzagged undefined conformation, instead of being well folded in helices.

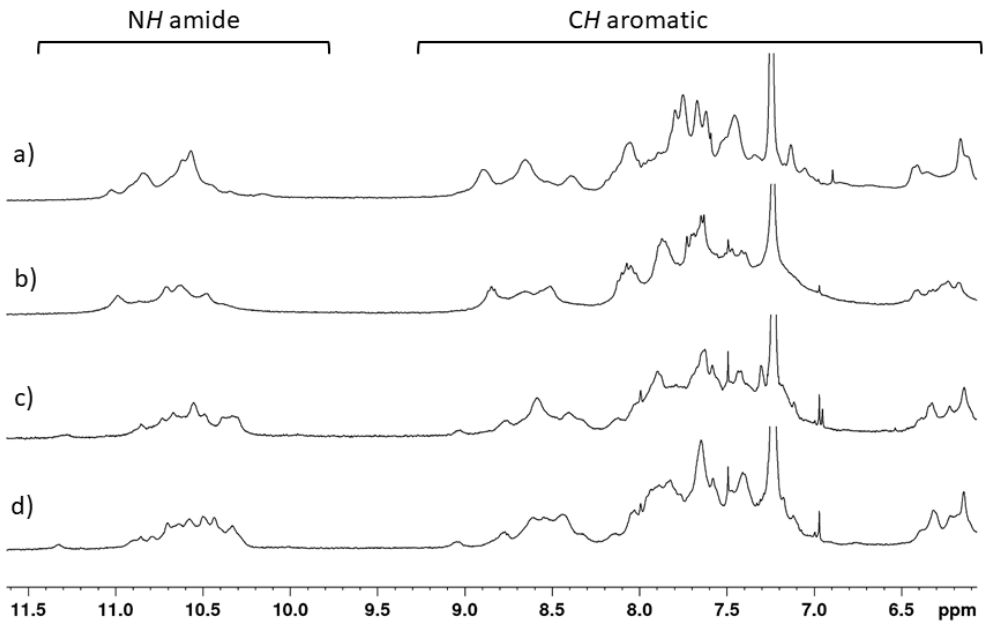

Figure 39. Part of ^{1}H NMR spectra (300 MHz, $CDCl_3$) of: a) macrocycle **29**, b) dodecamer amine acid, **28**, c) dodecamer amine, **27**, d) dodecamer **26**.

Surprisingly, only a single peak was observed during the macrocycle **29** purification using recycling GPC. After three cycles, macrocycle **29** was collected (Figure 40). The residual time of **29** is 24.58 mins, which is shorter than ocatmeric macrocycle **24** (25.01 mins) indicating that **29** has a higher MW than **24**. Mass analysis was also performed with **29** and **30**, a mass with $[M+2H]^{2+}$ = 1787.7156 was found, which corresponds to the macrocycle **29** (calcd for $[M+2H]^{2+}$: 1787.6894), the mass of **30** (calcd for $[M+2H]^{2+}$: 1562.0856) was found with $[M+2H]^{2+}$ = 1562.0332. While, the mass of $[2M+3H]^{3+}$ = 2082.7056 was also found corresponding to dimeric macrocycle **30** (calcd for $[2M+3H]^{3+}$: 2082.7795).

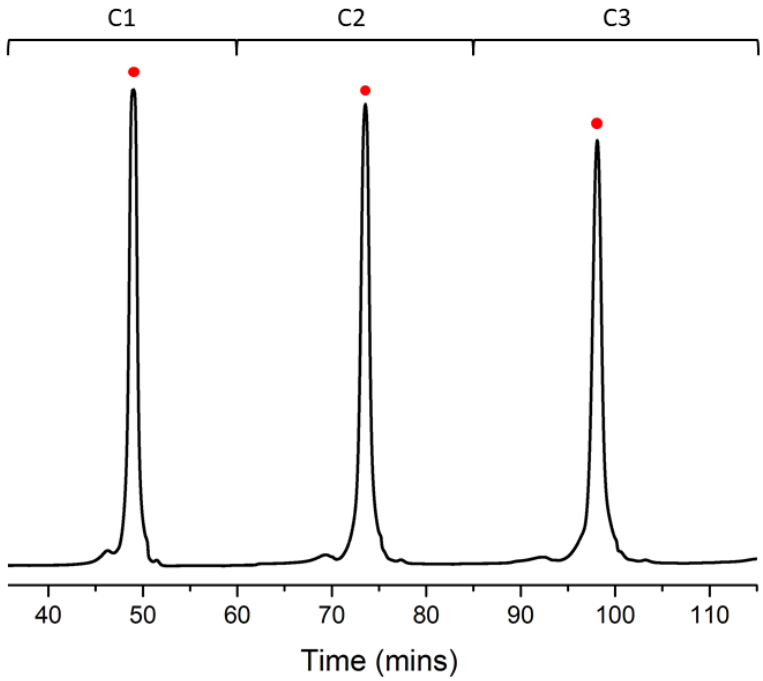

Figure 40. GPC Chromatogram of **29** purification. The peaks marked with red circle stand for **29**. The residual time can be calculated be the time between two cycles of same peaks.

NMR analysis was carried out on macrocycle **30** more easily as it has a much better solubility in chloroform than macrocycle **25**. On the contrary to tetramer macrocycle **19** or octamer macrocycle **25**, dodecamer **30** displayed well resolved resonances at room temperature for ^{1}H and ^{19}F NMR (Figures 41 and 42). In ^{1}H NMR, twelve signals were found which correspond to the theoretical number for a macrocyclic 12mer oligoamide as **30**. As for ^{19}F NMR, twelve resonances could also be found, on for each of the twelve Q^F building blocks. Interestingly, both in the ^{1}H and ^{19}F NMR one can observe 2 resonances that are distinct from the rest of the signals (10.4 and -118 ppm, respectively).

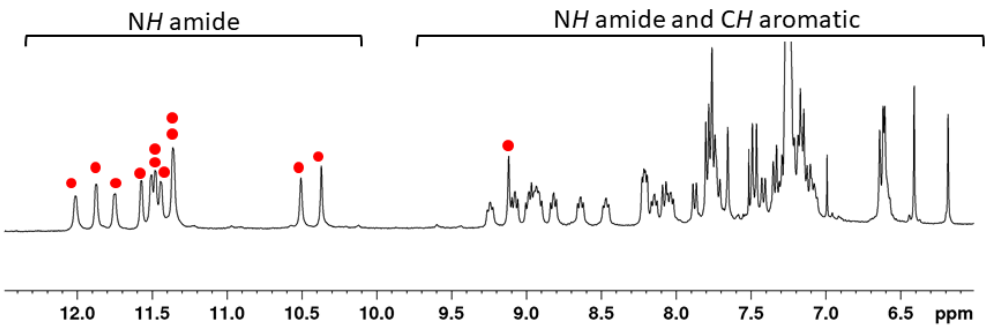

Figure 41. Part of ^{1}H NMR spectrum (400 MHz, 0.7mM, $CDCl_3$) of dodecamer macrocycle **30**.

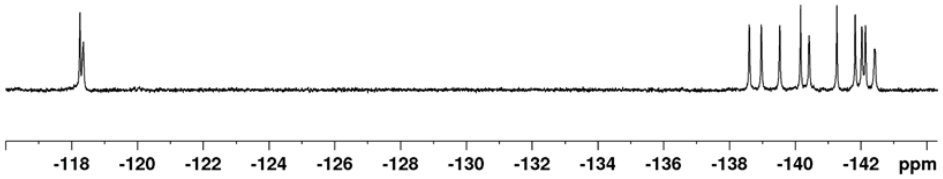

Figure 42. ^{19}F NMR spectrum (400 MHz, 0.7mM, $CDCl_3$) of dodecamer macrocycle **30**.

Some presumptions about the conformation of **30** were represented in Figure 43. We devised that as for **25**, dodecamer **30** could satisfy its propensity to fold as a helix by adopting "plectonemes" with three distinct cycles.[40] Three handedness arrangements of the helices exists and are: (P, P), (P, M) and (M, M). The middle units linking the two rings at each extremity of the structure describe a cycle from top view, yet they are not covalently bonded and will not be considered as a proper ring. In (P, P) and (M, M), all cycles have the same handedness and the band of compound twisted twice to form the "plectonemes" conformations. While in (P, M), consecutive crossings alternate their handedness without twist of compound, it has similar-looking figure that can be called "pseudoplectoneme".

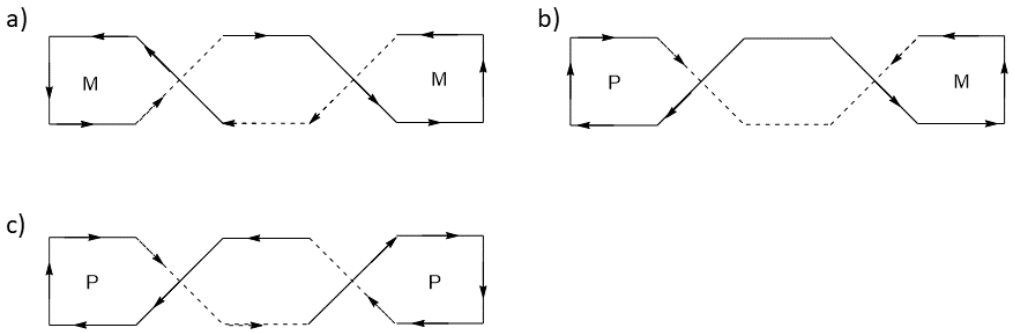

Figure 43. Schematic representation of theoretical macrocycles **30** folding. Straight line represent a Q^F unit, the solid line is in the front layer and dot line is in the back. Arrows represent handedness P or M.

4.5.2 Structure of macrocycles

Variable concentration and temperature experiments were used to assess the structure and dynamic behavior of the dodecamer macrocycle **30**. A variable concentration experiment were performed from 0.1 mM to 3.2 mM without any noticeable change of the ^1H NMR spectra.

40 Stępień, M.; Sprutta, N.; Latos-Grażyński, L. *Angew. Chem., Int. Ed.* **2011**, *50*, 4288-4340; Soya, T.; Kim, W.; Kim, D.; Osuka, A. *Chem.—Eur. J.* **2015**, *21*, 8341-8346.

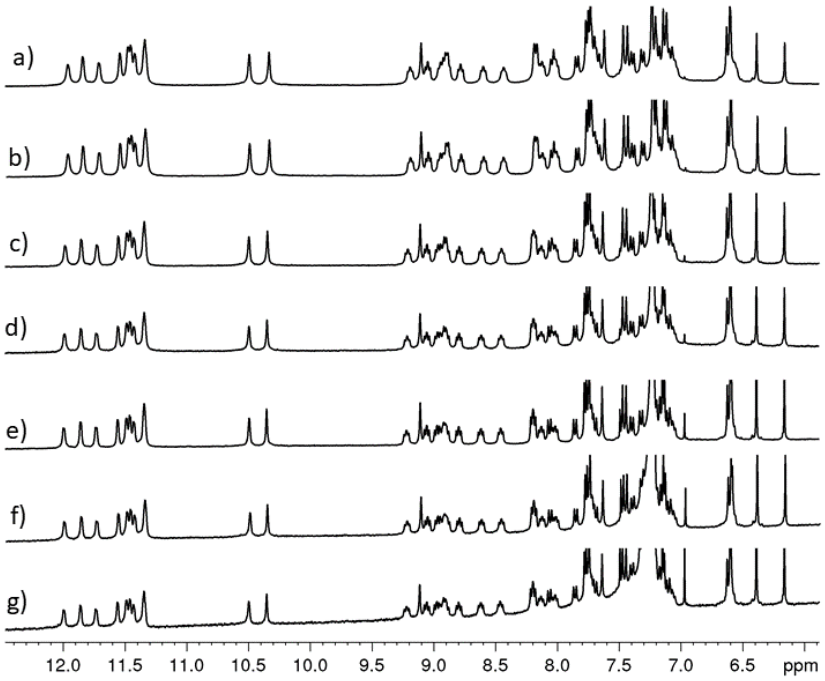

Figure 44. Part of ^{1}H NMR spectra (400 MHz, $CDCl_3$, 298 K) of dodecamer **30** at different concentrations, a) 3.20 mM, b) 2.37 mM, c) 1.57 mM, d) 0.98 mM, e) 0.49 mM, f) 0.24 mM, g) 0.1 mM.

Additionally variable temperature studies were carried out. Increasing the temperature from 273K to 353K in $C_2D_2Cl_4$ (Figure 45), did not reveal any change of the chemical shifts of the amide or aromatic resonances. No additional set of signal could be observed.

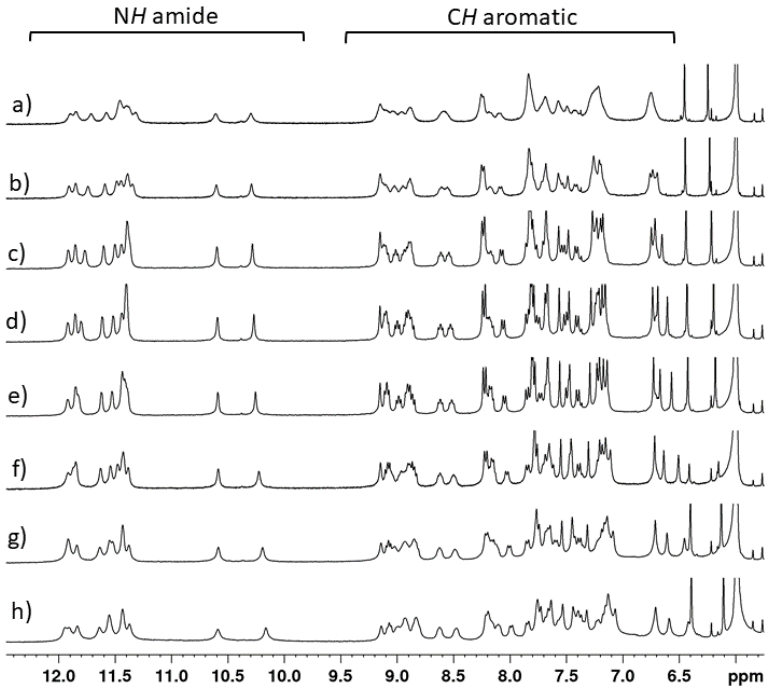

Figure 45. Part of ^{1}H NMR spectra (400 MHz, $C_2D_2Cl_4$) of dodecamer **30** in variable temperature, a) 353 K, b) 343 K, c) 333 K, d) 323 K, e) 313 K, f) 298 K, g) 283 K, h) 273 K.

Lowering the temperature from 298K from 258K in $CDCl_3$ did not reveal any change of ^1H NMR spectra (Figure 46), The variable temperatures experiments seemd to indicate that macrocycle **30** had a stable conformation yet it is difficult to assess whether it exists under a monomeric of dimeric form.

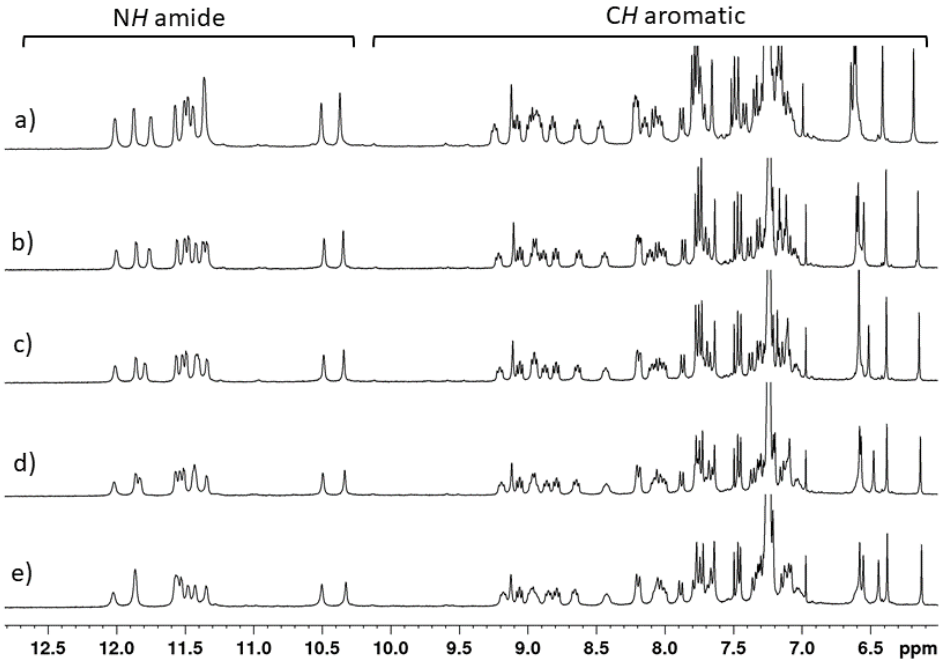

Figure 46. Part of ^1H NMR spectra (400 MHz, $CDCl_3$) of dodecamer **30** in variable temperature, a) 298 K, b) 288 K, c) 278 K, d) 268 K, e) 258 K.

To understand the structure of dodecamer **30**, X-ray crystallography was used. X-ray quality single crystals were grown by slow diffusion of *n*-hexane into a chloroform solution of **30** and the structure was resolved in the *P*-1 space group. As shown in Figure 47a, quite surprisingly macrocycle **30** exists as a dimer: two dodecamer macrocycles **30** dimerizes to form macrocycle dimer $(\mathbf{30})_2$. In the dotted cycle of Figure 47b, two Q^F unites had opposite orientation which could be confirmed by the position of their own F atoms (grey ball). As a result, dimerization of monomer **30** formed anti-parallel (head-to-tail) macrocycle dimer $(\mathbf{30})_2$. If we analyze the folding of a monomeric unit one can observe that independent rings with opposite chirality are linked by two curved segments constituted by two Q^F monomers and that resemble to slightly curve aromatic sheets (taupe color in Figure 47). The two segments are positioned on two different horizontal layers and the distance was measured as 6.5 Å. The two blue and red ring (P and M, respectively, Figure 47) are constituted by four well-folded Q^F

monomers. The size of blue and red cycles were determined to be ~ 6.6 Å. Diameter of the middle grey section was measure as 8.1 Å, due to the space distance between two divided parts. The distance between the aromatic units of the two independent macrocycles **30** was measured to be 3.3 Å a value that correspond to aromatic stacking (Figure 47b). This conformation of (**30**)$_2$ is consistent with the hypothesis formulated (P, M) (in Figure 43b, pseudoplectoneme), pseudoplectoneme is an untwisted conformation, the two middle grey segments are anti-parallel and arranged as "stair" shape (in Figure 47f), which provide the space and possibility for dimerization. While in plectonemes conformations (in Figure 43, (P, P) and (M, M)), the central cavity is closed by the cross of the middle segments.

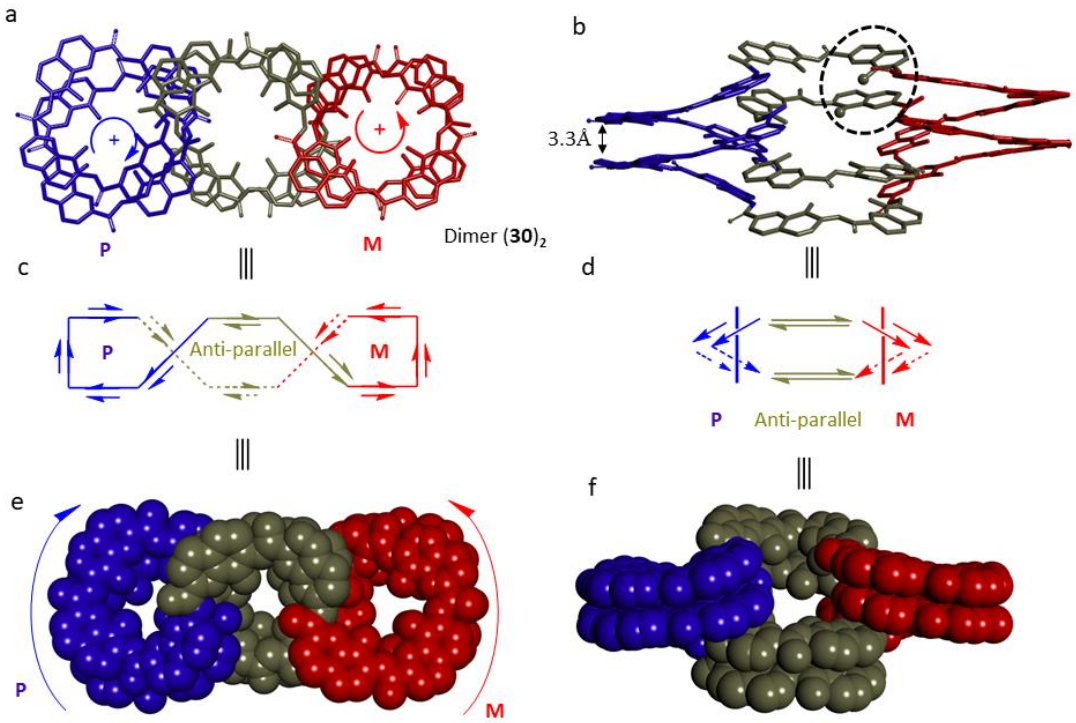

Figure 47. X-ray structure of dodecamer macrocycles dimeric (**30**)$_2$, a) Top view of (**30**)$_2$, opposite handedness cycles were marked as blue (P) and red (M), middle cycle was marked as grey, b) side view of (**30**)$_2$, the antiparallel Q^F units are highlighted in the dotted cycle and their F atoms were marked as ball style; c) top view of the schematic representation of (**30**)$_2$, straight line represent a Q^F unit, the solid line is in the front layer and dot line is in the back. Arrows denote the P or M handedness; d) side view of the schematic representation; e) top view and f) side view of dimeric (**30**)$_2$ in CPK style. Side chains (O*i*Bu groups) and included solvent molecules have been removed for clarity.

The symmetry of the dimeric architecture was also investigated. Fluorine atoms in Q^F units can be used to assign the orientation of macrocycles and to assess the symmetry. Monomeric macrocycle **30** contained two rings with opposite handedness, this conformation is noted (P, M)-**30** (Figure 48a). (P, M)-**30** possesses a center of symmetry which is marked as black dot (Figure 48 a, c), for any atom in the (P, M)-**30**, an identical atom exists diametrically opposite relative to the center and at distance from itself. Some F atoms in the rings are picked and shown with different colors (green and red) and can be used as examples. The distance between F atoms and inversion center was presented as arrows, all F atoms could find a corresponding atom in opposite position at equal distance from center. (P, M)-**30** is *Ci* symmetry.

Mirroring (P, M)-**30** through a plane allows to obtain **30**(mirror) (Figure 48, a → b), the overall helicity of **30** did not changed. While the orientation of all Q^F units is opposite from (P, M)-**30**, a 180° vertical rotation (Figure 48, b to d), allows to obtain the conformation (P, M)-**30** back. This confirms that monomeric macrocycle **30** has effectively an achiral centrosymmetrical conformation.

The symmetry of dimeric [(P, M)-**30**]$_2$ is clearly different and is showed in Figure 48. Unlike, the monomeric macrocycle (P, M)-**30**, [(P, M)-**30**]$_2$ does not present a centrosymmetry. Interestingly, as show in Figure 48e-f, one can observe that the dimeric macrocycle presents a C_2 axis that cross the structure through the two cycles and is perpendicular to both helical axis. A point that is worth noting is that if the self-assembly (i.e. dimerization) of two achiral centrosymmetrical macrocycles **30** leads to the formation of a C_2 symmetrical chiral entity that is [(P, M)-**30**]$_2$. Such an emergence of chirality is, to the best of our knowledge, not very common.

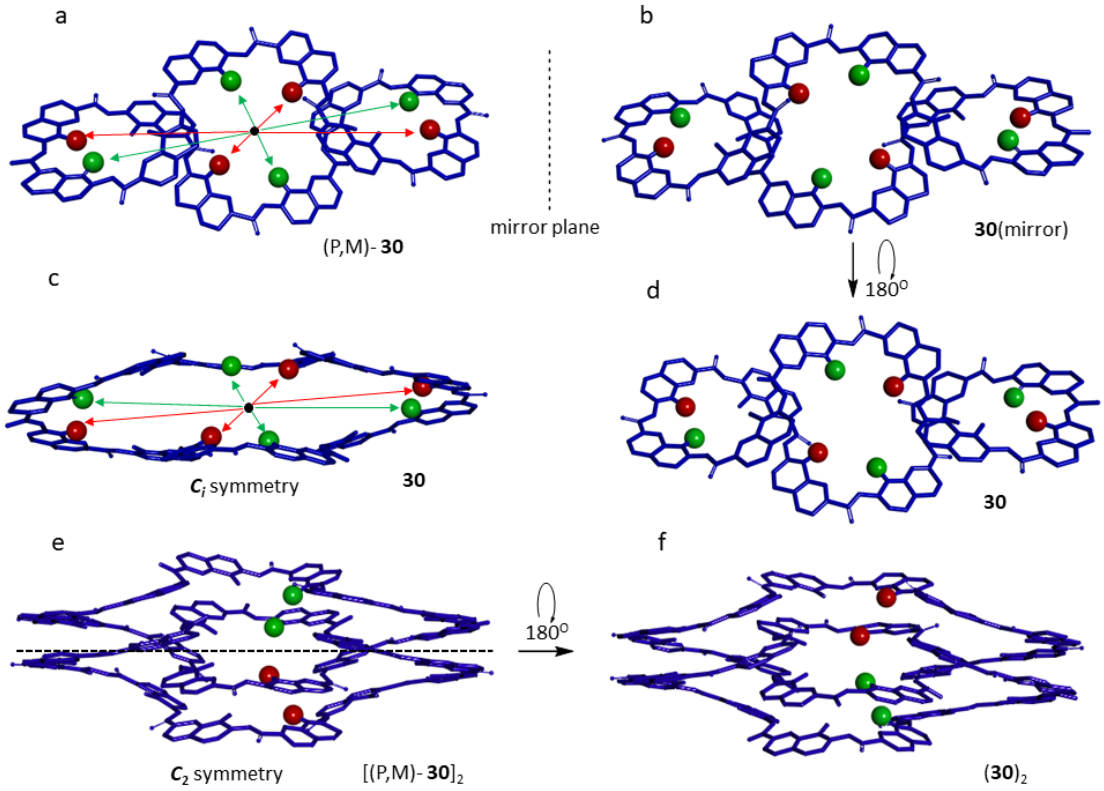

Figure 48. X-ray structure of macrocycle monomer and dimer, a)top view of macrocycle monomeric (P, M)-**30**, picked F atoms were marked as green and red balls, inversion center was marked as black cycle, equal distance between a pair of antipodal F atoms and inversion center were marked as different color arrow (green and red); b) top view of mirror structure of (P, M)-**30**; c) front view of **30**; d) top view of **30**, rotated 180° horizontal from b); e) side view of macrocycle dimeric [(P, M)-**30**]$_2$; f) side view of (**30**)$_2$, rotated 180° vertical from e). Side chains (O*i*Bu groups) and included solvent molecules have been removed for clarity.

In monomeric macrocycle (P, M)-**30**, the twelve amide groups showed a *trans* configuration, while four of them did not display a classical hydrogen bonding pattern with the NH of the amide group pointing towards the exterior of the ring (green, Figure 49). In these amide groups, the carbonyl group is flipped towards the F atom of the adjacent Q^F allowing the adjacent Q^F unit to flip to other side acting as handedness inversion center. The four amide highlighted in green in Figure 49 are located between the central cycle (taupe) and the external cycles (blue and red). As a result, the dodecamer macrocycle adopts a "pseudoplectoneme" shape.

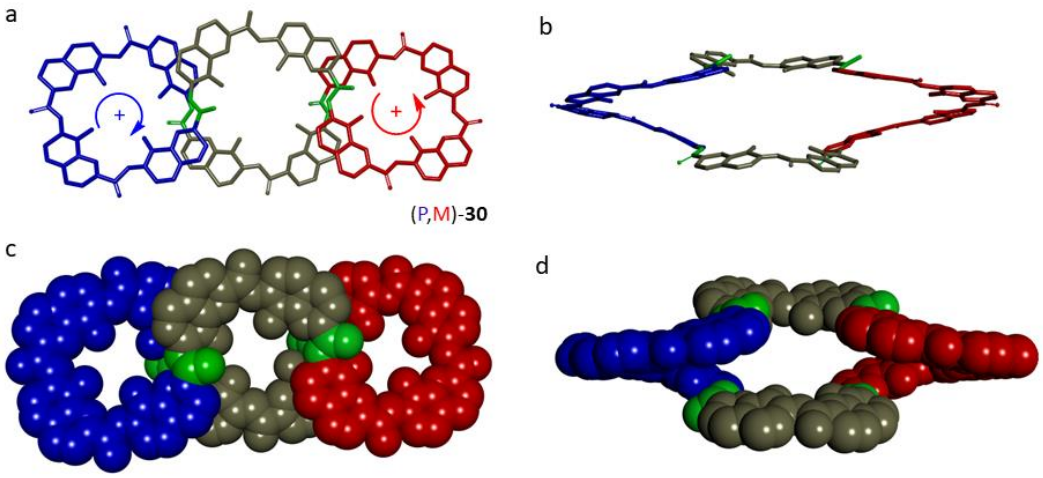

Figure 49. The X-ray structure of dodecamer monomeric macrocycle (P, M)-**30**, a) Top view of (P, M)-**30**, P helicity was marked as blue and M helicity was marked as red, divided cycle was marked as grey, flipped amide groups were marked as green, b) side view of (P, M)-**30**; CPK style for c) top view of (P, M)-**30**, d) side view of (P, M)-**30**. Side chains (O*i*Bu groups) and included solvent molecules have been removed for clarity.

4.6 Size of macrocycles

Macrocycle's size can be assessed by the number of consecutive atoms in the cyclic framework.[41] Consideration of the cyclic structure included saturated, unsaturated, and aromatic system, which are monocyclic, some of which have small rings fused or contain bridges that connect rings. The atoms number is counted according to the smallest internal macrocycle, as shown in figure 50, the atoms and bonds colored in red are used to determine the size of the macrocycle. The varying size of Q^F macrocycles that have been produced during this study is listed in the table 1.

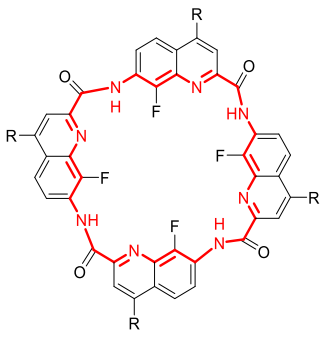

Figure 50. The smallest ring in the macrocycle for the atom number counting (red).

41 Frank, A. T.; Farina, N. S.; Sawwan, N.; Wauchope, O. R.; Qi, M.; Brzostowska, E. M.; Chan, W.; Grasso, F. W.; Haberfield, P.; Greer, A. *Mol. Divers.* **2007**, *11*, 115-118.

Compound	**7**	**13**	**19**	**25**	**30**
Number of Q^F units	4	4	6	8	12
Ring size	28	28	42	56	84

Table 1. Ring size of macrocycles

5. Conclusions and perspectives

Shaped-persistent planar structures can be prepared using the protection of the removable DMB groups, which worked as amide conformational disruptors to ensure the precursors can be cyclized. Using this strategy, we prepared Q^F containing macrocycles with varying sizes ranging from tetramer to dodecamer. Their structural conformations were confirmed by X-ray crystallography, mass spectrometry and NMR. Contrary to analogous helices, those macrocycles showed restricted backbones. This strategy can be extended to longer sequence giving rise to larger macrocycles using double segment strategy (8mer → 16mer → 32mer).

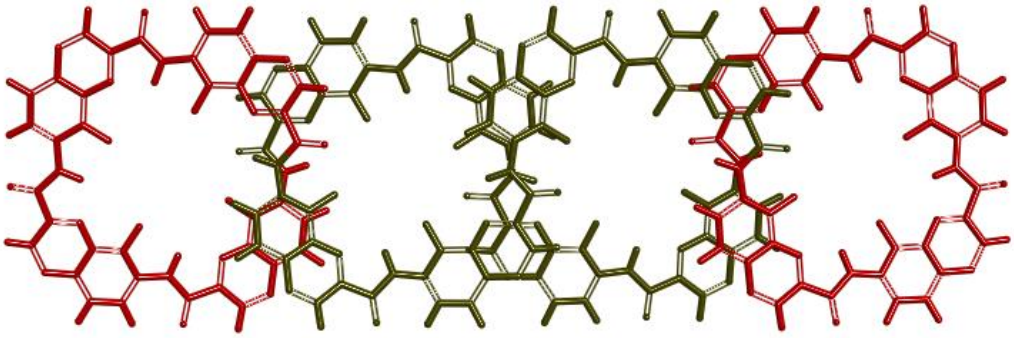

Figure 51. Energy minimized molecular models of the macrocycle 16-mer.

6. Experiments

6.1 Methods for NMR

NMR spectra were recorded on 3 different NMR spectrometers: (1) an Avance II NMR spectrometer (Bruker Biospin) with a vertical 7,05T narrow-bore/ultrashield magnet operating

at 300 MHz for ^{1}H observation and 75 MHz for ^{13}C observation by means of a 5-mm direct BBO H/X probe with Z gradient capabilities; (2) an Avance 400 NMR spectrometer (Bruker Biospin) with a vertical 9.4T narrow-bore/ultrashield magnet operating at 400 MHz for ^{1}H observation by means of a 5-mm direct QNP $^{1}H/^{13}C/^{31}P/^{19}F$ probe with gradient capabilities; (3) an Avance III NMR spectrometer (Bruker Biospin) with a vertical 16.45T narrowbore/ ultrashield magnet operating at 700 MHz for ^{1}H observation by means of a 5-mm TXI $^{1}H/^{13}C/^{15}N$ probe with Z gradient capabilities. Chemical shifts are reported in parts per million (ppm, δ) relative to the 1H residual signal of the deuterated solvent used. 1H NMR splitting patterns with observed first-order coupling are designated as singlet (s), doublet (d), triplet (t), or quartet (q). Coupling constants (*J*) are reported in hertz. Data processing was performed with Topspin 3.6 software.

6.2 Methods for GPC

Preparative recycling GPC (gel permeation chromatography) were performed on JAIGEL 20*600 mm columns (Japan Analytical Industry) at a flow rate of 7 mL min^{-1} with a mobile phase composed of 1% (vol/vol) ethanol and 0.5% (vol/vol) Et_3N in chloroform. Monitoring was carried out by UV detector at 254 nm, 280 nm, 300 nm and 360 nm.

6.3 Methods for X-ray crystallography

Crystallography Single crystal X-ray diffraction experiments were performed at IECB X-ray facility (CNRS UMS 3033 – INSERM US001, University of Bordeaux) on a 3kW microfocus Rigaku FRX rotating anode. The source is equipped with high flux Osmic Varimax HF mirrors. The FRX generator is combined with a hybrid Dectris Pilatus 200K detector. All data were collected at the copper kα wavelength with a partial chi goniometer that decreases blind areas and enables automatic axial adjustment. Data were processed with the CrysAlisPro suite version 1.171.38.43. Empirical absorption correction using spherical harmonics, implemented in SCALE3 ABSPACK scaling algorithm was used. Structures were solved with Shelxt and refined by full-matrix least-squares method on F2 with Shelxl-2014 within Olex2. For all atoms, anisotropic atomic parameters were used. Hydrogen atoms were place at

idealized position sand refined as riding of their carriers with Uiso(H)=1.2Ueq(CH, CH2, NH) and Uiso(H)=1.5Ueq(CH3). DFIX and AFIX instructions were used to improve the geometry of molecules and RIGU to model atomic displacement parameters. Severely disordered solvent molecules were removed using the SQUEEZE procedure from the PLATON suite. For search and analysis of solvent accessible voids in the structures default parameters were utilized: grid 0.20 Å, probe radius 1.2 Å and NStep 6. Calculated total potential solvent accessible void volumes and electron counts per unit cell are given in the CIF files that were checked using IUCR's checkcif algorithm. Due to the characteristics of the crystals, i.e. large volume fractions of disordered solvent molecules, weak diffraction intensity, incompleteness of the data and moderate resolution, a number of A -level and B -level alerts remain in the check cif file. These alerts are inherent to the data and refinement procedures and do not reflect errors. Rather, they illustrate the limited practicality of the checkcif tool for medium size molecule crystallography.

Name	**7**	**18a**	**25**	**30**
Formula	$C_{74}H_{72}F_4N_8O_{12}$	$C_{98}H_{89}F_5N_{12}O_{16}$	$2(C_{112}H_{104}F_8N_{16}O_{16})$	$2(C_{168}H_{156}F_{12}N_{24}O_{24})$
M.W	1341.42	1785.85	2082.14	6246.44
Space group	*P*-1	*P*-1	P21/c	*P*-1
a	14.0065(3)	16.6273(7)	36.4661(5)	24.6529(8)
b	16.5952(3)	17.9333(6)	42.5825(5)	28.2336(8)
c	21.9975(5)	19.7845(6)	20.4587(3)	32.8540(10)
α	68.842(2)	77.595(3)	90	76.853(2)
β	82.911(2)	66.569(3)	99.813(1)	72.246(3)
γ	66.752(2)	63.592(4)	90	74.952(3)
Cell volume	4380.18	4842.91	31303.8	20756.7
Packing Coefficient	0.598886	0.600331	0.449211	0.58284

6.4 Methods for chemical synthesis

All reactions were carried out under a dry nitrogen atmosphere. Commercial reagents were purchased from Sigma-Aldrich, Alfa-Aesar or TCI and were used without further purification

unless otherwise specified. Tetrahydrofurane (THF) and dichloromethane (CH_2Cl_2) were dried over alumina columns; chloroform ($CHCl_3$), triethylamine (Et_3N) and diisopropylethylamine (DIEA) were distilled over calcium hydride (CaH_2) prior to use. Reactions were monitored by thin layer chromatography (TLC) on Merck silica gel 60-F254 plates and observed under UV light. Column chromatography purifications were carried out on Merck GEDURAN Si60 (40-63µm). ESI mass spectra were obtained from the Mass Spectrometry Laboratory at the European Institute of Chemistry and Biology (UMS 3033 - IECB), Pessac, France.

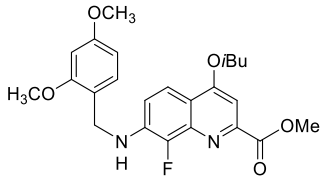

2

Compound **2**: **1** (610 mg, 1.98 mmol), 2,4-dimethoxybenzaldehyde (659 mg, 3.97mmol) were dissolved in 1,2-dichloroethane (5 ml), under inert atmosphere of N_2. The slurry was stirred at room temperature for 2 hours. Then sodium triacetoxyborohydride (841 mg, 3.97 mmol) was added to the slurry. The mixture was stirred at room temperature under a N_2 atmosphere for 18 h. The reaction mixture was quenched by adding aqueous saturated $NaHCO_3$, and the product was extracted with dichloromethane. The organic layer was washed with brine, and dried over anhydrous $MgSO_4$. After the solvent was removed in vacuo, the residue was purified by flash column chromatography (silica gel, ethyl acetate / cyclohexane = 1 / 6) to give **2** as yellow solid (731 mg, 83 %.). ^{1}H NMR (300 MHz, $CDCl_3$, 298 K) δ 7.90 (dd, *J*(H, H) = 1.5, *J*(H, H) = 9.1, 1H), 7.37 (s, 1H), 7.26-7.18 (m, 2H), 6.50 (d, *J*(H, H) = 2.3, 1H), 6.45-6.41 (m, 1H), 4.91 (br, 1H), 4.49 (d, *J*(H, H) = 6.2, 2H), 4.07 (s, 3H), 4.03 (d, *J*(H, H) = 6.4, 2H), 3.87 (s, 3H), 3.81 (s, 3H), 2.34-2.20 (m, 1H), 1.15 (s, 3H), 1.12 (s, 3H) ^{13}C NMR (100 MHz, $CDCl_3$) δ 166.4, 162.7, 160.4, 158.4, 149.6, 145.3, 142.8, 138.9, 136.9, 129.3, 118.9, 117.5, 116.0, 114.7, 103.8, 98.7, 98.3, 74.9, 55.3, 53.0, 42.9, 28.1, 19.2. HRMS (ESI): m/z calcd for $C_{24}H_{28}FN_2O_5$ $[M+H]^+$ 443.1977, found 443.1989

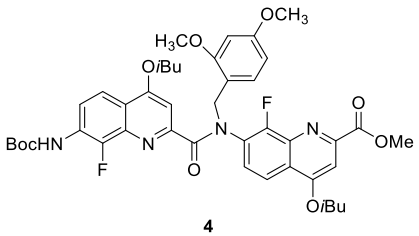

4

Compound **4**: A solution of **3** (645 mg, 1.7 mmol) in dry $CHCl_3$ (3 mL) was cooled to 0°C. 1-Chloro-N,N,2-trimethyl-1-propenylamine (0.75 mL, 3.0 eq.) was added. The solution was stirred at room temperature for 3 h under inert atmosphere of N_2. The solvent was removed under high-vacuum for at least 2 hours to yield the corresponding acid chloride. The resulting acid chloride was dissolved in dry $CHCl_3$ (3 mL) and added to a solution of **2** (630 mg, 0.9 eq.) and dry DIPEA (0.73 mL, 4.0 eq.) in dry $CHCl_3$ (1 mL). The mixture was stirred for 12 h. The solvent was removed under reduced pressure and the residue was dissolved in dichloromethane, washed with saturated aqueous NH_4Cl, saturated aqueous $NaHCO_3$ and brine, dried over $MgSO_4$, filtered and concentrated in vacuo. The residue was purified by flash column chromatography (silica gel, ethyl acetate / cyclohexane = 1 / 4) to give **4** as yellow solid (1.1 g, 89 %.). ^{1}H NMR (300 MHz, $CDCl_3$, 298 K) δ 8.19 (t, *J*(H, H) = 7.9, 1H), 7.82 (t, *J*(H, H) = 10.9, 2H), 7.58-7.49 (m, 3H), 7.25 (s, 1H), 6.75 (s, 1H), 6.46 (d, *J*(H, H) = 8.1, 1H), 6.30 (s, 1H), 5.21 (dd, *J*(H, H) = 14.5, 2H), 4.01 (br, 7H), 3.78 (s, 3H), 3.47 (s, 3H), 2.35-2.18 (m, 2H), 1.52 (s, 9H), 1.15-1.10 (m, 12H) ^{13}C NMR (100 MHz, $CDCl_3$) δ 168.6, 165.9, 162.4, 162.0, 160.4 158.5, 154.6, 154.1, 152.1, 151.6, 149.3, 146.6, 144.1, 138.9, 136.9, 131.6, 131.3, 129.6, 126.6, 122.2, 118.9, 117.9, 117.1, 116.9, 116.0, 104.1, 101.6, 100.2, 98.1, 81.4, 75.2, 75.0, 55.2, 54.9, 53.2, 47.7, 38.6, 37.0, 35.5, 28.2, 28.1, 28.0, 19.1. HRMS (ESI): m/z calcd for $C_{43}H_{49}F_2N_4O_9$ $[M+H]^+$ 803.3462, found 803.3486

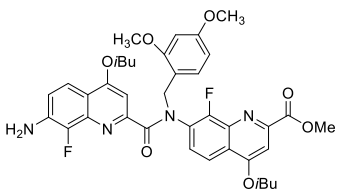

Synthesis of compound **5**: **4** (200 mg, 0.24 mmol) was dissolved in dioxane (0.2 mL). HCl in dioxane (4M, 2mL) was added to the solution, and stirred at room temperature for 4 h. The mixture was diluted with DCM, the organic layer was washed with saturated aqueous $NaHCO_3$

and brine, dried over MgSO4, filtered and concentrated in vacuo to give **5** as yellow solid (169 mg, 98%).^{1}H NMR (400 MHz, $CDCl_3$, 298 K) δ 7.82 (d, *J*(H, H) = 8.9, 1H), 7.64 (d, *J*(H, H) = 8.8, 1H), 7.55 (t, *J*(H, H) = 7.8, 1H), 7.49-7.47 (m, 2H), 7.12 (s, 1H), 6.84 (t, *J*(H, H) = 8.1, 1H), 6.42 (d, *J*(H, H) = 8.1, 1H),6.27 (s, 1H), 5.19 (dd, *J*(H, H) = 14, 2H), 3.98-3.94 (m, 7H), 3.75 (s, 3H), 3.44 (s,3H), 2.30-2.16 (m, 2H), 1.12-1.06 (m, 12H). ^{13}C NMR (100 MHz, $CDCl_3$) δ 168.9, 165.9, 162.4, 162.1, 160.3, 158.5, 154.3, 151.6, 149.2, 144.9, 142.5, 139.0, 138.9, 138.1, 138.0, 133.8, 131.6, 131.4, 129.8, 122.2, 118.2, 117.0, 116.0, 115.2, 104.1, 101.5, 98.8, 98.1, 75.2, 74.8, 67.0, 55.2, 54.9, 53.2, 47.7, 28.2, 19.1. HRMS (ESI): m/z calcd for $C_{38}H_{40}F_2N_4O_7$ $[M+H]^+$ 702.7558, found 703.7089.

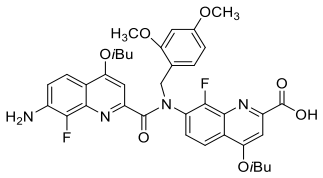

Compound **6**: **5** (120 mg, 0.17 mmol) was dissolved in a mixture of THF (10 mL) and H_2O (2 mL). To this solution was added LiOH (35.8 mg, 5.0 equiv.). The solution was stirred at room temperature for 3 h. Then solution was neutralized with 1N HCl to pH = 4~5, and concentrated under reduced pressure to remove THF. H_2O (30 mL) was added to the residue. The aqueous phase was extracted with CH_2Cl_2 (3×20 mL). The combined organic phases were dried over Na_2SO_4, filtered, then evaporated to give dimer acid 6 as a yellow solid(115 mg, 98%). ^{1}H NMR (400 MHz, $CDCl_3$, 298 K) δ 7.82 (d, *J*(H, H) = 8.5, 1H), 7.66 (d, 1H), 7.53-7.46 (m, 3H), 7.17 (s, 1H), 6.67 (t, *J*(H, H) = 8.1, 1H), 6.44 (d, *J*(H, H) = 6.8, 1H),6.26 (s, 1H), 5.37 (d, *J*(H, H) = 13.2, 1H), 5.08 (d, *J*(H, H) = 13.2, 1H), 4.02 (d, *J*(H, H) = 6.3, 2H), 3.96 (d, *J*(H, H) = 6.4, 2H), 3.75 (s, 3H), 3.42 (s, 3H), 2.34-2.16 (m, 2H), 1.12-1.06 (m, 12H). ^{13}C NMR (100 MHz, $CDCl_3$)δ 168.5, 164.3, 163.7, 160.5, 158.5, 154.1, 147.4, 131.7, 129.7, 118.4, 117.4, 116.9, 116.5, 115.1, 104.1, 99.3, 98.8, 98.1, 74.9, 67.9, 55.3, 54.9, 28.1, 19.2.

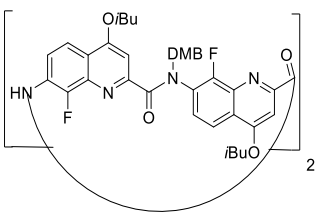

Compound **7**: **6** (270 mg, 0.39 mmol) and triphenylphosphine (411 mg, 4 eq.) were mixed in dry chloroform (2 mL) and then trichloroacetonitrile (0.15 mL, 4 eq.) and dry DIPEA (0.40 mL, 6 eq.) were added. The mixture was stirred at room temperature for 48 h under inert atmosphere of N_2. The solvent was removed under reduced pressure and the residue was dissolved in dichloromethane and washed with saturated aqueous NH_4Cl, $NaHCO_3$ and extracted with chloroform. The organic layer was washed with brine, and dried over anhydrous $MgSO_4$. After the solvent was removed in vacuo, the residue was purified by column chromatography (silica gel, ethyl acetate / n-hexane = 1 / 2) and GPC to give **7** as yellow solid (86 mg, 32%). ^{1}H NMR (300 MHz, $CDCl_3$, 298 K) δ 10.40 (s, 2H), 8.25 (t, *J*(H, H) = 5.2, 2H) 7.86 (d, *J*(H, H) = 9.2, 2H), 7.55-7.47 (m, 6H), 7.13 (s, 2H), 6.68 (t, *J*(H, H) = 5.0, 2H), 6.45 (dd, *J*(H, H) = 3.5, 2H),6.24 (d, *J*(H, H) = 3.5, 2H), 5.45 (d, *J*(H, H) = 14.1, 2H), 4.98 (d, *J*(H, H) = 14.1, 2H), 4.05-3.90 (m, 8H), 3.75 (s, 6H), 3.34 (s, 6H), 2.28-2.09 (m, 4H), 1.01 (d, *J*(H, H) = 6.5, 12H), 1.03-1.00 (m, 12H). HRMS (ESI): m/z calcd for $C_{74}H_{73}F_4N_8O_{12}$ $[M+H]^+$ 1341.5312, found 1341.5396.

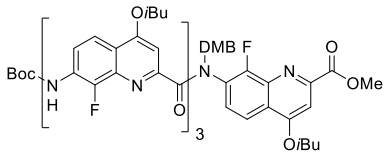

Compound **10**: A solution of **5** (845 mg, 1.3 mmol) in dry $CHCl_3$ (3 mL) was cooled to 0°C. 1-Chloro-N,N,2-trimethyl-1-propenylamine (0.27 mL, 1.5 eq.) was added. The solution was stirred at room temperature for 3 h under inert atmosphere of N_2. The solvent was removed under high-vacuum for at least 2 hours to yield the corresponding acid chloride. The resulting acid chloride was dissolved in dry $CHCl_3$ (3 mL) and added to a solution of **9** (929 mg, 1.0 eq.) and dry DIPEA (0.70 mL, 3.0 eq.) in dry $CHCl_3$ (2 mL). The mixture was stirred for 12 h. The solvent was removed under reduced pressure and the residue was dissolved in dichloromethane and washed with saturated aqueous NH_4Cl, saturated aqueous $NaHCO_3$ and brine, dried over $MgSO_4$, filtered and concentrated in vacuo. The residue was purified by flash column chromatography (silica gel, ethyl acetate / cyclohexane = 1 / 4) to give **10** as yellow solid (1.3 g, 74 %.). ^{1}H NMR (300 MHz, $CDCl_3$, 298 K) δ10.96 (s, 1H), 10.59 (s, 1H), 8.87 (q, *J*(H, H) = 6.8, 1H), 8.60 (t, *J*(H, H) =7.9, 1H), 8.53 (q, *J*(H, H) =5.3, 1H), 8.12 (q, *J*(H, H) =3.5, 1H), 8.04

(d, *J*(H, H) =5.2, 1H), 7.91(d, *J*(H, H) =8.9, 2H), 7.74 (s, 1H), 7.69 (s, 1H), 7.60 (t, *J*(H, H) =7.9, 1H), 7.55 (s, 1H), 7.50 (s, 1H), 7.47 (s, 1H), 7.31 (s, 1H), 6.45 (q, *J*(H, H) =3.4, 1H), 6.31 (s, 1H), 5.47 (d, *J*(H, H) =7.3, 1H), 4.97(d, *J*(H, H) =7.3, 1H), 4.14-4.09 (m, 4H), 4.02-3.98 (m, 7H), 3.76 (s, 3H), 3.50 (s, 3H), 2.40-2.12 (m, 4H), 1.59 (s, 9H), 1.17-1.10 (m, 24H).^{13}C NMR (100 MHz, $CDCl_3$) δ 168.6, 166.0, 163.5, 163.4, 162.7, 162.6, 162.4, 162.1, 160.5, 158.7, 154.7, 152.4, 151.4, 151.2, 149.4, 148.6, 147.1, 145.2, 143.8, 137.8, 137.6, 137.3, 131.6, 130.0, 127.8, 126.8, 126.0, 122.5, 120.9, 120.0, 119.1, 118.8, 117.8, 116.3, 104.2, 101.8, 100.7, 98.3, 97.9, 81.8, 75.6, 75.3, 55.4, 55.1, 53.3, 48.0, 30.4, 29.8, 28.1, 19.1. HRMS (ESI): m/z calcd for $C_{71}H_{74}F_4N_8O_{13}$ $[M+H]^+$ 1323.4096, found 1324.5714.

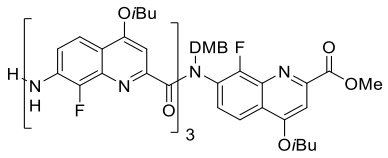

Compound **11**: **10** (0.20 g, 0.15 mmol) was dissolved in dioxane (0.2 mL). HCl in dioxane (4M, 2mL) was added to the solution, and stirred at room temperature for 4 h. The mixture was diluted with DCM, the organic layer was washed with saturated aqueous $NaHCO_3$ and brine, dried over $MgSO_4$, filtered and concentrated in vacuo to give **11** as yellow solid (180 mg, 98%).^{1}H NMR (300 MHz, $CDCl_3$, 298 K) δ 11.07 (s, 1H), 10.64 (s, 1H), 8.90 (q, *J*(H, H) =5.3, 1H), 8.61 (t, *J*(H, H) =7.8, 1H), 8.12 (d, *J*(H, H) =9.1, 1H), 7.98-7.89 (m, 3H), 7.70-7.64 (m, 3H), 7.55 (s, 1H), 7.50 (d, *J*(H, H) =8.3, 1H), 7.32 (s, 1H), 7.14 (t, *J*(H, H) =8.3, 1H), 6.47 (d, *J*(H, H) =8.2, 1H), 6.34 (s, 1H), 5.50 (d, *J*(H, H) =14.6, 1H), 4.98 (d, *J*(H, H) =14.6, 1H), 4.13-3.99 (m, 8H), 3.79 (s, 3H), 3.72 (s, 3H), 3.53 (s, 3H), 2.34-2.16 (m, 4H), 1.26 (s, 3H), 1.18-1.12 (m, 18H), 0.97 (d, *J*(H, H) =6.6, 3H). ^{13}C NMR (100 MHz, $CDCl_3$) δ 168.8, 166.0, 163.3, 162.9, 162.7, 162.3, 162.0, 160.6, 158.7, 154.6, 151.2, 150.7, 149.4, 148.2, 145.2, 144.9, 142.0, 139.1, 138.4, 137.4, 135.3, 131.5, 130.1, 127.0, 126.8, 125.9, 122.6, 120.3, 119.5, 119.2, 118.8, 117.5, 117.1, 116.5, 115.9, 104.3, 101.8, 100.5, 98.4, 98.1, 96.4, 75.5, 75.2, 67.2, 55.4, 55.2, 53.3, 48.1, 31.7, 29.8, 28.2, 22.7, 19.3, 19.1, 14.2. HRMS (ESI): m/z calcd for $C_{66}H_{66}F_4N_8O_{11}$ $[M+H]^+$ 1223.2926, found 1224.5142.

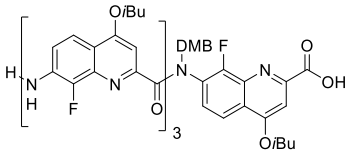

Compound **12**: **11** (140 mg, 0.15 mmol) was dissolved in a mixture of THF (10 mL) and H_2O (2 mL). To this solution was added LiOH (35.8 mg, 5.0 equiv.). The solution was stirred at room temperature for 3 h. Then solution was neutralized with 1N HCl to pH = 4~5, and concentrated under reduced pressure to remove THF. H_2O (30 mL) was added to the residue. The aqueous phase was extracted with CH_2Cl_2 (3×20 mL). The combined organic phases were dried over Na_2SO_4, filtered and concentrated in vacuo to give **12** as yellow solid (125 mg, 95%). ^{1}H NMR (300 MHz, $CDCl_3$, 298 K) δ 11.10 (s, 1H), 10.57 (s, 1H), 8.90 (q, *J*(H, H) =5.3, 1H), 8.62 (t, *J*(H, H) =7.8, 1H), 8.09 (d, *J*(H, H) =9.3, 1H), 7.90 (t, *J*(H, H) =8.9, 3H), 7.76 (d, *J*(H, H) =5.3 3H), 7.55 (s, 1H), 7.50 (d, *J*(H, H) =8.3, 1H), 7.32 (s, 1H), 7.14 (t, *J*(H, H) =9.0, 1H), 7.68 (d, *J*(H, H) =5.3, 2H), 7.59 (s, 2H), 7.50 (d, *J*(H, H) =8.1, 1H), 7.13 (t, *J*(H, H) =8.4, 1H), 6.43 (d, *J*(H, H) =8.1, 1H), 6.24 (s, 1H), 5.46 (d, *J*(H, H) =14.7, 1H), 4.97 (d, *J*(H, H) =14.7, 1H), 4.09 (d, *J*(H, H) =6.4, 4H), 4.00 (d, *J*(H, H) =6.4, 2H), 3.94 (d, *J*(H, H) =6.4, 2H), 3.75 (s, 3H), 3.37 (s, 3H), 2.31-2.12 (m, 4H), 1.26 (s, 3H), 1.30-1.21 (m, 12H), 1.15-1.10 (m, 12H).

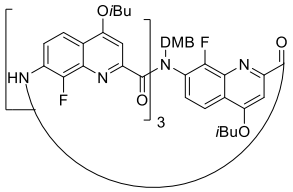

Compound **13**: **12** (120 mg, 0.39 mmol) and triphenylphosphine (260 mg, 4 eq.) were mixed in dry chloroform (2 mL) and then trichloroacetonitrile (0.12 mL, 10 eq.) and dry DIPEA (0.25 mL, 15 eq.) were added. The mixture was stirred at room temperature for 48 h. The solvent was removed under reduced pressure and the residue was dissolved in dichloromethane and washed with saturated aqueous NH_4Cl, $NaHCO_3$ and extracted with chloroform. The organic layer was washed with brine, and dried over anhydrous $MgSO_4$. After the solvent was removed in vacuo, the residue was purified by column chromatography (silica gel, ethyl acetate / n-hexane = 1 / 2) and GPC to give **13** as yellow solid (32 mg, 26%). ^{1}H NMR (300 MHz, $CDCl_3$, 298 K) δ 12.27 (d, *J*(H, H) =4.8, 1H), 12.02 (d, *J*(H, H) =4.4, 1H), 11.72 (d, *J*(H, H) =3.8, 1H), 8.95 (q, *J*(H, H) =5.3, 1H), 8.84(q, *J*(H, H) =5.2, 1H), 8.74 (q, *J*(H, H) =5.2, 1H), 8.09 (d, *J*(H, H) =4.5, 3H),

7.95 (d, *J*(H, H) =8.2, 1H), 7.74 (s, 1H), 7.62 (d, *J*(H, H) =6.8, 3H), 7.53 (q, *J*(H, H) =5.1, 3H), 6.95 (s, 1H), 6.59 (d, *J*(H, H) =8.2, 1H), 6.32 (d, *J*(H, H) =2.2, 1H), 6.10 (q, *J*(H, H) =3.5, 1H), 5.40 (d, *J*(H, H) =14.5, 1H), 4.79 (d, *J*(H, H) =14.5, 1H), 4.13-4.02 (m, 8H), 3.69 (s, 3H), 2.36-2.25 (m, 4H), 1.17-1.14 (m, 24H). HRMS (ESI): m/z calcd for $C_{65}H_{62}F_4N_8O_{10}$ $[M+H]^+$ 1191.4598, found 1191.4616.

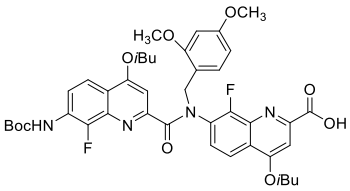

Compound **14**: Compound **4** (0.60 g, 0.74 mmol) was dissolved in a mixture of THF (10 mL) and H_2O (2 mL). To this solution was added LiOH (60 mg, 2.0 equiv.). The solution was stirred at room temperature for 3 h. Then solution was neutralized with 1N HCl to pH = 4~5, and concentrated under reduced pressure to remove THF. H_2O (30 mL) was added to the residue. The aqueous phase was extracted with CH_2Cl_2 (3×20 mL). The combined organic phases were dried over Na_2SO_4, filtered, then evaporated to give dimer acid **14** as a yellow solid (577 mg, 99%). ^{1}H NMR (400 MHz, $CDCl_3$, 298 K) δ 8.16 (t, *J*(H, H) = 7.9, 1H), 7.79-7.75 (m, 2H), 7.52 (s, 1H), 7.48-7.42 (m, 2H), 7.24 (s, 1H), 6.67 (s, 1H), 6.42 (d, *J*(H, H) = 8.1, 1H),6.24 (s, 1H), 5.19 (dd, *J*(H, H) = 14.5, 2H), 4.02-3.98 (m, 6H), 3.73 (s, 4H), 2.28-2.17 (m, 2H), 1.47 (s, 9H), 1.08-1.05 (m, 12H). ^{13}C NMR (100 MHz, $CDCl_3$) δ 168.3, 164.2, 163.7, 162.1, 160.5, 158.5, 154.4, 153.6, 152.1, 151.0, 147.6, 146.6, 144.1, 137.1, 131.8, 129.6, 122.4, 119.2, 117.8, 117.1, 116.8, 116.4, 81.5, 75.6, 75.1, 55.3, 47.7,38.6, 37.0, 35.5, 30.3, 28.2, 28.0, 19.1. HRMS (ESI): m/z calcd for $C_{42}H_{47}F_2N_4O_9$ $[M+H]^+$ 789.3306, found 789.3299.

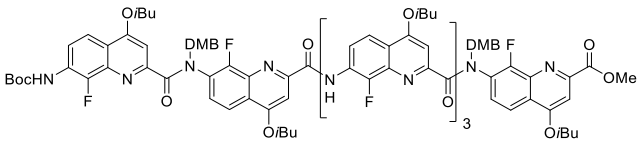

Compound **15**: A solution of **14** (106 mg, 0.13 mmol) in dry $CHCl_3$ (3 mL) was cooled to 0°C. 1-Chloro-N,N,2-trimethyl-1-propenylamine (0.05 mL, 3.0 eq.) was added. The solution was stirred at room temperature for 3 h under N_2 atmosphere. The solvent was removed under high-vacuum for at least 2 hours to yield the corresponding acid chloride. The resulting acid chloride

was dissolved in dry $CHCl_3$ (3 mL) and added to a solution of **11** (150 mg, 1.0 eq.) and dry DIPEA (63 μL, 3.0 eq.) in dry $CHCl_3$ (2 mL). The mixture was stirred for 12 h. The solvent was removed under reduced pressure and the residue was dissolved in dichloromethane and washed with saturated aqueous NH_4Cl, saturated aqueous $NaHCO_3$ and brine, dried over $MgSO_4$, filtered and concentrated in vacuo. The residue was purified by flash column chromatography (silica gel, ethyl acetate / cyclohexane = 1 / 3) and GPC to give **15** (147 mg 62%), as yellow solid. ^{1}H NMR (300 MHz, $CDCl_3$, 298 K) δ 10.81 (s, 1H), 10.67 (s, 1H), 10.50 (s, 1H), 8.83 (t, *J*(H, H) =7.7, 1H), 8.67 (t, *J*(H, H) =7.6, 1H), 8.53 (t, *J*(H, H) =7.5, 1H), 8.18-8.14 (m, 3H), 7.90 (d, *J*(H, H) =8.9, 2H), 7.81-7.73 (m, 6H), 7.54-7.42 (m, 4H), 6.72 (s, 1H), 6.42-6.21 (m, 5H), 5.42-5.27 (m, 2H), 4.97 (br, 2H), 4.18-4.11 (m, 6H), 4.01-3.93 (m, 9H), 3.72-3.64 (m, 6H), 3.46-3.40 (m, 6H), 2.37-2.13 (m, 6H), 1.48 (s, 9H), 1.20-0.95 (m, 36H).

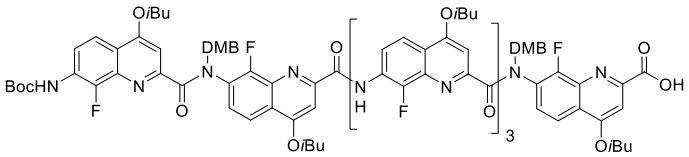

Compound **16**: **15** (130 mg, 0.06 mmol) was dissolved in a mixture of THF (3 mL) and H_2O (0.5 mL). To this solution was added LiOH (8.4 mg, 3.0 equiv.). The solution was stirred at room temperature for 3 h. Then solution was neutralized with 1N HCl to pH = 4~5, and concentrated under reduced pressure to remove THF. H_2O (30 mL) was added to the residue. The aqueous phase was extracted with CH_2Cl_2 (3×20 mL). The combined organic phases were dried over Na_2SO_4, filtered, then evaporated to give dimer acid **16** as a yellow solid (124 mg, 97%)^{1}H NMR (300 MHz, $CDCl_3$, 298 K) δ 10.85 (s, 1H), 10.73 (s, 1H), 10.47 (s, 1H), 8.85 (t, *J*(H, H) =7.9, 1H), 8.72 (t, *J*(H, H) =7.4, 1H), 8.61-8.48 (m, 1H), 8.15-8.12 (m, 3H), 7.92 (d, *J*(H, H) =8.0, 2H), 7.81-7.68 (m, 6H), 7.62-7.31 (m, 5H), 6.72 (s, 1H), 6.39 (br, 2H), 6.20 (s, 2H), 5.38-4.94 (m, 4H), 4.18-3.95 (m, 12H), 3.74-3.69 (m, 8H), 3.38 (s, 4H), 2.37-2.10 (m, 4H), 1.48 (s, 9H), 1.20-0.95 (m, 36H).

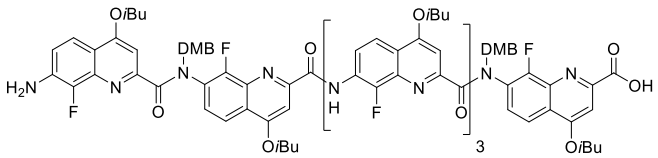

Compound **17**: **16** (124 mg, 0.06 mmol) was dissolved in dioxane (0.2 mL). HCl in dioxane (4M, 5mL) was added to the solution, and stirred at room temperature for 4 h. The mixture was diluted with DCM and the organic layer was washed with saturated aqueous $NaHCO_3$ and brine, dried over $MgSO_4$, filtered and concentrated in vacuo to give **17** as yellow solid (110 mg, 97%).^{1}H NMR (300 MHz, $CDCl_3$, 298 K) δ 10.79 (s, 2H), 10.52 (s, 1H), 8.78 (br, 2H), 8.55 (t, *J*(H, H) =7.2, 1H), 8.18-8.13 (m, 2H), 7.93-7.90 (m, 2H), 7.80-7.71 (m, 4H), 7.62-7.43 (m, 6H), 7.11-6.97 (m, 2H), 6.46-6.39 (m, 2H), 6.20 (s, 3H), 5.37-4.95 (m, 4H), 4.18-3.92 (m, 12H), 3.80-3.63 (m, 4H), 3.37 (s, 8H), 2.37-2.09 (m, 6H), 1.20-1.09 (m, 27H), 1.00-0.98 (m, 9H).

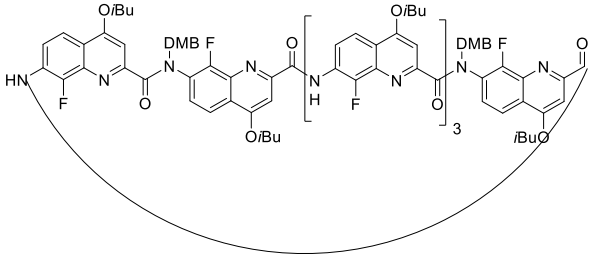

Compound **18**: **17** (110 mg, 0.06 mmol) and triphenylphosphine (156 mg, 10 eq.) were mixed in dry chloroform (2 mL) and then trichloroacetonitrile (79 μL, 12 eq.) and dry DIPEA (150 μL, 15 eq.) were added. The mixture was stirred at room temperature for 48 h under N_2 atmosphere. The solvent was removed under reduced pressure and the residue was dissolved in dichloromethane and washed with saturated aqueous NH_4Cl, $NaHCO_3$ and extracted with chloroform. The organic layer was washed with brine, and dried over anhydrous $MgSO_4$. After the solvent was removed in vacuo, the residue was purified by column chromatography (silica gel, ethyl acetate / n-hexane = 1 / 2) and GPC to give **18** as yellow solid (72 mg, 63%).^{1}H NMR (300 MHz, $CDCl_3$, 298 K) δ 11.28-10.27 (m, 4H), 8.98-8.59 (m, 3H), 8.10-7.86 (m, 3H), 7.84-7.59 (m, 6H), 7.54-7.30 (m, 4H), 6.45-6.15 (m, 2H), 5.85-4.92 (m, 4H), 4.13-4.06 (m, 12H), 3.83-3.36 (m, 12H), 2.28-1.85 (m, 6H), 1.13-1.11 (m, 36H). HRMS (ESI): m/z calcd for $C_{102}H_{98}F_6N_{12}O_{16}$ $[M+H]^+$ 1861.7201 found 1861.7244.

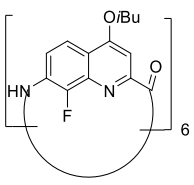

Compound **19**: Trifluoroacetic acid (5 mL) was added to **18** (20.0 mg, 0.01 mmol) and the mixture was stirred at 60°C for 2 h. The reaction mixture was quenched by adding sat. $NaHCO_3$ aq. and extracted with chloroform. The organic layer was washed with brine, and dried over $MgSO_4$. After the solvent was removed in vacuo, the residue was purified by GPC to give **19** as yellow solid (15.7 mg, quant.). ^1H NMR (400 MHz, $C_2D_2Cl_4$, 353 K) δ10.35 (s, 1H), 8.50 (q, *J*(H, H) =5.1, 1H), 8.13 (d, *J*(H, H) =9.0, 1H), 7.80 (s, 1H), 4.18 (d, *J*(H, H) =6.3, 2H), 2.39-2.32 (m, 2H), 1.20 (d, *J*(H, H) =6.6, 6H).

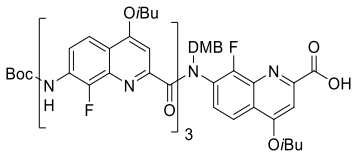

Compound **20**: **4** (750 mg, 0.56 mmol) was dissolved in a mixture of THF (10 mL) and H_2O (2 mL). To this solution was added LiOH (71 mg, 3.0 equiv.). The solution was stirred at room temperature for 3 h. Then solution was neutralized with 1N HCl to pH = 4~5, and concentrated under reduced pressure to remove THF. H_2O (30 mL) was added to the residue. The aqueous phase was extracted with CH_2Cl_2 (3×20 mL). The combined organic phases were dried over Na_2SO_4, filtered, then evaporated to give dimer acid **20** as a yellow solid (702 mg, 97%). ^1H NMR (300 MHz, $CDCl_3$, 298 K) δ 10.99 (s, 1H), 10.56 (s, 1H), 8.89 (q, *J*(H, H) =5.3, 1H), 8.61 (t, *J*(H, H) =7.6, 1H), 8.52 (t, *J*(H, H) =8.1, 1H), 8.12 (d, *J*(H, H) =9.5, 1H), 8.04 (d, *J*(H, H) =9.3, 1H), 7.91 (t, *J*(H, H) =7.8, 2H), 7.73 (s, 1H), 7.68 (s, 1H), 7.61 (s, 1H), 7.53 (t, *J*(H, H) =7.9, 1H), 7.45 (s, 1H), 7.36 (s, 1H), 6.47 (d, *J*(H, H) =7.7, 1H), 6.29 (s, 1H), 5.42 (d, *J*(H, H) =13.5, 1H), 5.08 (d, *J*(H, H) =14.8, 1H), 4.14-4.09 (m, 4H), 4.05-4.03 (m, 4H), 3.76 (s, 3H), 3.46 (s, 3H), 2.40-2.15 (m, 4H), 1.59 (s, 9H), 1.25 (s, 3H), 1.17-1.11 (m, 18H), 0.95 (s, 3H). ^{13}C NMR (100 MHz, $CDCl_3$) δ 168.3, 164.4, 163.9, 162.8, 162.5, 160.6, 158.7, 154.5, 152.5, 147.7, 145.1, 143.8, 137.7, 131.7, 129.9, 127.9, 126.9, 122.7, 120.9, 120.2, 119.9, 119.1, 118.8, 117.7, 117.0, 104.2, 100.63, 99.7, 98.3, 97.9, 81.7, 75.7, 75.6, 75.3, 55.4, 55.0, 31.7, 30.4, 29.8, 28.4, 28.2, 28.0, 22.7, 19.3, 19.1, 14.2. HRMS (ESI): m/z calcd for $C_{70}H_{72}F_4N_8O_{13}$ $[M+H]^+$ 1309.3823, found 1310.5554.

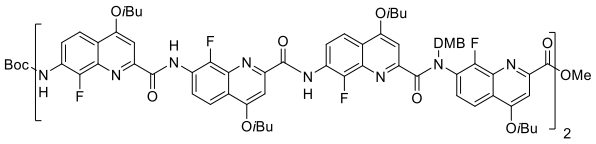

Compound **21**: A solution of **20** (400 mg, 0.30 mmol) in dry $CHCl_3$ (3 mL) was cooled to 0°C. 1-Chloro-N,N,2-trimethyl-1-propenylamine (0.10 mL, 2.2 eq.) was added. The solution was stirred at room temperature for 3 h under N_2. The solvent was removed under high-vacuum for at least 2 hours to yield the corresponding acid chloride. The resulting acid chloride was dissolved in dry $CHCl_3$ (3 mL) and added to a solution of **11** (377 mg, 1.0 eq.) and dry DIPEA (0.16 mL, 3.0 eq.) in dry $CHCl_3$ (2 mL). The mixture was stirred for 12 h. The organic layer was washed with saturated aqueous NH_4Cl, saturated aqueous $NaHCO_3$ and brine, dried over $MgSO_4$, filtered and concentrated in vacuo. The residue was purified by flash column chromatography (silica gel, ethyl acetate / cyclohexane = 1 / 3) to give **21** as yellow solid (594 mg, 77 %.). ^{1}H NMR (400 MHz, $CDCl_3$, 298 K) δ 11.44-10.28 (m, 5H), 9.09-8.33 (m, 5H), 8.16-7.31 (m, 20H), 7.19-6.97 (m, 2H), 6.51-5.99 (m, 3H), 5.47-4.85 (m, 4H), 4.12-3.36 (m, 31H), 2.39-2.09 (m, 8H), 1.66-1.51 (m, 12H), 1.22-1.07 (m, 45H).^{13}C NMR (100 MHz, $CDCl_3$) δ 167.6, 164.8, 162.1, 161.4, 160.9, 159.4, 159.2, 157.4, 153.5, 151.3, 150.2, 150.1, 149.9, 148.0, 146.8, 137.6, 136.4, 130.7, 130.2, 128.4, 128.1, 126.6, 125.8, 125.5, 124.8, 121.5, 120.8, 119.4, 118.9, 118.7, 118.1, 117.6, 116.4, 116.0, 115.3, 103.1, 99.7, 99.5, 98.2, 97.0, 76.2, 74.3, 74.0, 54.2, 54.1, 53.9, 52.0, 46.6. HRMS (ESI): m/z calcd for $C_{136}H_{136}F_8N_{16}O_{23}$ $[M+H]^+$ 2514.6602, found 2515.0552.

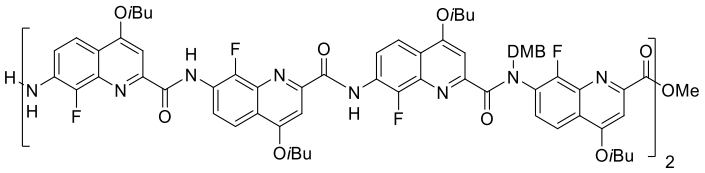

Compound **22**: **21** (100 mg, 0.039 mmol) was dissolved in dioxane (0.1 mL). HCl in dioxane (4M, 1.0 mL) was added to the solution, and stirred at room temperature for 4 h. The mixture was diluted with DCM and the organic layer was washed with saturated aqueous $NaHCO_3$ and brine, dried over $MgSO_4$, filtered and concentrated in vacuo to give **22** as yellow solid (93 mg, 97%).^{1}H NMR (400 MHz, $CDCl_3$, 298 K) δ 11.30-10.37 (m, 5H), 9.13-8.32 (m, 4H), 8.22-7.37 (m, 20H), 7.22-6.92 (m, 3H), 6.51-6.18 (m, 3H), 5.47-4.94 (m, 4H), 4.35-3.91 (m, 25H), 3.77-

3.36 (m, 6H), 2.42-2.11 (m, 8H), 1.72-1.62 (m, 6H), 1.24-0.95 (m, 42H). ^{13}C NMR (100 MHz, $CDCl_3$) δ 168.6, 165.8, 163.1, 162.7, 162.4, 161.9, 160.5, 160.3, 160.0, 158.6, 158.4, 154.6, 151.1, 150.5, 138.8, 137.7, 137.1, 135.1, 131.7, 11.4, 129.5, 126.9, 125.9, 122.5, 121.9, 120.0, 119.1, 118.9, 117.4, 117.0, 116.3, 104.1, 101.6, 101.2, 100.7, 100.4, 99.2, 98.1, 96.1, 95.3, 72.2, 71.1, 61.5, 59.4, 53.1, 47.6, 42.8, 37.6, 35.6, 30.2, 29.6. HRMS (ESI): m/z calcd for $C_{131}H_{128}F_8N_{16}O_{21}$ $[M+H]^+$ 2414.5432, found 2414.9951.

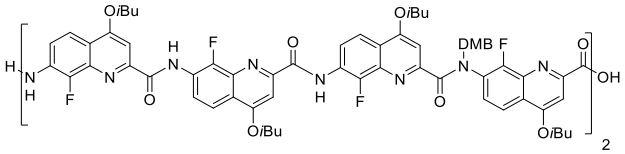

Compound **23**: **22** (90 mg, 0.037 mmol) was dissolved in THF (1.0 mL). LiOH (7.45 mg, 0.186 mmol) was added to the solution, followed with H_2O (0.1 mL) and stirred at room temperature for 4 h. The organic layer was washed with citric acid (5%, 25 mL) and brine, dried over $MgSO_4$, filtered and concentrated in vacuo to give **23** as yellow solid (82 mg, 98%).^{1}H NMR (400 MHz, $CDCl_3$, 298 K) δ 11.27-10.34 (m, 5H), 9.10-8.32 (m, 4H), 8.07-7.30 (m, 20H), 7.19-6.90 (m, 3H), 6.64-6.04 (m, 3H), 5.44-4.87 (m, 4H), 4.42-3.79 (m, 18H), 3.76-3.30 (m, 10H), 2.40-2.07 (m, 8H), 1.23-0.94 (m, 48H). ^{13}C NMR (100 MHz, $CDCl_3$) δ167.2, 163.2, 162.6, 162.1, 161.3, 160.9, 160.4, 159.5, 159.0, 157.5, 153.3, 150.0, 149.4, 146.6, 144.1, 136.1, 134.0, 130.7, 130.4, 128.7, 125.9, 124.8, 124.4, 121.4, 118.9, 118.1, 117.8, 116.4, 115.2, 114.6, 103.1, 102.9, 102.7, 102.5, 99.4, 98.0, 97.0, 95.0, 94.2, 66.9, 66.0, 58.4, 50.0, 47.0, 36.0, 34.5, 28.6, 28.4, 24.5. HRMS (ESI): m/z calcd for $C_{130}H_{126}F_8N_{16}O_{21}$ $[M+H]^+$ 2400.5162, found 2400.9805.

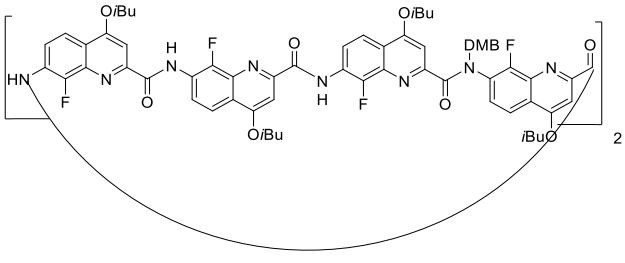

Compound **24**: **23** (350 mg, 0.15 mmol) and triphenylphosphine (582 mg, 15 eq.) were mixed in dry chloroform (5 mL) and then trichloroacetonitrile (250 μL, 17 eq.) and dry DIPEA (384 μL, 15 eq.) were added. The mixture was stirred at room temperature for 48 h. The solvent was removed under reduced pressure and the residue was dissolved in dichloromethane and washed

with saturated aqueous NH_4Cl, $NaHCO_3$ and extracted with chloroform. The organic layer was washed with brine, and dried over anhydrous $MgSO_4$. After the solvent was removed in vacuo, the residue was purified by column chromatography (silica gel, ethyl acetate / *n*-hexane = 1 / 2) and GPC to give **24** as yellow solid (127 mg, 36%). ^{1}H NMR (300 MHz, $CDCl_3$, 298 K) δ 11.15-10.80 (m, 2H), 10.68 (s, 2H), 10.44-10.23 (m, 2H), 8.97-8.46 (m, 4H), 8.37-8.26 (m, 2H), 8.17-8.02 (m, 3H), 7.95-7.40 (m, 11H), 7.30 (s, 4H), 6.59 (br, 1H), 6.40 (d, *J*(H, H) =7.9, 2H), 6.22-6.18 (m, 3H), 5.64 (d, *J*(H, H) =14.2, 2H), 5.03 (d, *J*(H, H) =14.2, 2H), 4.17-3.96 (m, 12H), 3.85 (s, 4H), 3.68 (s, 6H), 3.47-3.33 (m, 6H), 2.30-2.07 (m, 8H), 1.24-1.05 (m, 24H), 1.02-0.94 (m, 24H). HRMS (ESI): m/z calcd for $C_{130}H_{125}F_8N_{16}O_{20}$ $[M+2H]^{2+}$ 1191.9615, found 1191.8117.

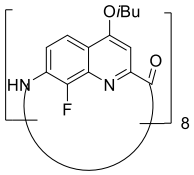

Compound **25**: Trifluoroacetic acid (5 mL) was added to **24** (100.0 mg, 0.04 mmol) and the mixture was stirred at 60°C for 2 h. The reaction mixture was quenched by adding sat. $NaHCO_3$ aq. and extracted with chloroform. The organic layer was washed with brine, and dried over $MgSO_4$. After the solvent was removed in vacuo, the residue was purified by GPC to give **25** as yellow solid (87.4 mg, quant.). ^{1}H NMR (300 MHz, $CDCl_3$, 298 K) δ 11.37-9.92 (m, 8H), 9.17-8.73 (m, 4H), 8.51-8.06 (m, 6H), 7.97-7.32 (m, 10H), 7.06-6.64 (m, 4H), 4.38-3.69 (m, 16H), 1.37-1.04 (m, 48H). HRMS (ESI): m/z calcd for $C_{112}H_{104}F_8N_{16}O_{16}$ $[3M+3H]^{3+}$ 2082.4450, found 2082.4993.

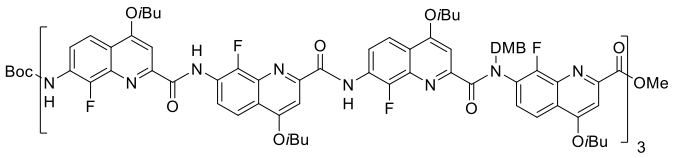

Compound **26**: A solution of **20** (107 mg, 0.08 mmol) in dry $CHCl_3$ (1 mL) was cooled to 0°C. 1-Chloro-N,N,2-trimethyl-1-propenylamine (0.04 mL, 3.0 eq.) was added. The solution was stirred at room temperature for 3 h. The solvent was removed under high-vacuum. The resulting acid chloride was dissolved in dry $CHCl_3$ (3 mL) and added to a solution of **22** (200 mg, 1.0 eq.) and dry DIPEA (0.05 mL, 3.0 eq.) in dry $CHCl_3$ (2 mL). The mixture was stirred for 12 h. The solvent was removed under reduced pressure and the residue was dissolved in

dichloromethane and washed with saturated aqueous NH_4Cl, saturated aqueous $NaHCO_3$ and brine, dried over $MgSO_4$, filtered and concentrated in vacuo. The residue was purified by flash column chromatography (silica gel, ethyl acetate / cyclohexane = 1 / 3) to give **26** as yellow solid (162 mg, 54%.). ^{1}H NMR δ (400 MHz, $CDCl_3$, 298 K) δ 10.96-10.40 (m, 8H), 9.01-8.51 (m, 8H), 8.10-7.48 (m, 28H), 6.48-6.24 (m, 9H), 5.50-4.96 (m, 6H), 4.24-3.83 (m, 27H), 3.73-3.67 (m, 9H), 3.52-3.41 (m, 9H), 2.43-2.11 (m, 12H), 1.32-1.00 (m, 81H). ^{13}C NMR (100 MHz, $CDCl_3$) δ 167.6, 167.1, 164.8, 162.0, 161.4, 160.8, 159.2, 157.4, 153.5, 151.3, 150.0, 148.1, 147.3, 146.7, 145.5, 145.0, 144.2, 137.7, 136.5, 130.5, 128.8, 125.7, 125.4, 124.5, 121.3, 120.1, 119.2, 118.7, 118.7, 118.2, 117.4, 116.4, 116.0, 115.2, 103.0, 100.5, 99.6, 97.0, 96.6, 80.3, 79.9, 74.3, 74.0, 54.1, 53.8, 46.8, 27.1, 18.2. HRMS (ESI): m/z calcd for $C_{201}H_{199}F_{12}N_{24}O_{33}$ $[M+H]^+$ 3706.4501, found 3706.4991.

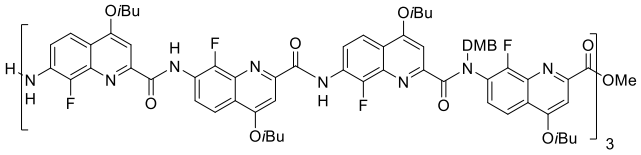

Compound **27**: **26** (80 mg, 0.021 mmol) was dissolved in dioxane (0.1 mL). HCl in dioxane (4M, 1mL) was added to the solution, and stirred at room temperature for 4 h. The mixture was diluted with DCM and washed with saturated aqueous $NaHCO_3$ and brine, the organic layer was dried over $MgSO_4$, filtered and concentrated in vacuo to give **26** as yellow solid (75 mg, 98%). ^{1}H NMR δ (400 MHz, $CDCl_3$, 298 K) 11.07-10.55 (m, 8H), 8.93-8.51 (m, 8H), 8.17-7.40 (m, 26H), 7.22-7.09 (m, 2H), 6.50-6.22 (m, 9H), 5.50-5.03 (m, 6H), 4.18-3.45 (m, 45H), 2.45-2.17 (m, 12H), 1.29-0.83 (m, 72H).

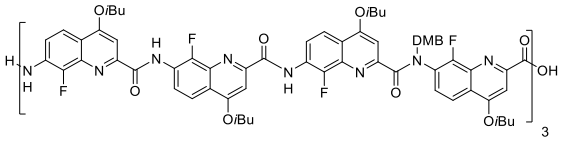

Compound **28**: **27** (80 mg, 0.021 mmol) was dissolved in THF (1.0 mL). LiOH (5.09 mg, 0.121 mL) was added to the solution, followed with H_2O (0.1 mL) and stirred at room temperature for 4 h. The organic layer was washed with citric acid (5%, 25 mL) and brine, dried over $MgSO_4$, filtered and concentrated in vacuo to give **28** as yellow solid (78 mg, 98%).^{1}H NMR (400 MHz,

$CDCl_3$, 298 K) δ 10.73-10.48 (m, 8H), 8.70-8.39 (m, 8H), 8.00-7.39 (m, 26H), 6.32-6.13 (m, 9H), 5.37-5.03 (m, 6H), 4.21-3.23 (m, 42H), 2.42-2.19 (m, 12H), 1.03-0.78 (m, 72H).

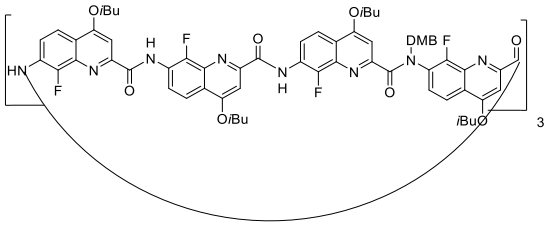

Compound **29**: **28** (85 mg, 0.023 mmol) and triphenylphosphine (93.4 mg, 15 eq.) were mixed in dry chloroform (3 mL) and then trichloroacetonitrile (47 μL, 17 eq.) and dry DIPEA (61 μL, 15 eq.) were added. The mixture was stirred at room temperature for 48 h under argon. The solvent was removed under reduced pressure and the residue was dissolved in dichloromethane and washed with saturated aqueous NH_4Cl, $NaHCO_3$ and extracted with chloroform. The organic layer was washed with brine, and dried over anhydrous $MgSO_4$. After the solvent was removed in vacuo, the residue was purified by column chromatography (silica gel, ethyl acetate / n-hexane = 1 / 2) and GPC to give **29** as yellow solid (52 mg, 61%).^{1}H NMR (400 MHz, $CDCl_3$, 298 K) δ 11.01-10.46 (m, 9H), 9.03-8.37 (m, 9H), 8.20-7.34 (m, 24H), 7.20-7.01 (m, 4H), 6.44-6.12 (m, 8H), 5.09 (br, 6H), 4.21-3.94 (m, 20H), 3.81-3.53 (m, 12H), 3.46-3.22 (m, 10H), 2.42-2.04 (m, 12H), 1.16-0.84 (m, 72H).

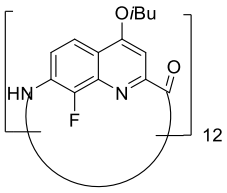

Compound **30**: Trifluoroacetic acid (5 mL) was added to **29** (56.0 mg, 0.015 mmol) and the mixture was stirred at 60°C for 2 h. The reaction mixture was quenched by adding sat. $NaHCO_3$ aq. and extracted with chloroform. The organic layer was combined and washed with brine, dried over $MgSO_4$. After the solvent was removed in vacuo, the residue was purified by GPC to give **30** as yellow solid (48.2 mg, quant.). ^{1}H NMR (400 MHz, $CDCl_3$, 298 K) δ 12.01 (s, 2H), 11.87 (s, 1H), 11.74 (s, 1H), 11.57 (s, 1H), 11.50 (s, 1H), 11.48 (s, 1H), 11.44 (s, 1H), 11.36 (s, 2H), 10.50 (s, 1H), 10.37 (s, 1H), 9.24 (t, *J*(H, H) =7.2, 1H), 9.11 (s, 1H), 9.07 (t, *J*(H, H) =7.8, 1H), 9.00-8.89 (m, 3H), 8.81 (t, *J*(H, H) =7.6, 1H), 8.63 (t, *J*(H, H) =7.3, 1H), 8.46 (t,

J(H, H) =7.2, 1H), 8.20 (q, *J*(H, H) =7.8, 2H), 8.14 (t, *J*(H, H) =7.2, 1H), 8.09 (s, 1H), 8.07-8.01 (m, 1H), 7.87 (d, *J*(H, H) =9.0, 1H), 7.80-7.71 (m, 4H), 7.65 (s, 1H), 7.51 (s, 1H), 7.47 (d, *J*(H, H) =11.0, 1H), 7.42 (d, *J*(H, H) =9.0, 1H), 7.35-7.29 (m, 2H), 7.18-7.07 (m, 5H), 6.99 (s, 1H), 6.64 (s, 1H), 6.60 (d, *J*(H, H) =4.6, 2H), 6.41 (s, 1H), 6.18 (s, 1H), 4.35 (br, 2H), 4.20-4.14 (m, 5H), 4.12-4.03 (m, 2H), 3.92-3.86 (m, 3H), 3.81-3.72 (m, 5H), 3.70-3.57 (m, 5H), 3.40 (t, *J*(H, H) =8.1, 1H), 3.03 (t, *J*(H, H) =8.1, 1H), 2.42-2.03 (m, 12H), 1.31-1.00 (m, 72H). HRMS (ESI): m/z calcd for $C_{168}H_{156}F_{12}N_{24}O_{24}$ $[M+2H]^{2+}$ 1562.0856, found 1562.0332, $[2M+3H]^{3+}$: 2082.7795, found 2082.7056 .

Chapter II: Photoswitchable guest binding using an aromatic oligoamide foldamer

1. Introduction

The design of molecular switches and triggers is common in the smart material and supramolecular areas.[1] Molecular or supramolecular switches have received a great deal of interest because their structures can be changed by an external stimulus, and in some cases, reverted to their original structures by applying another stimulus. Those changes can be triggered by physical and chemical stimuli, for example, photo-irradiation, redox, temperature, magnetic field and pH.[2]

1.1 Photo-switchable molecules

During those strategies, light is a non-invasive stimulus and photochemistry have various applications on controllable systems due to its easy processing and high efficiency. Photochromism is the reversible transformation of chemical species between two forms with different absorption spectra. The transformation, for example photoisomerization, can modulate molecular properties and functions, such as conformations, dielectric constant or refractive index. Molecules that reversibly transform light energy in this way are called "molecular photo-switches". A variety of photo-switches including azobenzenes,[3] anthracenes,[4] overcrowded alkenes[5], diaryethenes and spiropyrans have been studied, and their photochromic processes involves *cis-trans* isomerization, photocyclization, photoinduced electron transfer and keto-enol tautomerism (Figure 1).

1 Yang, C.; Inoue, Y. *Chem. Soc. Rev.* **2014**, *43*, 4123-4143; Vallavoju, N.; Sivaguru, J. *Chem. Soc. Rev.* **2014**, *43*, 4084-4101; Zhang, L.; Wang, H.-X.; Li, S.; Liu, M. *Chem. Soc. Rev.* **2020**, *49*, 9095-9120; Bisoyi, H. K.; Li, Q. *Angew. Chem. Int. Ed.* **2016**, *55*, 2994-3010; Wang, Y.; Xu, H.; Zhang, X. *Adv. Mater.* **2009**, *21*, 2849-2864; Yang, Y.-W.; Sun, Y.-L.; Song, N. *Acc. Chem. Res.* **2014**, *47*, 1950-1960; Kakuta, T.; Yamagishi, T.-a.; Ogoshi, T. *Acc. Chem. Res.* **2018**, *51*, 1656-1666; Baroncini, M.; Silvi, S.; Credi, A. *Chem. Rev.* **2020**, *120*, 200-268; Huang, C.-H.; Bassani, D. M. *Eur. J. Org. Chem.* **2005**, *2005*, 4041-4050.

2 Pianowski, Z. L. *Chem. Eur. J.* **2019**, *25*, 5128-5144; Yagai, S.; Kitamura, A. *Chem. Soc. Rev.* **2008**, *37*, 1520-1529.

3 Klajn, R.; Stoddart, J. F.; Grzybowski, B. A. Chem. Soc. Rev. 2010, 39, 2203-2237; Beharry, A. A.; Woolley, G. A. Chem. Soc. Rev. 2011, 40, 4422-4437.

4 Becker, H. D. Chem. Rev. 1993, 93, 145-172; Bouas-Laurent, H.; Castellan, A.; Desvergne, J.-P.; Lapouyade, R. Chem. Soc. Rev. 2000, 29, 43-55.

5 Wenger, O. S. *Chem. Soc. Rev.* **2012**, *41*, 3772-3779; Feringa, B. L. *J. Org. Chem.* **2007**, *72*, 6635-6652.

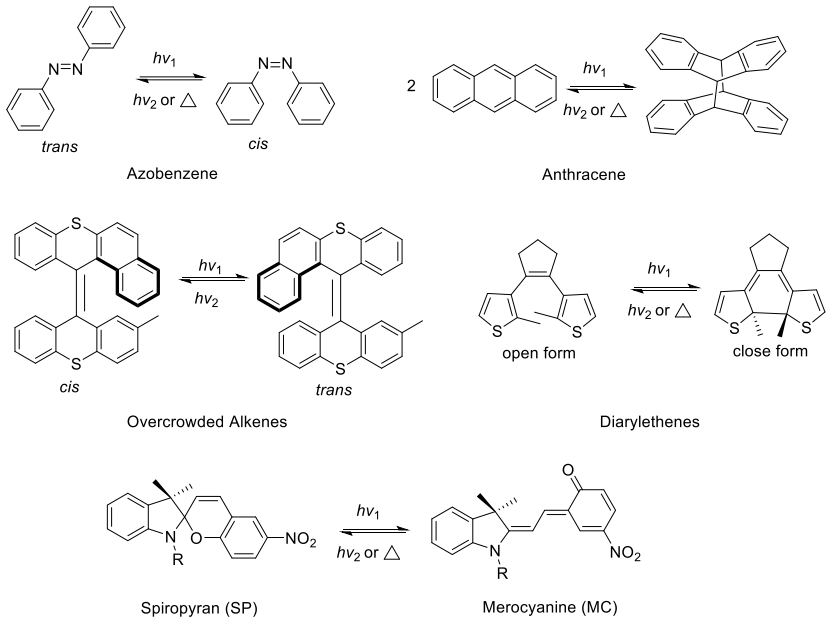

Figure 1. Molecular structure of typical photochromic molecules.

1.2 Photo-switchable chirality

Molecular photoswitches can be used to control the chirality and organization of dynamic helical polymers: chiral polyisocyanates is a good example. Polyisocyanates have a dynamic helical conformation,[6] obtained from achiral monomers such as hexylisocyanate. The corresponding polymer consists of a racemic mixture of P and M helical chains or helical segments in a long polymeric chain. In the presence of chiral side chains, the polymer chains become diastereomeric and may have a strong preference for one helical twist sense. This results from the incorporation of a small number of chiral side groups in copolymers. The high cooperativity which is leading to a strong amplification of chirality is called the "sergeants and soldiers" effect. Zentel and coworker have prepared polyisocyanates with chiral azobenzene side chains containing one or two stereogenic centers (Figure 2).[7] Upon irradiating at 365 nm the copolymer **2.1** exhibits a change in optical rotatory dispersion (ORD) and circular dichroism (CD) spectra indicating a change in the population of helical segments and the preferred helical sense was the same in both states. The same switching experiment for two stereocentres polymer **2.2** resulted in an inversion of the helical twist sense (Figure 2).

6 Feringa, B. L.; van Delden, R. A.; Koumura, N.; Geertsema, E. M. *Chem. Rev.* **2000**, *100*, 1789-1816.
7 Mueller, M.; Zentel, R. *Macromolecules* **1994**, *27*, 4404-4406.

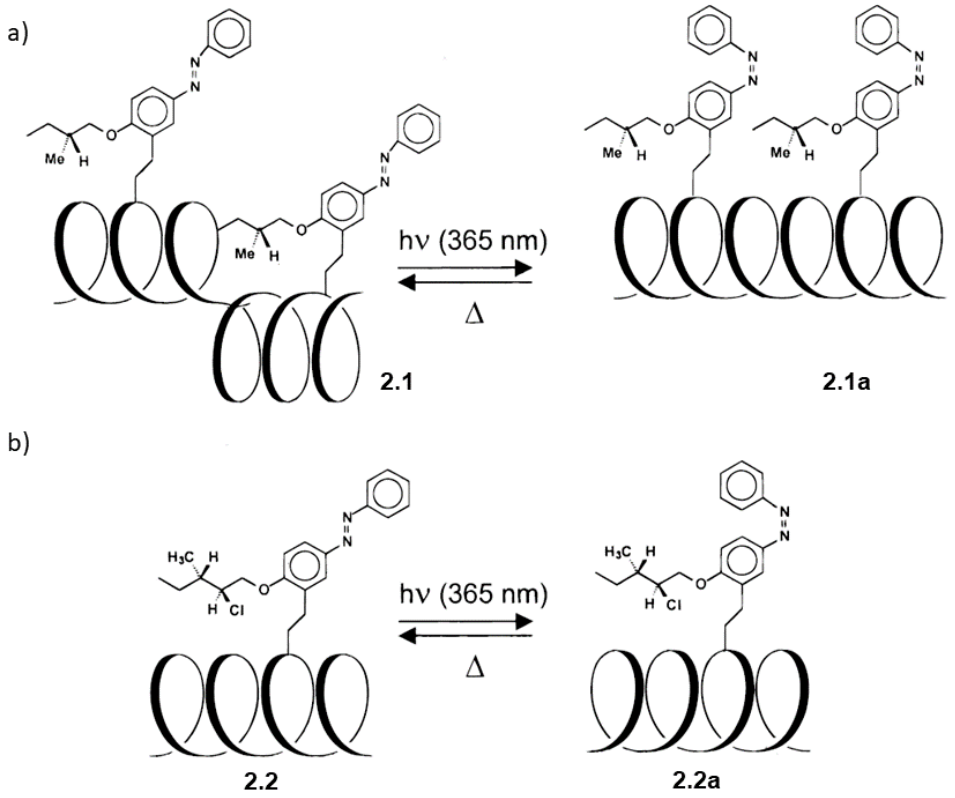

Figure 2. Chiral photoswitchable polyisocyanates: a) schematic representation of the shift in equilibrium between P and M helical upon irradiation. b) illustration of P and M helix transition in the polyisocyanates upon photoisomerization of the azobenzene unit.

The photocontrol of peptide helices have been studied by Woolley and coworker.[8] In the α-helices **2.4**, the distances between the pair of cysteines was adjusted precisely to the lengths between the ends of the azobenzene derivative **2.3** in both *trans* or *cis* forms (Figure 3). The distance of *trans*-**2.3** isomer fit well with the helical fold, while the *cis*-**2.3** isomer that has a shorter end-to-end conformation and a distance which is less compatible with the helical structure. Upon UV irradiation to process *trans* to *cis* isomerization, the space around cysteines peptide is reduced and the helical conformation was perturbed. Irradiation with visible light, to revert azobenzene from *cis* to *trans*, allows to recover a stable helix. In this system, the linker **2.3** worked as tilting energy landscape without altering the intrinsic conformational dynamics of the peptide (Figure 3).

8 Woolley, G. A. *Acc. Chem. Res.* **2005**, *38*, 486-493; Dugave, C.; Demange, L. *Chem. Rev.* **2003**, *103*, 2475-2532.

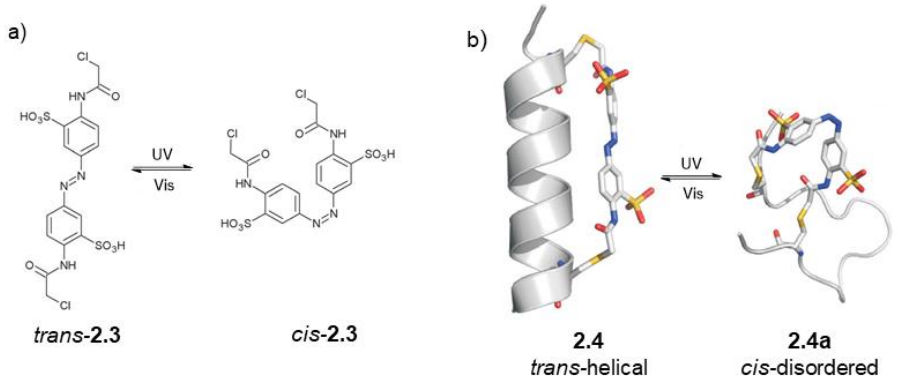

Figure 3. a) Photoisomerization of azobenzene derivative **2.3** from *trans* to *cis*; b) Conformations of α-helical peptides linked with azobenzene derivative **2.3**. Photoisomerization from *trans* to *cis* induces a decrease in helix content. Recovery from *cis* to *trans* allows a re-folding of the helix.

Feringa and coworkers built up an intramolecular transmission of chirality system,[9] which is triggered by photo-switch molecular, overcrowded alkenes (Figure 4). A dynamic helical polymer **2.5**, polyhexylisocyanate, was functionalized at one end with amide-substituted *trans* overcrowded alkenes motor. In solution, the polymer **2.5** preorganized a helical conformation and showed dynamically racemic, the polymer chains consist of equal amounts of interconverting right-handed and left-handed helices. After irradiation of the motor unit, the M-helical polymer **2.5b** is exclusively obtained due to the unstable *cis* form, while followed with the thermal isomerization of motor to the stable *cis* form that results in the change of helix conformation to the P-helical polymer **2.5c**. The racemic state of the polymer **2.5** can be achieved by completing the motor cycle and turn to starting *trans* state. As a result, the chirality of polymer can be switched between the racemic, M and P states by controlling the isomerization of the molecular motor (Figure 4).

9 van Leeuwen, T.; Lubbe, A. S.; Štacko, P.; Wezenberg, S. J.; Feringa, B. L. *Nat. Rev. Chem.* **2017**, *1*, 0096; Pijper, D.; Feringa, B. L. *Angew. Chem. Int. Ed.* **2007**, *46*, 3693-3696.

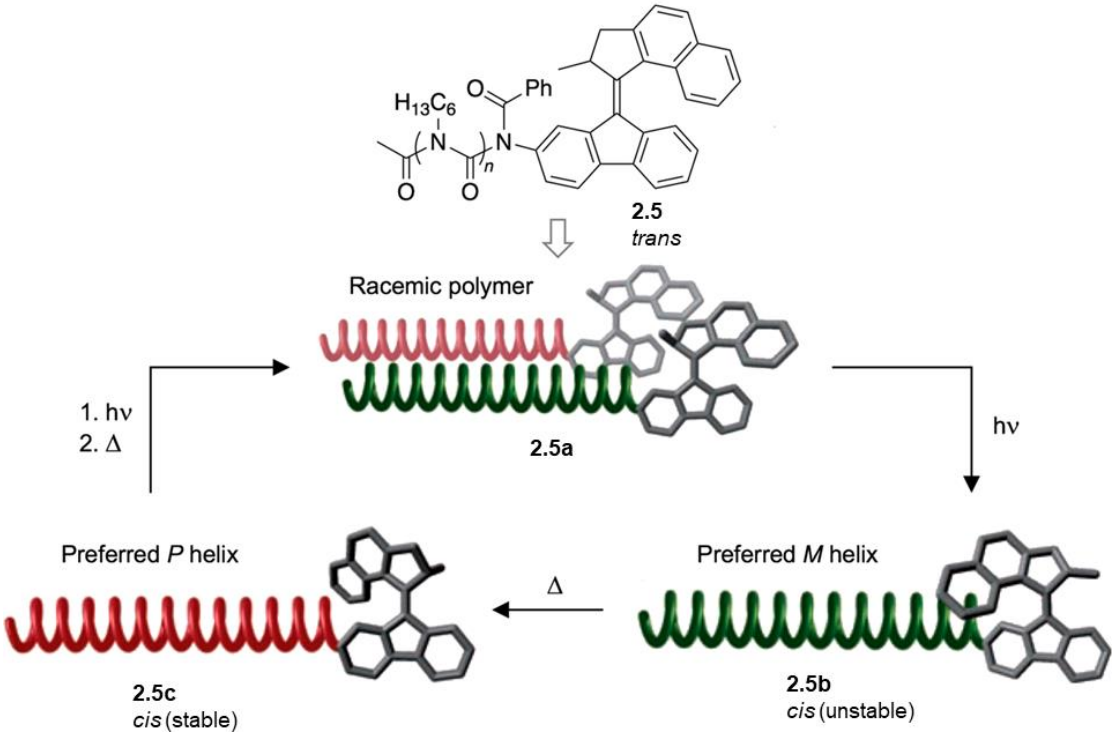

Figure 4. Structure formula of motor functional helical polymer and representation of the photo-switch control of the helicity of the polymer chain.

The overcrowded alkene motor was also used in another study by the same group.[10] Oligobipyridine ligands **2.6** were functionalized with unidirectional rotary motor (Figure 5). At the beginning, the motor moiety of oligomers is in the stable (*P,P*)-*trans* state, in the presence of Cu ions, oligomer chains **2.6** folded into a helicate **2.7**. Upon irradiation, the motor was stimulated to the less stable (*M,M*)-*cis* form and dissociated two molecular helix to yield intramolecular helicates **2.7a** with the same handedness (P). Then, thermal isomerization led to the stable (*P,P*)-*cis* form, and causes inversion of the chirality of the helicate **2.7b** from P to M. The two helicates can be restored by completing the rotary cycle and return to stable *trans* state with further irradiation and thermal interconversion. The content and chirality of helical oligomers can be controlled by the state of the alkene motor (Figure 5).

10 Zhao, D.; van Leeuwen, T.; Cheng, J.; Feringa, B. L. *Nat. Chem.* **2017**, *9*, 250-256.

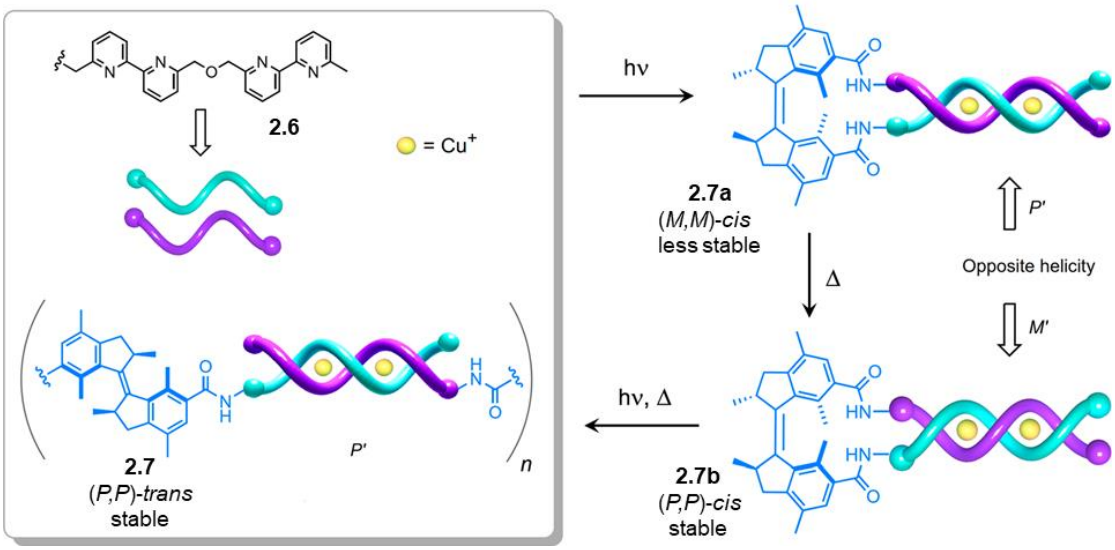

Figure 5. Formula of the oligomer combining molecular motor and bis(bipyridine) ligand components, represent the photo switching between oligomeric and monomeric double-stranded Cu helicates of different handedness.

1.3 Photo-switchable materials

Li and coworkers studied a reversible visible-light-switch system in both organic solvents and liquid-crystal media.[11] Two enantiomeric azo photoswitches, (*S*,*S*)-**2.8** and (*R*,*R*)-**2.8**, with axial chirality and large conjugation were prepared (Figure 6). These molecules exhibited a fast, reversible photoisomerization process needing only visible-light irradiation. When doped in an achiral liquid crystal with a high concentration, the molecules self-assembled into a helical conformation which proved to be tunable and dynamically reversible under irradiation with visible light. While if doped with only a low concentration in the liquid crystal, it formed an optically tunable achiral nematic phase and a helical structure could be obtained reversibly under irradiation of visible light (Figure 6).

11 Wang, Y.; Urbas, A.; Li, Q. *J. Am. Chem. Soc.* **2012**, *134*, 3342-3345.

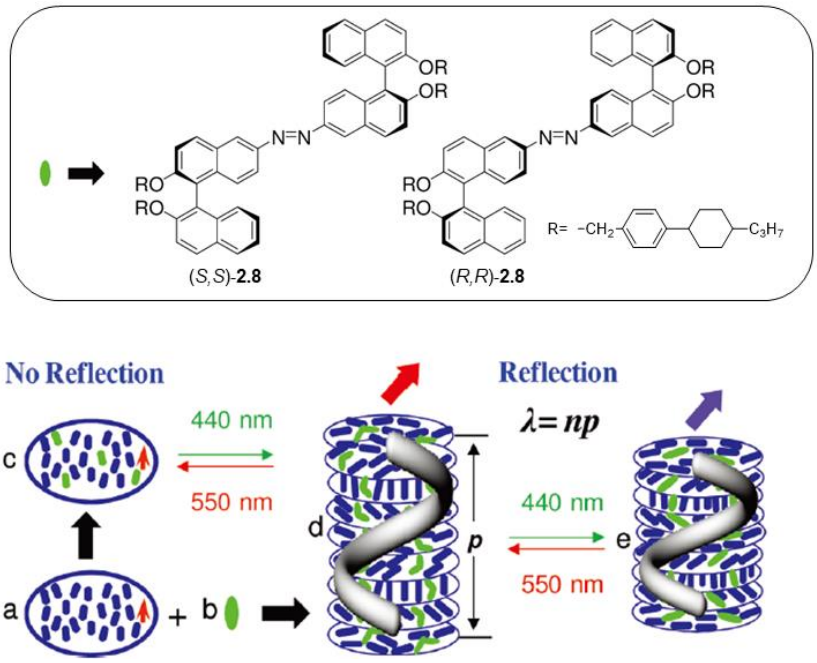

Figure 6. Structure of photo-control axially chiral switches (*S*,*S*)-**2.8** and (*R*,*R*)-**2.8**; Schematic presentation of process of the reflection wavelength of photo-driven chiral switches (*S*,*S*)-**2.8** and (*R*,*R*)-**2.8** (green) in an achiral liquid crystal (blue) reversibly tuned only by visible light: a) achiral nematic host; b) photo-driven chiral switch; c) achiral photoresponsive nematic phase; (d, e) photo-switchable chiral nematic phase which pitch length decrease from d) to e).

1.4 Photo controlled molecular machine

Leigh and coworker studied the first photo-driven catenane rotary motor **2.9** which can shift a complete circulation of one closed ring.[12] In [3]Catenane **2.9** (two of the small rings mechanically locked onto the bigger ring) the presence of the first small ring will block the rotational motion of the second small ring to ensure an overall stimuli-driven motion around the larger ring. The large ring is a track for the small rings, and possess four different stations: fumaramide (A, green), methyl-substituted tertiary fumaramide (B, red), succinamide (C, orange), and amide (D, purple). The four stations where the interlocked small rings can non-covalently bind were selected to display different affinities with the order A > B > C > D. As the fumaramide station A was attached with a benzophenone unit, the isomerization of this station can be photosensitized at 350nm a wavelength long enough to avoid the isomerization of station B. Different wavelengths were selected to switch the binding stations A and B.

12 Leigh, D. A.; Wong, J. K. Y.; Dehez, F.; Zerbetto, F. *Nature* **2003**, *424*, 174-179.

At the beginning, one of the small ring (pink ring) resides on the strongest binding station, A, then the second ring (blue ring) interlocked with the second favored station, B. After irradiation at 350 nm, the E→Z isomerization was carried out at station A, weakens its binding for the small ring and cause the motion of the pink ring to the succinic amide ester station, C (process 1). Due to the presence of the blue rings residing around the tertiary fumaramide station, B, the pink ring was forced to move with a counter-clockwise direction. Then, upon irradiating at 250 nm, isomerization of station B caused the blue ring to relocate to the single amide station, D (process 2). Again, this occurred counter-clockwise because the presence of pink ring blocked the direction of movement. The initial conformation can be restored using an irradiation under 400-670 nm with a stoichiometric amount of Br_2 or thermal back-isomerization with a catalytic amount of ethylenediamine (process 3). After three steps, the position of the two rings is swapped, thus the same sequence of three stimuli need to be carried on again to reset the system fully and shuttle the ring to their initial position (Figure 7).

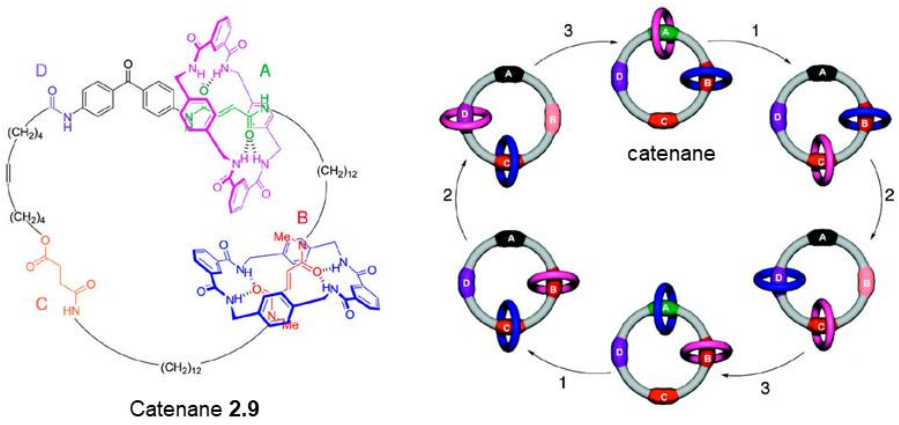

Figure 7. Stimuli-induced unidirectional rotation in a four-station ring. (1) photoisomerization of the fuaramide station (A, from green to black) under irradiation with 350 nm light; (2) photoisomerization of the tertiary fumaramide station (B, from red to pink) under irradiation with 250 nm light; (3) back reset of the A and B stations upon heating or by irradiation with 400-670 nm light in the presence of Br_2.

1.5 Photo-switchable capsule

Flood and coworkers prepared a photoswitchable system where light stimulus is employed to trigger the photo-dependent release and reuptake of chloride ions in organic solvent.[13] A

13 Hua, Y.; Flood, A. H. *J. Am. Chem. Soc.* **2010**, *132*, 12838-12840.

chiral aryl-triazole foldamer **2.10** terminated with two azobenzene groups has been prepared (Figure 8). It defines a folded host for chloride ions that unfolds with UV light to release the chloride. The *trans* dominated helical foldamer is more preorganized for the chloride binding and an ~10-fold reduction in binding affinity was induced by the photoisomerization in CH_3CN. A robust chloride binding and release cycle can be achieved by alternately irradiating the sample with UV and visible light.

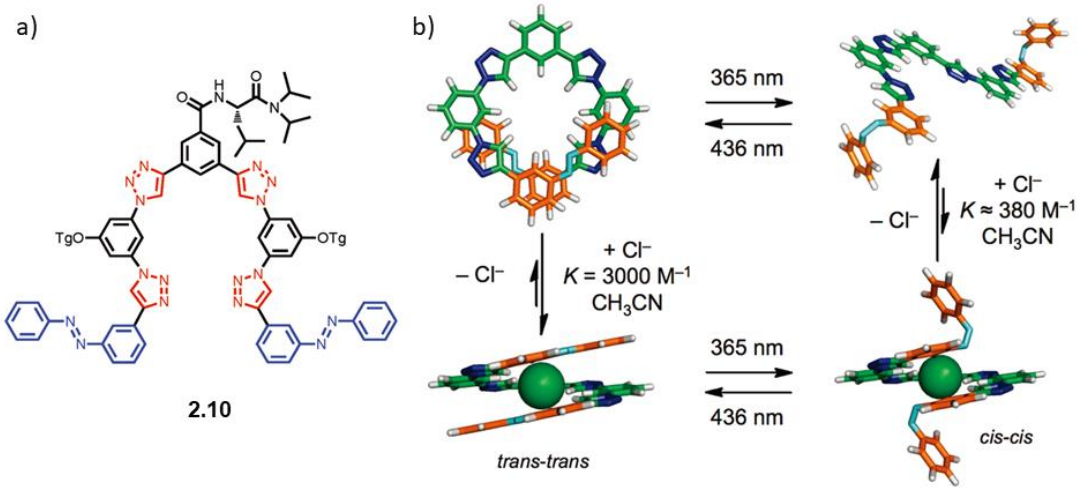

Figure 8. a) Structure of the aryl-trizaole foldamer; b) proposed cycle of photo-switch binding and release of chloride.

Rebek and co-workers reported the use of 4,4'- dimethylazobenzene **2.11** (Figure 9) to control the capture and release of guest compounds in a capsule.[14] In order to bind to capsule [**2.13**]$_2$, **2.12** need to adopt twisted conformation (Figure 9b), as a result, the *trans*-conformation of **2.11** showed a stronger affinity for host [**2.13**]$_2$ than **2.12**. In the mixture, **2.11** and [**2.13**]$_2$ favored to form complex. Upon irradiating with a 365 nm light, isomerization of **2.11** into its *cis* form caused its release from the capsule and allow uptake of another guest **2.12** from the solution. Since the process is reversed by heat, the *trans*/*cis* isomerization of **2.11** becomes a switch for host capsules to catch different kinds of guest.

14 Dube, H.; Ams, M. R.; Rebek, J. *J. Am. Chem. Soc.* **2010**, *132*, 9984-9985.

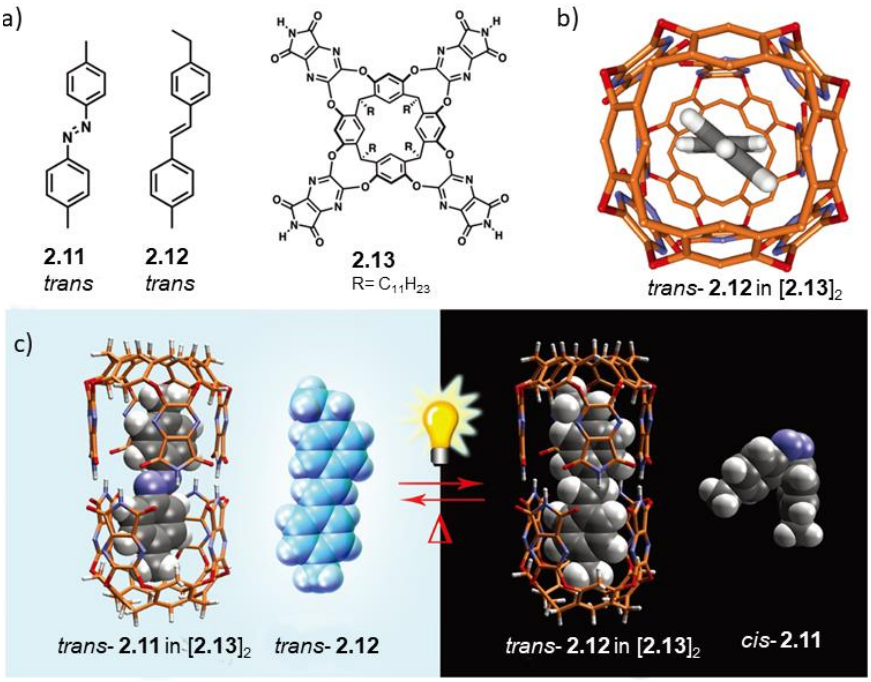

Figure 9. A supramolecular fluorescence-switching device; (a) structure of azobenzene **2.11**, stilbene **2.12**, and **2.13**; (b) encapsulated *trans*-stilbene **2.12** assumes a twisted conformation in [**2.13**]$_2$ (top view). (c) **2.12** fluoresces when it is free in solution. Upon irradiation azobenzene **2.11** is expelled from the capsule, **2.12** is encapsulated, and its fluorescence is quenched. Heating restores the starting point.

2. Compounds design

Over the last three decades, stimuli-responsive supramolecular systems have been extensively investigated for their application as molecular machines,[15] as molecular probes[16] and smart materials.[17] The conformations of molecules can be changed by tuning the properties of the environment, for example, temperature, pH and pressure, as a result, the properties and functions of those molecules can be affected by external stimulation. Controlling size and shape of molecule is an important feature of these systems. Incorporating stimuli-responsive groups into assemblies is always used as an efficient strategy to control their conformation.

Helix is a pattern commonly found in biomolecules such as proteins and nucleic acids.[18] Helical structures serve not only as structural components but also as functional units. Many helical structures are prepared using covalent linkages or non-covalent assemblies. Our group

15 Baroncini, M.; Silvi, S.; Credi, A. *Chem. Rev.* **2020**, *120*, 200-268; van Leeuwen, T.; Lubbe, A. S.; Štacko, P.; Wezenberg, S. J.; Feringa, B. L. *Nat. Rev. Chem.* **2017**, *1*, 0096.
16 Yagai, S.; Kitamura, A. *Chem. Soc. Rev.* **2008**, *37*, 1520-1529.
17 Tian, H.; Wang, Q.-C. *Chem. Soc. Rev.* **2006**, *35*, 361-374.
18 Guichard, G.; Huc, I. *Chem. Commun*. **2011**, *47*, 5933-5941.

has prepared the aromatic oligoamide sequences **H1** and **H2** (Figure 10), both of them can fold into helical architectures which are stabilized by hydrogen bonding, conjugation, electrostatic repulsions and aromatic stacking. Furthermore, **H1** and **H2** can also fold around dumbbell shape rod to form foldaxanes (Figure 11c and 12). This conformation is supported by the intermolecular hydrogen bonds between binding sites (Figure 10d), which are located at the extremity of the helix (P^C, namely 2,6-pyridinedicarboxamide, hydrogen-bond donors), and anchor points on the rod (carbonyl hydrogen-bond acceptors).

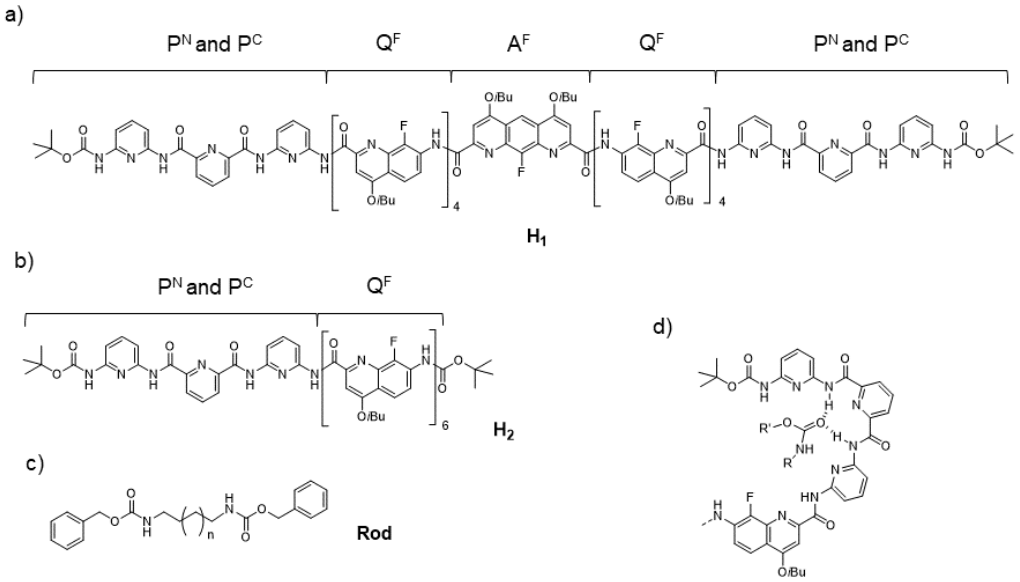

Figure 10. Formulas of aromatic helix **H1** (a), **H2** (b) and guest rod (c). Intermolecular hydrogen bonds (d) between helix and rod.

Symmetrical helix **H1** exist as single and double helical conformations,[19] (Figure 11). In solution, double helices prevail, signal of the single helices was barely detected at equilibrium by ^{1}H NMR. After the addition of rod, complexes consisting of a single helix and one equivalent of guest were confirmed by titration data and mass spectrometry. The binding affinity of the single helix for dumbbell shape guests is strong enough to overcome its propensity to form double helix. In the presence of a rod, a double helix can dissociate to single helices, then the single helix can unfold and refold around the rod to form a foldaxane.

19 Gan, Q.; Ferrand, Y.; Bao, C.; Kauffmann, B.; Grélard, A.; Jiang, H.; Huc, I. *Science* **2011**, *331*, 1172; Wang, X.; Wicher, B.; Ferrand, Y.; Huc, I. *J. Am. Chem. Soc.* **2017**, *139*, 9350-9358; Wang, X.; Gan, Q.; Wicher, B.; Ferrand, Y.; Huc, I. *Angew. Chem., Int. Ed.* **2019**, *58*, 4205-4209; Ferrand, Y.; Gan, Q.; Kauffmann, B.; Jiang, H.; Huc, I. *Angew. Chem. Int. Ed.* **2011**, *50*, 7572-7575.

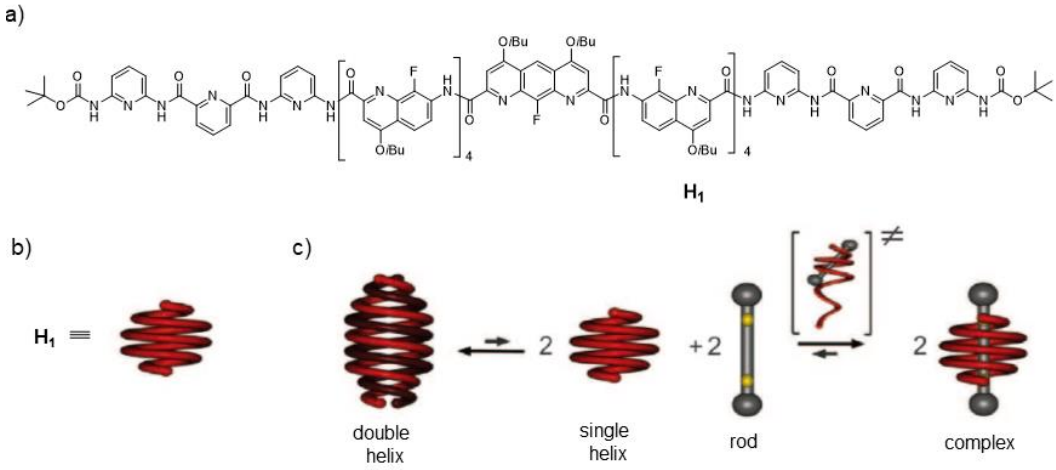

Figure 11. Formula (a) and cartoon (b) of **H1**. Equilibrium (c) between **H1** as double helices, single helices, or complexes with rod-like guests. The formation of a complex with a dumbbell guest requires the unfolding and refolding of the helix.

Later, unsymmetrical sequence **H2** was reported as a probe to assess the distance between the extremities of a rod and its conformational change.[20] **H2** can form parallel and antiparallel double helices (Figure 12). Only the antiparallel double helices can bind to dumbbell-shaped bichromophoric rods to form the so-called foldaxane. In solution, delayed luminescence can be detected because the reversible electronic energy transfer (REET) proceed between two chromophoric ends of the free and flexible rod. After binding with the double helix, the rod is rigidified and the distance between two chromophoric groups is locked. As a result, the chromophores showed their own photophysical properties without interaction between each other.

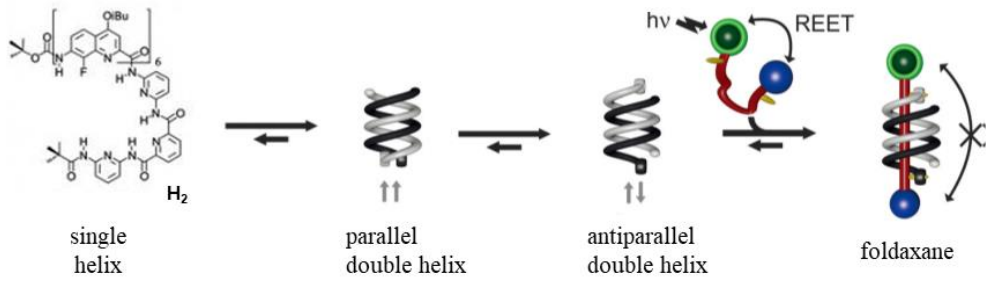

Figure 12. Representation of the equilibrium of single helix and double helix, double helix contains parallel and antiparallel conformations. Antiparallel can bind with rod and change its photophysical properties.

20 Denisov, S. A.; Gan, Q.; Wang, X.; Scarpantonio, L.; Ferrand, Y.; Kauffmann, B.; Jonusauskas, G.; Huc, I.; McClenaghan, N. D. *Angew. Chem. Int. Ed.* **2016**, *55*, 1328-1333.

Besides helical structures, aromatic sheets structure is another attractive secondary motif. Aromatic sheet structures formed not only thanks to hydrogen bonding, but also via aromatic stacking.[21]

Our group prepared two-stranded aromatic sheets **H$_3$** from turn units (**T**) and 1,8-diaza-2,7-anthracene-dicaboxylic acid (**A^H**).[22] The aromatic sheets **H$_3$** can adopt a parallel aromatic sheet conformation favored by a better π-π aromatic stake (Figure 13).

The photoreaction of free **A^H** units was first investigated, under light irradiation (320-390 nm), and only the antiparallel photoproduct was obtained due to dipolar replusion (Figure 13c). Furthermore, the same irradiation was also carried out with aromatic sheets **H$_3$**, and only the parallel photoproduct **H$_{3P}$** was observed (Figure 13b). The **T** units can induce the **A^H** at parallel orientation thus the [4+4] photocycloaddition leads quantitatively to the parallel photoproduct.

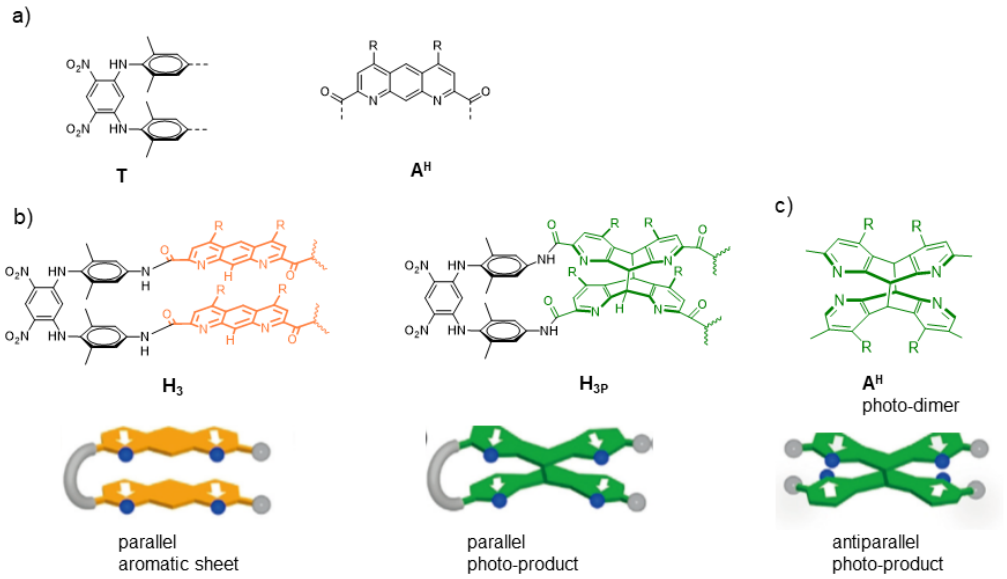

Figure 13. a) Structure of building segments **T** and **A^H**; b) the diazaanthracene-based aromatic sheet **H$_3$**, two diazaanthracene units are parallel with each other (orange) and corresponding photoproduct **H$_{3p}$** is also a parallel structure (green); c) photoproducts of free **A^H** adopt antiparallel structure.

Our group also designed the helix-sheet-helix architecture **H$_4$** based on three-stranded aromatic sheets (red and black, Figure 14a) and two helical segments (blue, Figure 14a)[23]. The three aromatic sheets (red, Figure 14a) were connected by two turn units (black, Figure 14a). **H$_4$** is C_2 symmetrical, three aromatic sheets have a parallel arrangement and they folded so as

21 Sebaoun, L.; Maurizot, V.; Granier, T.; Kauffmann, B.; Huc, I. *J. Am. Chem. Soc.* **2014**, *136*, 2168-2174.
22 Gole, B.; Kauffmann, B.; Maurizot, V.; Huc, I.; Ferrand, Y. *Angew. Chem. Int. Ed.* **2019**, *58*, 8063-8067.
23 Lamouroux, A.; Sebaoun, L.; Wicher, B.; Kauffmann, B.; Ferrand, Y.; Maurizot, V.; Huc, I. *J. Am. Chem. Soc.* **2017**, *139*, 14668-14675.

to form a basket like object, whose aperture size depends on the degree of curvature of the central monomers (Figure 14c). The opening cavity of **H4** can work as a window and pathway to bind and release a guest (Figure 14d), such as glycolic acid.

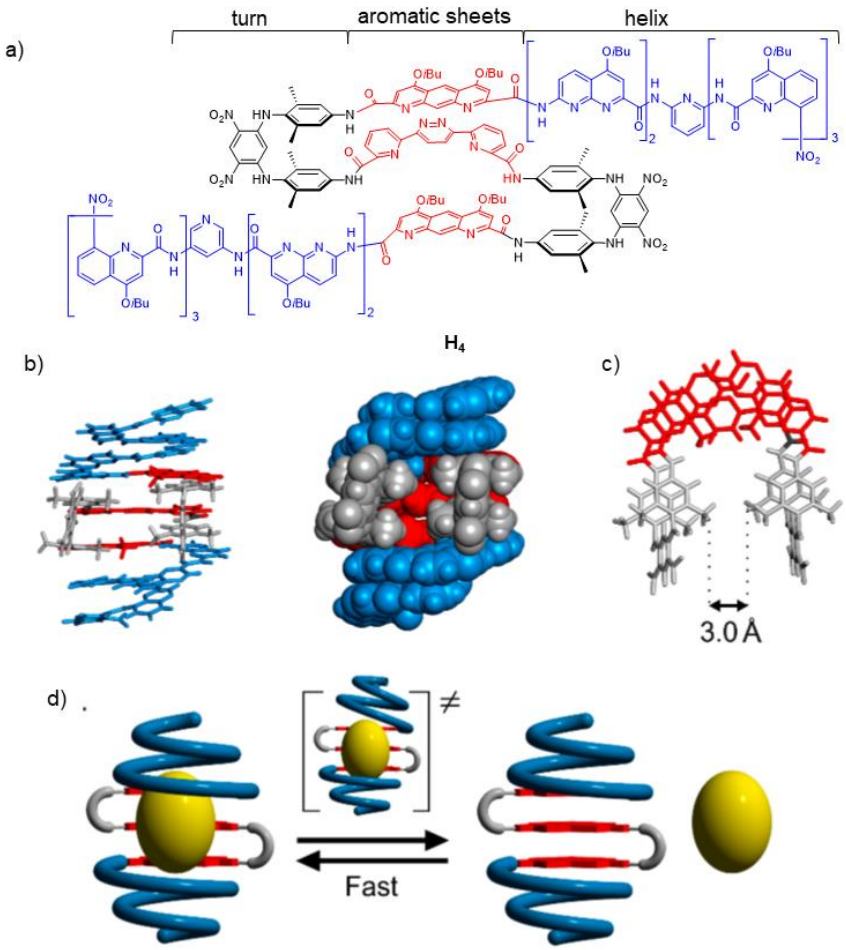

Figure 14. Representation of the aromatic foldamer-based helical capsules **H4**; a) formula of **H4**, contained helix (blue), central sheets (red) and turn units (black); X-ray single crystal structure of b) **H4** and c) aromatic sheets segment picked from crystal packing; d) schematic representation of helix-sheet-helix structure that can bind and release a guest.

In this chapter, we will show the design of a new multi-stranded foldamer which contained helices, aromatic sheets and turns (Figure 15a). We expect that it can form the similar structure as the one of **H4**, in which turn and aromatic sheet segments can form an opening cavity for the binding of guest molecules. While we also have bind site at each extremity of the helical segment, it will allow the foldamer to fold around rod-shape guest to form complex named foldaxane (Figure 15b, left pathway). The multiple binding site and the side aperture of **1** will also open up the possibility to bind to T-shaped guest (Figure 15b, right pathway).

Furthermore, photoreactions between aromatic sheets can also be performed under the light irradiation. Reversible [4+4] cycloaddition of two diazaanthracene sheets result in photodimer as **H3P** (Figure 13b). The photoreaction may change the size of cavity leading to the release of the guest.

In this work, I have several collaborators Dr. Bappaditya Gole, Dr. Mcclenaghan Nathan and Dr. Anh Thy Bui. The compounds were prepared with Bappa. Nathan and Anh Thy helped us a lot in the photoreaction.

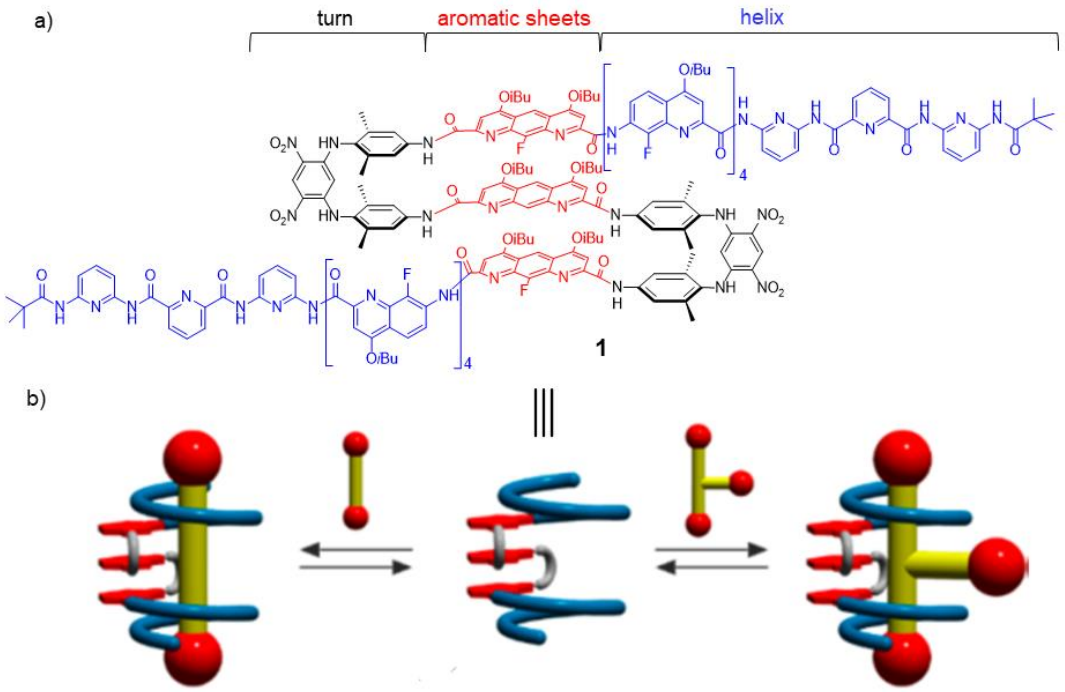

Figure 15. a) formula of **1**, contained helix (blue), central sheets (red) and turn units (black); b) Cartoon representation of **1** that can bind and release a dumbbell shape rod (left) or a T-shaped guest (right).

3. Result and discussion

3.1 Synthesis

3.1.1 Synthesis of foldamers

Six different aromatic monomers were used for the preparation of the helix-sheet-helix foldamer described in this chapter (Figure 16): 2,6-diaminopyridine ($\mathbf{P^N}$), 2,6-pyridinedicarboxylic acid ($\mathbf{P^C}$), 7-amino-8-fluoro-2-quinolinecarboxylic ($\mathbf{Q^F}$), 1,8-diaza-9-

fluror-2,7-anthracene-dicaboxylic acid ($\mathbf{A^F}$), 1,8-diaza-2,7-anthracene-dicaboxylic acid ($\mathbf{A^H}$) and dinitro-di(xylylamino)-phenyl turn (**T**).[24] Local preferential interactions between each amide and adjacent aryl rings set a favorable orientation at each aryl-amide linkage, which results in stable helical shape. The cavity of the helix depends on the size of monomer (i.e. number of aromatic rings) and positions of amine and acid substituents on aryl rings. This cavity allows the interpenetration of an alkyl chain, due to the hydrogen bonding between terminal 2,6-pyridinedicarboxamide units and carbamate groups of a guest (Figure 10d).

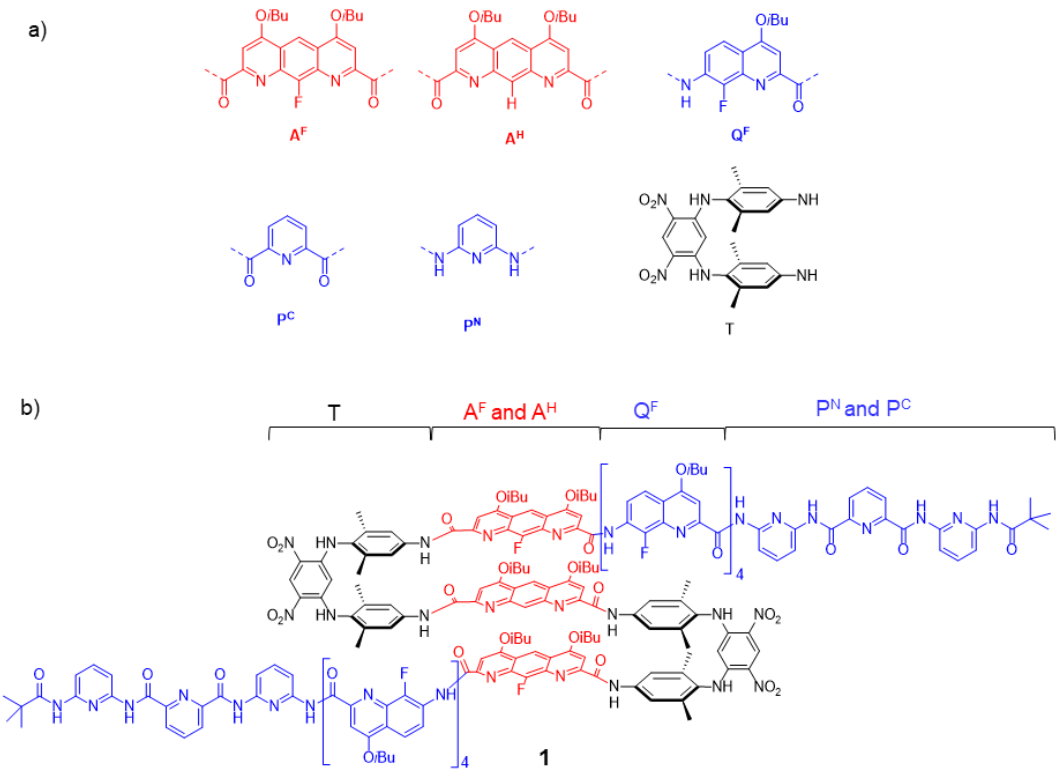

Figure 16. Representation of the aromatic foldamer **1**; a)color coded formula and corresponding letters of monomer units, $\mathbf{A^F}$ (red), $\mathbf{A^H}$ (red), $\mathbf{Q^F}$ (blue), $\mathbf{P^N}$ (blue), $\mathbf{P^C}$ (blue) and **T** (black); b) formula of **1**, contained helix, central sheets and turn units.

What should be mentioned first is that Q^F/P sequences (for example $Q^F{}_6P_3$ and $Q^F{}_4P_3$, Figure 11 and 12) can self-assemble in double helix in solution. For the coupling reaction between oligomers **9** and **13**, **13** was activated from acid to its corresponding acid chloride and then reacted it with amine **9**. If the precursors can form double helices, the reactivity of the amine group of Q^F units is drastically decreased as it may be hidden in the double helix. As a

24 Ferrand, Y.; Huc, I. *Acc. Chem. Res.* **2018**, *51*, 970-977.

consequence, dimethoxybenzyl (DMB) group was employed to prevent precursors to form double helices (see chapter I).

7-amino-8-fluoro-2-quinolinecarboxylic acid (Q^F) protected with Boc and methyl ester has been reported, and the synthetic strategy to prepare dimer acid **6** can be found in chapter I. Ghosez's reagent was used to convert **6** to its corresponding acid chloride and reacted with oligomer **7**[25] to afford the DMB protected sequence **8**. Trifluoroacetic acid (TFA) cannot be used to remove Boc groups due to its poor orthogonality with DMB groups, thus HCl (4M in dioxane) solution was used. The heptamer amide **9** was obtained in good yield after purification by GPC.

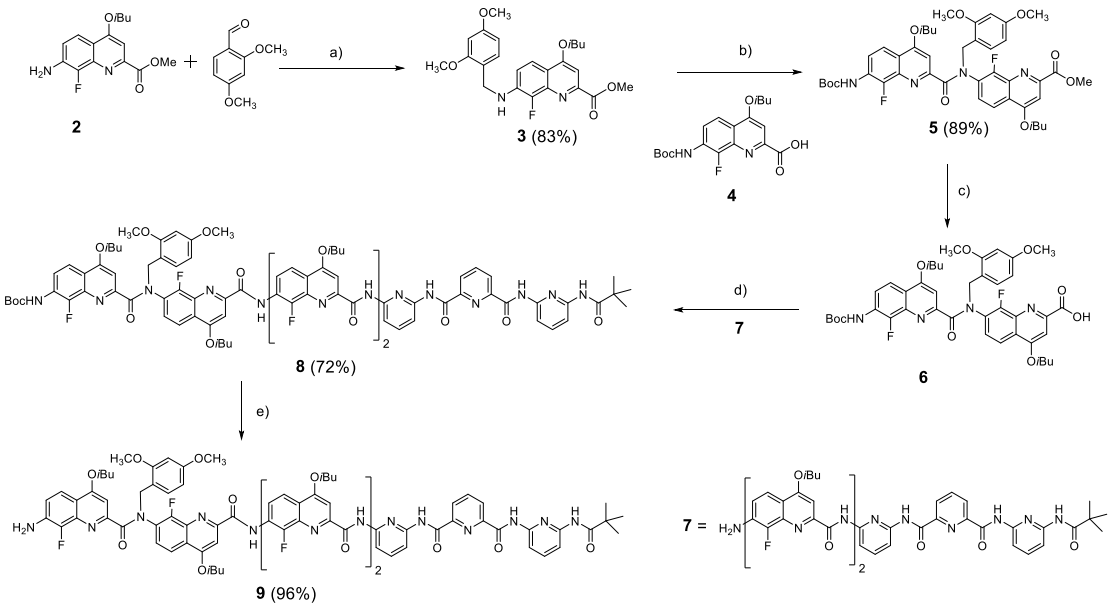

Scheme 1. Synthetic pathway of oligomer **9**. Reagents and conditions: (a) sodium triacetoxyborohydride, 1,2-dichloroethane, 18 hours; (b) (i) 1-Chloro-*N*,*N*,2-trimethyl-1-propenylamine, dry $CHCl_3$, 2 hours, room temperature; (ii) dry DIPEA, dry $CHCl_3$, 12 hours, room temperature; (c) NaOH, MeOH/H_2O/THF, 3 hours, room temperature; (d) (i) 1-Chloro-*N*,*N*,2-trimethyl-1-propenylamine, dry CH_2Cl_2, 2 hours, room temperature; (ii) dry DIPEA, dry CH_2Cl_2, 12 hours, room temperature; (e) dioxane, 4M HCl in dioxane, 3 hours, room temperature.

The synthesis of helix-sheet-helix **1** was achieved according to the route described in Scheme 2. The monostranded sheet **10** was prepared from A^F according to our previous procedures with minor changes.[26] Amino monostranded sheet **10** was coupled twice to the

25 Bao, C.; Gan, Q.; Kauffmann, B.; Jiang, H.; Huc, I. *Chem. Eur. J.* **2009**, *15*, 11530-11536.
26 Lamouroux, A.; Sebaoun, L.; Wicher, B.; Kauffmann, B.; Ferrand, Y.; Maurizot, V.; Huc, I. *J. Am. Chem. Soc.* **2017**, *139*, 14668-14675.

diaza-anthracene diacid **11** using PyBOP (benzotriazol-1-yloxytripyrrolidinophosphonium hexafluorophosphate) as activating agent to obtain the tristranded sheet **12**. Then, LiI is used to cleave the methyl ester of **12** and the corresponding diacid **13** was afforded. DMB protected helix-sheet-helix foldamers **14** was obtained by coupling twice oligomer **9** to diacid **13**. Finally, to deprotect DMB groups, the foldamer **14** was treated with TFA to afford final foldamer **1**.

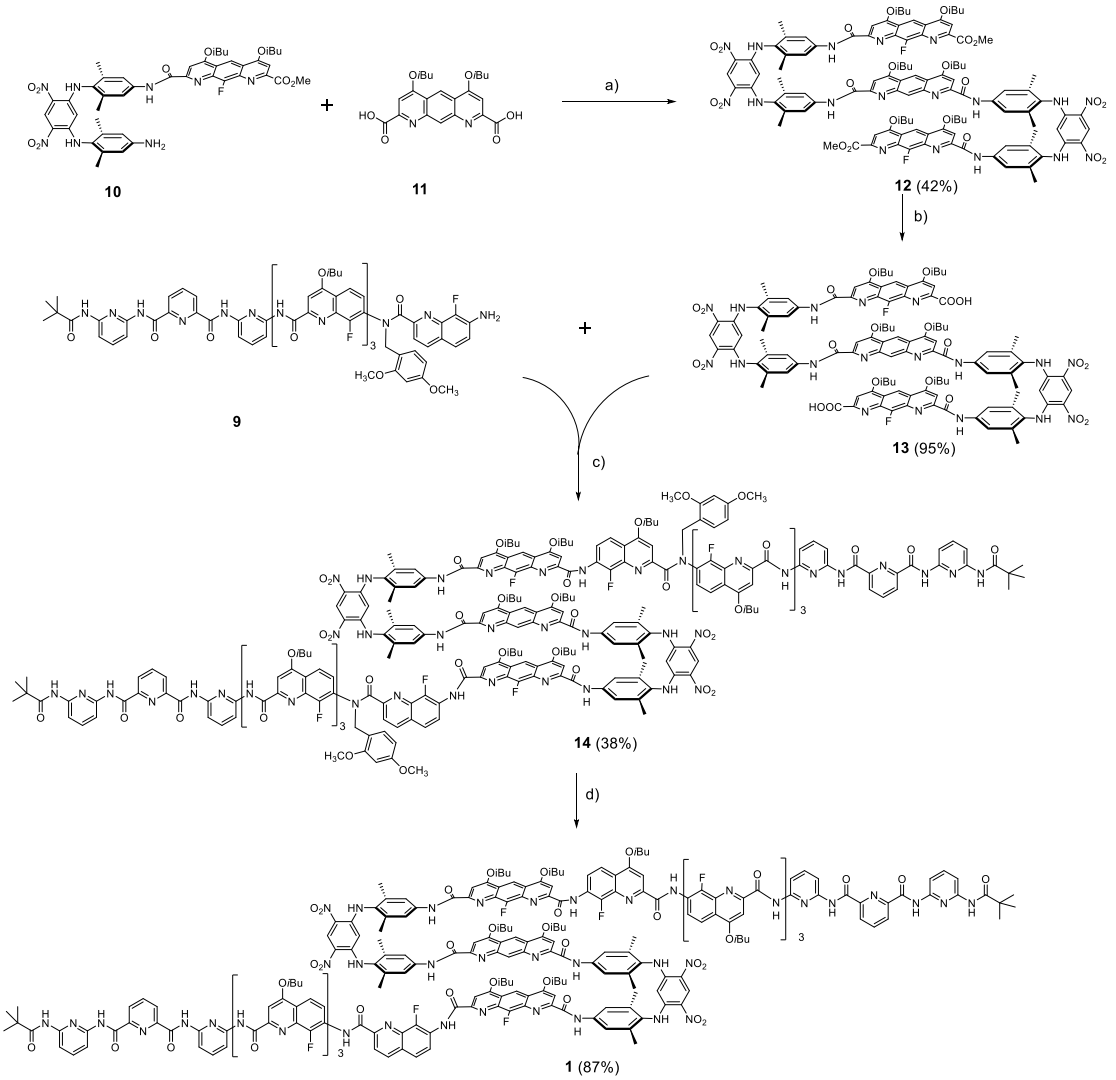

Scheme 2. Synthesis of oligomer **1**. Reagents and conditions: (a) PyBOP, DIPEA, $CHCl_3$, 2 days, 45 °C. (b) LiI, ethyl acetate, 12 hours, 78 °C; (c) (i) $(COCl)_2$, $CHCl_3$, 2 hours, room temperature. (ii) DIPEA, $CHCl_3$, 16 hours, room temperature; (d) $CHCl_3$, TFA, 36 hours, room temperature.

3.1.2 Synthesis of rod

Foldamer **1** was expected to fold around rod-like guest to form foldaxane, furthermore, turn and aromatic sheet segments in **1** can form an aperture on the side of the architecture thus

allowing the complexation of T-shape guest. Two types of rod were prepared in this chapter linear dumbbell shaped and T-shaped guest (Figure 17).

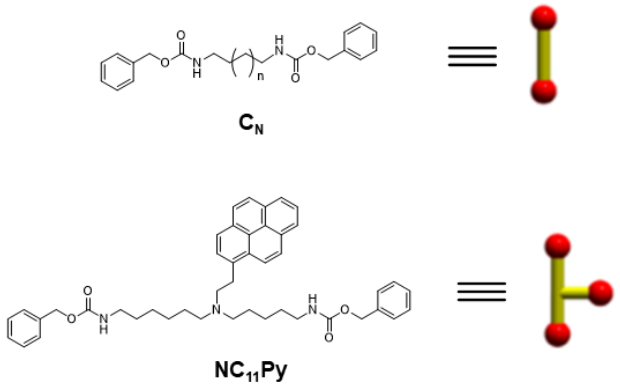

Figure 17. Representation of the rod-like ($\mathbf{C_N}$) and T-shape ($\mathbf{NC_{11}Py}$) guest.

Carbamate groups act as hydrogen-bond acceptors and are located at each extremity of the rod. The distance between two carbamate functions is determined by the number of carbon atoms in alkyl chain (Scheme 3). To achieve a strong binding between foldamer and rod, the length of rod should match the size of foldamer. Rod-like guest $\mathbf{C_{12}}$ was prepared directly from the reaction between benzyl chloroformate and 0.5 equivalent of diamine. In $\mathbf{C_{12}}$, twelve carbon atoms are between two carbamate functions which is expected as best length for foldamer **1** in our molecular modeling.

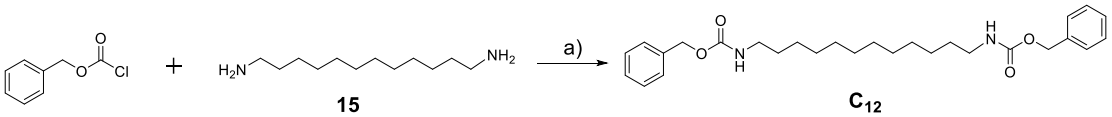

Scheme 3. Synthetic pathway of $\mathbf{C_{12}}$ rod. Reagents and conditions: (a) NaOH (4M aqueous), 16 hours, room temperature, 86%.

T-shaped, Pyrene functionalized dicarbamate rod was also prepared. To find the right size for this new rod, two rods were prepared (Scheme 4). Amine functionalized segment **18** was obtained from the coupling between benzyl chloroformate and mono-protected amine **17**. After deprotection of the Boc group in acidic medium, amine segment **19** was obtained. The second part of the rod was obtained through the tosylation of the hydroxyl groups of **20** that after reaction with **19** afford rod $\mathbf{NC_{11}}$.

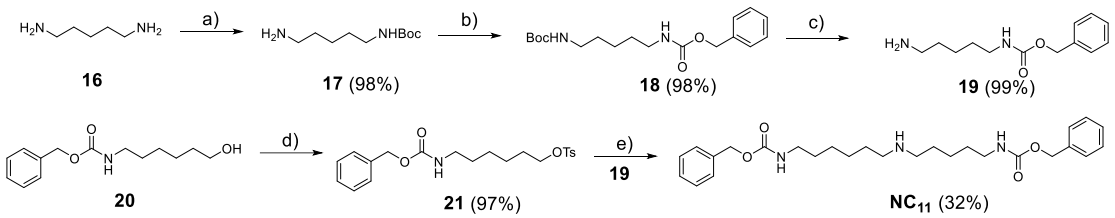

Scheme 4. Synthetic pathway of **NC$_{11}$** rod. Reagents and conditions: (a) Di-tert-butyl-dicarbonate, dry $CHCl_3$, 5 hours, room temperature; (b) Benzyl chloroformate, NaOH (4M aqueous), 16 hours, room temperature; (c) Trifluoroacetic acid, Dichloromethane, 3 hours, room temperature; (d) TsOCl, *N*,*N*-dimethylpyridin-4-amine, NEt_3, DCM, 6 hours; (e) Dry DMF, NEt_3, 16 hours, 80 °C.

Rod **NC$_{11}$** contains a secondary amine which can be functionalized with a pyrene moiety. The pyrene moiety was prepared as shown in Scheme 5. Carboxylic acid functionalized pyrene **22** was reduced to yield pyrene **23**. Then after a treatment with TsOCl, pyrene **24** was obtained and refluxed in acetonitrile with rod **NC$_{11}$** to give **NC$_{11}$Py** as as a T-shaped guest.

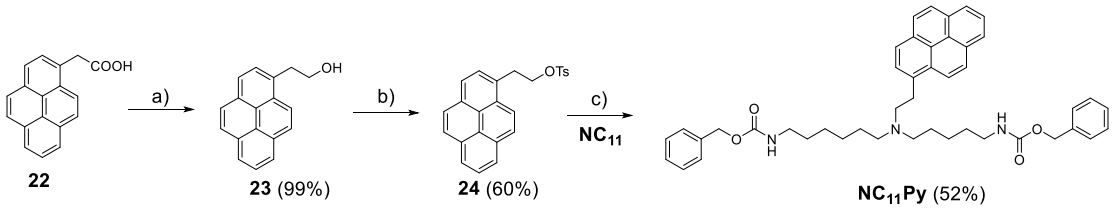

Scheme 5. Synthetic pathway of **NC$_{11}$Py** rod. Reagents and conditions: (a) $LiAlH_4$, dry THF, 12 hours, room temperature; (b) TsOCl, *N*,*N*-dimethylpyridin-4-amine, NEt_3, DCM, 6 hours; (c) K_2CO_3, dry acetonitrile, reflux, 24 hours.

3.2 Characterization of foldamer

To investigate the structure of foldamer **1**, NMR studies were first carried out (Figure 18). ^{1}H NMR spectra revealed a set of sharp peaks at room temperature in $CDCl_3$ indicating a single conformation of foldamer **1**. In the NH amide region, nine peaks marked with red cycles were identified whereas a single H_{ext} (the proton *ortho* to both nitro groups in turns) was found and marked with a green circle. This reveals that foldamer **1** has a symmetrical conformation.

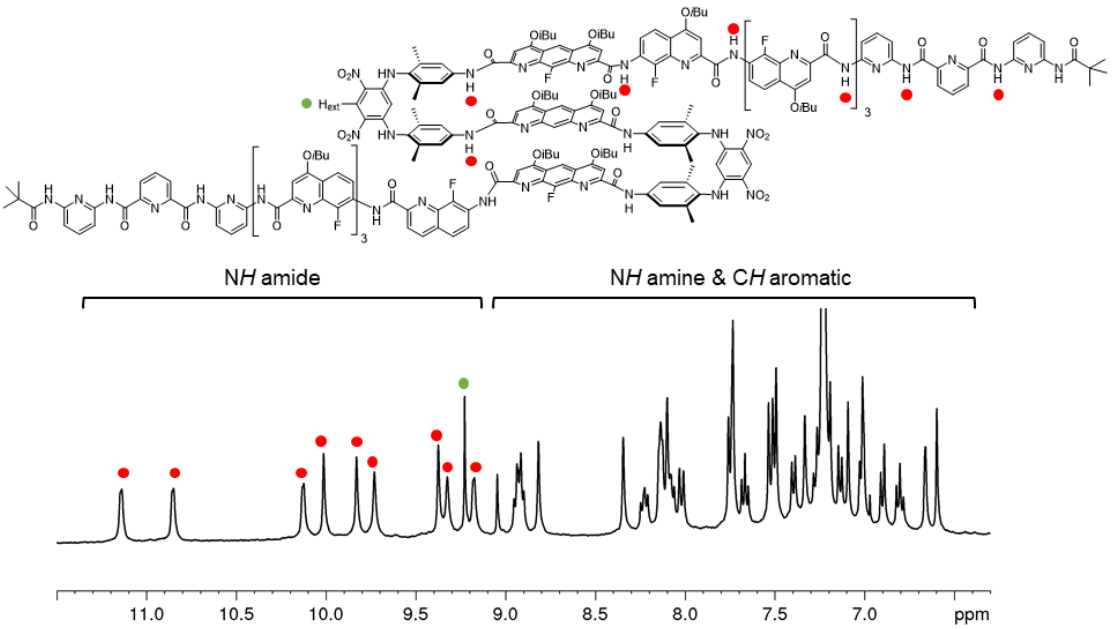

Figure 18. 400 MHz ^{1}H NMR spectrum at 298 K of oligomer **1** in $CDCl_3$. Amide and H_{ext} peaks were marked as red and green cycles, respectively.

^{19}F NMR was also employed to investigate the structure of foldamer **1** (Figure 19). Spectra showed five singlets, divided into two groups (4 & 1): a single signal at -129 ppm corresponding to A^F unit, whereas the second group containing four peaks around -143 ppm correspond to Q^F units. As **1** contains two A^Fs and eight Q^Fs, it means that observing only five peaks indicate a symmetrical structure.

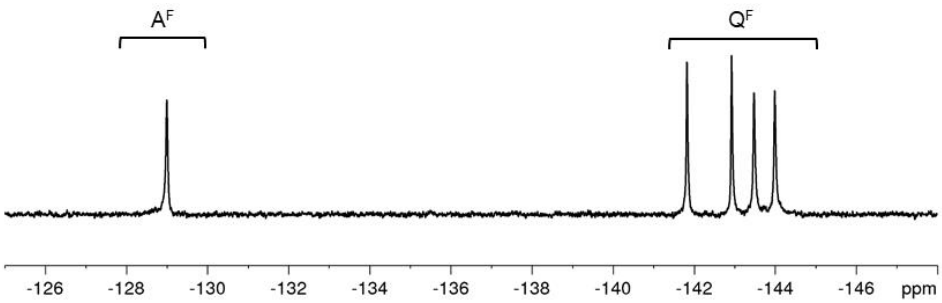

Figure 19. 376 MHz ^{19}F NMR spectrum at 298 K of oligomer **1** in $CDCl_3$. The four signals arising from the quinoline (Q^F) monomer and one signal arising from the diazaanthracene (A^F) monomer.

An energy minimized molecular model was built to understand the structure of foldamer **1** (Figure 20). The two helically folded segments stack above and below the aromatic sheet possess the same P or M helicity. The diazaanthracene units in the aromatic sheet segments revealed a parallel arrangement as they are connected with rigid turns. The model reveals an aperture in between the two turn units (Figure 20b), it will ultimately allow the helix-sheet-

helix to accommodate a T-shape guest. The rigid turns can keep a distance long enough to prevent an intramolecular folding of the two helical segments forming an intramolecular double helix conformation. Foldamer **1** shows an average C_2 symmetry axis perpendicular to the axis of the helix segments.

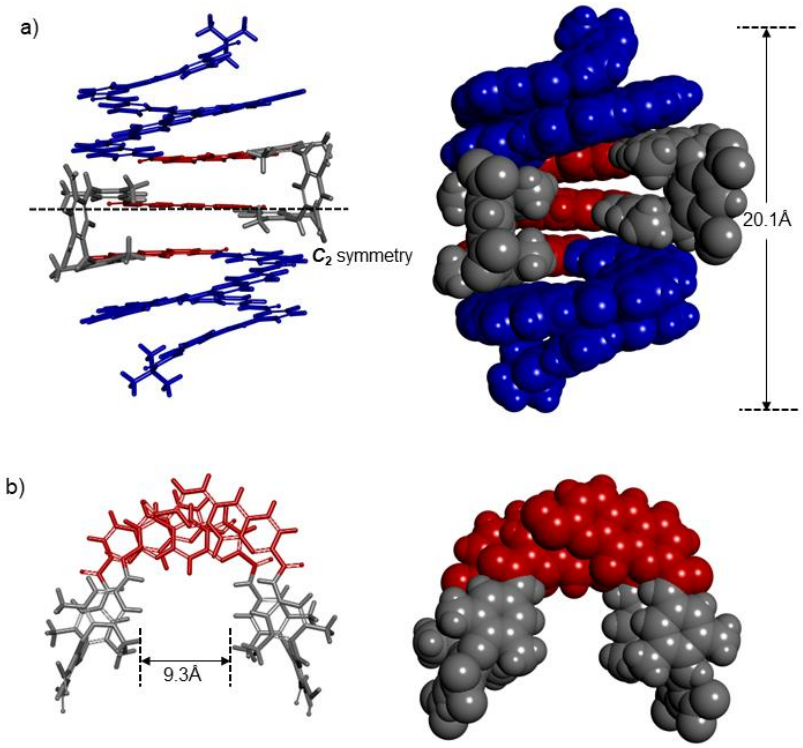

Figure 20. Energy minimized molecular models of the foldamer **1**; a) Side view of **1**, helical segments, diazaanthracene units and turns were marked as blue, red and grey, respectively; b) top view of turn and sheets segments of **1**, The models were produced with Maestro software package, using MMFFs force filed, chloroform as solvent and TNCG as minimization method.

3.3 Host/Guest chemistry

The ability of foldamer **1** to bind to alkyl rod was investigated by NMR. Dicarbamate **C12** rod was first added to foldamer **1**. Upon addition of the rod a new set of ^{1}H NMR signals appeared that can eventually be attributed to the helix-rod complex. The foldaxane is in slow exchange with the free foldamer at the NMR scale time (Figure 21). The intensity of the proton signals of the free foldamer and the complex represents the molar ratio of the corresponding species in solution. By applying the equation show in Figure 21, the binding constants between **1** and **C12** can be calculated as 9.70×10^3 L mol^{-1}. ^{19}F NMR was also performed to present to characterized the binding behavior of **1** (Figure 21, h to n). Upon adding **C12**, the ^{19}F signals

belonging to free **1** decreased and a new set of signals corresponding to foldamer-rod complex emerged, which clearly indicated the binding between foldamer **1** and rod $\mathbf{C_{12}}$.

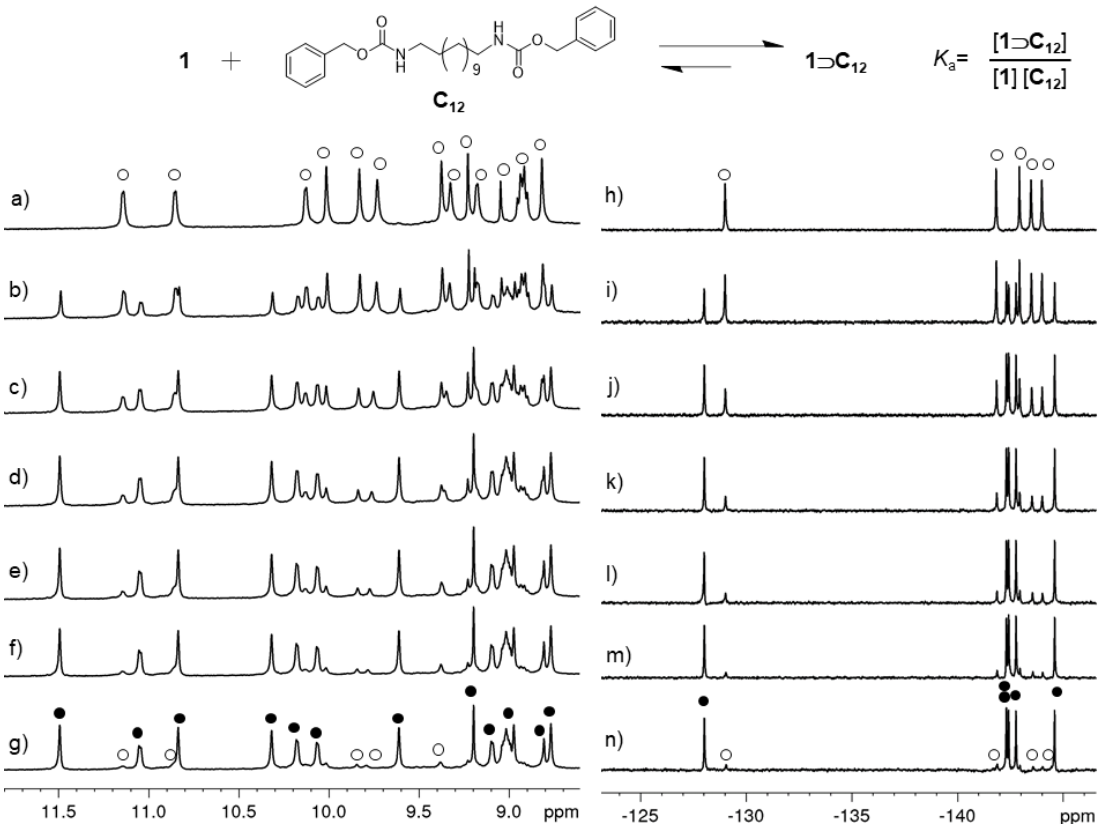

Figure 21. Schematic illustration showing encapsulation of $\mathbf{C_{12}}$ guest within foldamer **1**. Part of the 400 MHz ^{1}H NMR spectra of **1** (1 mM) at 298 K in $CDCl_3$ (a) and after addition of $\mathbf{C_{12}}$ (5 mM in $CDCl_3$) (b) 0.25 equiv.; (c) 0.5 equiv.; (d) 0.75 equiv.; (e) 1.0 equiv.; (f) 1.5 equiv. and (g) 2.0 equiv. The corresponding 376 MHz ^{19}F NMR spectra are given in (h) to (n), respectively. The signals correspond to the starting oligomer **1** are shown in empty cycles and for the host-guest complex, $\mathbf{1 \supset C_{12}}$, marked as black cycles.

The structure of complex $\mathbf{1 \supset C_{12}}$ was also confirmed by X-ray crystallography. Fortunately, we obtained single crystals suitable for X-ray analysis for $\mathbf{1 \supset C_{12}}$. The single crystals were grown by slow diffusion of hexane into a chloroform solution and the structure was solved in the *P*-1 space group. The structure revealed that the two helical segments remain above and below the tristranded aromatic sheet in a "canonical architecture". In the crystal structure, the carbamate of the rod is hydrogen bonded (Figure 22, green) to the peripheral 2,6-pyrindinedicarboamide ($\mathbf{P^C}$) units. The perfect match between the length of the carbamate groups and the rigid aromatic sheet promotes the stability of the complex. One can observe that $\mathbf{C_{12}}$ rod does not adopt a linear straight conformation, whereas the orientation of two carbamate

groups are dictated by the P^C monomers in **1**. The interactions between two carbamate groups allows the alkyl chain to slightly bend. In the top view (Figure 22c), aromatic sheets and turns fold with a crescent shape and describe an aperture for the cavity.

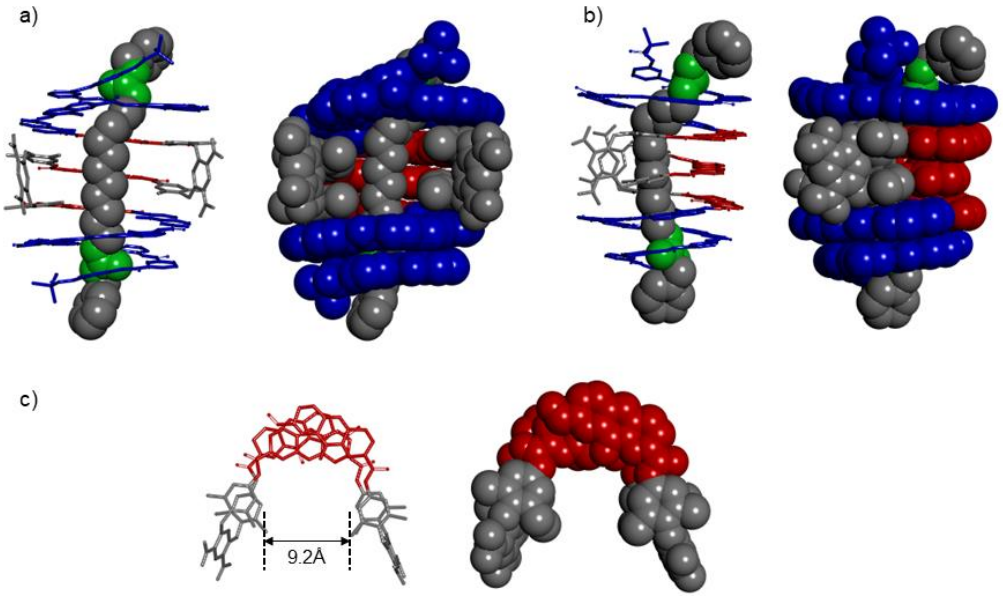

Figure 22. The X-ray structure of the complex **1⊃C$_{12}$**; a) side view of complex **1⊃C$_{12}$** is presented as stick and CPK mode, different segments were marked as corresponding color: helices (blue), sheets (red), turns (grey), alkyl chain and stopper in rod (grey), and carbamate groups (green); b) front view of complex **1⊃C$_{12}$**; c) top view of sheets and turns units in the crystal packing. Side chains (O*i*Bu groups) and included solvent molecules have been removed for clarity.

Similar titrations were also carried out with the T-shape pyrene functionalized rod **NC$_{11}$Py** and foldamer **1**. Upon adding **NC$_{11}$Py**, a new set of signals appeared on the ^{1}H NMR spectra which indicates that the binding between **1** and **NC$_{11}$Py** is also in slow exchange at the NMR timescale (Figure 23). The binding constants could be calculated by integration of proton signals of the free foldamer and host-guest complex as $K_a = 2.7 \times 10^3$ L mol^{-1}. Interestingly, **NC$_{11}$Py** is not symmetrical, thus the resulting complex **1 ⊃ NC$_{11}$Py** is desymmetrized. In the ^{1}H NMR spectra, the number of signals belonging to complex **1 ⊃ NC$_{11}$Py** is doubles compared to the symmetrical complex **1⊃C$_{12}$** (Figure 23g and Figure 22g). ^{19}F NMR measurements confirm the result as free **1** displayed five peaks, after forming complex, whereas ten resonances were observed for **1 ⊃ NC$_{11}$Py**, corresponding to two A^F and eight Q^F units.

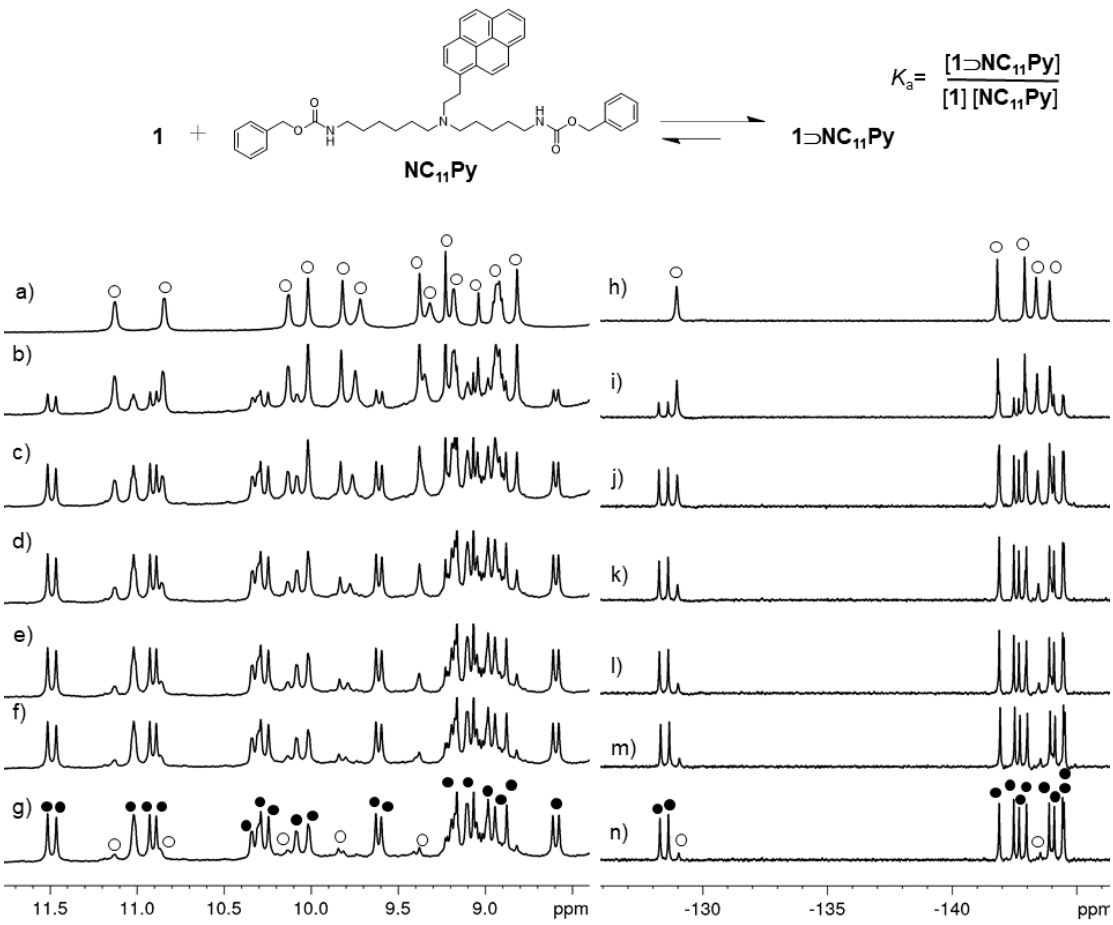

Figure 23. Schematic illustration showing encapsulation of **$NC_{11}Py$** guest within foldamer **1**. Part of the 400 MHz ^1H NMR spectra of **1** (1 mM) at 298 K in $CDCl_3$ (a) and after addition of **$NC_{11}Py$** (5 mM in $CDCl_3$) of (b) 0.50 equiv.; (c) 1.0 equiv.; (d) 1.5 equiv.; (e) 2.0 equiv.; (f) 2.5 equiv.; and (g) 3.0 equiv.. The corresponding 376 MHz ^{19}F NMR spectra are given in (h) to (n), respectively. The signals correspond to the starting oligomer **1** are shown in empty cycles and for the host-guest complex, **1 ⊃ $NC_{11}Py$**, in black cycles. Noted that number of signals become doubled after guest binding due to the asymmetric nature of the guest.

The conformation of complex **1 ⊃ $NC_{11}Py$** was also studied by crystallography (Figure 24). The X-ray quality single crystal were grown by slow diffusion of hexane into a chloroform solution of **1 ⊃ $NC_{11}Py$**. The structure was solved in the *P*-1 space group. As expected the structure revealed hydrogen bond between carbamate groups on the rod and peripheral $\mathbf{P^C}$ units. The pyrene moiety of the rod is located in the aperture of the cavity and stacked on one xylyl of aromatic sheet. Pyrene functions may flip from one side of the cavity to the other. The angle between pyrene function and remote turn unit is 75° (Figure 24c). The affinity for the pyrene rod is probably affected by the steric hindrance of pyrene group which led to the decrease of binding constants from 9.7×10^3 to 2.7×10^3 L mol^{-1}, compared with the complex **1⊃C_{12}**.

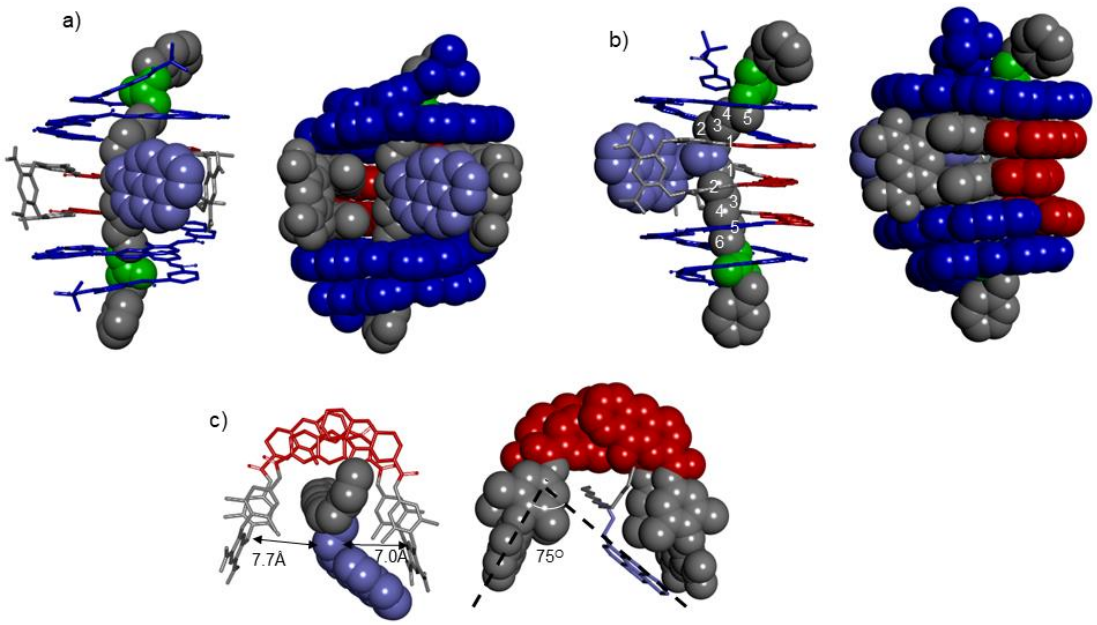

Figure 24. The X-ray structure of the complex **1⊃ NC$_{11}$Py**; a) side view of complex **1⊃ NC$_{11}$Py** was presented as stick and CPK mode, different segments were marked as corresponding color: helices (blue), sheets (red), turns (grey), alkyl chain and stopper in rod (grey), pyrene groups (purple) and carbamate groups (green); b) front view of complex **1⊃ NC$_{11}$Py**; c) top view of sheets, turns and pyrene units in the crystal packing. Side chains (O*i*Bu groups) and included solvent molecules have been removed for clarity.

3.4 Light irradiation of the helix-sheet-helix foldamer

Photoirradiation of diazaanthracenes led to their photocycloaddition, which is reversible upon heating. The photo-irradiation of turn **12** was first carried out and monitored by ^{1}H NMR (Figure 25). Upon irradiation, a new set of proton emerged which correspond to the [4+4] cycloaddition photoproduct **12a**. ^{19}F NMR spectra also showed the same result. Due to its symmetrical structure, **12** only displays a single peak at -128 ppm corresponding to the A^F units, yet after irradiation new peak emerged at -158 ppm corresponding to the dissymmetrical photoproduct **12a**. Photoconversion of **12** is efficient, after 75 mins of irradiation under 320-390 nm light, photoproduct **12a** can be obtained in high yield (>98%).

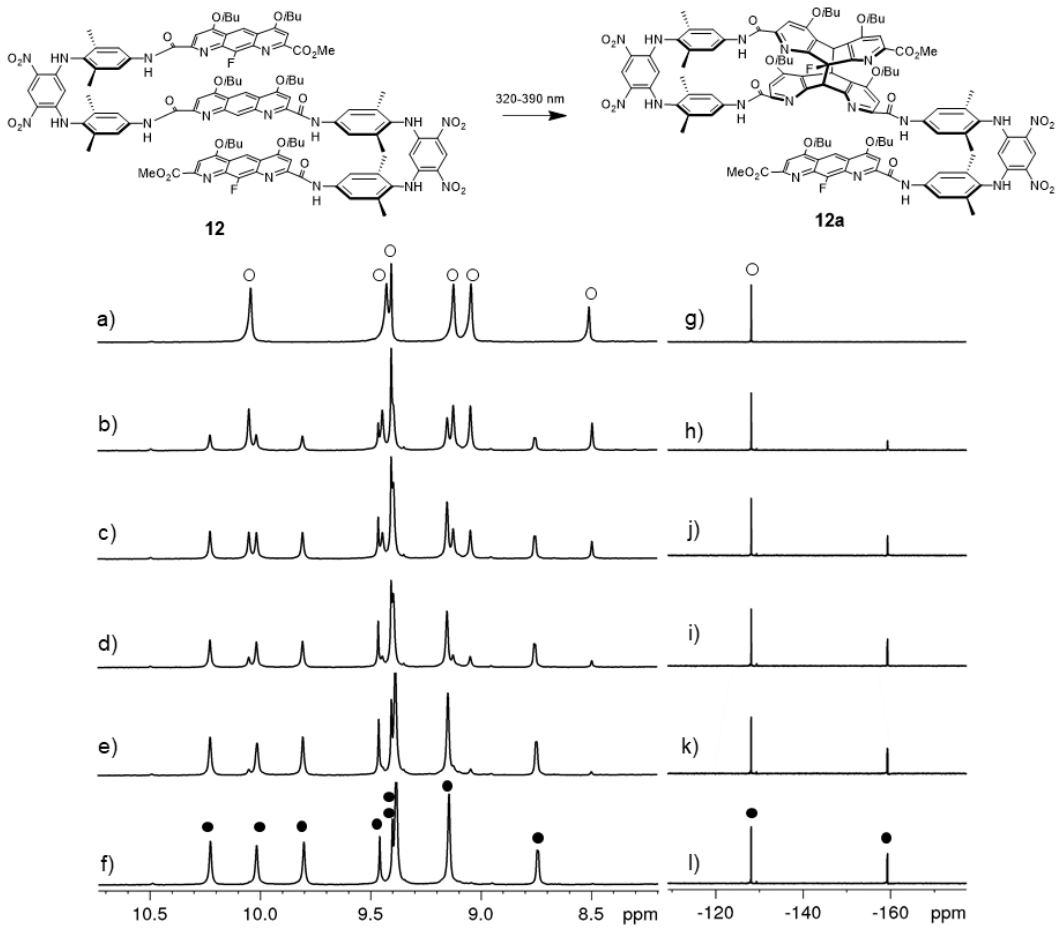

Figure 25. Schematic representation of photoirradiation (320 nm – 390 nm) induced adduct formation between two diazaanthracene (A_F and A_H) units in **12** to **12a**. Part of the 400 MHz ^{1}H NMR spectra of **12** at 298 K (1 mM in $CDCl_3$) under photoirradiation after (a) 0 min; (b) 15 min.; (c) 30 min; (d) 45 min; (e) 60 min; and (f) 75 min. The corresponding 376 MHz ^{19}F NMR spectra are given in (g) to (l), respectively. The signals correspond to the starting oligomer **12** are shown in empty cycles and for photoproduct, **12a,** in black cycles.

The photoconversion of helix-sheet-helix **1** was performed under 320-390 nm light. The process was monitored by ^{1}H NMR spectra (Figure 26), and upon irradiating the sample, a new set of signals appeared corresponding to photoproduct **1a.** After irradiating **1** for two hours, the original peaks totally disappeared, indicating the photoreaction was finished. Compare with aromatic sheets turn **12,** helix-sheet-helix **1** needed more time to achieve the photoproduct, it may because **1** need more energy overcome steric hindrance and intramolecular interaction of helix segments to carry on the photoreaction.

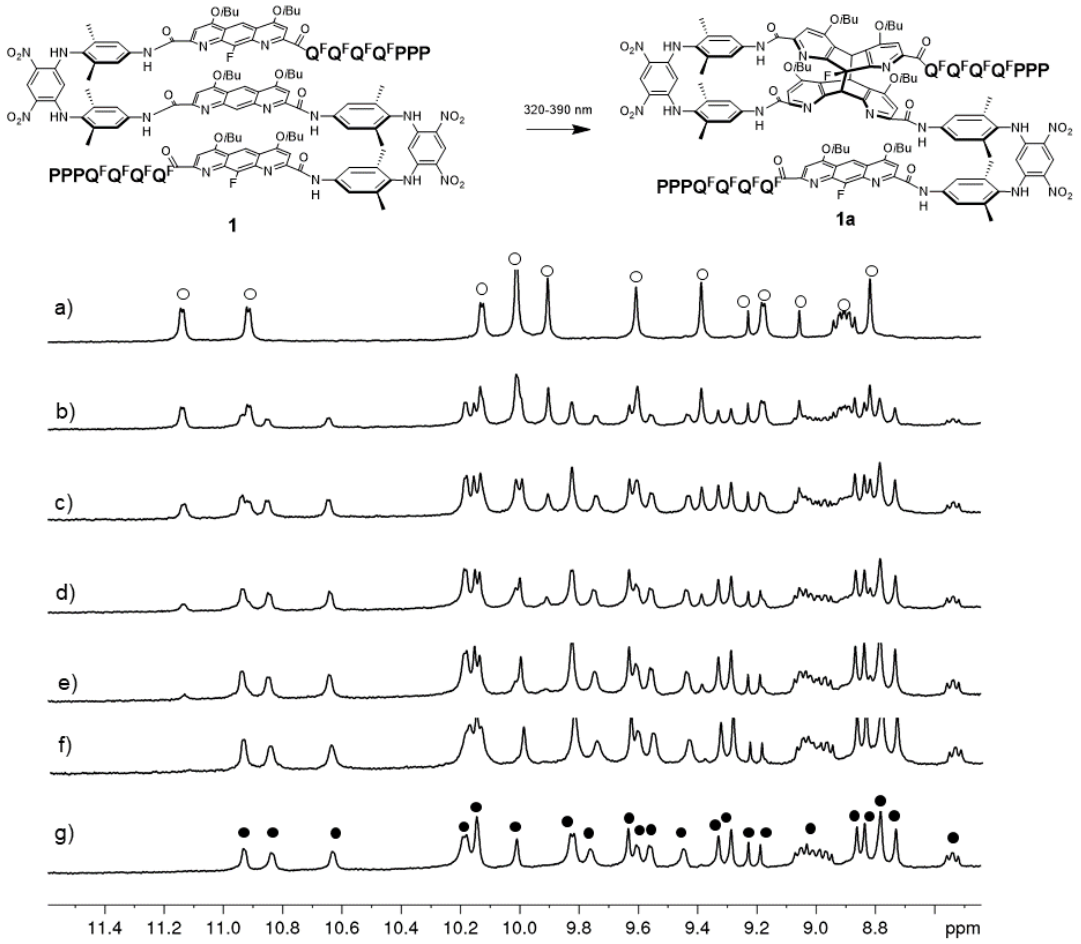

Figure 26. Schematic representation of photoirradiation (320 nm – 390 nm) induced adduct formation between two diazaanthracene (A_F and A_H) units in **1** to **1a**. Part of the 400 MHz ^{1}H NMR spectra of **1** at 298 K (1 mM in $CDCl_3$) under photoirradiation after (a) 0 min; (b) 15 min.; (c) 30 min; (d) 45 min; (e) 60 min; (f) 90 min; and (g) 120 min. The signals correspond to the starting oligomer **1** are shown in empty cycles and for photoproduct, **1a,** in black cycles.

^{19}F NMR spectra also clearly revealed the photocycloaddition. Contrary to helix-sheet-helix **1**, its photoproduct **1a** has an unsymmetrical structure, as a result, after two hours of irradiation, ten fluorine resonances could be identified (instead of 5 for **1**), one peak found at -127 ppm corresponding to the unreacted A^F unit and eight signals around -140 ppm for the eight Q^F units. The last peak at -161 ppm could be attributed to the photocycloadduct between one A^F and one A^H unit.

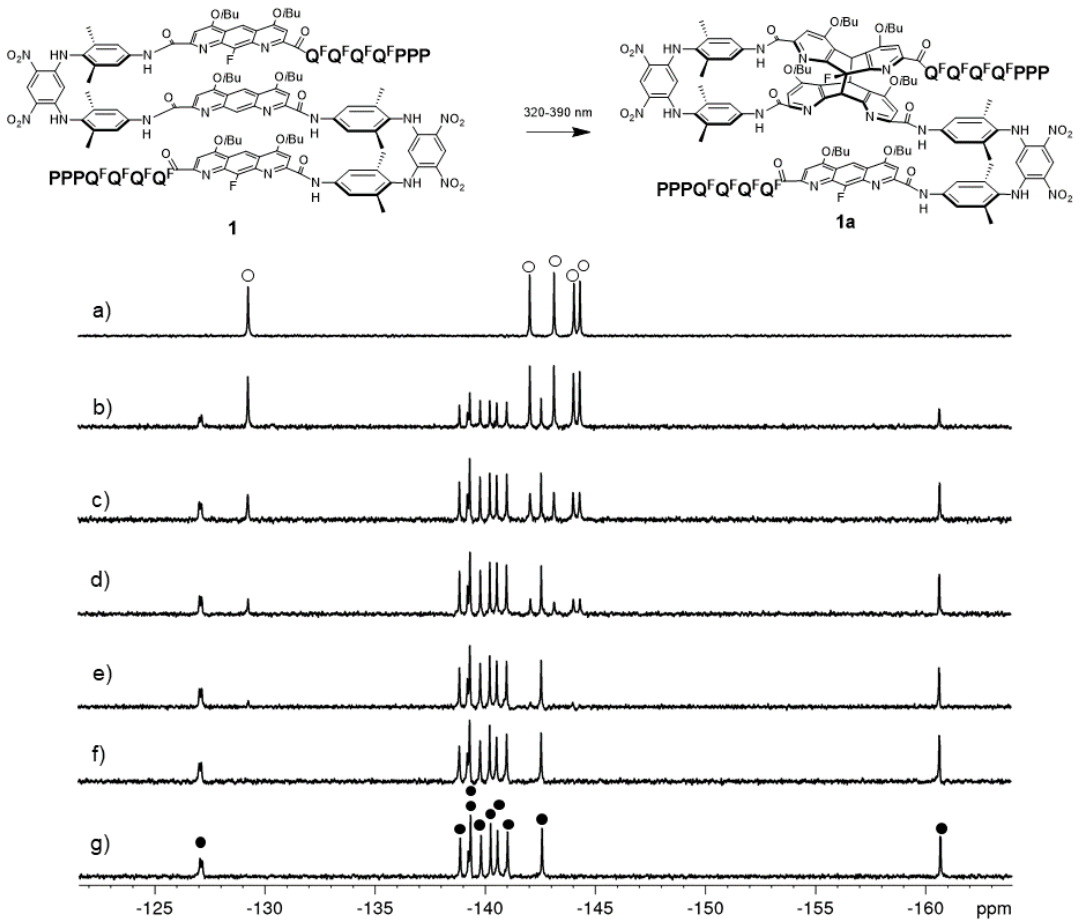

Figure 27. Schematic representation of photoirradiation (320 nm – 390 nm) induced adduct formation between two diazaanthracene (A_F and A_H) units in **1** to **1a**. Part of the 376 MHz ^{19}F NMR spectra of **1** at 298K (1 mM in $CDCl_3$) under photoirradiation after (a) 0 min; (b) 15 min.; (c) 30 min; (d) 45 min; (e) 60 min; (f) 90 min; and (g) 120 min. The signals correspond to the starting oligomer **1** are shown in empty cycles and for photoproduct, **1a,** in black cycles.

An energy minimized molecular model was built to understand the structure of foldamer **1a** (Figure 28). Two diazaanthracenes photocyclized adopting a butterfly-shaped conformation. The two helical segments remained above and below of the photo-modified sheet even if diazaanthracene units could not stack very well anymore. Compared to the conformer **1** the overall length of product **1a** increased from 20.1 Å to 20.9 Å. The distance between two turn units increased from 9.3 Å to 10.2 Å (Figure 28c). In conclusion, we devised that the longer length of the foldamer and its wider cavity may promote the release of guest.

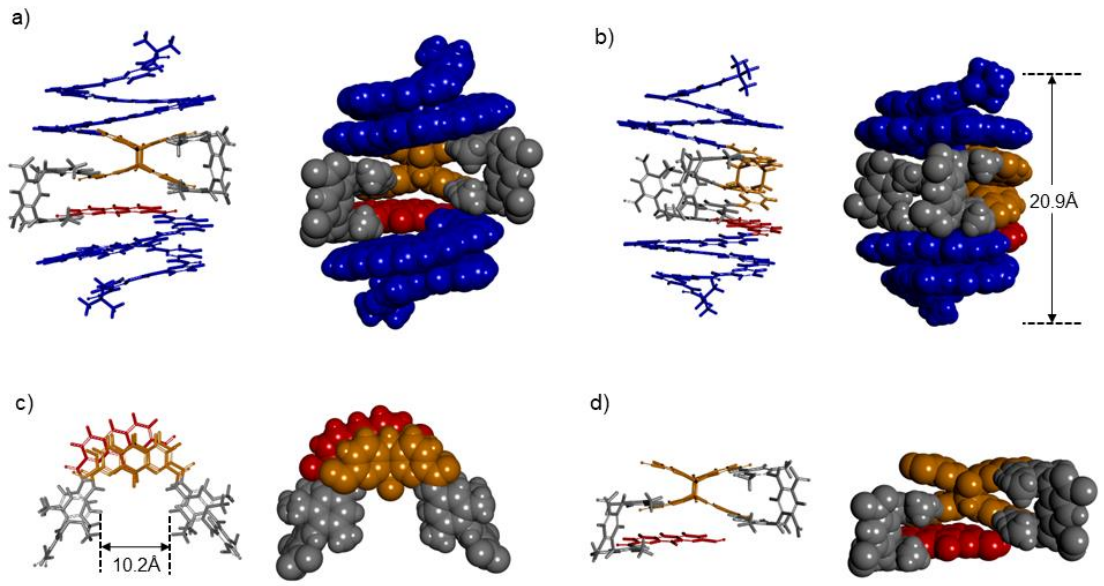

Figure 28. Energy minimized molecular models of the photoproduct **1a**; a) side view and b) front view of **1a**, helical segments, diazaanthracene units and turns were marked as blue, red and grey, respectively; c) top view and d) side view of turn and sheets segments of **1a**, The models were produced with Maestro software package, using MMFFs force filed, chloroform as solvent and TNCG as minimization method.

Photoirradiation of foldaxane **1⊃C12** was first followed by ^{1}H NMR (Figure 29, a-f). Upon irradiating a sample of **1⊃C12** in $CDCl_3$, a new set of signals emerged which corresponds to photoproduct **1a**. In parallel, the signals corresponding to **1⊃C12** decreased. Interestingly, the fact that the new set of signals (Figure 29f) corresponds to photoproduct **1a** (Figure 29g), indicate that **1a** could not bind to **C12**, in another word, irradiation of complex **1⊃C12** could disassociate the binding interaction to afford free rod and photoproduct. ^{19}F NMR spectra also lead to a similar observation, symmetrical complex **1⊃C12** convert to the unsymmetrical photoproduct **1a** and free rod in solution by photoreaction.

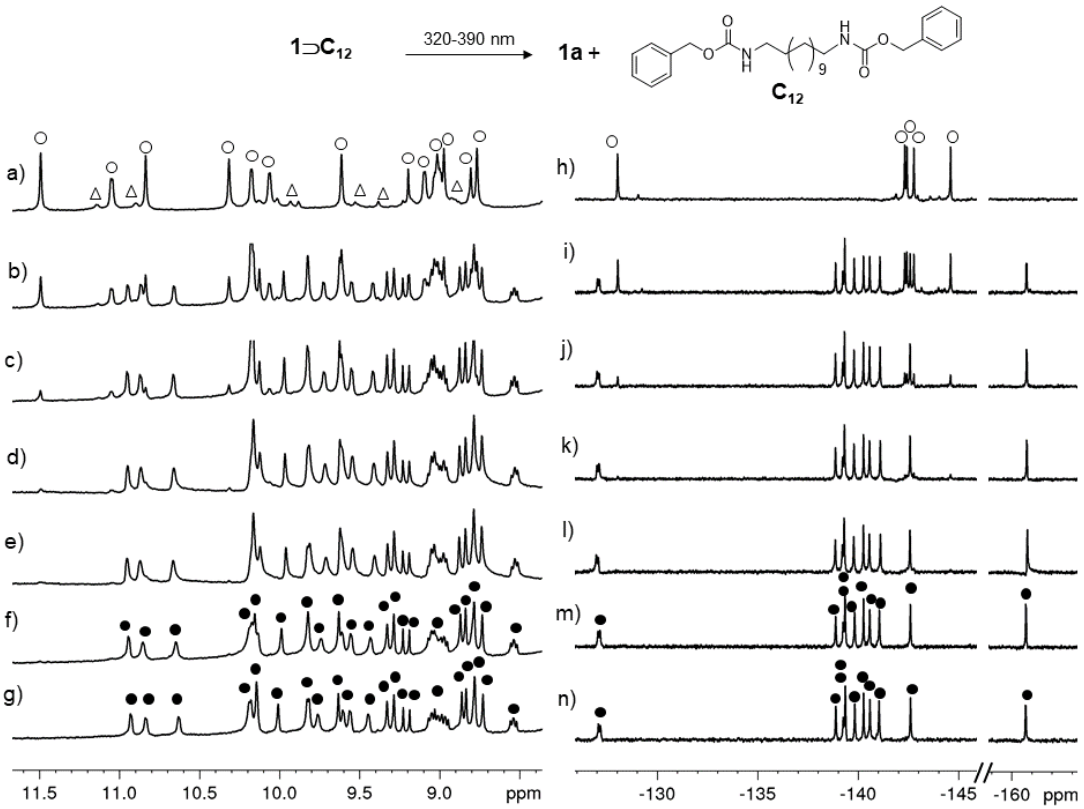

Figure 29. Schematic illustration of photoirradiation (320 nm – 390 nm) induced guest, $\mathbf{C_{12}}$, release from a host-guest complex, $\mathbf{1 \supset C_{12}}$, upon photoadduct formation between two diazaanthracene (A_F and A_H) units. Part of the 400 MHz ^{1}H NMR spectra of (a) host-guest complex, $\mathbf{1 \supset C_{12}}$, at 298 K in $CDCl_3$ and after (b) 30 min; (c) 60 min.; (d) 90 min; (e) 120 min; and (f) 150 min. (g) The 400 MHz ^{1}H NMR spectra of **1a,** when produced by irradiation of **1**, given for comparison. (h-n) The corresponding 376 MHz ^{19}F NMR, respectively. The signals marked as empty cycles, empty triangles and dark cycles correspond to the $\mathbf{1 \supset C_{12}}$, free **1** and **1a**.

Chloroform can convert slowly in air to poisonous phosgene and release HCl, irradiation under powerful lamp can also accelerate the process. While HCl will violently disturb the fold of **1** and then dissociate the complex $\mathbf{1 \supset NC_{11}Py}$. So irradiation of foldaxane $\mathbf{1 \supset NC_{11}Py}$ was performed in CD_2Cl_2 with triethylamine buffer. As observed previously, the ^{1}H NMR spectra (Figure 30) revealed the appearance of signals corresponding to photoproduct **1a**, whereas the signals of $\mathbf{1 \supset NC_{11}Py}$ progressively disappeared upon irradiating the sample. In the process of irradiation, we observed the mixture of photoproduct **1a**, foldaxane $\mathbf{1 \supset NC_{11}Py}$ and side product of photoreaction.

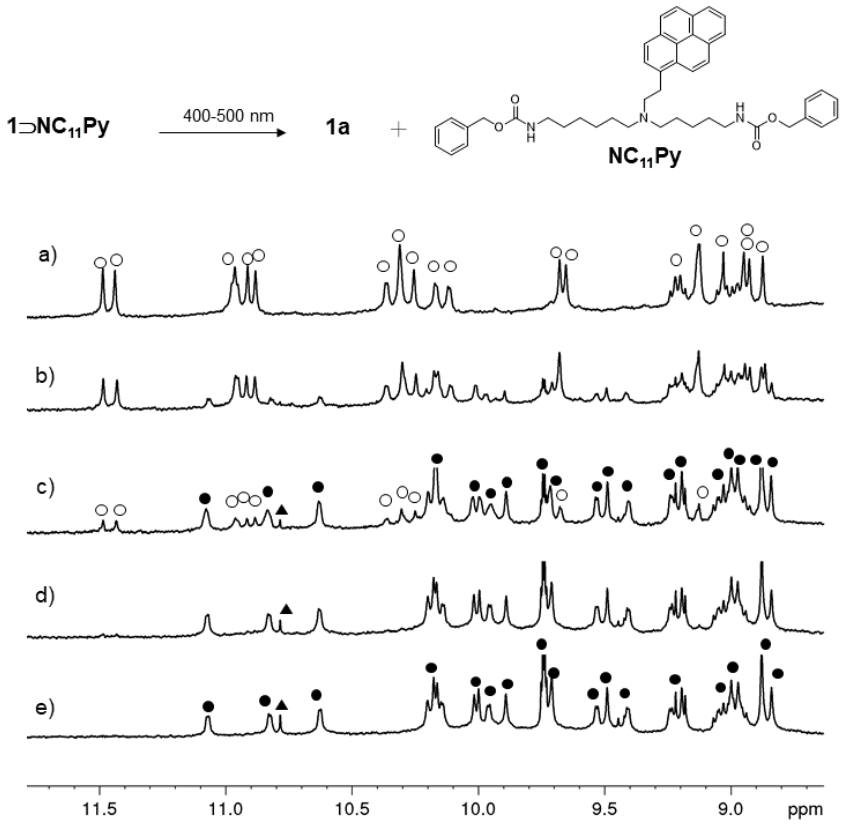

Figure 30. Schematic illustration of photoirradiation (427 nm) induced guest, **$NC_{11}Py$**, release from a host-guest complex, **$1\supset NC_{11}Py$**, upon photoadduct formation between two diazaanthracene (A_F and A_H) units. Part of the 600 MHz ^1H NMR spectra of (a) host-guest complex, **$1 \supset NC_{11}Py$**, at 298 K in CD_2Cl_2 and after (b) 8 mins; (c) 15 mins; (d) 30 mins; (e) 60 mins irradiation. The signals marked as empty cycles and dark cycles correspond to the **$1\supset NC_{11}Py$** and **1a,** side product was marked as dark triangles.

3.5 Thermal treatment to reverse photoproduct

The photocycloadduct obtained from two diazaanthracenes is reversible as it can most of the time be thermally reverted. The thermal reversibility of **1a** (in the presence of the guest **C_{12}**) was tested by heating the photoproduct in $CDCl_3$ at 333 K and a complete reversibility was achieved after 24 hours. Upon heating (Figure 31), a new set of signals emerged progressively and was found to correspond to **$1\supset C_{12}$**. In short, Photoproduct **1a** was converted back slowly to sequence **1** that can subsequently bind to rod **C_{12}** to form complex **$1\supset C_{12}$**. As a result, the ^1H and ^{19}F NMR revealed restored compound **$1\supset C_{12}$**.

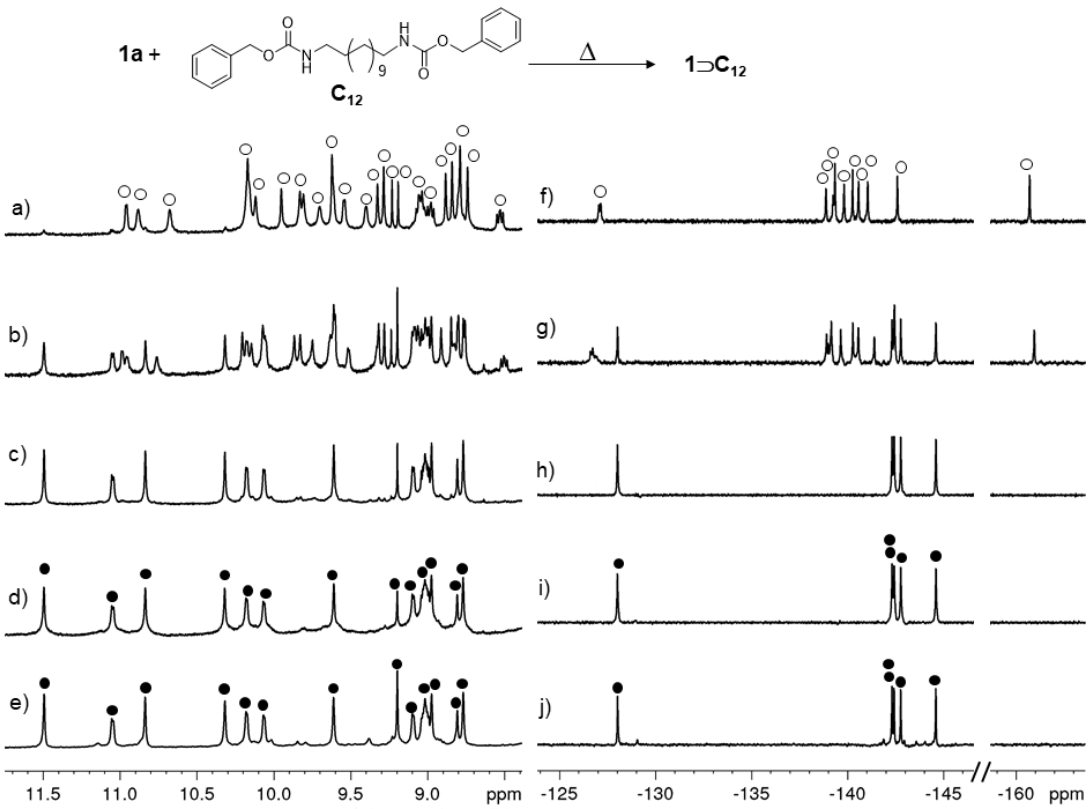

Figure 31. Schematic illustration showing thermally activated cleavage of photoproduct **1a** to **1** and subsequent binding of $\mathbf{C_{12}}$ when present in the medium. Part of the 400 MHz ^{1}H NMR spectra at 298 K in $CDCl_3$ of (a) **1a** (1 mM) in the presence of 2 equivalent of $\mathbf{C_{12}}$ and after heating the mixture at 333 K for (b) 3 hours; (c) 20 hours; and (d) 24 hours. (e) The 400 MHz ^{1}H NMR spectra of $\mathbf{1\supset C_{12}}$, obtained from different experiment, given for comparison. (f-j) The corresponding 376 MHz ^{19}F NMR, respectively. The signals marked with empty cycles and black cycles correspond to **1a** and $\mathbf{1\supset C_{12}}$.

Irradiation of foldaxane $\mathbf{1\supset NC_{11}Py}$ was performed in CD_2Cl_2, but the boiling point of CD_2Cl_2 is not enough for the thermal treatment, so $CDCl_3$ was employed for the thermal reversion. The mixture of photoproduct **1a** and rod $\mathbf{NC_{11}Py}$ were heated at 333 K. The reversion was also monitored by NMR. As the same with complex $\mathbf{1\supset C_{12}}$, photoproduct **1a** was reversed back to foldamer **1** then bind with rod to form complex $\mathbf{1\supset NC_{11}Py}$. Opposite to photoproduct **1a**, the side product of photoreaction is irreversible, the signal marked as dark triangle has no change during the thermal treatment.

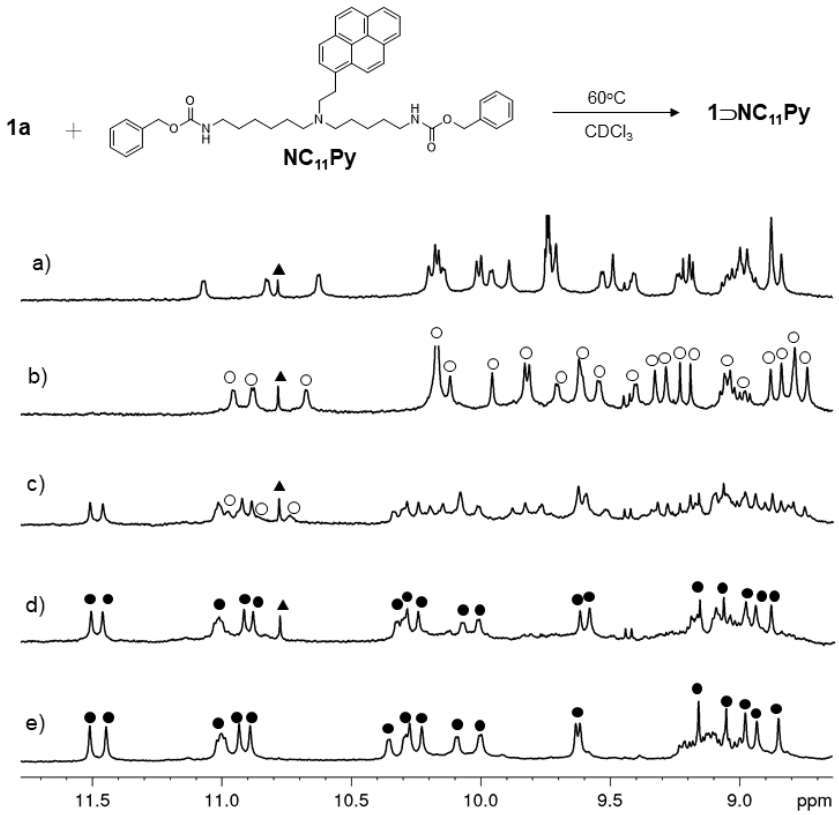

Figure 32. Part of the 400 MHz ^{1}H NMR spectra at 298 K of **1a** (0.5 mM) in the presence of 2.5mM of **$NC_{11}Py$** (a) in CD_2Cl_2; b) in $CDCl_3$; after heating the mixture at 333 K in $CDCl_3$ for (c) 15 hours; (d) 24 hours; (e) spectra of **1⊃$NC_{11}Py$** in $CDCl_3$, obtained from different experiment, given for comparison. The signals marked with empty cycles and black cycles correspond to **1a** and **1⊃$NC_{11}Py$**, side product was marked as dark triangles.

3.6 Repeated cycles: between photoreaction and thermal treatment

The reversible cycles between photoreaction and thermal treatment could be repeated for multiple times. As shown in the figure 33, each step of photoreactions and thermal treatments were monitored by NMR in CD_2Cl_2.The conversion and reversion between **1** and photoproduct **1a** were efficient, at the end of each step, we observed the expected product was main compound. After two cycles (Figure 33e), the signals belong to host/guest complex **1⊃$NC_{11}Py$** was obtained, while no remarkable signals corresponding to photoproduct **1a** were found. This reversible system can be repeated at least twice.

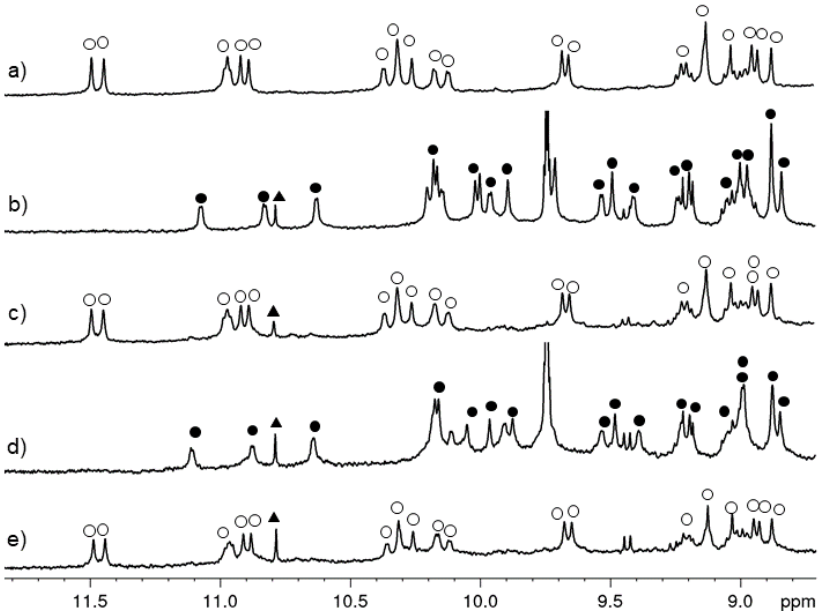

Figure 33. Part of the 400 MHz ^{1}H NMR spectra at 298 K of **1a** (0.5 mM) in CD_2Cl_2 (a) with 2.5 mM of **$NC_{11}Py$**; b) after irradiation; (c) after thermal treatment; (d) after second irradiation; (e) followed with second thermal treatment. The signals marked with black cycles and empty cycles correspond to **1a** and **1 ⊃ $NC_{11}Py$**, side product was marked as dark triangles.

4. Conclusion

We designed and synthesized a canonical and symmetrical helix-sheet-helix foldamers that can bind efficiently to dumbbell and T shape guests both solution and solid state. The quantitative photocycloaddition of diazaanthracenes within aromatic sheet produces dissymmetrical architectures that causes the dissociation of rod from the helix. A thermal treatment allows to recover the initial conformation and the re-formation of the helix-rod complex. The high efficiency of the photo-cycloaddition suggests that it could be implemented multiple times within a given aromatic foldamer sequence. More functional rods can also be designed to bind to helix-sheet-helix foldamer, as for example the ruthenium rod show below. This represents a future object and can give access to new application like the development of diazaanthracene photocycloaddition via triplet-triplet annihilation.

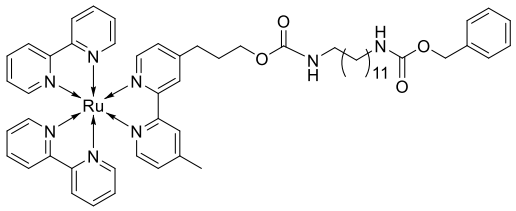

Figure 34. Structure of Ru ion functional rod.

5. Experimental part

5.1 Nuclear Magnetic Resonance

NMR spectra were recorded on 3 different NMR spectrometers: (1) an Avance II NMR spectrometer (Bruker Biospin, Wissembourg, France) with a vertical 7.05 T narrow-bore/ultrashield magnet operating at 300 MHz for ^{1}H spectra and 75 MHz for ^{13}C spectra by means of a 5mm BBFO $^{1}H/^{15}N$-^{31}P-^{19}F probe with Z gradient capabilities; (2) a Avance III HD 400 NMR spectrometer (Bruker Biospin, Wissembourg, France) with a vertical 9.4 T narrow-bore/ultrashield magnet operating at 400 MHz for ^{1}H spectra and 100MHz for ^{13}C spectra by means of a 5mm Smartprobe BBFO $^{1}H/^{15}N$-^{31}P-^{19}F probe with Z gradient capabilities; (3) an Avance NEO NMR spectrometer (Bruker Biospin, Wissembourg, France) with a vertical 16.45 T narrowbore/ultrashield magnet operating at 700 MHz for ^{1}H spectra by means of a 5mm TXI $^{1}H/^{13}C/^{15}N$ probe with Z gradient capabilities. Chemical shifts are reported in parts per million (ppm, δ) relative to the ^{1}H residual signal of the deuterated solvent used. ^{1}H NMR splitting patterns with observed first-order coupling are designated as singlet (s), doublet (d), triplet (t), or quartet (q). Coupling constants (J) are reported in hertz. Samples were not degassed otherwise it is specified. Data processing was performed with Topspin 3.5 software.

5.2 Spectroscopic studies

Electronic absorption spectra were measured on a UV-vis-NIR spectrophotometer. Steady-state emission spectra were recorded on a spectrofluorometer fitted with a PMT detector and

exciting with a 450W Xe-lamp across a double monochromator and were corrected for instrumental response.

5.3 Molecular modeling

Molecular Models calculation were done using MacroModel version 8.6 (Schrödinger Inc.) with the Merck Molecular Force Field static (MMFFs) as implemented in this software. Energy minimized structures were obtained using 500 steps of Truncated Newton Conjugate Gradient (TNCG), chloroform as implicit solvent and the extended Cutoff option.

5.4 Crystallography

Single crystal X-ray diffraction experiments were performed at the IECB X-ray facility (CNRS UMS 3033 – INSERM US001, University of Bordeaux) on a 3kW microfocus Rigaku FRX rotating anode. The source is equipped with high flux Osmic Varimax HF mirrors. The FRX generator is combined with a hybrid Dectris Pilatus 200K detector. All data were collected at the copper kα wavelength with a partial chi goniometer that decreases blind areas and enables automatic axial adjustment. Data were processed with the CrysAlisPro suite version 1.171.38.43.[1] Empirical absorption correction using spherical harmonics, implemented in SCALE3 ABSPACK scaling algorithm was used. Structures were solved with Shelxt[2] and refined by full-matrix least-squares method on F2 with Shelxl-2014[2] within Olex2.[3] For all atoms, anisotropic atomic parameters were used. Hydrogen atoms were place at idealized position sand refined as riding of their carriers with Uiso(H)=1.2Ueq(CH, CH2, NH) and Uiso(H)=1.5Ueq(CH3). DFIX and AFIX instructions were used to improve the geometry of molecules and RIGU to model atomic displacement parameters. Severely disordered solvent molecules were removed using the SQUEEZE procedure from the PLATON suite.[4] For search and analysis of solvent accessible voids in the structures default parameters were utilized: grid 0.20 Å, probe radius 1.2 Å and NStep 6. Calculated total potential solvent accessible void volumes and electron counts per unit cell are given in the CIF files that were checked using IUCR's checkcif algorithm. Due to the characteristics of the crystals, i.e. large volume fractions of disordered solvent molecules, weak diffraction intensity, incompleteness of the data and

moderate resolution, a number of A -level and B -level alerts remain in the check cif file. These alerts are inherent to the data and refinement procedures and do not reflect errors. Rather, they illustrate the limited practicality of the checkcif tool for medium size molecule crystallography.

Name	**1⊃C_{12}**	**1 ⊃ $NC_{11}Py$**
Formula	$C_{286}H_{280}F_{10}N_{50}O_{44}$	$C_{303}H_{291}F_{10}N_{51}O_{44}$
M.W	5311.6760	5540.9580
Space group	*P*-1	*P*-1
a	24.1978(3)	23.7615(5)
b	35.7135(6)	24.0825(5)
c	44.821(1)	35.9358(6)
α	82.497(2)	101.204(2)
β	81.642(1)	91.486(1)
γ	78.235(1)	111.906(2)
Cell volume	37313.1	18605.6
Packing Coefficient	0.52043	0.495605

5.5 Photochemistry

Photo-irradiation experiments were carried out in NMR tubes. Respective compounds were placed in NMR tubes, degassed and filled with argon. Subsequently, argon purged deuterated solvents were used to dissolve the compounds. The solutions were then subjected to irradiation by UV resources, they are EXFO Lite (Model No. E3000-01) portable device having light source of 320 - 390 nm with 50 W lamp, Kessil science (PR160L) LED photoreaction lighting 370 nm (43 W) and 427 nm (45 W). NMR were checked at different time intervals to follow the photo-product formation. The experiments were repeated several times to establish reproducibility. Thermal reversibility experiments were performed in NMR tubes. The anthracene derivatives were dissolved in the appropriate deuterated solvent (CD_2Cl_2 or $CDCl_3$). The tube was heated to 333 K for $CDCl_3$, respectively. The kinetic reversibility was followed by ^1H NMR.

kessil

5.6 Methods for chemical synthesis

All reactions were carried out under a dry inert atmosphere otherwise it is specified. Commercial reagents were purchased from Sigma Aldrich, TCI Chemicals or Alfa-Aesar and were used without further purification. Tetrahydrofurane (THF) and dichloromethane (CH_2Cl_2) were dried over alumina columns (MBRAUN SPS-800 solvent purification system); chloroform ($CHCl_3$) and diisopropylethylamine (DIPEA) were distilled over P_2O_5 and calcium hydride (CaH_2) respectively prior to use. Reactions were monitored by thin layer chromatography (TLC) on Merck silica gel 60-F254 plates and observed under UV light. Column chromatography purifications were carried out on Merck GEDURAN Si60 (40-63 µm). Preparative recycling GPC (gel permeation chromatography) were performed on JAIGEL 20*600 mm columns (Japan Analytical Industry) at a flow rate of 7 mL min^{-1} with a mobile phase composed of 1% (vol/vol) ethanol and 0.5% (vol/vol) Et_3N in chloroform. Monitoring was carried out by UV detector at 254 nm, 280 nm, 300 nm and 360 nm. ESI mass spectra were obtained from the Mass Spectrometry Laboratory at the European Institute of Chemistry and Biology (UMS 3033 & US01 - IECB), Pessac, France.

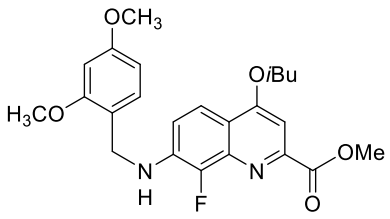

3

Synthesis of compound 3: Quinoline amine **2** (610 mg, 1.98 mmol) and 2,4-dimethoxybenzaldehyde (659 mg, 3.97 mmol) were dissolved in 1,2-dichloroethane (5 ml) in a 10 mL round-bottom flask filled with argon. The slurry was stirred at room temperature for 2 hours. Then sodium triacetoxyborohydride (841 mg, 3.97 mmol) was added to the slurry. The mixture was stirred at room temperature under argon atmosphere for 18 h. The reaction mixture was quenched by adding aqueous saturated $NaHCO_3$, and the product was extracted with dichloromethane. The organic layer was washed with brine and dried over anhydrous $MgSO_4$. After the solvent was removed in vacuo, the residue was purified by column chromatography (silica gel, ethyl acetate and cyclohexane (1:6) as eluent) to give **2** as yellow solid (731 mg,

83%). ^{1}H NMR (300 MHz, $CDCl_3$, 298 K, δ ppm): 7.90 (dd, *J* = 1.5, *J* = 9.1, 1H), 7.37 (s, 1H), 7.26 – 7.18 (m, 2H), 6.50 (d, *J* = 2.3, 1H), 6.45 – 6.41 (m, 1H), 4.91 (br, 1H), 4.49 (d, *J* = 6.2, 2H), 4.07 (s, 3H), 4.03 (d, *J* = 6.4, 2H), 3.87 (s, 3H), 3.81 (s, 3H), 2.34 – 2.20 (m, 1H), 1.15 (s, 3H), 1.12 (s, 3H). ^{13}C NMR (100 MHz, $CDCl_3$, 298 K, δ ppm): 166.4, 162.7, 160.4, 158.4, 149.6, 145.3, 142.8, 138.9, 136.9, 129.3, 118.9, 117.5, 116.0, 114.7, 103.8, 98.7, 98.3, 74.9, 55.3, 53.0, 42.9, 28.1, 19.2. HRMS (ESI): m/z calcd for $C_{24}H_{28}FN_2O_5$ $[M+H]^+$ 443.1977, found 443.1989.

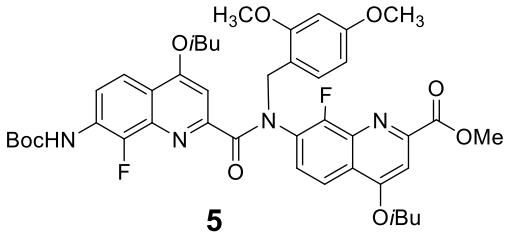

5

Synthesis of dimer 5: A solution of acid, **3** (645 mg, 1.7 mmol) in dry $CHCl_3$ (3 mL) was cooled to 0°C. 1-Chloro-N,N,2-trimethyl-1-propenylamine (0.75 mL, 3.0 eq.) was added. The solution was stirred at room temperature for 3 h under N_2 atmosphere. The solvent was removed under high vacuum for at least 2 hours to yield the corresponding acid chloride. The resulting acid chloride was dissolved in dry $CHCl_3$ (3 mL) and added to a solution of **3** (630 mg, 0.9 eq.) and dry DIPEA (0.73 mL, 4.0 eq.) in dry $CHCl_3$ (1 mL). The mixture was stirred for 12 h. The organic layer was washed with saturated aqueous NH_4Cl, saturated aqueous $NaHCO_3$ and brine, dried over $MgSO_4$, filtered and concentrated in vacuo. The residue was purified by column chromatography (silica gel, ethyl acetate and cyclohexane (1:4) as eluent) to give **5** as yellow solid (1.1 g, 89%). ^{1}H NMR (300 MHz, $CDCl_3$, 298 K, δ ppm): 8.19 (t, *J* = 7.9, 1H), 7.82 (t, *J* = 10.9, 2H), 7.58 – 7.49 (m, 3H), 7.25 (s, 1H), 6.75 (s, 1H), 6.46 (d, *J* = 8.1, 1H), 6.30 (s, 1H), 5.21 (dd, *J* = 14.5, 2H), 4.01 (br, 7H), 3.78 (s, 3H), 3.47 (s, 3H), 2.35 – 2.18 (m, 2H), 1.52 (s, 9H), 1.15 – 1.10 (m, 12H). ^{13}C NMR (100 MHz, 298 K, δ ppm): 168.6, 165.9, 162.4, 162.0, 160.4 158.5, 154.6, 154.1, 152.1, 151.6, 149.3, 146.6, 144.1, 138.9, 136.9, 131.6, 131.3, 129.6, 126.6, 122.2, 118.9, 117.9, 117.1, 116.9, 116.0, 104.1, 101.6, 100.2, 98.1, 81.4, 75.2, 75.0, 55.2, 54.9, 53.2, 47.7, 38.6, 37.0, 35.5, 28.2, 28.1, 28.0, 19.1. HRMS (ESI): m/z calcd for $C_{43}H_{49}F_2N_4O_9$ $[M+H]^+$ 803.3462, found 803.3486.

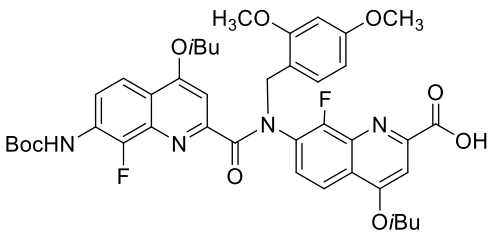

6

Synthesis of dimer acid 6: Compound **5** (0.60 g, 0.74 mmol) was dissolved in a mixture of THF (10 mL) and H_2O (2 mL). To this solution LiOH (60 mg, 2.0 equiv.) dissolved in MeOH was added dropwise. The solution was stirred at room temperature for 3 h. Then solution was neutralized with 1N HCl to pH = 4 ~ 5 and concentrated under reduced pressure to remove THF. Some more H_2O (30 mL) was added to the residue. The aqueous phase was extracted with CH_2Cl_2 (3×20 mL). The combined organic phases were dried over Na_2SO_4, filtered, evaporated to give dimer acid **6** as a yellow solid. ^{1}H NMR (400 MHz, $CDCl_3$, 298 K, δ ppm): 8.16 (t, *J* = 7.9, 1H), 7.79 – 7.75 (m, 2H), 7.52 (s, 1H), 7.48 – 7.42 (m, 2H), 7.24 (s, 1H), 6.67 (s, 1H), 6.42 (d, 1H), 6.24 (s, 1H), 5.19 (dd, *J* = 14.5, 2H), 4.02 – 3.98 (m, 6H), 3.73 (s, 4H), 2.28 – 2.17 (m, 2H), 1.47 (s, 9H), 1.08 – 1.05 (m, 12H). ^{13}C NMR (100 MHz, $CDCl_3$, 298 K, δ ppm): 168.3, 164.2, 163.7, 162.1, 160.5, 158.5, 154.4, 153.6, 152.1, 151.0, 147.6, 146.6, 144.1, 137.1, 131.8, 129.6, 122.4, 119.2, 117.8, 117.1, 116.8, 116.4, 81.5, 75.6, 75.1, 55.3, 47.7, 38.6, 37.0, 35.5, 30.3, 28.2, 28.0, 19.1. HRMS (ESI): m/z calcd for $C_{42}H_{47}F_2N_4O_9$ $[M+H]^+$ 789.3306, found 789.3299.

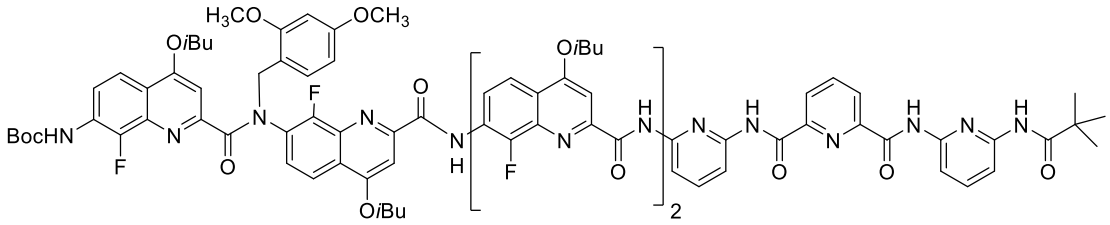

8

Synthesis of oligomer 8: Dimer acid **6** (100 mg, 0.126 mmol) was dried in vacuo, and then dissolved in dry CH_2Cl_2 (4 mL) in a 10 mL round bottom flask. To this 1-chloro-N,N,2-trimethylpropenylamine (32 μL, 1.5 equiv.) was added. The reaction mixture was stirred at room temperature for 2 h resulting in a homogeneous solution, and then evaporated to provide the corresponding acid chloride. To a solution of the amine **7** (120 mg, 0.126 mmol) in CH_2Cl_2

(2 mL) containing DIEA (65 μL, 0.37 mmol) was added a solution of acid chloride in CH_2Cl_2 (2 mL) via syringe. The reaction mixture was stirred at room temperature for 12 h. The solution was evaporated, and the product was purified by chromatography (silica gel, ethyl acetate and cyclohexane 1:2) to get yellow solid (145 mg, 72 %). ^{1}H NMR (400 MHz, $CDCl_3$, 298 K, δ ppm): 10.77 (s, 1H), 10.68 (s, 2H), 10.16 (s, 1H), 10.06 (s, 1H), 8.78 (t, *J* = 5.2, 2H), 8.39 (d, *J* = 7.6, 1H), 8.23 (t, *J* = 6.7, 2H), 8.11 – 8.05 (m, 4H), 7.96 – 7.86 (m, 4H), 7.74 – 7.65 (m, 4H), 7.44 – 7.36 (m, 2H), 7.32 – 7.28 (m, 1H), 7.13 (s, 1H), 6.74 (s, 1H), 6.39 (d, 1H), 6.16 (s, 1H), 5.01 (dd, *J* = 13.9, 2H), 4.18 (d, *J* = 6.3, 4H), 4.10 (d, *J* = 6.1, 2H), 3.93 (d, *J* = 5.8, 2H), 3.73 (s, 3H), 3.32 (s, 3H), 2.35 – 2.22 (m, 3H), 2.18 – 2.09 (m, 1H), 1.45 (s, 9H), 0.88 (s, 9H). ^{13}C NMR (100 MHz, $CDCl_3$, 298 K, δ ppm): δ175.8, 167.1, 162.1, 161.4, 161.2, 160.9, 160.7, 160.3, 159.4, 157.4, 153.6, 152.9, 151.1, 150.2, 150.1, 149.6, 148.8, 148.6, 148.3, 147.9, 147.5, 147.2, 145.6, 144.6, 144.4, 143.1, 139.7, 139.3, 138.0, 136.9, 136.5, 136.1 136.0, 130.8, 130.4, 128.3, 125.7, 125.6, 124.6, 124.4, 121.3, 120.6, 119.9, 118.7, 118.0, 116.7, 116.0, 109.5, 109.1, 108.7, 103.0, 99.0, 98.0, 97.2, 97.0, 80.3, 74.4, 73.9, 54.2, 53.8, 46.6, 38.3. HRMS (ESI): m/z calcd for Chemical Formula: $C_{92}H_{94}F_4N_{15}O_{15}$ $[M+H]^+$ 1725.7018, found 1725.7174.

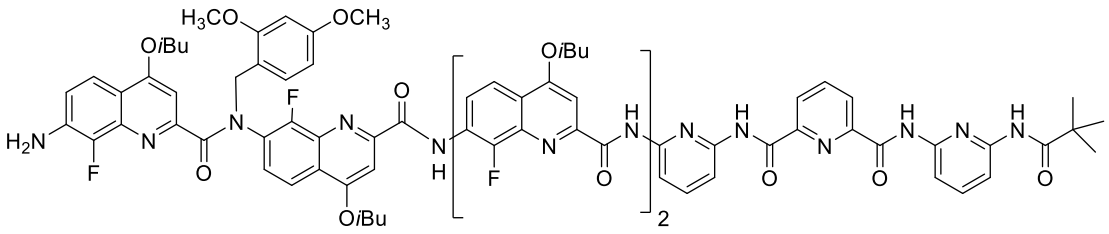

9

Synthesis of oligomer amine 9: Oligomer **8** (0.42 g, 0.24 mmol) was dissolved in dioxane (2 mL), and HCl (4M in dioxane, 5 mL) was added. The mixture was stirred at room temperature for 3h. The solvent was evaporated, and the residue was dissolved in CH_2Cl_2 (20 mL), washed with saturated $NaHCO_3$, dried over Na_2SO_4 and then evaporated to give amine **9** as a yellow solid (375mg, 96%). It was dried in vacuum and used without further purification. ^{1}H NMR (400 MHz, $CDCl_3$, 298 K, δ ppm): 10.77 (s, 1H), 10.67 (s, 2H), 10.19 (s, 1H), 10.09 (s, 1H), 8.79 – 8.73 (m, 2H), 8.36 (d, *J* = 7.5, 1H), 8.20 (t, *J* = 7.1, 2H), 8.09 (d, *J* = 9.0, 2H), 8.02 (d, *J* = 7.6, 1H), 7.94 – 7.87 (m, 4H), 7.75 – 7.67 (m, 5H), 7.53 (d, *J* = 8.8, 1H), 7.43 (t, *J* = 7.7, 1H), 7.38 (d, *J* = 8.2, 1H), 7.33 (t, *J* = 7.3, 1H), 7.02 (s, 1H), 6.79 (t, *J* = 8.1, 1H), 6.39 (d, *J* = 7.6,

1H), 6.16 (s, 1H), 5.01 (dd, *J* = 13.9, 2H), 4.12 – 4.02 (m, 8H), 3.93 (d, *J* = 5.8, 2H), 3.73 (s, 3H), 3.32 (s, 3H), 2.34 – 2.22 (m, 3H), 2.07 – 2.01 (m, 1H), 0.88 (s, 9H). ^{13}C NMR (100 MHz, $CDCl_3$, 298 K, δ ppm): 176.8, 168.3, 163.2, 162.5, 162.4, 161.9, 161.8, 161.2, 160.4, 158.4, 154.4, 154.1, 151.5, 151.1, 150.6, 149.9, 149.5, 149.3, 148.9, 148.6, 148.3, 145.6, 144.9, 142.5, 140.6, 139.1, 138.2, 138.1, 137.5, 134.1, 134.0, 131.8, 129.4, 126.8, 126.7, 126.6, 125.7, 125.5, 122.3, 121.1, 119.9, 119.8, 118.2, 117.6, 117.1, 116.1, 114.9, 110.5, 110.2, 109.8, 109.7, 104.0, 98.9, 98.6, 98.0, 75.4, 74.7, 55.3, 54.8, 47.5, 39.3. HRMS (ESI): m/z calcd for $C_{87}H_{86}F_4N_{15}O_{13}$ $[M+H]^+$ 1625.6494, found 1625.6615.

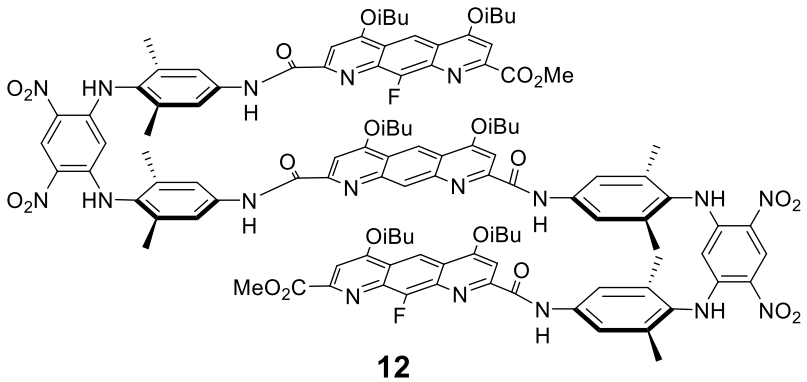

12

Oligomer 12. Tetramer amine **10** (0.185 g, 0.214 mmol), diacid **11** (0.04 g, 0.1 mmol) and PyBOP (0.208 g, 0.4 mmol) were placed in a 5 mL round-bottom flask filled with argon. Freshly distilled $CHCl_3$ (2 mL) and DIPEA (70 μL, 0.4 mmol) were then successively added. The solution was stirred at 45 °C for two days. The solvent was removed under reduced pressure and the residue was dissolved in dichloromethane, washed with 5% NH_4Cl, distilled water and brine. The organic layer was dried over Na_2SO_4, filtered and concentrated under reduced pressure. The crude product was purified by recycling GPC and compound **12** was obtained as a yellow solid (0.087 g, 42% yield). ^{1}H NMR (300 MHz, $CDCl_3$, 298 K, δ ppm): 9.99 (s, 2H), 9.38 (s, 2H), 9.35 (s, 2H), 9.07 (s, 2H), 8.99 (s, 2H), 8.45 (s, 1H), 7.88 (d, *J* = 1.9 Hz, 2H), 7.53 – 7.29 (m, 11H), 7.16 (s, 2H), 6.57 (s, 2H), 4.77 (s, 2H), 4.02 (t, *J* = 6.7 Hz, 8H), 3.83 (s, 6H), 3.21 (d, *J* = 6.8 Hz, 4H), 2.34 – 2.25 (m, 3H), 2.14 (s, 12H), 2.05 (s, 12H), 1.99 – 1.75 (m, 3H), 1.27 – 1.19 (m, 12H), 1.16 (m, 12H), 0.90 (d, *J* = 6.7 Hz, 12H). ^{13}C NMR (75 MHz, $CDCl_3$, 298 K, δ ppm): 165.18, 162.62, 162.17, 161.02, 160.91, 152.78, 152.40, 151.18, 150.69, 148.36, 148.16, 145.19, 137.28, 137.23, 137.20, 135.64, 134.30, 134.17, 130.49, 130.47, 129.34,

127.43, 125.07, 125.03, 121.23, 121.16, 120.41, 119.10, 118.99, 115.35, 109.78, 99.52, 96.16, 94.65, 77.36, 75.21, 74.67, 53.27, 28.45, 28.43, 27.96, 19.28, 19.26, 18.88, 18.05, 18.03. ^{19}F NMR (282 MHz, $CDCl_3$, 298 K, δ ppm): -128.15. HRMS (ESI): m/z calcd for $C_{112}H_{115}F_2N_{18}O_{22}$ $[M+H]^+$ 2102.8435, Found 2102.8297.

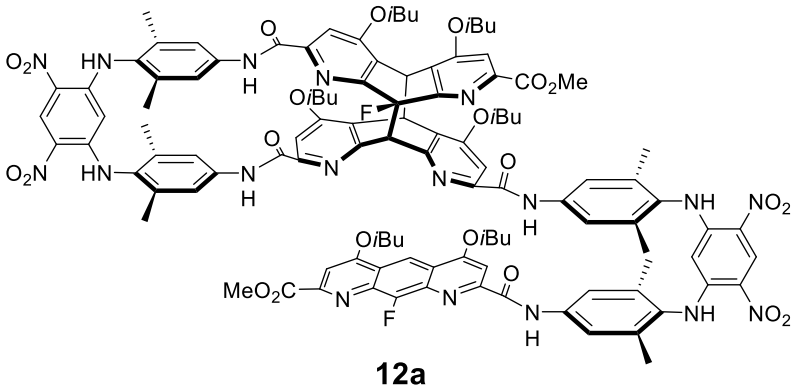

12a

Photoproduct 12a. Oligomer **12** was irradiated in $CDCl_3$ as described above and the progress was followed by ^{1}H NMR spectroscopy. After 2 hours of photoirradiation, 98% of photoproduct formation was observed. ^{1}H NMR (700 MHz, $CDCl_3$, 298 K, δ ppm): 10.18 (s, 1H), 9.96 (s, 1H), 9.77 (s, 1H), 9.42 (s, 1H), 9.37 (s, 1H), 9.35 (s, 2H), 9.34 (s, 1H), 9.11 (s, 2H), 8.71 (s, 1H), 7.94 (s, 1H), 7.88 (s, 1H), 7.87 (s, 1H), 7.68 (s, 1H), 7.45 (s, 1H), 7.44 (s, 1H), 7.39 (s, 2H), 7.36 (s, 1H), 7.32 (s, 1H), 7.31 (s, 1H), 7.22 (s, 1H), 6.61 (s, 1H), 6.51 (s, 1H), 5.69 (d, *J* = 11.3 Hz, 1H), 5.64 (d, *J* = 11.3 Hz, 1H), 5.20 (s, 1H), 5.14 (d, *J* = 28.95 Hz, 1H), 4.70 (s, 1H), 4.11-4.07 (m, 2H), 4.06 (s, 3H), 3.85-3.80 (m, 4H), 3.76-3.73 (m, 1H), 3.75 (s, 3H), 3.72-3.68 (m, 4H), 3.61-3.59 (m, 1H), 2.36-2.31 (m, 2H), 2.17 (s, 3H), 2.16 (s, 3H), 2.15-2.12 (m, 2H), 2.14 (s, 3H), 2.12 (s, 3H), 2.11 (s, 3H), 2.07 (s, 3H), 2.06 (d, *J* = 2.1 Hz, 6H), 2.04-2.00 (m, 2H), 1.18-1.17 (m, 6H), 1.09-1.02 (m, 24H), 0.95-0.92 (m, 6H). ^{13}C NMR (175 MHz, $CDCl_3$, 298 K, δ ppm): 165.7, 165.1, 163.2, 162.9, 161.9, 161.7, 161.6, 161.2, 160.8, 160.6, 160.5, 160.3, 159.8, 154.1, 153.2, 152.7, 151.0, 150.2, 149.3, 149.2, 148.3, 148.2, 147.9, 137.2, 137.0, 136.9, 136.7, 136.6, 136.5, 136.2, 136.0, 134.9, 130.4, 130.1, 130.0, 129.7, 129.5, 126.9, 126.6, 124.9, 124.8, 124.1, 123.8, 122.0, 121.8, 120.5, 120.3, 120.1, 119.5, 119.1, 118.8, 110.9, 108.1, 104.6, 104.1, 99.4, 97.1, 96.6, 93.6, 93.3, 93.1, 75.3, 75.1, 75.0, 64.9, 64.8, 33.2, 33.1, 32.9, 32.7, 32.5, 31.9, 31.4, 30.9, 30.3, 29.7, 29.4, 29.3, 29.2, 29.1, 28.2, 27.8, 27.5, 27.2, 26.9, 25.6, 19.2, 19.1, 18.9, 18.8, 18.3, 18.2, 18.1, 18.0, 17.7, 14.1.

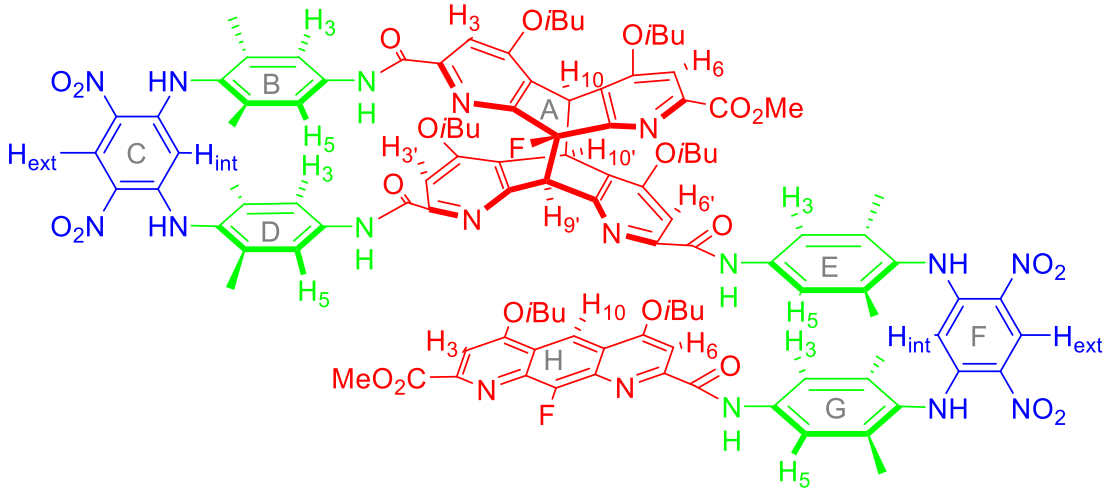

	Proton	^{1}H Chemical shift	^{13}C Chemical shift
A	H_3	7.36	104.6
	H_6	7.32	108.1
	H_{10}	5.64	32.7
	H_3’	7.31	104.1
	H_6’	7.45	104.6
	H_{10}’	5.69	32.9
	H_9’	5.14	64.8
B	NH	9.77	/
	H_3	7.94	119.5
	H_5	6.61	119.1
C	NH-B	9.11	/
	NH-D	9.11	/
	H_{ext}	9.37	124.8
	H_{int}	4.69	93.3
D	H_3	7.87	119.1
	H_5	6.51	118.8
	NH	9.34	/
E	H_3	7.22	120.5
	H_5	7.88	120.1
	NH	9.96	/
F	NH-E	9.35	/
	NH-G	9.35	/
	H_{ext}	9.42	124.9
	H_{int}	5.20	93.6
G	NH	10.18	/
	H_3	7.68	120.1
	H_5	7.44	120.3
H	H_3	7.39	97.1

	H_6	7.39	99.4
	H_{10}	8.71	110.9

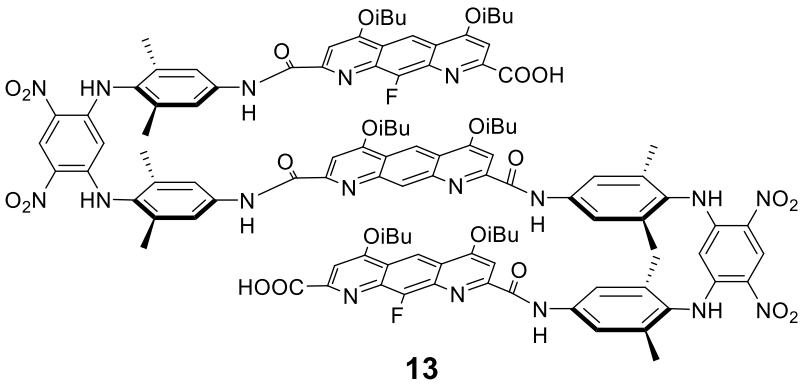

13

Oligomer diacid 13. In a round bottom flask, oligomer **12** (0.08 g, 0.038 mmol) was taken along with lithium iodide (0.05 g, 0.38 mmol) and freshly dried ethyl acetate (2 mL) was added under nitrogen atmosphere. The mixture was refluxed at 78 °C for 5 hours before it cooled down to room temperature. Solvent was removed under reduced pressure, followed by diethyl ether was added to obtained precipitate. The precipitate was filtered, and 5% aqueous citric acid solution was added. Finally, the precipitate was washed with water (three times) and cold methanol followed by dried under vacuum to obtain yellow powder which was used without further purification (0.074 g, 95% yield). ^{1}H NMR (400 MHz, $CDCl_3$, 298 K, δ ppm): 9.91 (s, 2H), 9.39 (s, 2H), 9.33 (s, 2H), 9.18 (s, 2H), 9.08 (s, 2H), 8.68 (s, 1H), 7.83 (s, 2H), 7.47 (s, 11H), 6.34 (s, 2H), 4.91 (s, 2H), 4.12 (d, J = 6.6 Hz, 8H), 3.26 (d, J = 6.6 Hz, 4H), 2.40 – 2.26 (m, 3H), 2.18 (s, 12H), 2.11 (s, 12H), 2.02 – 1.89 (m, 3H), 1.25 (d, J = 6.6 Hz, 12H), 1.21 (d, J = 6.6 Hz, 12H), 0.97 (d, J = 6.6 Hz, 12H). ^{19}F NMR (376 MHz, $CDCl_3$, 298 K, δ ppm): -129.85. HRMS (ESI): m/z calcd for $C_{110}H_{111}F_2N_{18}O_{22}$ $[M+H]^+$ 2074.8122, Found 2074.7951.

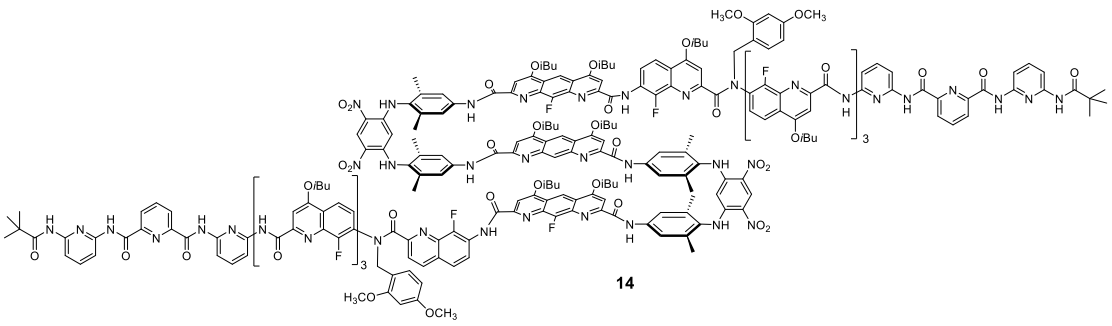

14

Oligomer 14. Diacid **13** (67 mg, 0.032 mmol) was suspended in anhydrous $CHCl_3$ (1 mL), then oxalyl chloride (27 µL, 0.32 mmol) was added and the reaction was allowed to stir at room temperature for 2 hours. The solvent and excess oxalyl chloride were removed under reduced pressure and the residue was dried under high vacuum for 3 hours to yield the corresponding acid chloride as a yellow solid. The solution of amine **9** (109 mg, 0.067 mmol) and distilled DIPEA (17 µL, 0.096 mmol) in anhydrous $CHCl_3$ (1 mL) was added dropwise via a syringe to solution of the freshly prepared acid chloride dissolved in anhydrous $CHCl_3$ (0.5 mL). The reaction was allowed to proceed at room temperature for 16 hours. After evaporation of the solvents, the crude product was purified by recycling GPC. Oligomer **14** was obtained as a yellow product (64 mg, 38% yield). ^{1}H NMR data not given due to the broadness of the peaks. ^{19}F NMR (282 MHz, $CDCl_3$, 298 K, δ ppm): -129.89, -130.59, -141.37, -141.80, -142.56. HRMS (ES+): m/z calcd for $C_{284}H_{278}F_{10}N_{48}O_{46}$ $[M+2H]^{2+}$ 2644.5410, found 2644.5188.

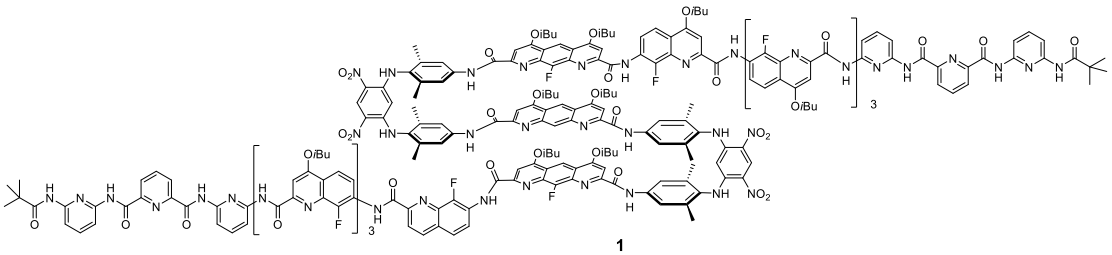

1

Oligomer 1. Dimethoxy benzyl protected oligomer **14** was taken in a 5 mL round bottom flask. To that 1 mL $CHCl_3$ and 1 mL trifluoroacetic acid added subsequently under argon atmosphere. The mixture was kept for stirring for 36 hours at room temperature. The solution poured into saturated aqueous solution of $NaHCO_3$ to neutralize, extracted with DCM, washed with water and brine respectively. The organic part was dried over anhydrous Na_2SO_4. Evaporation of organic part resulted yellow solid, which was further purified by recycling GPC. Oligomer **1** was obtained as a yellow product (49 mg, 87% yield). ^{1}H NMR (400 MHz, $CDCl_3$, 298 K, δ ppm): 11.17 (s, 2H), 10.87 (s, 2H), 10.16 (s, 2H), 10.04 (s, 2H), 9.84 (s, 2H), 9.69 (s, 2H), 9.40 (s, 2H), 9.28 (s, 2H), 9.25 (s, 2H), 9.21 (s, 2H), 9.07 (s, 1H), 8.96 (q, *J* = 6.3 Hz, 4H), 8.84 (s, 2H), 8.37 (s, 2H), 8.29 – 8.22 (m, 2H), 8.17 (d, *J* = 6.8 Hz, 5H), 8.11 (d, *J* = 13.0 Hz, 4H), 8.05 (d, *J* = 8.8 Hz, 3H), 7.78 (s, 3H), 7.76 (s, 4H), 7.69 (t, *J* = 7.5 Hz, 2H), 7.56 (s, 2H), 7.54 (s, 2H), 7.52 (s, 2H), 7.43 (s, 1H), 7.41 (s, 1H), 7.34 (s, 3H), 7.31 (s, 1H), 7.30 (s, 2H), 7.28 (s,

2H), 7.22 (s, 2H), 7.17 (s, 1H), 7.15 (s, 1H), 7.12 (s, 2H), 7.06 (s, 1H), 7.04 (s, 3H), 6.95 (s, 1H), 6.93 (s, 1H), 6.83 (t, *J* = 7.8 Hz, 2H), 6.69 (s, 2H), 6.63 (s, 2H), 6.21 (s, 1H), 6.14 (s, 2H), 5.75 (s, 2H), 5.67 (s, 2H), 4.36 (t, *J* = 7.6 Hz, 2H), 4.15 (dd, *J* = 15.6, 8.1 Hz, 10H), 4.05 (q, *J* = 7.1 Hz, 11H), 3.98 – 3.81 (m, 8H), 3.63 (t, *J* = 7.9 Hz, 3H), 3.49 (d, *J* = 7.7 Hz, 3H), 3.38 (dt, *J* = 14.7, 7.7 Hz, 1H), 3.28 (q, *J* = 7.5 Hz, 1H), 3.20 – 3.06 (m, 3H), 2.98 (t, *J* = 6.9 Hz, 2H), 2.38 (tq, *J* = 13.8, 7.4 Hz, 14H), 2.24 – 2.07 (m, 6H), 1.97 (s, 8H), 1.67 (s, 8H), 1.41 (t, *J* = 7.3 Hz, 5H), 1.35 – 1.15 (m, 84H), 1.11 (td, *J* = 7.2, 5.1 Hz, 9H), 1.04 (dd, *J* = 14.3, 6.7 Hz, 18H), 0.65 (s, 7H), 0.27 (s, 18H). ^{19}F NMR (376 MHz, $CDCl_3$, 298 K, δ ppm): -128.95, -141.78, -142.88, -143.34, -143.92. HRMS (ES+): m/z calcd for $C_{266}H_{259}F_{10}N_{48}O_{42}$ $[M+3H]^{3+}$ 1663.3177, found 1663.3151.

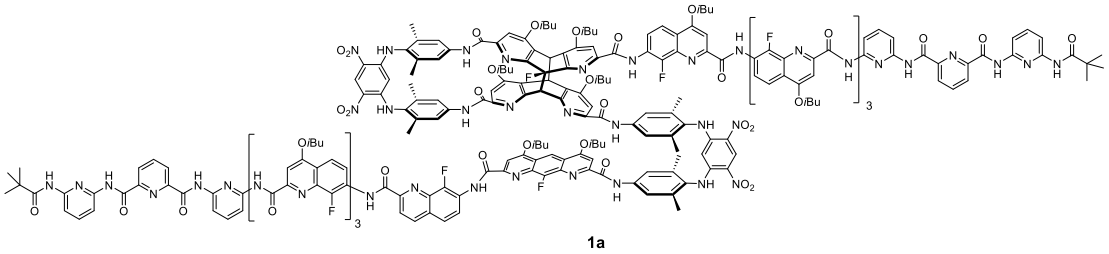

1a

Photoproduct 1a. Oligomer **1** was irradiated in $CDCl_3$ as described above and the progress was followed by ^{1}H NMR spectroscopy. After 2 hours of photoirradiation, 98% of photoproduct formation was observed. ^{1}H NMR (400 MHz, $CDCl_3$, 298 K, δ ppm): 10.95 (s, 1H), 10.86 (s, 1H), 10.65 (s, 1H), 10.21 (s, 3H), 10.17 (s, 3H), 10.03 (s, 1H), 9.84 (s, 3H), 9.78 (s, 2H), 9.66 (s, 1H), 9.63 (s, 1H), 9.58 (s, 2H), 9.47 (s, 1H), 9.35 (s, 1H), 9.31 (s, 1H), 9.25 (s, 1H), 9.21 (s, 1H), 9.11 – 8.95 (m, 4H), 8.89 (s, 1H), 8.86 (s, 2H), 8.81 (s, 3H), 8.76 (s, 2H), 8.61 – 8.51 (m, 1H), 8.32 – 8.20 (m, 3H), 8.20 – 7.98 (m, 12H), 7.96 (s, 1H), 7.93 (s, 3H), 7.81 (s, 2H), 7.78 (s, 1H), 7.76 (s, 1H), 7.72 (s, 2H), 7.67 (s, 3H), 7.55 (s, 3H), 7.52 (s, 1H), 7.42 (d, *J* = 7.0 Hz, 4H), 7.34 (s, 1H), 7.32 (s, 1H), 7.22 (s, 2H), 7.20 (s, 1H), 7.16 (s, 3H), 7.14 (s, 3H), 7.07 (s, 4H), 7.03 (s, 1H), 7.00 (s, 2H), 6.98 (s, 1H), 6.95 (s, 1H), 6.93 (s, 2H), 6.90 (s, 2H), 6.88 (s, 1H), 6.85 (d, *J* = 2.8 Hz, 3H), 6.83 (s, 2H), 6.79 (s, 1H), 6.77 (s, 1H), 6.75 (s, 2H), 6.73 (s, 2H), 6.70 (s, 1H), 6.68 (s, 2H), 6.65 (s, 4H), 6.61 (s, 3H), 6.55 (s, 2H), 6.44 (d, *J* = 7.9 Hz, 3H), 6.26 (d, *J* = 7.8 Hz, 1H), 6.20 (s, 2H), 6.12 (s, 1H), 6.10 (s, 1H), 5.48 (s, 1H), 5.34 (s, 1H), 5.30 (s, 1H), 5.27 (s, 1H), 5.24 (s, 1H), 5.07 (s, 1H), 5.06 (s, 2H), 5.03 (s, 1H), 5.00 (s, 2H), 4.86 (s, 1H),

4.37 – 4.06 (m, 24H), 3.86 – 3.05 (m, 35H), 2.77 – 2.58 (m, 3H), 2.46 (dq, *J* = 12.9, 6.7 Hz, 13H), 2.35 (t, *J* = 7.5 Hz, 4H), 2.30 – 2.14 (m, 11H), 2.02 (s, 22H), 1.91 (s, 8H), 1.88 (s, 7H), 1.80 (s, 10H), 1.44 (d, *J* = 6.7 Hz, 84H), 1.38 – 0.72 (m, 18H), 0.43 (s, 7H), 0.33 (s, 18H). ^{19}F NMR (376 MHz, $CDCl_3$, 298 K, δ ppm): -127.07, -127.17, -138.88, -139.25, -139.35, -139.83, -140.27, -140.58, -141.03, -142.60, -160.68. ^{19}F NMR (376 MHz, Proton coupled, $CDCl_3$, 298 K, δ ppm): -127.17, -138.89, -139.25, -139.36, -139.83, -140.27, -140.58, -141.04, -142.60, -160.71 (d, *J* = 37.6 Hz). HRMS (ES+): m/z calcd for $C_{266}H_{258}F_{10}N_{48}O_{42}$ $[M+2H]^{2+}$ 2494.4729, found 2494.4624.

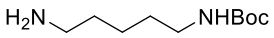

17

Synthesis of 17. In a 100 mL round bottom flask, 1,5-pentanediamine **16** (3.1 g, 30 mmol) was taken. The mixture was degassed and filled with argon. To that 50 mL of dry chloroform was added. To that solution Di-tert-butyl-dicarbonate (1.31 g 6 mmol) in 20 mL of dry chloroform was added dropwise through a dropping funnel over a period of 3 hours at room temperature. The mixture was allowed to stir for another 2 hours. Then the organic mixture was washed with water (100 mL, three times), dried over anhydrous Na_2SO_4 and solvent was evaporated to dryness to obtain **17** (1.2 g 98%) as colorless oil. The ^{1}H-NMR indicated that the crude product was highly pure and, therefore, no further purification was performed. ^{1}H NMR (300 MHz, $CDCl_3$, 298 K, δ ppm): 4.53 (s, br, 1H), 3.11 (q, *J* = 6.6 Hz, 2H), 2.68 (t, *J* = 6.8 Hz, 2H), 1.62 – 1.07 (m, 15H).

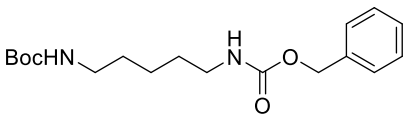

18

Synthesis of 18. In a 25 mL round bottom flask, Boc-protected amine **17** (1.1 g 5.4 mmol) was taken. To that 16 mL aqueous NaOH (4M) and followed by benzyl chloroformate (0.85 mL, 6.5 mmol) was added. The mixture was stirred at room temperature for 16 hours. The crude product was extracted with ethyl acetate. The organic layer was washed with brine and dried over anhydrous Na_2SO_4. After solvent was removed in vacuo, the residue was purified by column

chromatography (silica gel, ethyl acetate and cyclohexane as eluent) to get **18** as colorless liquid (1.8 g, 98%). ^{1}H NMR (300 MHz, $CDCl_3$, 298 K, δ ppm): 7.40 – 7.28 (m, 5H), 5.09 (s, 2H), 4.78 (s, 1H), 4.53 (s, 1H), 3.28 – 2.99 (m, 4H), 1.56 – 1.19 (m, 15H). ^{13}C NMR (75 MHz, $CDCl_3$, 298 K, δ ppm): 156.59, 156.19, 136.75, 128.70, 128.65, 128.27, 128.23, 127.78, 127.12, 66.75, 41.00, 40.43, 29.84, 29.69, 28.56, 23.92. HRMS (ESI): m/z calcd for $C_{18}H_{28}N_2O_4Na$ $[M+Na]^+$ 359.1941, found 359.2114.

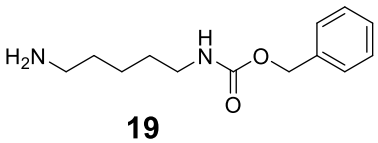

19

Synthesis of 19. In a 10 mL round-bottom flask, **18** (1.6 g, 4.75 mmol) was dissolved in 3 mL dichloromethane and subsequently, 3 mL TFA was added dropwise. The mixture was allowed to stir for 3 hours at room temperature. A saturated aqueous solution of $NaHCO_3$ was added to quench the excess acid. Then, the solution was extracted with CH_2Cl_2, washed with water, dried over Na_2SO_4 and evaporated. The amine **19** was obtained without any further purification as a colorless liquid (1.1 g, 99% yield). ^{1}H NMR (300 MHz, $CDCl_3$, 298 K, δ ppm): 7.40 – 7.28 (m, 5H), 5.09 (s, 2H), 4.76 (s, 1H), 3.20 (q, *J* = 6.7 Hz, 2H), 2.68 (t, *J* = 6.8 Hz, 2H), 1.73 – 1.21 (m, 6H). ^{13}C NMR (75 MHz, $CDCl_3$, 298 K, δ ppm): 156.57, 136.75, 128.61, 128.25, 128.19, 127.58, 127.02, 66.68, 41.71, 41.02, 39.85, 32.59, 29.81, 29.71, 24.00. HRMS (ESI): m/z calcd for $C_{26}H_{41}N_4O_4$ $[2M+H]^+$ 473.3122, found 473.3176.

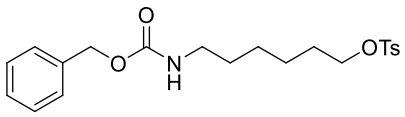

21

Synthesis of 21. In a 50 mL round bottom flask, **20** (1 g 3.98 mmol), 4-toluenesulfonyl chloride (1.14 g, 6 mmol), *N*,*N*-dimethylpyridin-4-amine (49 mg, 0.4 mmol) were taken. The mixture was degassed and filled with argon. Subsequently, 20 mL dry dichloromethane and followed by triethylamine (2.78 mL, 20 mmol) was added when temperature was maintained at 0 °C by ice water bath. The mixture was stirred at 0 °C for 1 hour and then brought to room temperature where it was stirred for another 5 hours. The mixture was neutralized by 2M aqueous HCl solution and extracted with dichloromethane. The organic layer was washed with 5% aqueous

$NaHCO_3$, brine and dried over anhydrous Na_2SO_4. After the solvent was removed in vacuo, the residue was purified by column chromatography (silica gel, dichloromethane and cyclohexane as eluent) to give **21** as white solid (1.56 g, 97%). ^{1}H NMR (300 MHz, $CDCl_3$, 298 K, δ ppm): 7.83 – 7.74 (m, 2H), 7.40 – 7.28 (m, 7H), 5.09 (s, 2H), 4.70 (s, 1H), 4.01 (t, *J* = 6.4 Hz, 2H), 3.15 (q, *J* = 6.7 Hz, 2H), 2.45 (s, 3H), 1.63 (t, *J* = 7.1 Hz, 2H), 1.44 (d, *J* = 8.0 Hz, 2H), 1.29 (dtd, *J* = 14.3, 7.1, 3.7 Hz, 4H). ^{13}C NMR (75 MHz, $CDCl_3$, 298 K, δ ppm): 156.50, 144.84, 136.74, 133.31, 129.97, 128.67, 128.26, 128.02, 70.54, 66.77, 40.99, 29.91, 28.86, 26.16, 25.17, 21.78. HRMS (ESI): m/z calcd for $C_{21}H_{27}NNaO_5S$ $[M+Na]^+$ 428.1502, found 428.1596.

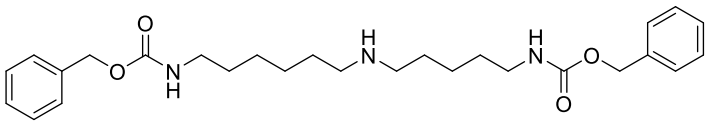

NC_{11}

Synthesis of NC_{11}. In a 10 mL round bottom flask, compounds **19** (709 mg, 3 mmol) and **21** (1.216 g, 3 mmol) were taken. The mixture was degassed and filled with argon. To that 5 mL dry dimethylformamide (DMF) was added followed by triethylamine (1.25 mL, 9 mmol). The mixture was stirred at 80 °C for 16 hours. Solvent was removed under vacuum. The mixture was neutralized with 5% citric acid (aqueous). At this point some white precipitate was obtained. The precipitate was filtered and neutralized by aqueous NaOH solution (4M) to obtain **NC_{11}** (450 mg, 32%) as white solid, which is highly pure as indicated by the ^{1}H-NMR. ^{1}H NMR (300 MHz, $CDCl_3$, 298 K, δ ppm): 7.43 – 7.29 (m, 10H), 5.09 (s, 4H), 4.76 (s, 2H), 3.26 – 3.09 (m, 4H), 2.57 (td, *J* = 7.1, 3.0 Hz, 4H), 1.62 – 1.4 (m, 8H), 1.41 – 1.20 (m, 6H). ^{13}C NMR (75 MHz, $CDCl_3$, 298 K, δ ppm): 156.54, 136.79, 128.66, 128.26, 128.23, 66.73, 50.07, 50.00, 41.15, 30.16, 30.03, 29.91, 27.13, 26.75, 24.65. HRMS (ESI): m/z calcd for $C_{27}H_{40}N_3O_4$ $[M+H]^+$ 470.3013, found 470.3098.

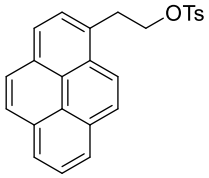

24

Synthesis of 24. In a 50 mL round bottom flask, **23** (900 mg, 3.65 mmol), 4-toluenesulfonyl chloride (1 g, 5.5 mmol), *N*,*N*-dimethylpyridin-4-amine (45 mg, 0.4 mmol) were taken. The mixture was degassed and filled with argon. Subsequently, 20 mL dry dichloromethane and followed by triethylamine (2.5 mL, 18 mmol) was added when temperature was maintained at 0 °C by ice water bath. The mixture was stirred at 0 °C for 1 hour and then brought to room temperature where it was stirred for another 5 hours. The mixture was neutralized by 2M aqueous HCl solution and extracted with dichloromethane. The organic layer was washed with brine and dried over anhydrous Na_2SO_4. After the solvent was removed in vacuo, the residue was purified by column chromatography (silica gel, dichloromethane and cyclohexane as eluent) to get **24** as pale-yellow solid (875 mg, 60%). ^{1}H NMR (300 MHz, $CDCl_3$, 298 K, δ ppm): 8.19 (td, *J* = 7.3, 1.2 Hz, 2H), 8.10 – 7.97 (m, 6H), 7.80 (d, *J* = 7.8 Hz, 1H), 7.36 – 7.29 (m, 2H), 6.73 – 6.66 (m, 2H), 4.45 (t, *J* = 6.8 Hz, 2H), 3.68 (t, *J* = 6.9 Hz, 2H), 1.87 (s, 3H). HRMS (ESI): m/z calcd for $C_{25}H_{20}NaO_3S$ $[M+Na]^+$ 423.1025, found 423.1111.

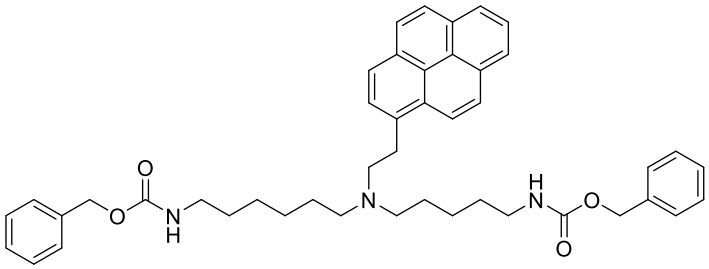

$NC_{11}Py$

Synthesis of $NC_{11}Py$. In a 10 mL round bottom flask, **NC_{11}** (70 mg, 0.15 mmol), **24** (72 mg, 0.18 mmol) and K_2CO_3 (124 mg, 0.9 mmol) were taken. The mixture was degassed and filled with argon. Subsequently, 5 mL dry acetonitrile was added. The mixture was refluxed for 1 day and then brought to room temperature. The solvent was removed under vacuum. The crude product was purified by column chromatography (silica gel, dichloromethane and methanol as eluent) to get **$NC_{11}Py$** as pale-yellow solid (54 mg, 52%). ^{1}H NMR (300 MHz, $CDCl_3$, 298 K, δ ppm): 8.29 (d, *J* = 9.2 Hz, 1H), 8.21 – 8.07 (m, 4H), 8.05 – 7.96 (m, 3H), 7.87 (d, *J* = 7.8 Hz, 1H), 7.41 – 7.27 (m, 10H), 5.08 (s, 4H), 4.75 (br, 2H), 3.51 (br, 2H), 3.27 – 3.03 (m, 4H), 2.93 (br, 2H), 2.61 (br, 4H), 1.82 – 1.10 (m, 14H). HRMS (ESI): m/z calcd for $C_{45}H_{52}N_3O_4$ $[M+H]^+$ 698.3952, found 698.3975.

Chapter III: Prusik Knot: from real world to molecular world

1. Introduction

Knots are the common and basic units of topologic structures which are widely employed in sports, architecture, agriculture, navigation and medical treatment. We can see knots in our life every days and everywhere. From ancient time, human make great effort to develop the ability to tie knots, enabling people to make advanced tools such as fishing nets and wave fabrics. In some case, knots can even be used to record and deliver information.[1]

At the molecular level, knots are also found in DNA and around 1% of proteins.[2] They are formed by polymeric chains which have enough length and flexibility. In 1989, the first synthetic molecular trefoil knot was reported,[3] knot theory and chemistry were connected together. The interest for knots encouraged scientists to investigate different molecular knot topologies.

Figure 1. Representation of some of basic knots in the real word.

In mathematics, a knot is theoretically defined as an embedding of a topological circle. Different with the open strings used to tie knots in our daily life (Figure 1), the mathematical knots are closed circles. There are no ends or terminals to tie or untie on a mathematical knot.

Alexander–Briggs notation is the most traditional way to classify knots:[4] knots have been catalogued in terms of crossing numbers. Every knot is represented as X_Y, where X corresponds

1 Mann, C. C. *Science* **2005**, *309*, 1008-1009; Fielden, S. D. P.; Leigh, D. A.; Woltering, S. L. *Angew. Chem. Int. Ed.* **2017**, *56*, 11166-11194.
2 Wasserman, S. A.; Cozzarelli, N. R. *Science* **1986**, *232*, 951; Sułkowska, J. I.; Rawdon, E. J.; Millett, K. C.; Onuchic, J. N.; Stasiak, A. *Proc. Natl. Acad. Sci. USA* **2012**, *109*, E1715; Frank-Kamenetskii, M. D.; Lukashin, A. V.; Vologodskii, A. V. *Nature* **1975**, *258*, 398-402.
3 Dietrich-Buchecker, C. O.; Sauvage, J.-P. *Angew. Chem. Int. Ed.* **1989**, *28*, 189-192.
4 Alexander, J. W.; Briggs, G. B. *Ann. Math.* **1926**, *28*, 562-586.

to the number of crossings and Y is the index number to denote its order from all knots with that number of crossings (Figure 2). This order is sorted by increasing torsion number in the knots with a determined crossing number. A knot without any crossing is termed as "unknot", and corresponds to a macrocycle at the molecular level (Figure 2). Trefoil knot (3_1) contains the minimum number of crossings and it is the simplest sample of a nontrivial knot.

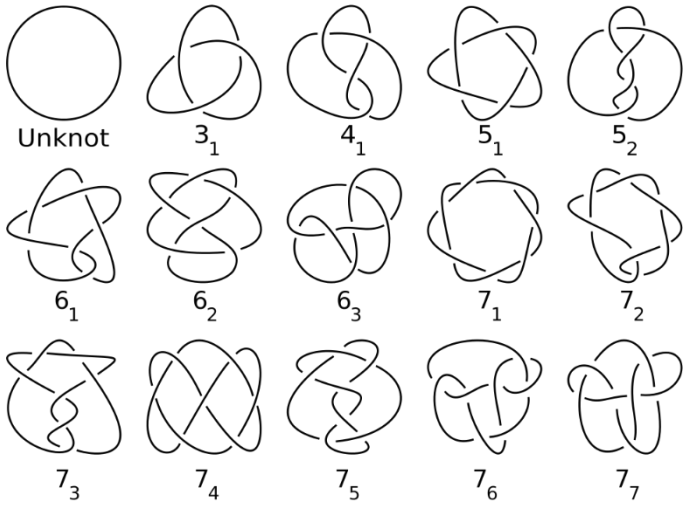

Figure 2. Knot table of all prime knots having up to seven crossings including the "unknot".

In diagrammatic form of knots, the transformation between different knot diagrams corresponding to the same knot can be achieved by a sequence of three types of operations in the diagram. These operations were independently discovered by Reidemeister as well as Alexander and Briggs, and are termed *Reidemeister moves* (Figure 3).[5] They are: (Reidemeister move I, RI) add or reduce a twist to a single strand in any direction; (Reidemeister move II, RII) move one strand entirely over another; (Reidemeister move III, RIII) move one strand over or under a crossing of two other strands.

5 Reidemeister, K. *Abh.Math.Semin.Univ.Hambg*. **1927**, *5*, 24-32.

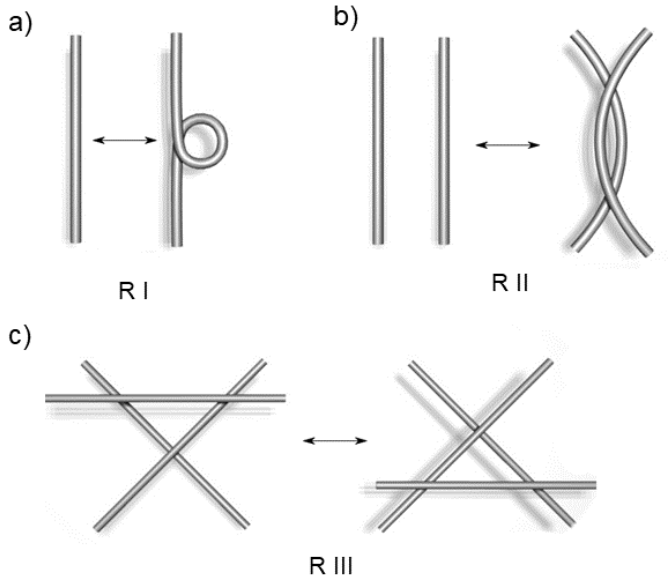

Figure 3. Schematic representation of Reidemeister moves; a) Reidemeister move I, add or reduce a twist to strand, RI changes the overall writhe of the knot by adding or reducing a nugatory crossing; b) Reidemeister move II, move one strand entirely over another, RII creates two new crossing points; c) Reidemeister move III, move one strand over or under a crossing of two other strands.

The synthesis of trefoil knot 3_1 was first reported by Sauvage and coworkers with their double-stranded metal helicate strategy.[6] In their design, 1,10-phenanthroline units were used to fold around a metallic template (Cu^I) to form a double helical complex, like (**3.1a**)$_2$. After connecting the ends of the helical complex, the metal-assembled precursor **3.2a** was obtained. The topology of the precursor was confirmed by X-ray crystallography (Figure 4b) as the complex showed a D_2 symmetry. In their first example **3.3**, alkyl chains were used to link two phenanthroline units and was obtained in low yield (8%). Thus, phenylene groups were employed as spacers between two phenanthroline units (**3.1a** and **3.1b**), so that they can promote the preorganization of the helical complex improving the overall yield of the precursor **3.2a** to 29%. Ring closing metathesis (RCM) was carried out with **3.2b** to yield the knot (74%).

6 Dietrich-Buchecker, C. O.; Guilhem, J.; Pascard, C.; Sauvage, J.-P. *Angew. Chem. Int. Ed.* **1990**, *29*, 1154-1156; Dietrich-Buchecker, C. O.; Sauvage, J.-P.; De Cian, A.; Fischer, J. *Chem. Commun.* **1994**, 2231-2232.

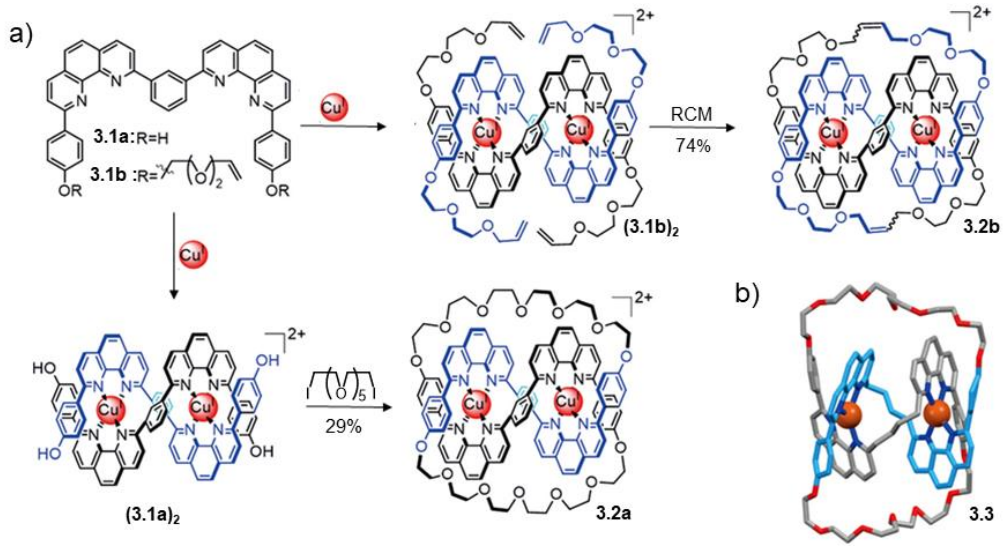

Figure 4. The synthesis of trefoil knot with metal helicate strategy; a) preparation of knot **3.2a** and **3.2b**. Williamson ether synthesis was performed with **$(3.1a)_2$** to obtain **$Cu_2$3.2a.** RCM could remarkably improve the yield of **3.2b**; b) X-ray structure of the **3.3**, the initial design with short alkyl chain as linker between phenanthroline units leads to low yield.

D_2 symmetric **3.3** was obtained as helix-metal complex, it was also the precursor of trefoil knot 3_1.[7] After demetalation of the Cu^I templates, the *D_2*-symmetric helical compound **3.3a** was obtained. A *D_3*-symmetric knot 3_1 was obtained after a sequence of Reidemeister moves (Figure 5a). The process can also be double-checked in the real world knots (Figure 5c).

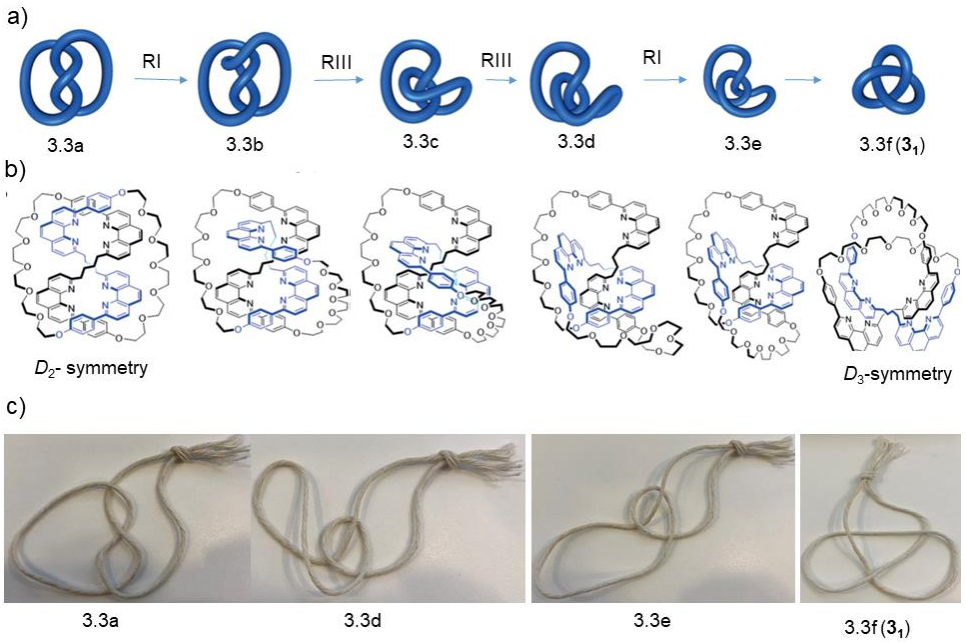

7 Dietrich-Buchecker, C. O.; Sauvage, J.-P. *Angew. Chem. Int. Ed.* **1989**, *28*, 189-192.

Figure 5. Schematic representation of formation of trefoil knot $\mathbf{3_1}$; a) Reidemeister move sequences processed from a D_2-symmetric double helix conformation to a D_3-symmetric diagram; b) the molecular structures correspond to each step in a); c) real world knot moved with the same Reidemeister move sequences with a) and b).

Leigh and co-worker reported another efficient synthesis of a left-handed trefoil knot **3.5** starting from oligomer **3.4** composed of three 2,6-pyridinedicarboxamide ligands (Figure 6).[8] The oligomer folds around a lanthanide ion to form a knot complex with a single handedness. Joining the end groups by ring-closing olefin metathesis affords the trefoil knot in 90% yield. The trefoil knot is D_3-symmetric and was used as an effective catalyst for the asymmetric Mukaiyama aldol reaction.

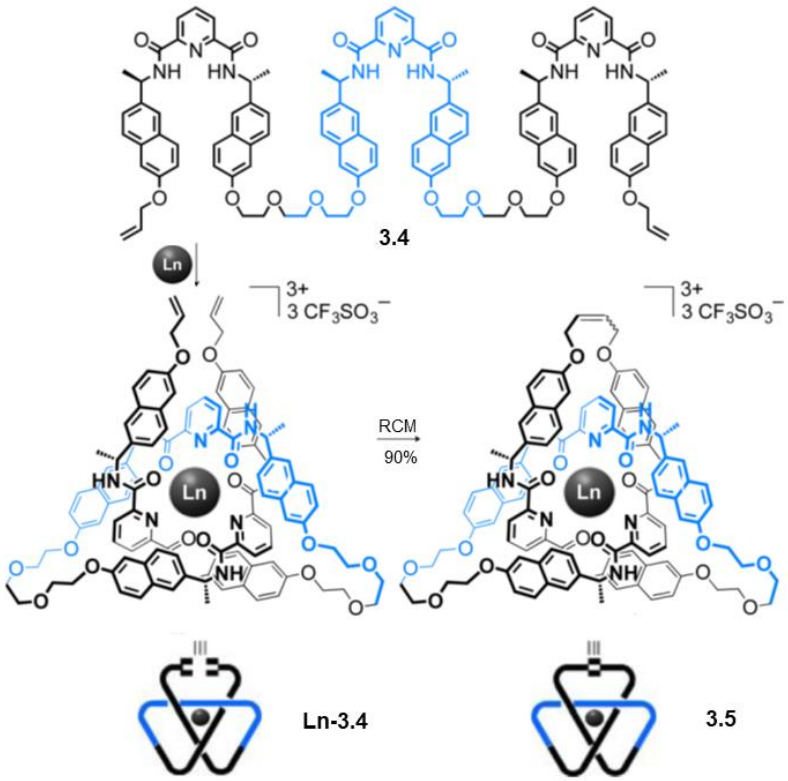

Figure 6. Synthesis of a 3_1 knot **3.5** with Ln(III)- tris(2,6-pyridinedicarboxamide) complex.

Leigh and co-workers also reported a strategy to synthesize a pentafoil knot (5_1) based on a Fe(II)-tri(bipyridine) complex (Figure 7).[9] Upon mixing the tri(bipyridine) ligand strand **3.6**

8 Gil-Ramírez, G.; Hoekman, S.; Kitching, M. O.; Leigh, D. A.; Vitorica-Yrezabal, I. J.; Zhang, G. *J. Am. Chem. Soc.* **2016**, *138*, 13159-13162.

9 Ayme, J.-F.; Beves, J. E.; Leigh, D. A.; McBurney, R. T.; Rissanen, K.; Schultz, D. *Nat. Chem.* **2012**, *4*, 15-20; Ayme, J.-F.; Beves, J. E.; Leigh, D. A.; McBurney, R. T.; Rissanen, K.; Schultz, D. *J. Am. Chem. Soc.* **2012**, *134*, 9488-9497; Beves, J. E.; Campbell, C. J.; Leigh, D. A.; Pritchard, R. G. *Angew. Chem. Int. Ed.* **2013**, *52*, 6464-6467; Marcos, V.; Stephens, A. J.; Jaramillo-Garcia, J.; Nussbaumer, A. L.; Woltering, S. L.; Valero, A.; Lemonnier, J.-F.; Vitorica-Yrezabal, I. J.; Leigh, D. A. *Science* **2016**, *352*, 1555.

with $FeCl_2$, pentameric circular helicate $[Fe_5\mathbf{3.6}_5]Cl$ was formed. It adopts a circular conformation while placing the alkene termini of **3.6** strands very close one to the other. The RCM was performed with $[Fe_5\mathbf{3.6}_5]Cl$ to obtain the pentafoil knot **3.7** in 98% yield. The conformation of the architecture was confirmed by X-ray crystallography (Figure 7b). Pentafoil knot **3.7** could be demetalated under basic conditions without decomposition.

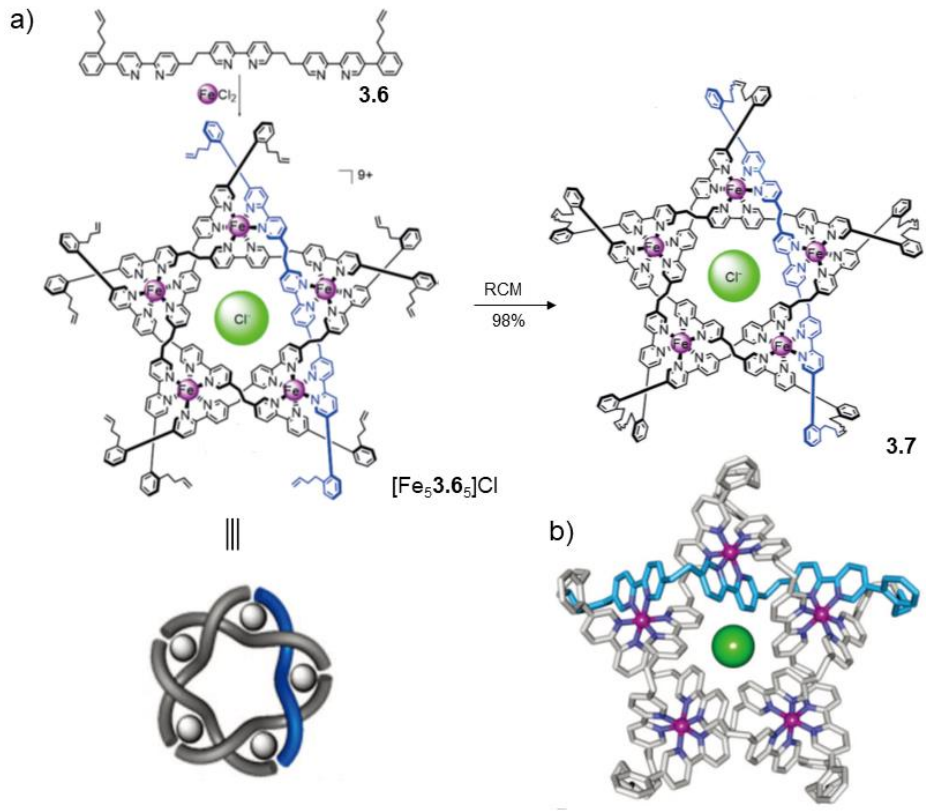

Figure 7. Schematic representation of formation of pentafoil knot **3.7**; a) pentafoil knot **3.7** can be obtained in high yield from the precursor complex $[Fe_5\mathbf{3.6}_5]Cl$, which contained closer end groups for RCM process; b) solid-state structure of **3.7**.

Leigh and co-workers also reported the preparation of the higher order knot 8_{19} **3.9** with Fe(II)-tri(bipyridine) complex (Figure 8).[10] Although different from **3.7**, the complex was built up with Fe(II) ion and three bipyridine containing strands. The complexation of $FeCl_2$ to **3.8** formed a circular triple helicate. The knot complex Fe_4**3.9** can be obtained using RCM in 62% yield. Following the treatment of NaOH, the demetalled 8_{19} knot **3.9** can be afforded.

10 Danon, J. J.; Krüger, A.; Leigh, D. A.; Lemonnier, J.-F.; Stephens, A. J.; Vitorica-Yrezabal, I. J.; Woltering, S. L. *Science* **2017**, *355*, 159.

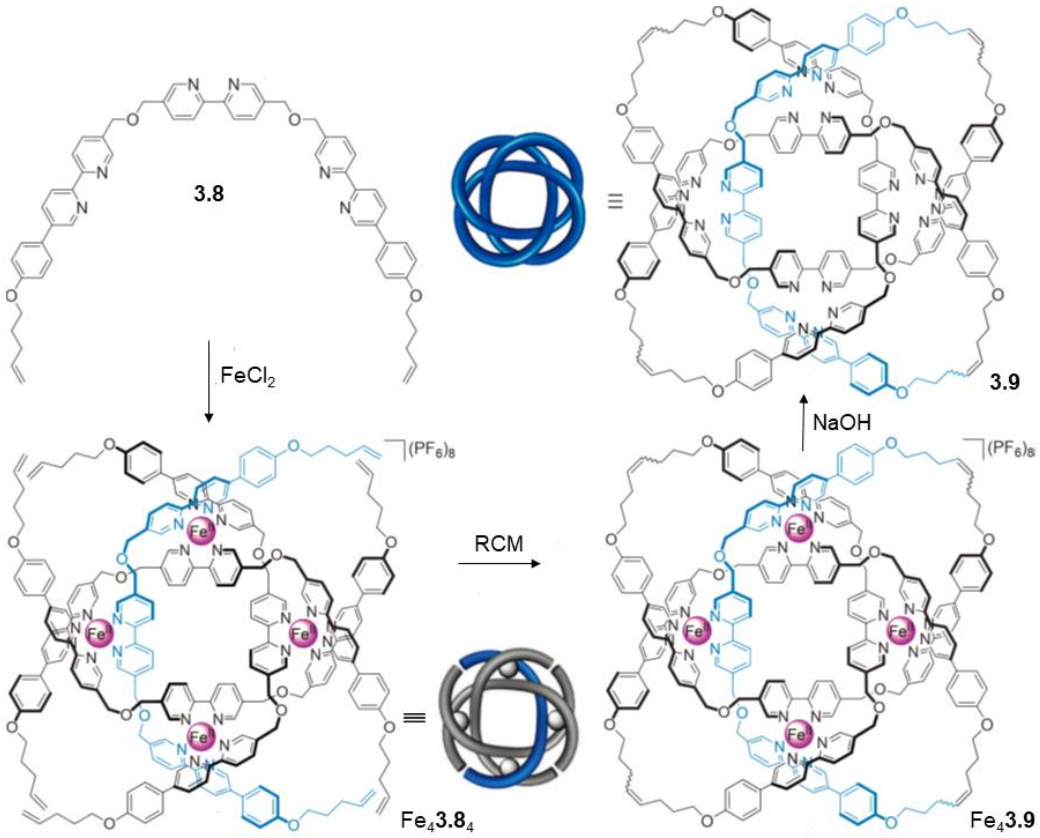

Figure 8. Synthesis of a 8_{19} knot **3.9** with Fe(II)-tri(bipyridine) complex.

2. The Prusik knot

2.1 Prusik knot in our world

In mathematics, knots are defined as closed topological circles. The area of mathematics which studies knots is known as knot theory. With the development of chemistry, scientists found that knot theory and chemistry can be related closely. Afterwards, more and more scientists were attracted to explore the property and structure of knots at the molecular level.

Knots also play a significant role in our living world, countless knots are employed in various areas. In this section, we will focused on a peculiar structure, the Prusik knot (Figure 9a). A Prusik knot can be constructed by attaching a loop of cord around a rope. It is widely used in climbing, caving, mountaineering, rope rescue and gardening. Prusik knot is easily tied by wrapping a double strap around a rope for a number of times (Figure 9b), the end of the double strap then hangs out from the middle of turn.

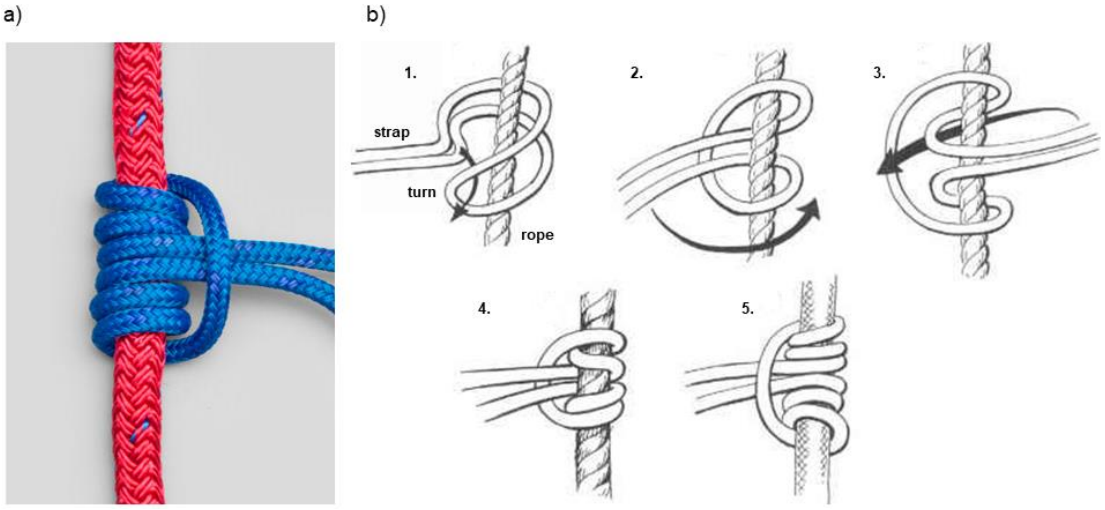

Figure 9. Representation of Prusik knots in daily life; a) the Prusik knots, b) strategy to tie a Prusik knot. Step 1-2, wrap a double strap around the rope for 1st time; Step 3-4, wrap for 2nd time; Step 5, take the ends of strap out from middle of turn.

When the ends of a strap are weighted or forced, the turn of knot are tightened and give a slight bent in the rope. As a result, the position of the knot is fixed on the rope and it is impossible to move or slide any more (Figure 10a). After the weight is cleared away, the knot can slide along the rope with manual pushing (Figure 10b). The use of Prusik knot in climbing, allows to keep the climber safe and efficient. Below one can find an example for ascending the line by using two Prusik knots (Figure 10c). The top knot is directly linked to the safety belt and the bottom one is equipped with a foot-long length of cord which can be reached by one foot. At first the climber can "stand up" in the foot cord and slide the top Prusik knot to a higher positon (bottom knot is weighted and tightened to keep him safe), then he can "sit" down and move the bottom knot up around the rope (top knot is tightened and bottom knot is free to move), after that he can "stand" up in the foot cord again to move the top knot to further, repeat the "stand and sit" process can make climber efficient and safe.

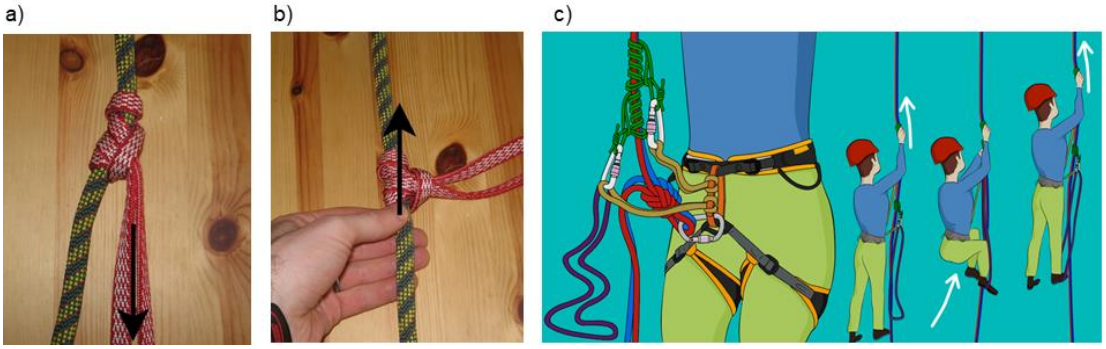

Figure 10. Representation of property of Prusik knots; a) when the knot is weighted, it forms a tight structure and fix its own position in the rope; b) when the knot is free, it can slide along the rope; c) process of using two Prusik knots to ascend around a rope, tighten and move between two knots alternately make climb efficient.

2.2 Designing a molecular Prusik knot: turns and aromatic sheets

In the past two decades, chemists have reported numerous non-natural foldamer backbones adopting well-defined conformations analogous to the secondary motifs of biopolymers, such as helices, sheets and turns.[11] This new paradigm holds great promise for molecular design. Among these motifs, foldamer helices attracted great attention while only few examples of artificial sheets and turns were reported.

To explore more complex architectures, our group incorporated turn segments into helical structures to form helix-turn-helix motifs. Those motifs form "super secondary structures" that are different to simple isolated helix or aromatic sheet. Those "super secondary structures" are prepared using aromatic oligoamide helical segments and turn units.

2.2.1 Dinitrobenzene units

Aromatic oligoamide sheets stabilized by π-π interactions were introduced between short linear segments and rigid turn units such as **T_1** and **T_{1a}** that can adopt face-to-face orientation (Figure 11).[12] **T_1** and **T_{1a}** present a well-organized conformation containing parallel xylyl rings, the distance between two parallel rings imparted by the dinitrobenzene unit is 4.8 Å. Four methyl groups *ortho* to the aromatic amine functions are the key points to hold the two xylyl rings parallel to each other and perpendicular to the dinitrobenzene units. Furthermore rigid aromatic interactions were found to favor elongation of the linear segments, further development of aromatic sheet structures are based on the xylyl hairpin turn motif due to its well-organized architecture.

11 De, S.; Chi, B.; Granier, T.; Qi, T.; Maurizot, V.; Huc, I. *Nat. Chem.* **2018**, *10*, 51-57.
12 Sebaoun, L.; Kauffmann, B.; Delclos, T.; Maurizot, V.; Huc, I. *Org. Lett.* **2014**, *16*, 2326-2329; Sebaoun, L.; Maurizot, V.; Granier, T.; Kauffmann, B.; Huc, I. *J. Am. Chem. Soc.* **2014**, *136*, 2168-2174; Lamouroux, A.; Sebaoun, L.; Wicher, B.; Kauffmann, B.; Ferrand, Y.; Maurizot, V.; Huc, I. *J. Am. Chem. Soc.* **2017**, *139*, 14668-14675.

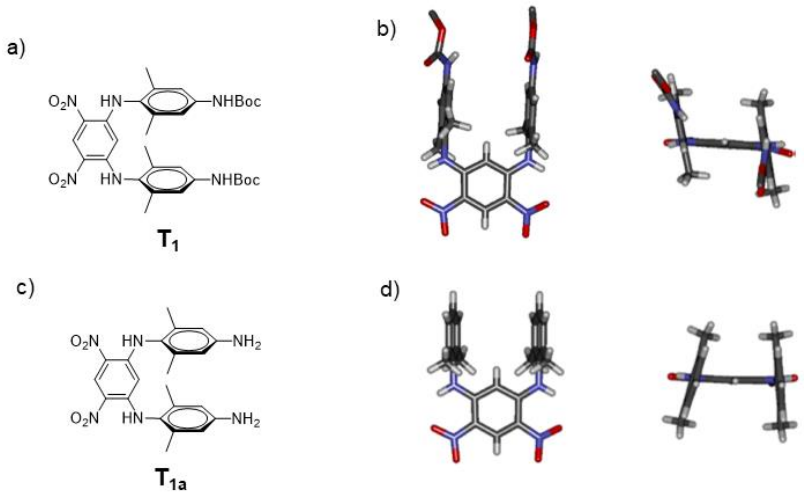

Figure 11. Schematic representation of xylyl hairpin turn a) $\mathbf{T_1}$ and c) $\mathbf{T_{1a}}$; side view and front view of the crystal structures of b) $\mathbf{T_1}$ and d) $\mathbf{T_{1a}}$.

2,5-dialkoxy-terephthalic acid units were used as linear segments to connect the hairpin turns to form a macrocycle (Figure 12a).[13] The 2,5-alkoxy substituents act as hydrogen bond acceptors which favor coplanar orientation of the aryl and adjacent amide bonds. The macrocyclic aromatic sheets represent tight models of two-stranded sheets. Rotation of the central terephthalamide was also observed, followed with a slower rotation of the xylyl units. The rotation of central units resulted in the coexistence of parallel and anti-parallel orientation of the terephtalamide segments, while the electrostatic effects favored anti-parallel conformer over the parallel conformer.

Multi-turn aromatic sheet structures were also reported (Figure 12b, 12c), the three-stranded (two turns) structure of $\mathbf{T_3}$ and five-stranded (four turns) structure of $\mathbf{T_4}$ showed a similar folding, with the xylyl rings perpendicular to the dinitrophenyl moieties. The central segments of each strand forms a face-to-face stack of three or five terephthalamide units at a 3.5 Å distance for $\mathbf{T_3}$ and $\mathbf{T_4}$ respectively. The aryl-aryl distance between the xylyl groups imparted by the dinitrobenzene group was measured to be 4.8 Å, which indicates an attractive interaction between stacked sheets. Similarly to $\mathbf{T_2}$ adjacent central terephthalamides in both $\mathbf{T_3}$ and $\mathbf{T_4}$ showed an anti-parallel orientation, stabilized by the stacked aromatic.

13 Sebaoun, L.; Maurizot, V.; Granier, T.; Kauffmann, B.; Huc, I. *J. Am. Chem. Soc.* **2014**, *136*, 2168-2174.

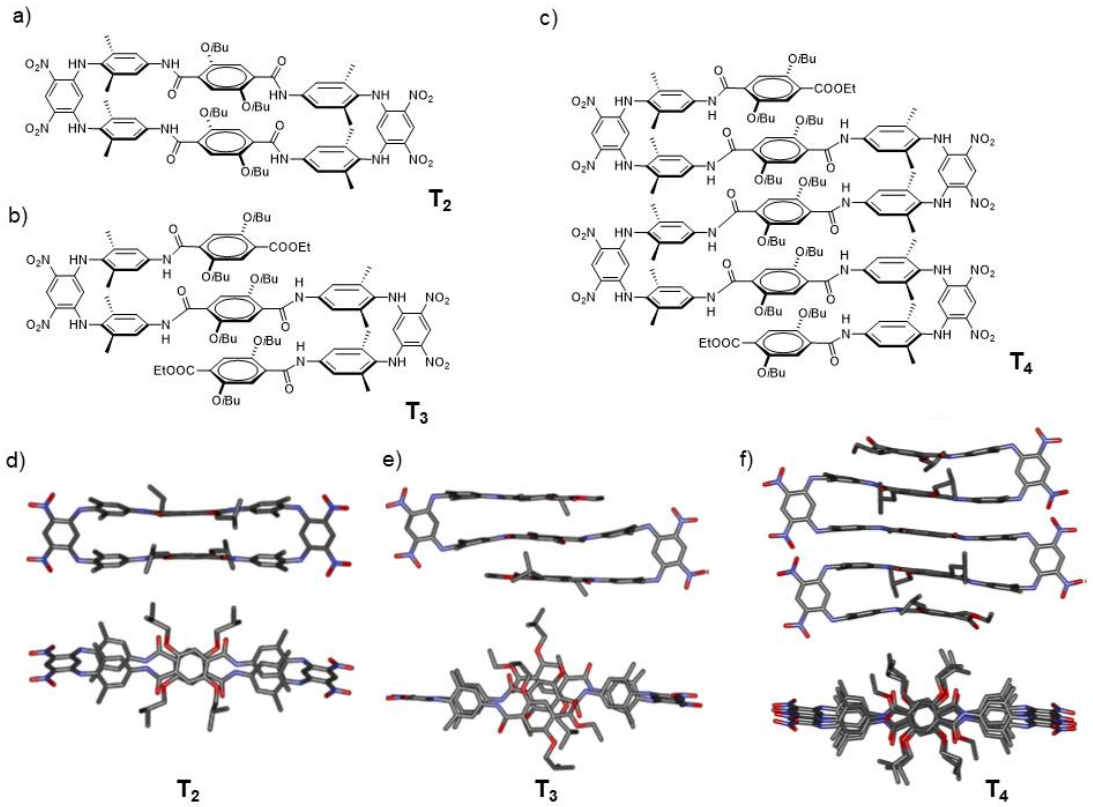

Figure 12. Schematic representation of a) macrocyclic aromatic sheets **T2,** b) three-stranded sheet **T3**, c) five-stranded aromatic sheet **T4**, d) the energy minimized conformation of **T2**; side view and top view of the crystal structures of e) **T3** and f) **T4**.

2.2.2 Squaramides units

A new hairpin turn units was designed using tertiary squaramides (Figure 13).[14] The design of turn **T5** was based on the conformational preference of N,N'-diaryl squaramides which favours *cis-cis* conformations, implying that the two aryl rings of **T5** are close to parallel. A significant aspect is the orientation of the protected amine and acid groups of **T5**. Substitution at *para* and *meta* positions is designed for substituents to be oriented in the same direction. The methoxy group adjacent to the ester of **T5** allows a control of the orientation of a secondary amide by hydrogen bonding.

14 Atcher, J.; Nagai, A.; Mayer, P.; Maurizot, V.; Tanatani, A.; Huc, I. *Chem. Commun*. **2019**, *55*, 10392-10395.

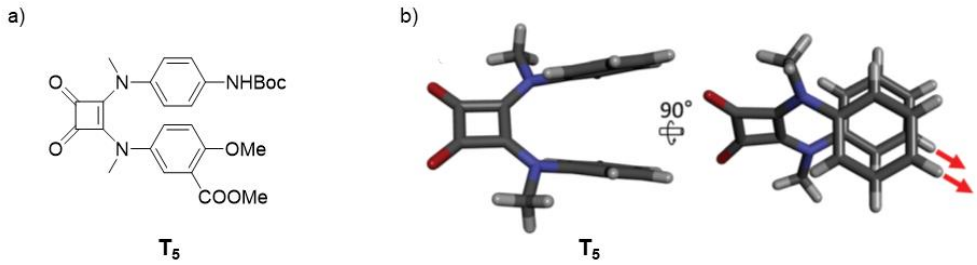

Figure 13. Schematic representation of tertiary squaramide based turn unit **T5**. Side and top view of the crystal structure of **T5**.

Larger aromatic units 1,8-diaza-anthracenes were attached to **T5** to prepare new architectures. Macrocyclic sheets **T6** contains two turns, *cis-cis* squaramides and parallel (head-to-head) anthracene units (Figure 14a). The twist of the squaramide plane confers an inherent chirality, resulting in overall C_2-symmetry.

T7 was found to have more degrees of freedom than **T6** because it is not cyclic (Figure 14b). Two anthracene units in **T7** revealed to be in head-to-tail conformation which results in a minimal overlap between aromatic rings and extensive overlap between each anthracene unit and an isobutoxy side chain of the other units.

Three-stranded (two turns) structure was used to investigate the effect of an additional aromatic layer (Figure 14c). In the crystal structure of **T8**, one turn leads to a head-to-head arrangement of anthracene units while the other turn dose not promote a well folded sheet formation. Its N- and C- termini do not point in the same direction, the turn is flipped at 180° to keep terminal anthracene units in the same plane.

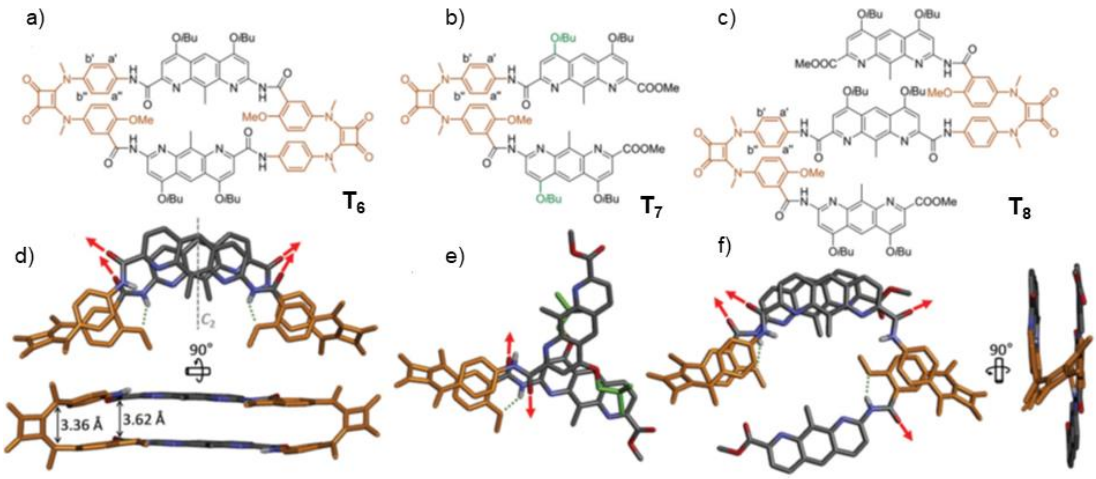

Figure 14. Chemical structures (a–c) and crystal structures (d–f) of compounds **T6, T7** and **T8**. Some 1,8-diaza-anthracene units derive from an amino acid, others from a diacid. In the crystal structures the non-

polar hydrogen atoms are omitted for clarity. *i*Bu side-chains are also omitted except in (e), where two of them are shown in green. In (d–f) red arrows show the orientation of the amides adjacent to the squaramide turn. Green dotted lines indicate hydrogen bonds within the turn unit.

2.2.3 Pyridine-dicarboxamide motifs

A new kind of multi-turn aromatic sheet structures was designed with two different turns,[15] a short turn **T_{1a}** that is constituted of a dinitrobenzene group (Figure 15a) and larger turn **T_9** (Figure 15b) that is constituted of a N,N'-dibenzyl 2,6-pyridine-dicarboxamide motif. Strand curvature associated to the anthracene units gives rise to a head-to-head arrangement of stacked aromatics within a curved two stranded sheet (Figure 15e). **T_{11}** dimerized through a reciprocal intercalation for which the N-oxide P^{NO} function of one strand and 2,6-pyridine-dicarboxamide derivatives amide NH of the other strand act as hydrogen bond acceptor and donor, respectively.

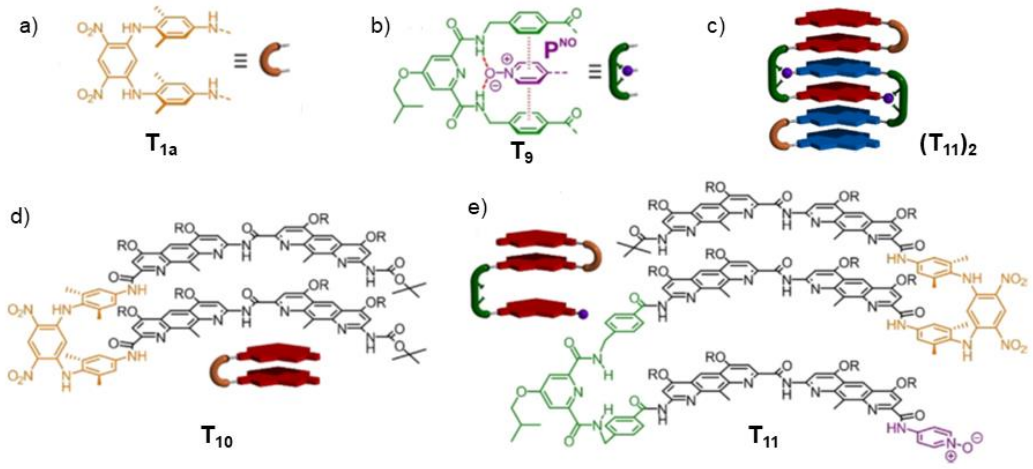

Figure 15. a-b) Chemical structures of **T_{1a}**, **T_9** and **P^{NO}**, and association mode of the latter two (dashed lines depict hydrogen bonds while hashes show aromatic stacking); c) Schematic representation of a self-assembled aromatic sheet **$(T_{11})_2$**; chemical structure and schematic representation of d) two-stranded aromatic sheet **T_{10}** and **e)** two-stranded aromatic sheet **T_{11}** (R=-$CH_2CH(CH_2CH_3)_2$).

2.3 Designing a molecular Prusik knot

As shown above, in the macroscopic world the Prusik knot can be tied by two loops. At the molecular level, we can envisage to use a folded structure such as an aromatic oligoamide helix-turn-helix to obtain such a knot. To design a Prusik knot, we devise that using an aromatic

15 Atcher, J.; Mateus, P.; Kauffmann, B.; Rosu, F.; Maurizot, V.; Huc, I. *Angew. Chem. Int. Ed.* **2021**, *60*, 2574-2577.

helix-turn-helix architecture composed of two helices linked by a single turn unit would be a good starting point. A critical point is that the two helical segments have to adopt an opposite handedness (M, red and P, blue, Figure 16a). They will flank, above and below, the aromatic turn unit (grey, Figure 16a), that will act as a handedness inversion center (Figure 16a). Moreover, the helix-turn-helix architecture must have the ability to bind a linear rod. For that purpose we can use our experience in foldaxane design. We anticipate that positioning polar pinchers at each extremity of the architecture would allow to bind dicarbamate containing guest. The complex of the helix-turn-helix and the rod is named foldaxane (Figure 16b). Finally, to obtain a fully functional Prusik knot, one must join the two ends of the helical segments using for example a long alkyl chain that form a closed loop.

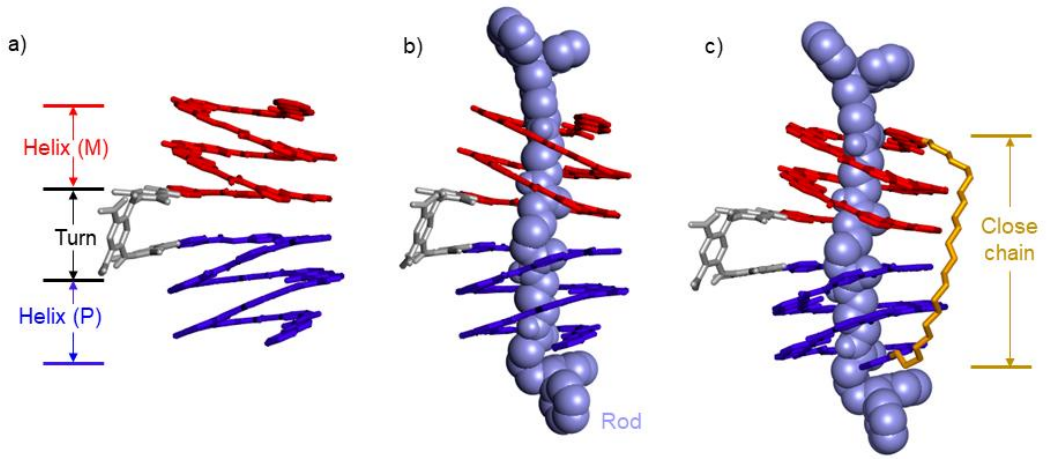

Figure 16. Energy minimized molecular models of molecular Prusik knot; a) side view of the helix-turn-helix architecture containing two helical segments with different handedness (*M* and *P*) and aromatic sheet (grey); b) side view of the corresponding foldaxane, composed by helix-turn-helix architecture and a dumbbell shape rod (light blue, in CPK style); c) side view of the molecular Prusik knot. The models have been produced with Maestro software package, using MMFFs force filed, TNCG as minimization method.

The two aromatic amide helical segments are composed of three types of monomers: 2,6-diaminopyridine (P^N), 2,6-pyridinedicarboxylic acid (P^C) and 7-amino-8-fluoro-2-quinolinecarboxylic (Q^F).[16] The Q^F part provide a cylindrical cavity that can accommodate alkyl chain whereas P^N and P^C units form a pyridine pincher that act as a hydrogen bond donor with carbamate groups (Figure 17b).

16 Gan, Q.; Ferrand, Y.; Bao, C.; Kauffmann, B.; Grélard, A.; Jiang, H.; Huc, I. *Science* **2011**, *331*, 1172.

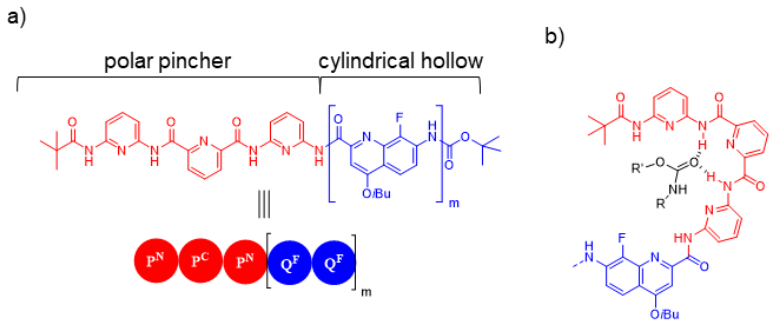

Figure 17. Formulas of (a) aromatic helix **H** and guest rod; b) intermolecular hydrogen bonds between helix and rod.

To maximize our chance of reaching a correct fold we tested three different turn units (Figure 18a) for the helix-turn-helix architecture: 2,7-diisobutoxy-3,6-naphthalenediamine (T^N), 4,6-dinitro-1,3-phenylenediamine (T^B) and N,N'-dibenzyl 2,6-pyridine-dicarboxamide (T^{py}). They can all adopt a hairpin conformation and induce an opposite helical handedness for the helices.

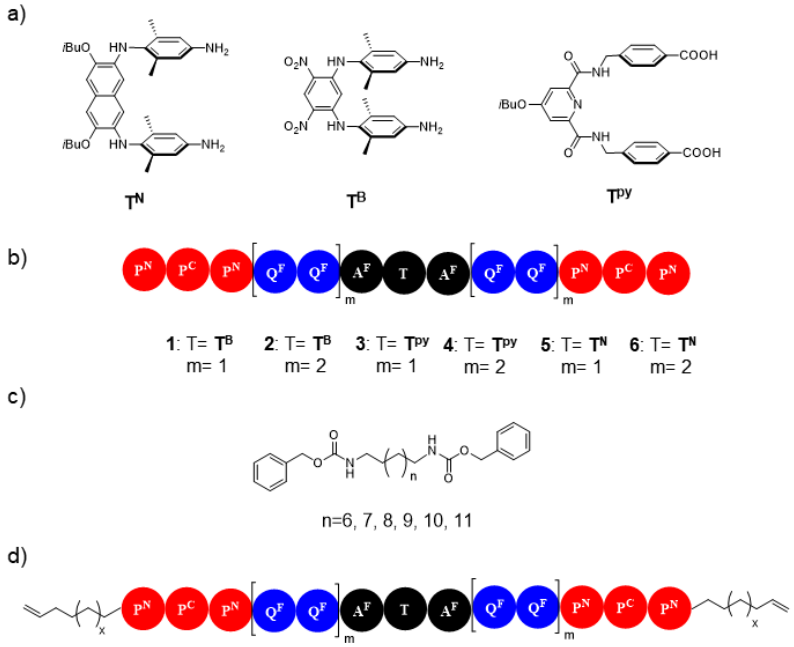

Figure 18. Chemical and color coded formula of a) turn units T^N, T^B, and T^{py}; b) oligomer sequence **1-6**; c) different dumbbell-like rods functioned with Carbamate groups; d) helix-turn-helix structure with alkyl chains.

The helical segment with varying length, $P_3Q^F_2$ and $P_3Q^F_4$, and turn units T^N, T^B, and T^{py} were chosen accordingly to prepare the helix-turn-helix structures. In total, six sequences were envisaged (Figure 18b), in all of them, the two helices are connected by a turn unit and possess a symmetry plane.

Rods with carbamates functions were used as guests and their length had to strictly match with the distance between two $\mathbf{P_3}$ polar pinchers. The length of the rods can be estimated using modeling. A series of dumbbell-like rod was prepared to screen the different helix-turn-helix structures (Figure 18c). To finalize the knot structure, we anticipate that long alkyl chains can be introduced as side chains of the $\mathbf{P^N}$ monomers and ring closing metathesis can be used to close this lateral loop (Figure 18d).

To prepare a Prusik knot, several hurdles needed to be passed: i. Prepare a helix-turn-helix structure, it adopts a similar conformation with the precursor of Prusik knot (Figure 16a); ii. Find a suitable rod for helix-turn-helix, they can form stable foldaxane complex (Figure 16b); iii. Close the ends of foldaxane to form a lateral loop (Figure 16c).

In this chapter, I focused on the first and second steps, thus several kinds of helix-turn-helix architectures were prepared and their folding and binding properties evaluated.

3. Results and discussion

3.1 Synthesis

The synthesis of foldamer **7** and **8** were already discussed in Chapter II. In short, preparation of **7** and **8** involved the coupling of a P_3 amino segment with the acid chloride of $Q^{F}{}_2$-Boc dimer, after Boc cleavage in acidic medium, **7** was obtained. One more coupling step with DMB protected Q^F dimer and Boc-deprotection were repeated to give **8** in overall 60% yield. The preparation of T^B, T^N and T^{py} units has been discussed and prepared by our group (Figure 19).[17] Jiaming Huang a PhD student from the group prepared the turn T^N.

17 Sebaoun, L.; Maurizot, V.; Granier, T.; Kauffmann, B.; Huc, I. *J. Am. Chem. Soc.* **2014**, *136*, 2168-2174; Sebaoun, L.; Kauffmann, B.; Delclos, T.; Maurizot, V.; Huc, I. *Org. Lett.* **2014**, *16*, 2326-2329; Lamouroux, A.; Sebaoun, L.; Wicher, B.; Kauffmann, B.; Ferrand, Y.; Maurizot, V.; Huc, I. *J. Am. Chem. Soc.* **2017**, *139*, 14668-14675; Atcher, J.; Mateus, P.; Kauffmann, B.; Rosu, F.; Maurizot, V.; Huc, I. *Angew. Chem. Int. Ed.* **2021**, *60*, 2574-2577.

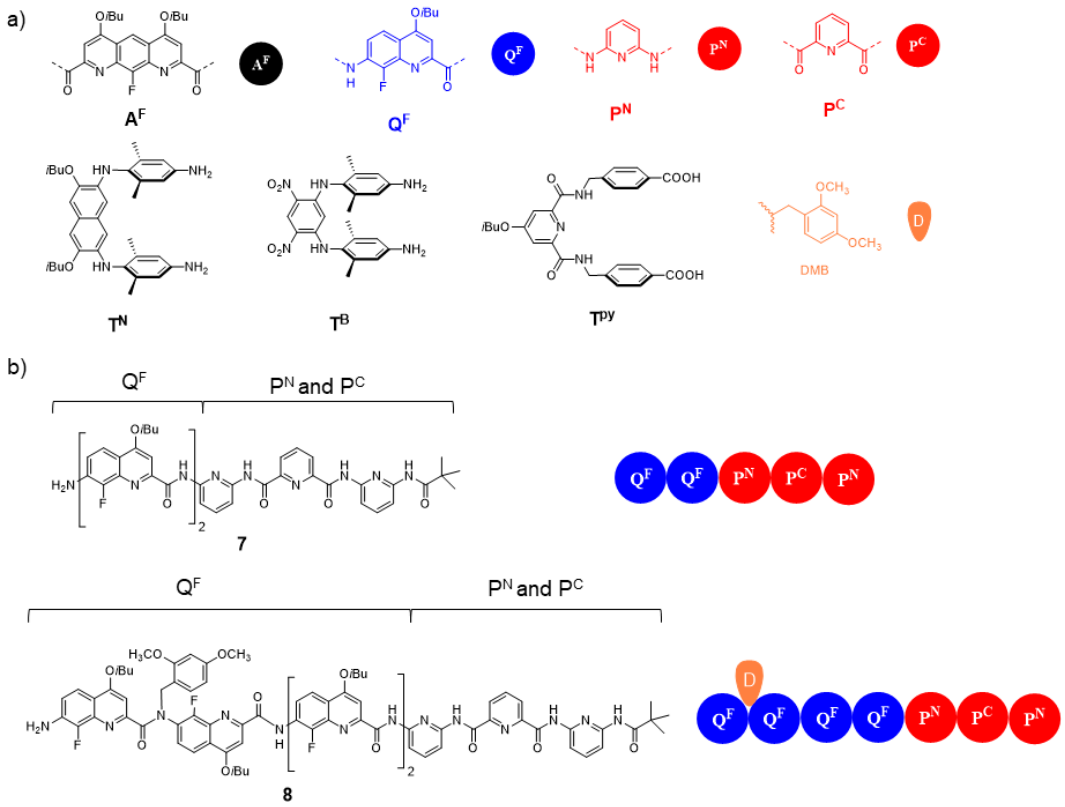

Figure 19. a) color coded formula and associated letters corresponding to A^F, P^N, P^C, Q^F monomers and T^B, T^{py}, T^N turn units; b) chemical and color coded formula of aromatic oligoamide foldamers **7** and **8**.

Diazaanthracene amino acid derivatives were developed from monoacid **9** which was obtained via the mono-saponification of the corresponding diesters of A^F. Diphenylphoshporylazide (DPPA) was used to convert the monoacid **9** into the Boc protected amino acid **10** via Curtius rearrangement. The Boc was cleaved in acidic medium to afford the amino anthracene **11**, which was then coupled with 4-(boc-aminomethyl)benzoic acid using PyBOP to obtain **12** with 45% yield. After saponification of the ester, acid **13** was obtained.

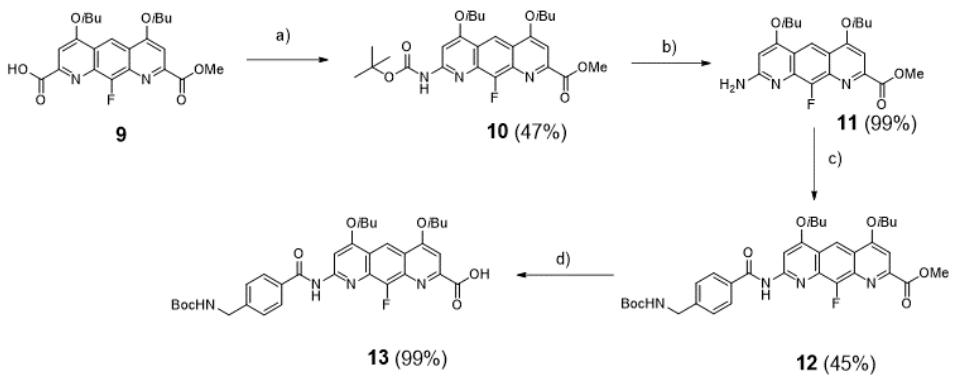

Scheme 1. Synthetic pathway of **13**. Reagents and conditions: a) diphenylphoshporyl azide, toluene, DIEA, *tert*-butanol, 100°C, 3 hours; b) CH_2Cl_2, TFA, room temperature, 3 hours; c) 4-(boc-aminomethyl)benzoic acid, PyBOP, DIEA, $CHCl_3$, 30°C, 24 hours; d) LiOH, THF, H_2O, room temperature, 4 hours.

According to literature,[18] 1,8-diphenylnaphthalene groups were prepared. In our case, 2,7-diisobutoxy-3,6-naphthalenediamine functional turn **16** was reduced under H_2 atmosphere using of Pd/C catalyst to obtain diamine **17** (T^N) with 95% yield.

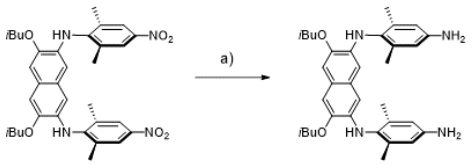

16 **17** (95%)

Scheme 2. Synthesis of naphthalene functional turn **17**. a) Pd/C, H_2, THF, 12 hours, room temperature.

The helix-turn-helix based on 4,6-dinitro-1,3-phenylenediamine (T^B) units were prepared according to the strategy shown in scheme 4. Compound **15** previously reported by our group,[19] was obtained by the saponification of diester **14**. Oxalyl chloride was used to convert diacid **15** to its corresponding acid chloride, then it was reacted with oligomer amine **7** and **8** to obtain the helix-turn-helix **1** and **18**, respectively. Compounds **1** and **18** were obtained after GPC purification with 63% and 27% yield. Foldamer **18** which contained two DMB groups, was subsequently treated with trifluoroacetic acid (TFA) to afford the final foldamer **2**.

18 Prabhakaran, P.; Puranik, V. G.; Chandran, J. N.; Rajamohanan, P. R.; Hofmann, H.-J.; Sanjayan, G. J. *Chem. Commun.* **2009**,3446-3448.

19 Lamouroux, A.; Sebaoun, L.; Wicher, B.; Kauffmann, B.; Ferrand, Y.; Maurizot, V.; Huc, I. *J. Am. Chem. Soc.* **2017**, *139*, 14668-14675.

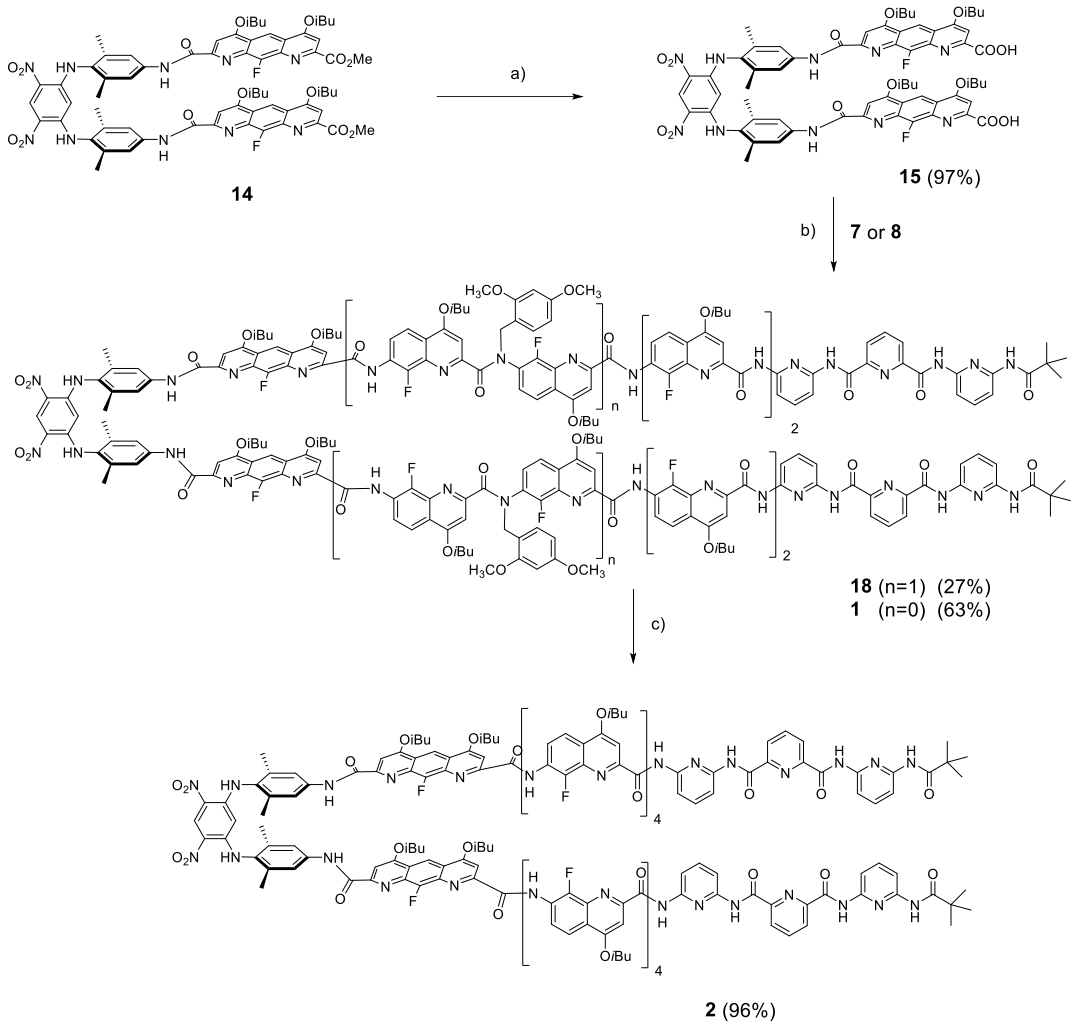

Scheme 3. Synthesis of oligomer **1** and **2**. Reagents and conditions: a) LiOH, THF, H_2O, room temperature, 4 hours; b) (i) $(COCl)_2$, $CHCl_3$, 2 hours, room temperature. (ii) DIPEA, $CHCl_3$, 16 hours, room temperature; c) $CHCl_3$, TFA, 4 hours, room temperature.

Derivatives of 2,6-pyridine-dicarboxamide were incorporated into foldamers to work as turn motif. The synthesis of pyridine based helix-turn-helix architectures were presented in scheme 5. Amino terminated oligomer **7** and **8** were coupled to acid **13** which was expected to provide face-to-face stacking aromatic rings in the conformation of final foldamer. During the process, 1-chloro-*N*,*N*,2-trimethyl-1-propenylamine (Ghosez's reagent) was used to convert **13** to its corresponding acid chloride, as its alternative oxalyl chloride could not be used because it generates HCl during the acid chloride formation which may affect the Boc group. Oligomer **19** and **20** were obtained with 55% and 54% yield, respectively. After Boc cleavage in acidic medium, amine **21** and **22** were prepared. Pyridine diacid 29 was coupled with oligomer amine **21** and **22** using PyBOP as an activating agent then purified by GPC to afford **3** and **23** with

48% and 35% yield, respectively. To cleave DMB groups, foldamer **23** was treated with TFA to afford free product **4**.

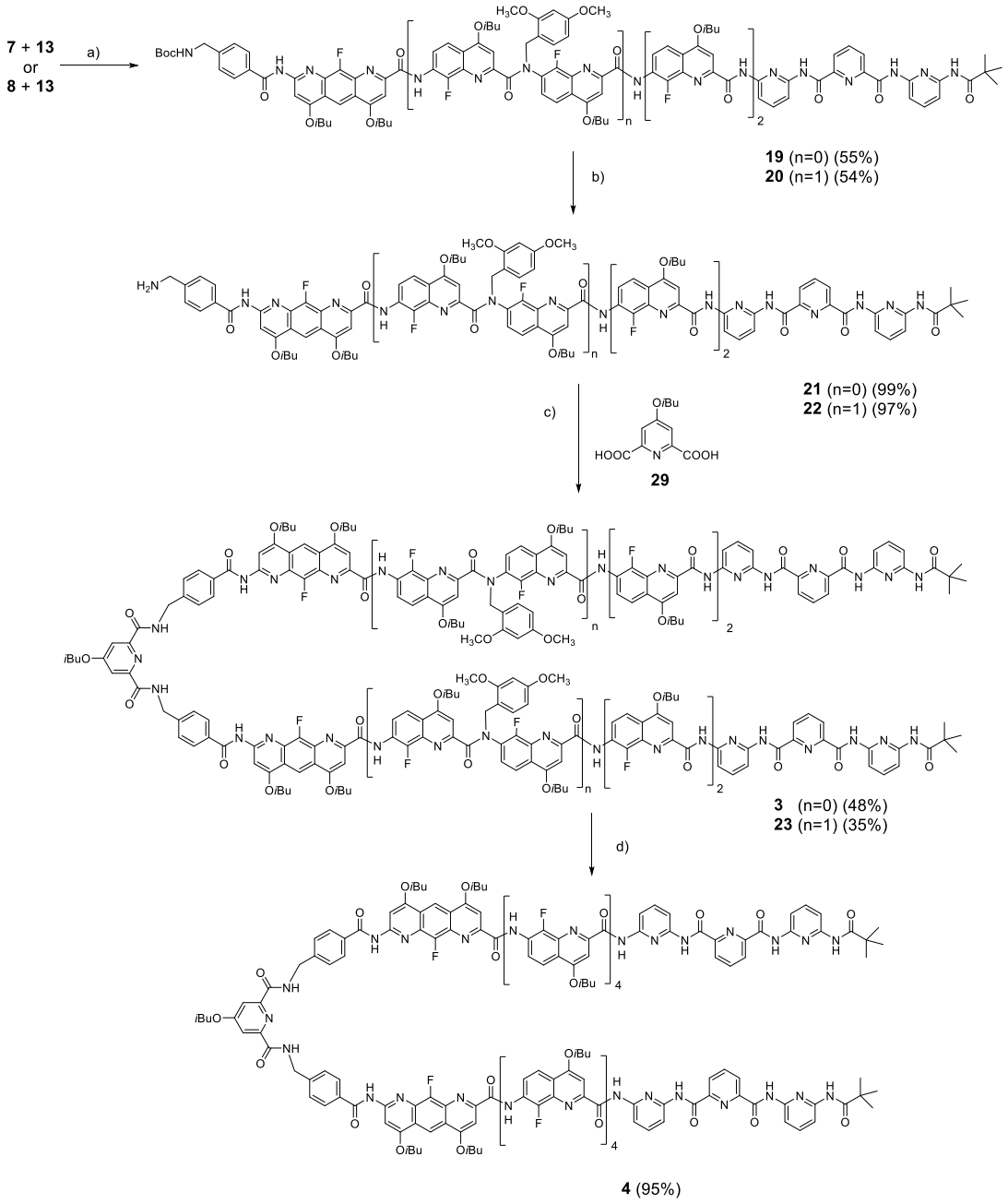

Scheme 4. Synthesis of oligomers **3** and **4**. Reagents and conditions: a) (i) 1-Chloro-*N*,*N*,2-trimethyl-1-propenylamine, dry $CHCl_3$, 2 hours, room temperature; (ii) dry DIPEA, dry $CHCl_3$, 12 hours, room temperature; b) dioxane, 4M HCl in dioxane, 3 hours, room temperature; c) PyBOP, DIPEA, $CHCl_3$, 2 days, 45 °C; d) $CHCl_3$, TFA, 4 hours, room temperature.

3,6-naphthalenediamine ($\mathbf{T^N}$) functional helix-turn-helix architectures were also prepared. The mono acid diazaanthracene **9** was converted to its corresponding acid chloride using oxalyl

chloride, then coupled with amine **7** and **8** to afford oligomers **24** and **25** with 46% and 57% yield, respectively. The saponification of **24** and **25** were carried out using LiOH in a mixture of THF/H_2O to obtain oligomer acid **26** and **27**, respectively. Naphthalene based turn **17** was coupled with oligomer acids **26** and **27** using PyBOP then purified by GPC to afford **5** and **28** with 41% and 37% yield, respectively. The final foldamer **6** was obtained after TFA cleavage of the DMB groups of precursor **28**.

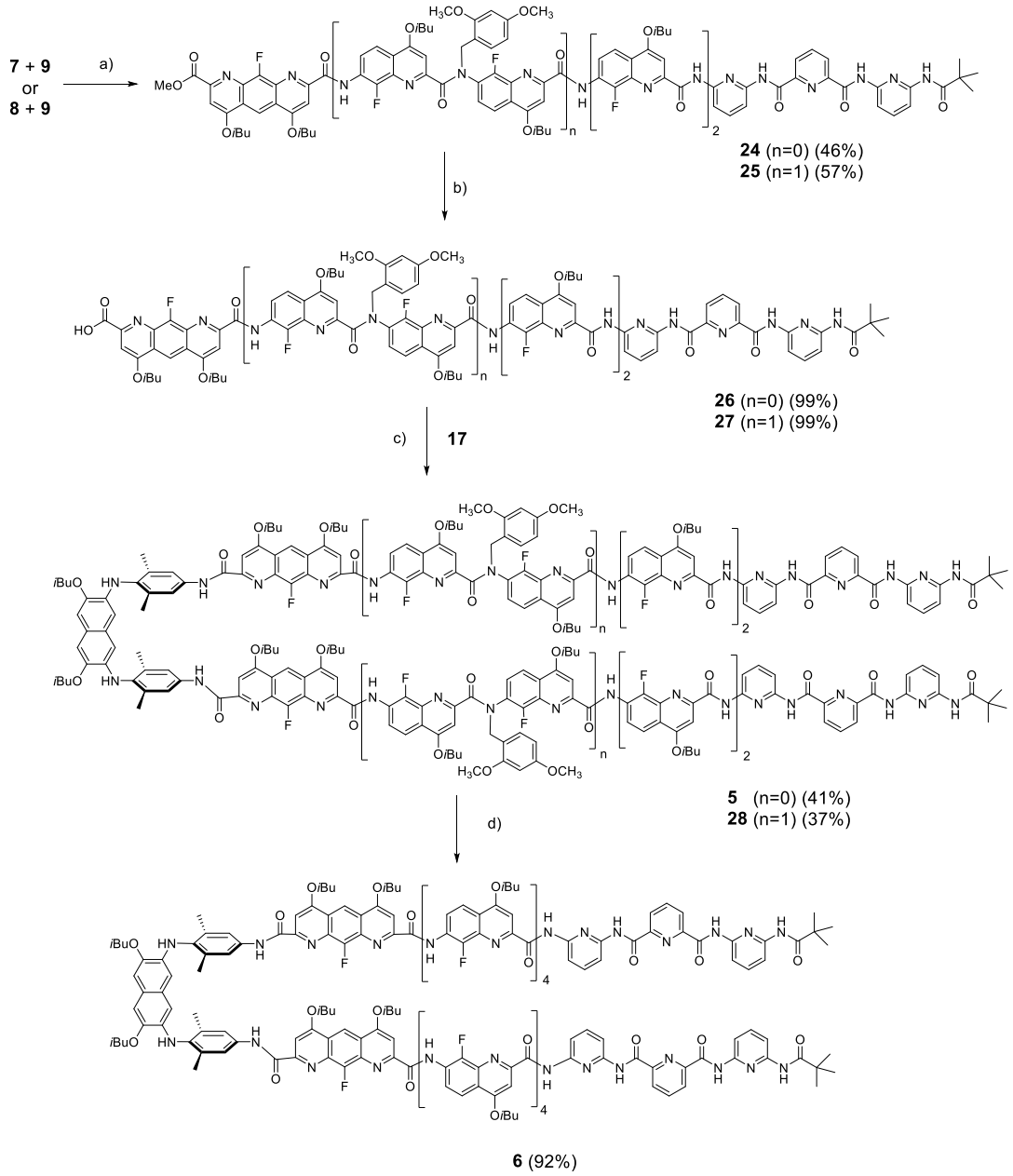

Scheme 5. Synthesis of oligomers **5** and **6**. Reagents and conditions: a) (i) $(COCl)_2$, $CHCl_3$, 2 hours, room temperature. (ii) DIPEA, $CHCl_3$, 16 hours, room temperature; b) LiOH, THF, H_2O, room

temperature, 4 hours; c) PyBOP, DIPEA, $CHCl_3$, 2 days, 45 °C; d) $CHCl_3$, TFA, 4 hours, room temperature.

3.2 Structure elucidation

3.2.1 T^b containing foldamer

NMR analysis was first employed to study the conformation of foldamers **1** and **2**. The NMR revealed complex and broad spectra for both oligomer in chloroform at room temperature. In the amide region (beyond 9.0 ppm), a set of resonances (Figure 20. red cycles) was observed corresponding to the amide and H_{ext} (the proton *ortho* to both nitro groups in turn). 11 signals were observed indicating that each amide and H_{ext} had different chemical environment as a result, the helix-turn-helix motifs **1** and **2** revealed a dissymmetrical architectures. We speculate, that the broadness of the signals may originate from the intermolecular aggregation of foldamers.

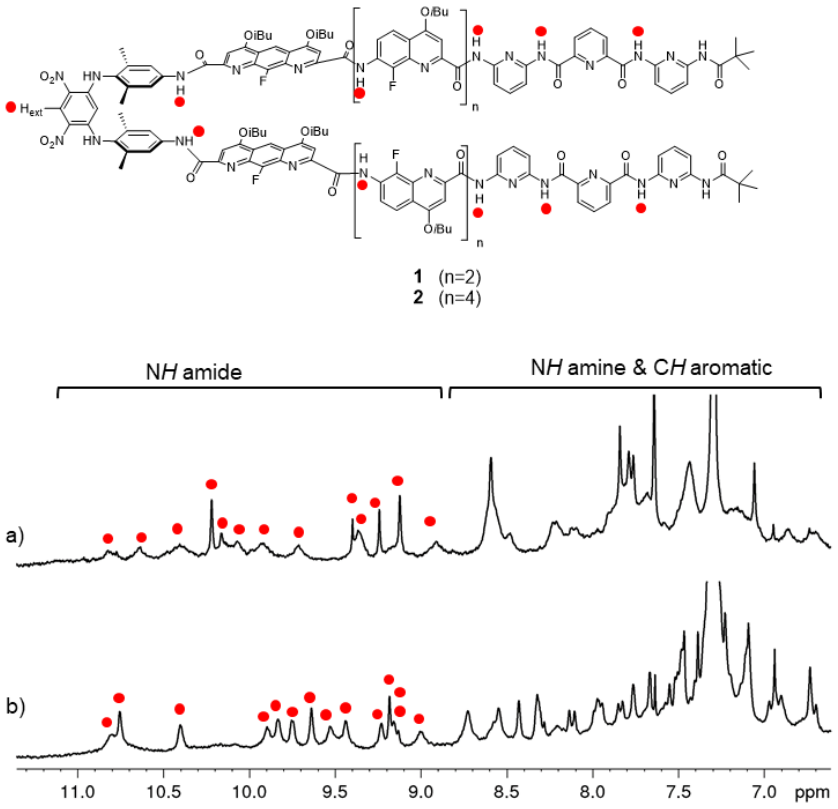

Figure 20. Chemical structure of foldamer **1** and **2**; 400 MHz ^{1}H NMR spectra at 298 K of **1** and **2** in $CDCl_3$. Amide and H_{ext} peaks were marked as red cycles.

Variable temperature NMR experiments were performed in $C_2D_2Cl_4$ to study the dynamic behavior of foldamer **1** (Figure 21). In $C_2D_2Cl_4$, we can only observe broad peaks in 298K which is totally different with $CDCl_3$. Upon raising the temperature from 298K to 378K, sharpening of the signals was observed.

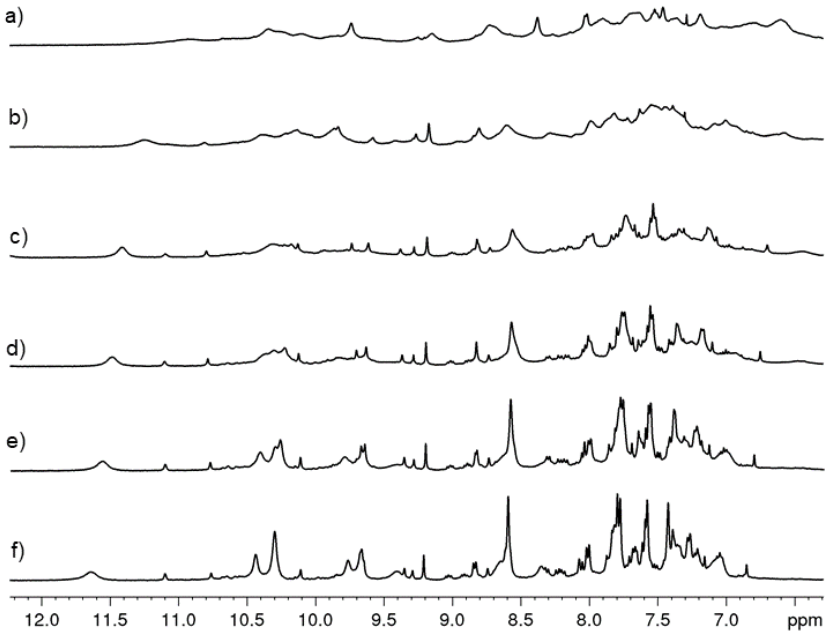

Figure 21. Part of ^{1}H NMR spectra (400 MHz, $C_2D_2Cl_4$) for variable temperature foldamer **1**, a) 298 K, b) 328 K, c) 348 K, d) 358 K, e) 368 K, f) 378 K.

Further characterizations of foldamer **1** were carried out by X-ray crystallography. X-ray quality single crystals were grown by slow diffusion of methanol into a chloroform solution of **1** and the structure was resolved in the *P*-1 space group.

Structure of monomeric foldamer **1** was picked up from crystal packing of dimeric $\mathbf{1}_2$. Monomeric helix-turn-helix motif 1 showed a "cone" shape conformation, in which a helical domain (blue, Figure 22) flipped at180^o to intercalate in the other helix segment (red, Figure 22) to form a head-to-head (parallel) double-helical structure. The two helical segments adopt the same handedness P (or M as the structure is centro-symmetric) and are connected by the aromatic sheets, which stabilize the double helix. The cavity of the double helical cone could be used to bind a guest.

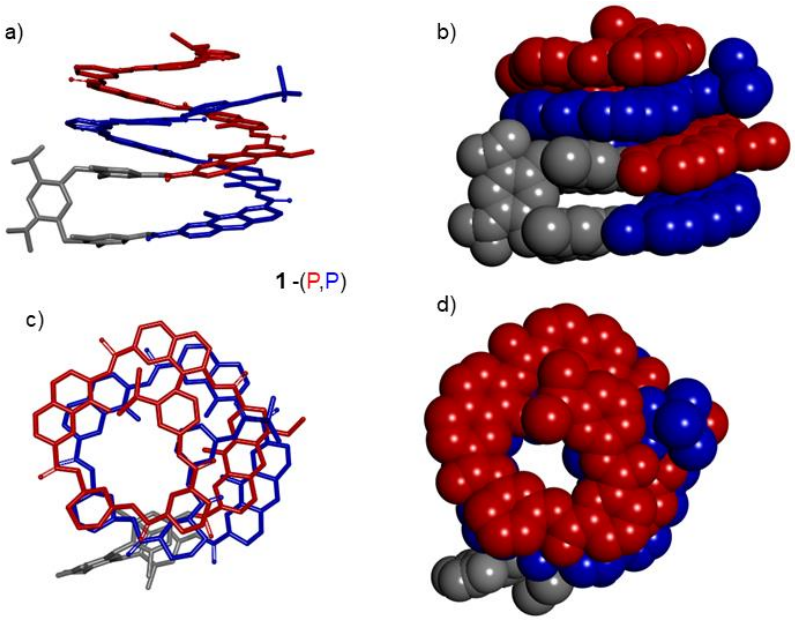

Figure 22. X-ray structure of foldamer monomeric **1**, a) front view of **1**, two helical segments were marked as blue and red. Aromatic sheets turns were marked as grey, b) front view of dimeric **1** in CPK style; c) side view of **1**; d) side view of dimeric **1** in CPK style; Side chains (O*i*Bu groups) and included solvent molecules have been removed for clarity

The crystal packing of the structure revealed that two cones of **1** can stacked with each other to form dimeric $\mathbf{1}_2$ due to the large flat aromatic surface of monomeric **1** (Figure 23a). Two dinitrobenzene groups in the crystal packing showed parallel arrangement (Figure 23c), the horizontal distance between two groups is 9.1Å. Helical segments self-assembled and stacked to double helical conformation, the distance between two segments is 3.7 Å. All helices have the same helicity (P). The crystal packing $\mathbf{1}_2$ presented C_2-symmetric conformation around the horizontal axis (Figure 23b).

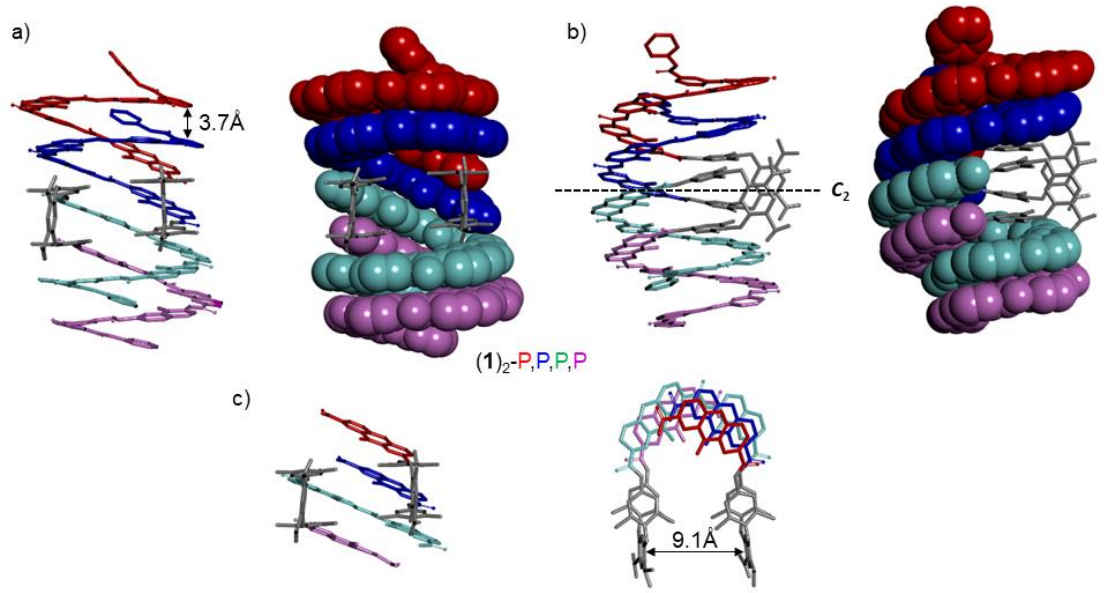

Figure 23. X-ray structure of foldamer dimeric $\mathbf{1}_2$, a) front view of $\mathbf{1}_2$, four helical segments were marked as blue, red, green and pink, respectively, turn units were marked as grey, b) side view of dimeric $\mathbf{1}_2$, the C_2 axis was presented as dot line; c) turn and diazaanthracene units were picked from crystal packing; Side chains (O*i*Bu groups) and included solvent molecules have been removed for clarity.

3.2.2 T^{py} containing foldamer

Foldamers **3** and **4** were also studied by ^{1}H NMR. In figure 24, the NMR revealed a complex and broad signal pattern in chloroform which may originate from the intermolecular aggregation of foldamers. In the amide region, several set of signals could be observed (red cycles, Figure 24).

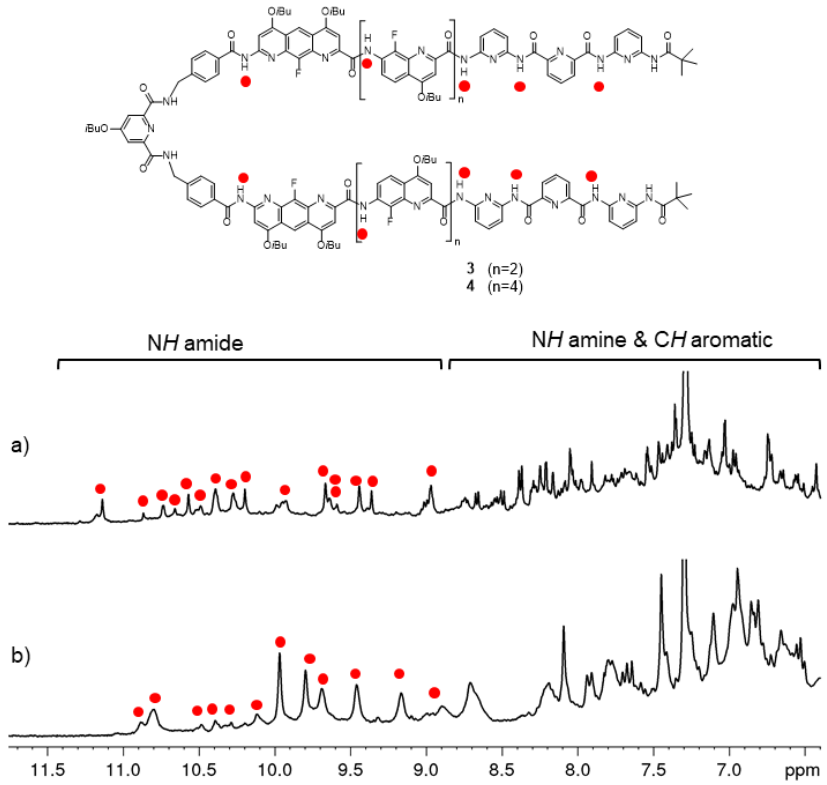

Figure 24. Chemical structure of foldamer **3** and **4**; 400 MHz ^{1}H NMR spectra at 298 K of **3** and **4** in $CDCl_3$. Amide peaks were marked as red cycles.

Variable temperature NMR experiments were performed in $C_2D_2Cl_4$ to study the dynamic behavior of foldamer **4**. Contrary to chloroform, broad signals were observed for **4** at room temperature. When temperature was raised from 298 K to 378 K, the broad peaks converted to sharp peaks.

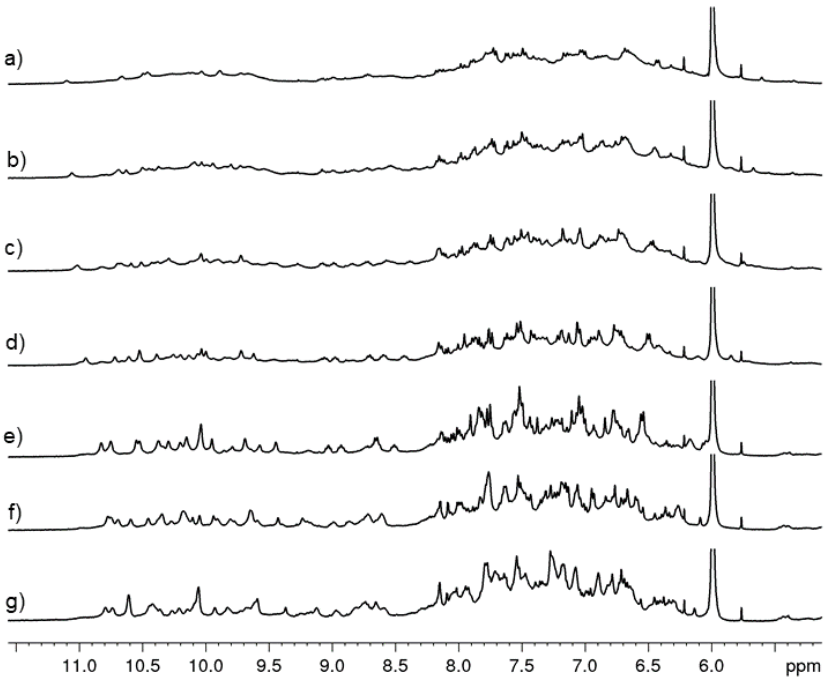

Figure 25. Part of ^{1}H NMR spectra (400 MHz, $C_2D_2Cl_4$) for variable temperature foldamer **4**, a) 298K, b) 308K, c) 318K, d) 328K, e) 338K, f) 343K, g) 353K.

To decipher the structure of foldamer **4**, X-ray crystallography was used. X-ray quality single crystals were grown by slow diffusion of *n*-hexane into a chloroform solution of **4** and the structure was resolved in the *P*-1 space group. To our surprise, pyridine based turn units and aromatic sheets adopt helical conformation (Figure 26), because the aromatic stack interaction between aryl rings is not strong enough to fold into parallel hairpin structure in the solvent. Turn units and aromatic sheets worked as bridges to connect their own two helical segments and incorporated into the helical conformation. In the monomeric foldamer **4**, two helical segments adopted consistent helicity (P) which is not changed by the pyridine based "turn" unit (Figure 26c). Two monomeric foldamer **4** self-assembled and stacked to head-to-tail (antiparallel) to form the double helical conformation $\mathbf{4}_2$, the distance between two monomeric helix is 3.1Å. The crystal packing $\mathbf{4}_2$ presented C_2-symmetric conformation around the horizontal axis (Figure 26b).

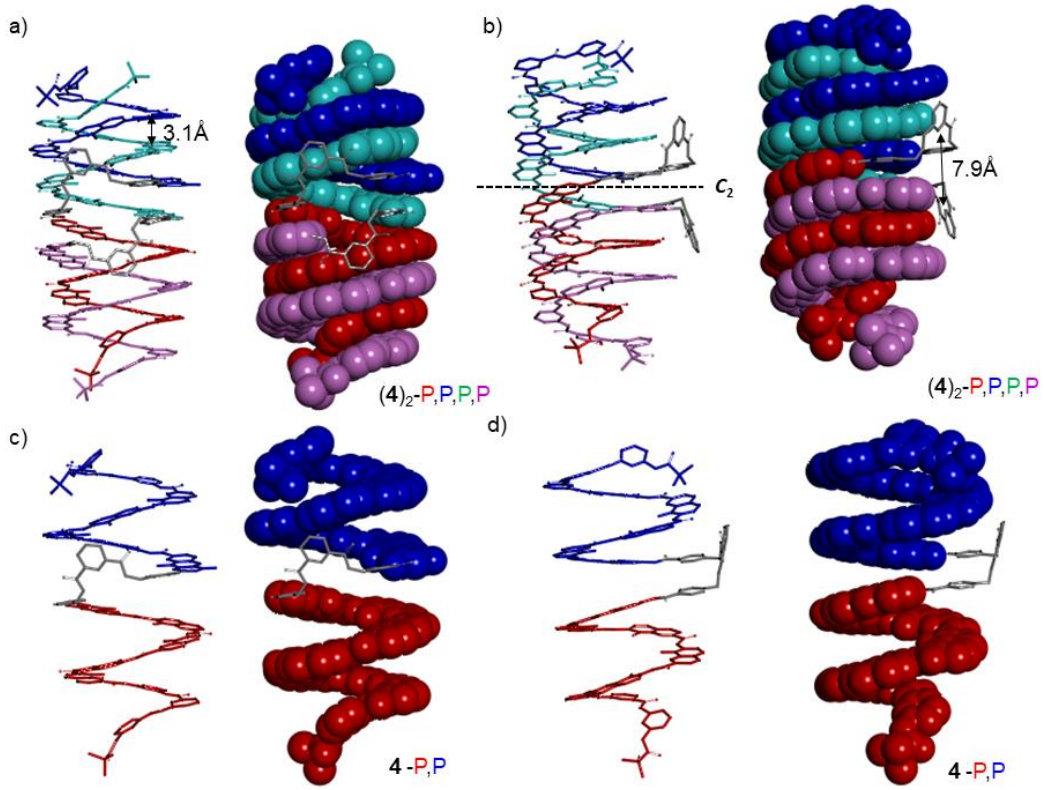

Figure 26. X-ray structure of foldamer dimeric $\mathbf{4}_2$; a) front view of $\mathbf{4}_2$, four helical segments were marked as blue, red, green and pink, respectively. Pyridine based aromatic turns were marked as grey; b) side

view of $\mathbf{4}_2$, the C_2 axis was presented as dot line; c) front view and d) side view of monomeric **4**, picked from crystal packing; Side chains (O*i*Bu groups) and included solvent molecules have been removed for clarity.

3.2.3 T^N containing foldamer

Similarly to the previous examples, ^{1}H NMR was employed to study the conformation of foldamer **5** and **6**. The NMR revealed sharp and simple spectra in chloroform at room temperature. In the amide region (beyond 9.0 ppm), a series of peaks (red cycles, Figure 27) were corresponding to the amide, the number of amide peaks were counted as 12 and 8 for foldamer **5** and **6**, respectively. It indicates that each amide of foldamer **5** has a different chemical environment and thus that **5** possess a dissymmetrical conformation. **6** contained two more Q^F units in each helix segment compared **5**, less amide signals were observed (8) confirming a symmetrical structure.

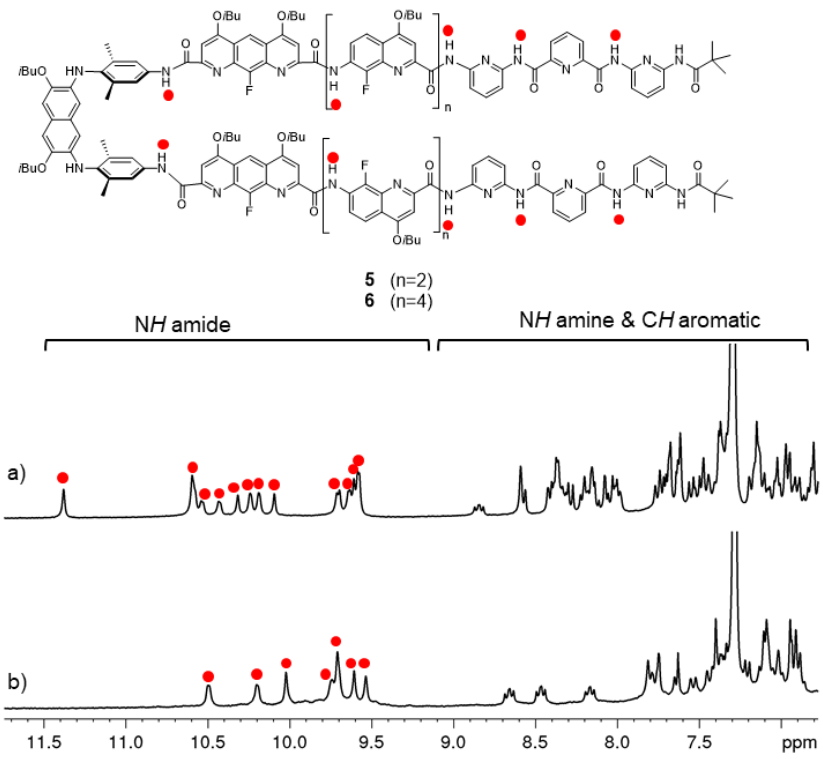

Figure 27. Chemical structure of foldamer **5** and **6**; 400 MHz ^{1}H NMR spectra at 298 K of **5** and **6** in $CDCl_3$. Amide peaks were marked as red cycles.

Additionally variable temperature studies were carried out. Increasing the temperature from 298K to 348K in $C_2D_2Cl_4$ (Figure 28), the spectra revealed changes of chemical shifts of the amide resonances. No additional set of signal could be observed. The variable temperatures experiments indicate that foldamer **6** had a stable conformation.

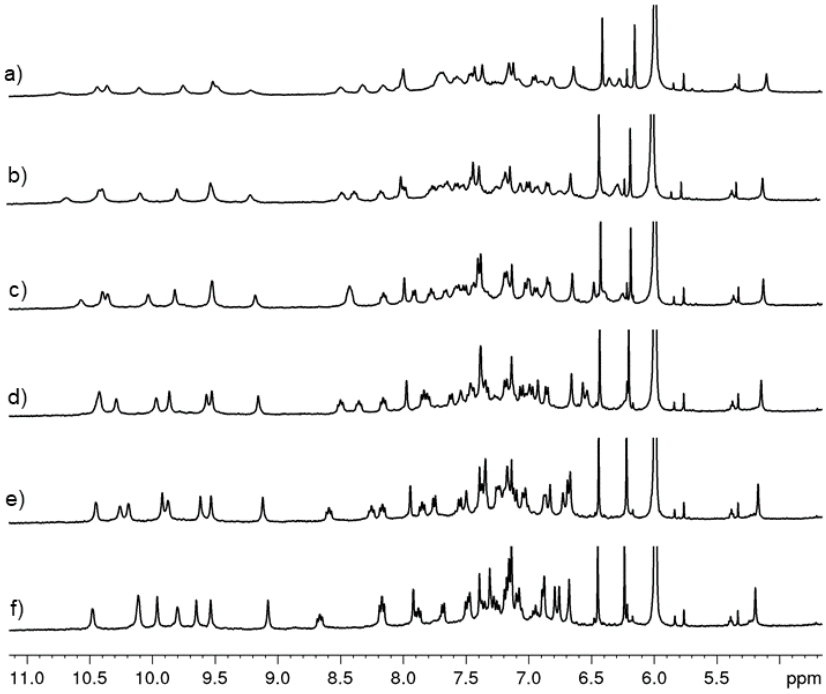

Figure 28. Part of ^{1}H NMR spectra (400 MHz, $C_2D_2Cl_4$) for variable temperature foldamer **6**, a) 298 K, b) 308 K, c) 318 K, d) 328 K, e) 338 K, f) 348 K.

The conformation of **5** was further confirmed by X-ray crystallography. The suitable single crystals were grown by slow diffusion of hexane into a chloroform solution and the structure was resolved in the *P*-1 space group. As shown in figure 29, foldamer **5** had an unexpected conformation. Two foldamer **5** self-assembled into dimeric foldamer $\mathbf{5}_2$, in which one helical segment of each monomeric 5 (red and pink, Figure 29) could fold into full helical conformation. The other segments (blue and green, Figure 29) flipped into the same side and stacked underneath the previous red and pink helix, they adopted M helicity. In blue helix, Q^F units can participated in the helical structure with red helix to form multiple-helix, while P_3 units flipped into opposite orientation and helicity (P).

Two helical segments were connected by a naphthalene turn (grey, Figure 29) which folded into hairpin conformation as expected. Naphthalene functional turn present a pretty long distance between two parallel aromatic sheets which was enough for the intercalation of an

aromatic group. As a result, P units of one strand intercalate into the hairpin turn. The distance between two parallel aromatic rings of the naphthalene functional turn was measured as 7.2Å. The crystal packing $\mathbf{5}_2$ presented C_2-symmetric conformation around the horizontal axis (Figure 29a), while monomeric **5** is asymmetry.

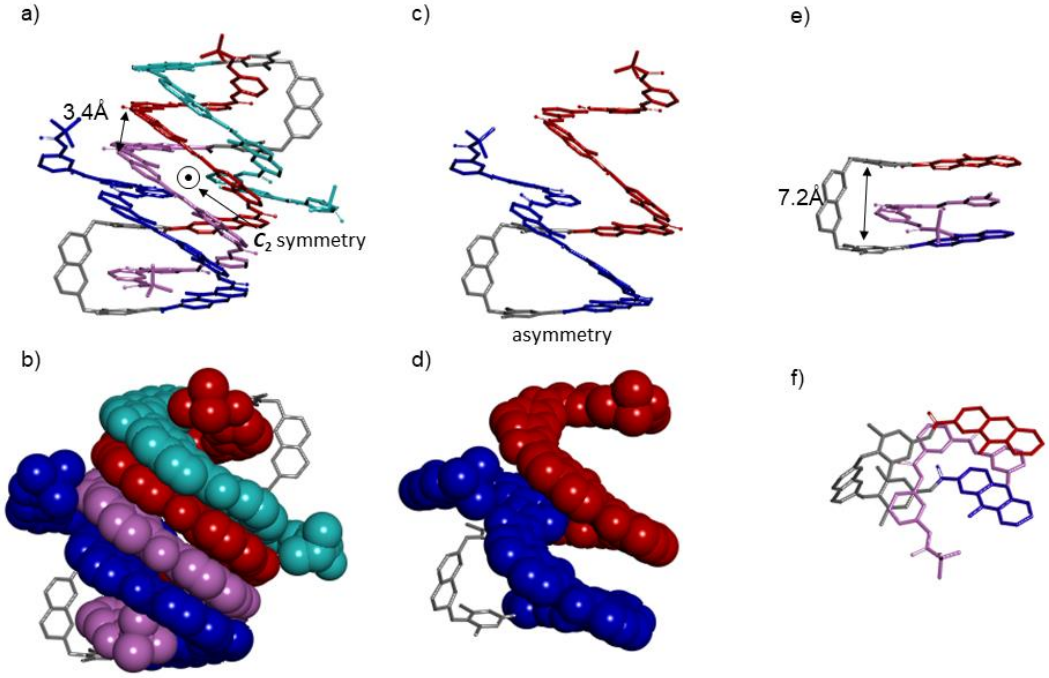

Figure 29. X-ray structure of foldamer $\mathbf{5}_2$, a) front view of $\mathbf{5}_2$, four helical segments were marked as blue, red, green and pink, respectively, turns units were marked as grey, b) front view of dimeric $\mathbf{5}_2$, helical segments were presented in CPK style; side view of monomeric **5** c) in stick style; d) helical segments were presented in CPK style; e) front view of Naphthalene functional turn with P_3 segment in crystal packing, presented in grey and red, respectively; f) top view of e); Side chains (O*i*Bu groups) and included solvent molecules have been removed for clarity.

The conformation of **6** was also confirmed by X-ray crystallography. The suitable single crystals were grown by slow diffusion of hexane into a chloroform solution and the structure was resolved in the *P*-1 space group. The crystal packing showed us a double helical conformation, two strand of **6** dimerized into a double helixes $(\mathbf{6})_2$, and the double helixes contained both C_2 symmetry and C_i symmetry.

Monomer Foldamer **6** showed a symmetrical conformation with two opposite handedness helices (P and M), and parallel arrangement of aromatic rings in turn segment (Figure 30). Two different handedness helices resided above and below the turn unit. Aromatic turn folded into

the hairpin shape and connected two helical segments as expected. **6** adopts a plane-symmetrical conformation, the plane of symmetry could be found in the center of foldamer **6**.

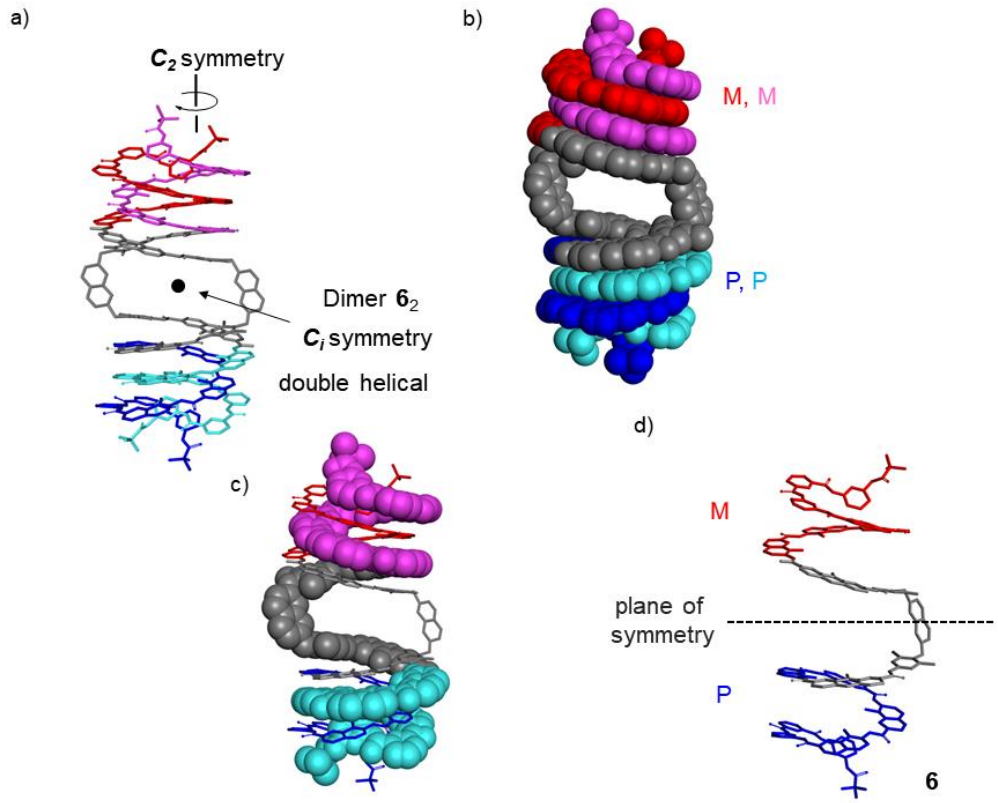

Figure 30. X-ray structure of foldamer **6**, a) front view of $(\mathbf{6})_2$, the center of C_i symmetry was marked as black dot, $(\mathbf{6})_2$ was C_2 symmetrical around vertical axis; b) one strand was showed as CPK style; c) in CPK style; d) monomer foldamer **6**, opposite handedness helical segments were marked as blue (M) and red (P), aromatic sheets were marked as grey. Side chains (O*i*Bu groups) and included solvent molecules have been removed for clarity.

The structure of **6** is similar with the precursor of Prusik knot that we have searched for a long time. From the top, we can also observe that it contains a cavity for the rod like guest. NMR titrations with different size of rods were carried out, but to our surprise, no binding could be observed with many different rods (Figure 31).

The formation of a foldaxane is achieved via slow folding of a single helix around a dumbbell shape rod. Yet this process can be hampered by the dimerization of single helix in a double helix. Although this process being reversible, the high stability of the double helical architecture do not allow its dissociation in the single helix and thus forbid the formation of the helix/rod complex. In all the examples presented above, upon adding rods to sequences **1**-**6**, no

foldaxane was observed. We surmise that the design of sequences that can adopt a well behaved single helix sheet helix (monomeric) would allow us to form foldaxane more easily.

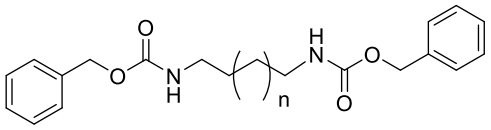

n=6, 7, 8, 9, 10, 11

Figure 31. Chemical formula of different size rods we titrated with foldamer **6**.

4. Conclusion

We designed and prepared several kinds of helix-turn-helix motifs based on different turn units (T^B, T^{py} and T^N) and helices. NMR and crystallographic analysis showed T^B contained foldamer **1** adopted a "cone" like conformation, foldamer **4** built with T^{py} folded into double helix structure. Foldamer **5** and **6** contain the same turn unit, T^N, while 5 adopt intra multiple helix conformation and 6 shown Prusik knot like structure.

We will continue to dissociate 6 into single helix and prepare the foldaxane with dumbbell rod to form the precursor of molecular Prusik knot.

Finally, foldamer **1**, **4** and **5** also showed interesting structure, we can explore more meaningful and important topology structure and then toward implementation of complex function.

5. Experiments

5.1 Methods for NMR

NMR spectra were recorded on 3 different NMR spectrometers: (1) an Avance II NMR spectrometer (Bruker Biospin) with a vertical 7,05T narrow-bore/ultrashield magnet operating at 300 MHz for ^1H observation and 75 MHz for ^{13}C observation by means of a 5-mm direct BBO H/X probe with Z gradient capabilities; (2) an Avance 400 NMR spectrometer (Bruker Biospin) with a vertical 9.4T narrow-bore/ultrashield magnet operating at 400 MHz for ^1H

observation by means of a 5-mm direct QNP $^{1}H/^{13}C/^{31}P/^{19}F$ probe with gradient capabilities; (3) an Avance III NMR spectrometer (Bruker Biospin) with a vertical 16.45T narrowbore/ ultrashield magnet operating at 700 MHz for ^{1}H observation by means of a 5-mm TXI $^{1}H/^{13}C/^{15}N$ probe with Z gradient capabilities. Chemical shifts are reported in parts per million (ppm, δ) relative to the 1H residual signal of the deuterated solvent used. 1H NMR splitting patterns with observed first-order coupling are designated as singlet (s), doublet (d), triplet (t), or quartet (q). Coupling constants (*J*) are reported in hertz. Data processing was performed with Topspin 3.6 software.

5.2 Methods for GPC

Preparative recycling GPC (gel permeation chromatography) were performed on JAIGEL 20*600 mm columns (Japan Analytical Industry) at a flow rate of 7 mL min^{-1} with a mobile phase composed of 1% (vol/vol) ethanol and 0.5% (vol/vol) Et_3N in chloroform. Monitoring was carried out by UV detector at 254 nm, 280 nm, 300 nm and 360 nm.

5.3 Methods for X-ray crystallography

Crystallography Single crystal X-ray diffraction experiments were performed at IECB X-ray facility (CNRS UMS 3033 – INSERM US001, University of Bordeaux) on a 3kW microfocus Rigaku FRX rotating anode. The source is equipped with high flux Osmic Varimax HF mirrors. The FRX generator is combined with a hybrid Dectris Pilatus 200K detector. All data were collected at the copper kα wavelength with a partial chi goniometer that decreases blind areas and enables automatic axial adjustment. Data were processed with the CrysAlisPro suite version 1.171.38.43. Empirical absorption correction using spherical harmonics, implemented in SCALE3 ABSPACK scaling algorithm was used. Structures were solved with Shelxt and refined by full-matrix least-squares method on F2 with Shelxl-2014 within Olex2. For all atoms, anisotropic atomic parameters were used. Hydrogen atoms were place at idealized position sand refined as riding of their carriers with Uiso(H)=1.2Ueq(CH, CH2, NH) and Uiso(H)=1.5Ueq(CH3). DFIX and AFIX instructions were used to improve the geometry

of molecules and RIGU to model atomic displacement parameters. Severely disordered solvent molecules were removed using the SQUEEZE procedure from the PLATON suite. For search and analysis of solvent accessible voids in the structures default parameters were utilized: grid 0.20 Å, probe radius 1.2 Å and NStep 6. Calculated total potential solvent accessible void volumes and electron counts per unit cell are given in the CIF files that were checked using IUCR's checkcif algorithm. Due to the characteristics of the crystals, i.e. large volume fractions of disordered solvent molecules, weak diffraction intensity, incompleteness of the data and moderate resolution, a number of A -level and B -level alerts remain in the check cif file. These alerts are inherent to the data and refinement procedures and do not reflect errors. Rather, they illustrate the limited practicality of the checkcif tool for medium size molecule crystallography.

Name	1	4	5	6
Formula	$C_{166}H_{160}F_6N_{32}O_{26}$	$2(C_{225}H_{217}F_{10}N_{39}O_{33})$	$2(C_{178}H_{180}F_6N_{30}O_{24})$	$C_{234}H_{232}F_{10}N_{38}O_{32}$
M.W	3133.2944	4185.4350	3237.5744	4278.6480
Space group	*P*-1	*P*-1	*P*-1	
a	22.647(1)	27.2431(6)	29.2465(14)	21.7204(11)
b	27.4215(12)	28.5466(7)	30.5136(9)	24.844(2)
c	32.7053(13)	39.7025(9)	32.3500(13)	32.4522(18)
α	108.090(4)	91.942(2)	62.463(4)	100.787(6)
β	100.339(4)	97.702(2)	69.170(4)	103.974(5)
γ	105.525(4)	105.854(2)	63.542(4)	112.907(6)
Cell volume	17821.2	29353.5	22507.2	14858.8
Packing Coefficient	0.607279	0.534552	0.580523	0.565885

5.4 Methods for chemical synthesis

All reactions were carried out under a dry nitrogen atmosphere. Commercial reagents were purchased from Sigma-Aldrich, Alfa-Aesar or TCI and were used without further purification unless otherwise specified. Tetrahydrofurane (THF) and dichloromethane (CH_2Cl_2) were dried over alumina columns; chloroform ($CHCl_3$), triethylamine (Et_3N) and diisopropylethylamine

(DIEA) were distilled over calcium hydride (CaH_2) prior to use. Reactions were monitored by thin layer chromatography (TLC) on Merck silica gel 60-F254 plates and observed under UV light. Column chromatography purifications were carried out on Merck GEDURAN Si60 (40-63μm). ESI mass spectra were obtained from the Mass Spectrometry Laboratory at the European Institute of Chemistry and Biology (UMS 3033 - IECB), Pessac, France.

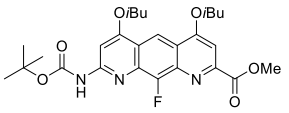

10

Compound **10**: In a dry 100 mL round bottomed flask equipped with a stir bar, **9** (300 mg, 0.67 mmol), DPPA (287 μL, 1.34 mmol, 2 equiv), DIPEA (227 μL, 1.34 mmol, 2 equiv) and tert-butanol (383 μL, 4.03 mmol, 6 equiv) was slurried in 25 mL of dry toluene under a nitrogen atmosphere. The flask was then heated to a 100 °C and the mixture stirred for 3 h. Solvent was removed on a rotary evaporator, and the crude material was precipitated from MeOH to obtain product **10** as a light yellow solid (162 mg, 47%). ^{1}H NMR (300 MHz, $CDCl_3$, 298 K) δ 8.90 (s 1H), 7.86 (s, 1H), 7.77 (s, 1H), 7.51 (s, 1H), 4.17-4.14 (m, 4H), 4.12 (s, 3H), 2.43-2.33 (m, 2H), 1.61 (s, 9H), 1.23-1.20 (m, 12H).

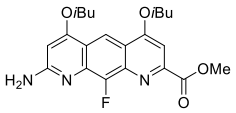

11

Compound **11**: **10** (150 mg, 0.290 mmol) was dissolved in CH_2Cl_2 (3 mL). To this solution trifluoroacetic acid (300 μL) was added. The solution was stirred at room temperature for 3 h. The solution poured into saturated aqueous solution of $NaHCO_3$ to neutralize, extracted with DCM, washed with water and brine respectively. The organic part was dried over anhydrous Na_2SO_4. Evaporation of organic part resulted yellow solid, compound **11** was obtained (119 mg, 99% yield). ^{1}H NMR (300 MHz, $CDCl_3$, 298 K) δ 8.72 (s 1H), 7.41 (s, 1H), 6.05 (s, 1H), 4.10-4.06 (m, 4H), 4.05 (s, 3H), 2.34-2.26 (m, 2H), 1.16-1.13 (m, 12H).

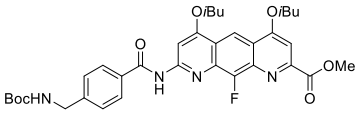

12

Compound **12**: Amine **11** (120 mg, 0.288mmol), 4-(boc-aminomethyl)benzoic acid (80 mg, 0.317 mmol) and PyBOP (750 mg, 1.44 mmol) were placed in a 10 mL round-bottom flask filled with argon. Freshly distilled $CHCl_3$ (2 mL) and DIPEA (300 μL, 1.72 mmol) were then successively added. The solution was stirred at 45 °C for two days. The solvent was removed under reduced pressure and the residue was dissolved in dichloromethane, washed with 5% NH_4Cl, distilled water and brine. The organic layer was dried over Na_2SO_4, filtered and concentrated under reduced pressure. The crude product was purified by recycling GPC and compound **12** was obtained as a yellow solid (84 mg, 45% yield). ^{1}H NMR (300 MHz, $CDCl_3$, 298 K) δ 9.03 (s 1H), 8.89 (s, 1H), 8.14 (s, 1H), 7.97 (s, 1H), 7.95 (s, 1H), 7.47 (s, 1H), 7.44 (s, 1H), 7.42 (s, 1H), 4.93 (s, 1H), 4.39 (d, *J* = 4.2 Hz, 2H), 4.13 (t, *J* = 7.3 Hz, 4H), 4.07 (s, 3H), 2.34-2.26 (m, 2H), 1.46 (s, 9H), 1.17 (d, *J* = 6.5 Hz, 12H).

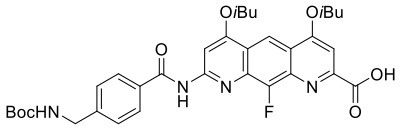

13

Compound **13**: **12** (180 mg, 0.27 mmol) was dissolved in a mixture of THF (3 mL) and H_2O (600 μL). To this solution was added LiOH (58.2 mg, 1.38 mmol, 5.0 equiv.). The solution was stirred at room temperature for 3 h. Then solution was neutralized with 1N HCl to pH = 4~5, and concentrated under reduced pressure to remove THF. H_2O (30 mL) was added to the residue. The aqueous phase was extracted with CH_2Cl_2 (3×20 mL). The combined organic phases were dried over Na_2SO_4, filtered, then evaporated to give dimer acid **13** as a yellow solid (169 mg, 99%). ^{1}H NMR (300 MHz, $CDCl_3$, 298 K) δ 9.08 (s, 1H), 8.97 (s, 1H), 8.23 (s, 1H), 8.04 (s, 1H), 8.01 (s, 1H), 7.59 (s, 1H), 7.52 (s, 1H), 7.49 (s, 1H), 5.00 (s, 1H), 4.46 (d, *J* = 5.9 Hz, 2H), 4.21 (d, *J* = 2.5 Hz, 4H), 2.45-2.37 (m, 2H), 1.46 (s, 9H), 1.23 (d, *J* = 6.7 Hz, 12H).

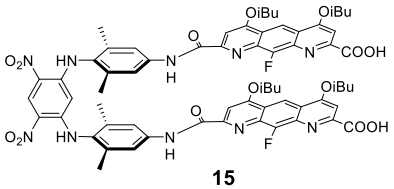

15

Compound **15**: **14** (180 mg, 0.27 mmol) was dissolved in a mixture of THF (3 mL) and H_2O (600 μL). To this solution was added LiOH (58.2 mg, 1.38 mmol, 5.0 equiv.). The solution was stirred at room temperature for 3 h. Then solution was neutralized with 1N HCl to pH = 4~5, and concentrated under reduced pressure to remove THF. H_2O (30 mL) was added to the residue. The aqueous phase was extracted with CH_2Cl_2 (3×20 mL). The combined organic phases were dried over Na_2SO_4, filtered, then evaporated to give acid **15** as a yellow solid (169 mg, 99%). ^{1}H NMR (300 MHz, DMSO-d_6, 298 K) δ 10.13 (s, 2H), 9.45 (s, 2H), 9.08 (s, 1H), 8.19 (s, 2H), 7.65 (s, 2H), 7.40 (s, 2H), 7.17 (s, 2H), 4.64 (s, 1H), 4.16 (d, *J* = 5.7 Hz, 4H), 4.83 (d, *J* = 5.5 Hz, 4H), 2.28-2.18 (m, 4H), 2.05 (s, 12H), 1.16 (d, *J* = 6.6 Hz, 12H), 1.06 (d, *J* = 6.6 Hz, 12H).

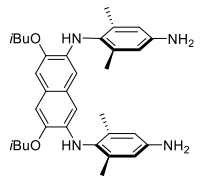

17

Compound **17**: In a 50 mL round bottom flask, **16** (60 mg, 0.099 mmol) and Pd/C (50 mg) were taken. To the mixture 15 mL of THF was added and nitrogen gas was purged. Subsequently, a balloon filled with hydrogen gas was fitted overhead. The mixture was stirred vigorously at room temperature for 16 hours. The mixture was filtered through celite pad to remove Pd/C and washed with fresh ethanol. Solvent was removed to get a powder **28** (50.7 mg, 95%). The ^{1}H-NMR indicated that the crude product was highly pure and, therefore, no further purification was performed. ^{1}H NMR (300 MHz, $CDCl_3$, 298 K) δ 6.95 (s, 2H), 6.50 (s, 4H), 6.00 (s, 2H), 5.59 (s, 2H), 3.93(d, *J* = 6.5 Hz, 4H), 3.53 (br, 4H), 2.33-2.20 (m, 2H), 2.12 (s, 12H), 1.10 (d, *J* = 6.7 Hz, 12H).

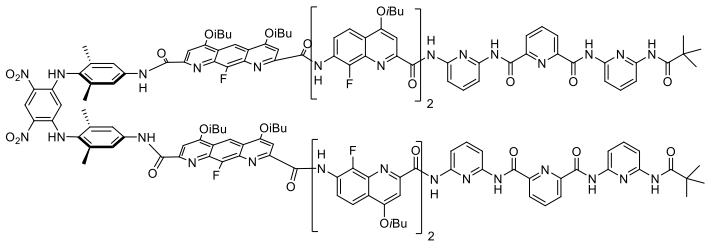

1

Oligomer 1. Diacid **15** (66 mg, 0.052 mmol) was suspended in anhydrous $CHCl_3$ (1 mL), then oxalyl chloride (44 µL, 0.52 mmol) was added and the reaction was allowed to stir at room temperature for 2 hours. The solvent and excess oxalyl chloride were removed under reduced pressure and the residue was dried under high vacuum for 3 hours to yield the corresponding acid chloride as a yellow solid. The solution of amine **7** (100 mg, 0.104 mmol) and distilled DIPEA (54 µL, 0.314 mmol) in anhydrous $CHCl_3$ (1 mL) was added dropwise via a syringe to solution of the freshly prepared acid chloride dissolved in anhydrous $CHCl_3$ (0.5 mL). The reaction was allowed to proceed at room temperature for 16 hours. After evaporation of the solvents, the crude product was purified by recycling GPC. Oligomer **14** was obtained as a yellow product (103 mg, 63% yield). ^{1}H NMR (300 MHz, $CDCl_3$, 298 K) δ 11.36 (s, 1H), 11.03 (s, 1H), 10.68 (s, 1H), 10.53 (s, 1H), 10.32 (s, 1H), 10.23 (s, 1H), 9.89 (s, 1H), 9.59 (s, 1H), 9.32 (s, 1H), 9.24 (s, 1H), 9.06 (s, 1H), 8.84 (s, 1H), 8.71-8.53 (m, 4H), 8.47-8.28 (m, 4H), 7.97-7.69 (m, 8H), 7.66-7.52 (m, 4H), 7.49-7.36 (m, 6H), 7.22-7.08 (m, 6H), 7.05-6.73 (m, 6H), 6.66-6.47 (m, 6H), 4.33-4.16 (m, 8H), 4.06-3.74 (m, 8H), 3.68(s, 1H), 2.54-2.28 (m, 8H), 1.62 (s, 12H), 1.41-1.18 (m, 48H).

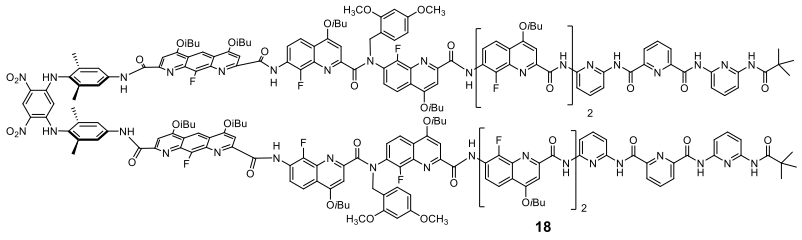

18

Oligomer 18. Diacid **15** (55 mg, 0.043 mmol) was suspended in anhydrous $CHCl_3$ (1 mL), then oxalyl chloride (36 µL, 0.43 mmol) was added and the reaction was allowed to stir at room temperature for 2 hours. The solvent and excess oxalyl chloride were removed under reduced pressure and the residue was dried under high vacuum for 3 hours to yield the corresponding

acid chloride as a yellow solid. The solution of amine **8** (156 mg, 0.104 mmol) and distilled DIPEA (60 µL, 0.344 mmol) in anhydrous $CHCl_3$ (1 mL) was added dropwise via a syringe to solution of the freshly prepared acid chloride dissolved in anhydrous $CHCl_3$ (0.5 mL). The reaction was allowed to proceed at room temperature for 16 hours. After evaporation of the solvents, the crude product was purified by recycling GPC. Oligomer **14** was obtained as a yellow product (25 mg, 27% yield). ^{1}H NMR (300 MHz, $CDCl_3$, 298 K) δ 11.12-10.26 (m, 10H), 10.14-9.84 (m, 7H), 9.33-8.94 (m, 5H), 8.70-8.44 (m, 4H), 8.25-7.50 (m, 30H), 7.07-6.19 (m, 21H), 5.41 (br, 2H), 4.89 (br, 2H), 4.38-4.00 (m, 24H), 3.83-3.73 (m, 12H), 2.56-2.32 (m, 12H), 1.86 (s, 18H), 1.38-1.01 (m, 72H).

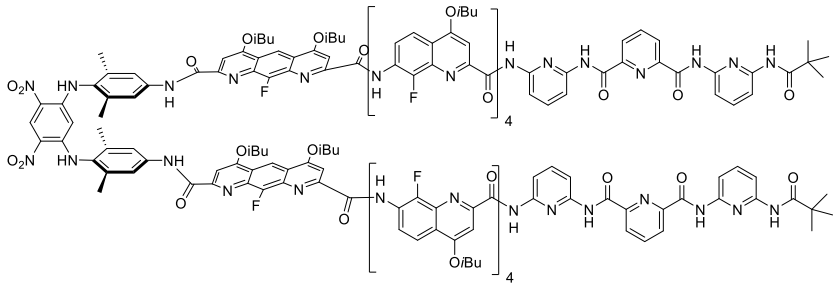

2

Oligomer 1. Dimethoxy benzyl protected oligomer **18** was taken in a 5 mL round bottom flask. To that 1 mL $CHCl_3$ and 1 mL trifluoroacetic acid added subsequently under argon atmosphere. The mixture was kept for stirring for 12 hours at room temperature. The solution poured into saturated aqueous solution of $NaHCO_3$ to neutralize, extracted with DCM, washed with water and brine respectively. The organic part was dried over anhydrous Na_2SO_4. Evaporation of organic part resulted yellow solid, which was further purified by recycling GPC. Oligomer **2** was obtained as a yellow product (25 mg, 96% yield). ^{1}H NMR (300 MHz, $CDCl_3$, 298 K) δ 10.08 (s, 1H), 10.75 (s, 2H), 10.40 (s, 1H), 9.89 (s, 1H), 9.83 (s, 1H), 9.75 (s, 1H), 9.63 (s, 1H), 9.53 (s, 1H), 9.44 (s, 2H), 9.23 (s, 1H), 9.18-9.13 (m, 3H), 9.00 (s, 2H), 8.72 (s, 2H), 8.54 (s, 3H), 8.43 (s, 2H), 8.32 (s, 3H), 8.24-8.18 (m, 2H), 8.13 (s, 1H), 8.10 (s, 1H), 8.00-7.94 (m, 4H), 7.85 (s, 1H), 7.83 (s, 1H), 7.76 (s, 2H), 7.66 (s, 4H), 7.58-7.40 (m, 8H), 7.15-7.09 (m, 6H), 6.97-6.90 (m, 4H), 6.73-6.69 (m, 4H), 6.49-6.44 (m, 4H), 6.21 (s, 2H), 5.90 (s, 2H), 4.26-4.03 (m, 25H), 2.53-2.30 (m, 12H), 1.73 (s, 18H), 1.39-1.26 (m, 72H).

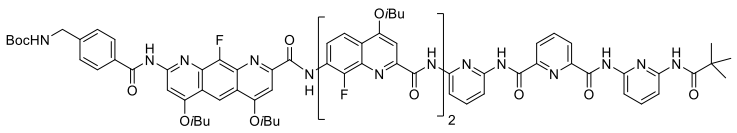

19

Oligomer 19: Acid **13** (50 mg, 0.078 mmol) was dried in vacuo, and then dissolved in dry CH_2Cl_2 (1 mL) in a 10 mL round bottom flask. To this 1-chloro-N,N,2-trimethylpropenylamine (20 μL, 4.5 equiv.) was added. The reaction mixture was stirred at room temperature for 2 h resulting in a homogeneous solution, and then evaporated to provide the corresponding acid chloride. To a solution of the amine **7** (75 mg, 0.078 mmol) in CH_2Cl_2 (1 mL) containing DIEA (40 μL, 0.234 mmol) was added a solution of acid chloride in CH_2Cl_2 (2 mL) via syringe. The reaction mixture was stirred at room temperature for 12 h. The solution was evaporated, and the product was purified by chromatography (silica gel, ethyl acetate and cyclohexane 1:2) to get yellow solid (67 mg, 55 %).^{1}H NMR (300 MHz, $CDCl_3$, 298 K) δ 10.85 (s, 1H), 10.63 (s, 2H), 10.18 (s, 3H), 9.08 (s, 1H), 8.69 (s, 2H), 8.29 (s, 1H), 7.97-7.80 (m, 4H), 7.69-7.61 (m, 5H), 7.46-7.34 (m, 3H), 7.22-7.18 (m, 3H), 6.97-6.93 (m, 4H), 4.23-4.08 (m, 8H), 2.46-2.40 (m, 4H), 1.97 (s, 9H), 1.49 (s, 9H), 1.32-1.27 (m, 24H).

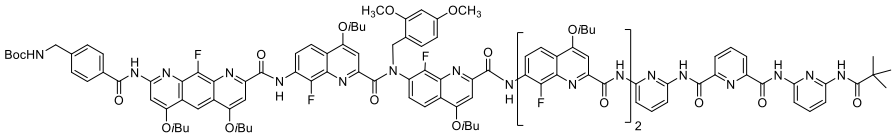

20

Oligomer 20: Acid **13** (90 mg, 0.141 mmol) was dried in vacuo, and then dissolved in dry CH_2Cl_2 (1 mL) in a 10 mL round bottom flask. To this 1-chloro-N,N,2-trimethylpropenylamine (60 μL, 3.0 equiv.) was added. The reaction mixture was stirred at room temperature for 2 h resulting in a homogeneous solution, and then evaporated to provide the corresponding acid chloride. To a solution of the amine **8** (229 mg, 0.141 mmol) in CH_2Cl_2 (3 mL) containing DIEA (73 μL, 0.423 mmol) was added a solution of acid chloride in CH_2Cl_2 (2 mL) via syringe. The reaction mixture was stirred at room temperature for 12 h. The solution was evaporated, and the product was purified by chromatography (silica gel, ethyl acetate and cyclohexane 1:2) to get yellow solid (171 mg, 54 %).^{1}H NMR (300 MHz, $CDCl_3$, 298 K) δ 11.14 (s, 1H), 10.95 (s, 1H), 10.74 (s, 1H), 10.66 (s, 1H), 10.35 (s, 1H), 10.19 (s, 1H), 10.11 (s, 1H), 9.26 (s, 1H), 8.83

(s, 2H), 8.57-8.48 (m, 2H), 8.39 (d, *J* = 6.7 Hz, 1H), 8.29-8.27 (m, 1H), 8.17-8.12 (m, 3H), 8.05-7.94 (s, 5H), 7.85-7.70 (s, 5H), 7.64-7.61 (m, 2H), 7.51-7.47 (m, 3H), 7.43-7.35 (m, 2H), 7.21-7.11 (m, 2H), 6.60-6.45 (m, 2H), 6.26-6.12 (m, 2H), 5.24 (d, *J* = 13.3 Hz, 1H), 4.95 (d, *J* = 13.3 Hz, 1H), 4.50 (s, 2H), 4.28-3.99 (m, 12H), 3.81 (m, 4H), 2.52-2.24 (m, 6H), 1.83 (s, 9H), 1.51-1.45 (m, 9H), 1.28-1.19 (m, 36H).

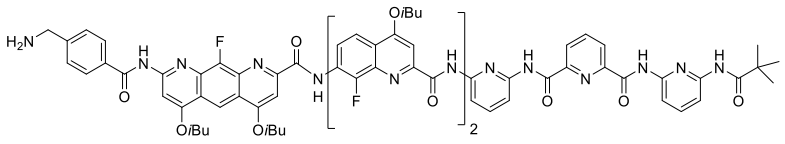

21

Oligomer 1. Dimethoxy benzyl protected oligomer **19** (40 mg, 0.025 mmol) was taken in a 5 mL round bottom flask. To that 1 mL $CHCl_3$ and 200 μL trifluoroacetic acid added subsequently under argon atmosphere. The mixture was kept for stirring for 3 hours at room temperature. The solution poured into saturated aqueous solution of $NaHCO_3$ to neutralize, extracted with DCM, washed with water and brine respectively. The organic part was dried over anhydrous Na_2SO_4. Evaporation of organic part resulted yellow solid, which was further purified by recycling GPC. Oligomer **1** was obtained as a yellow product (36 mg, 99% yield). ^{1}H NMR (300 MHz, DMSO-d_6, 298 K) δ 11.46 (s, 1H), 11.02 (s, 1H), 10.72 (s, 1H), 10.50 (s, 1H), 10.27 (s, 1H), 8.97 (s, 1H), 8.46-8.27 (m, 4H), 8.00-7.66 (m, 6H), 7.50-7.15 (m, 6H), 6.86-6.60 (m, 6H), 4.23-4.07 (m, 8H), 2.36-2.28 (m, 4H), 1.30-1.18 (m, 24H), 0.60 (s, 9H).

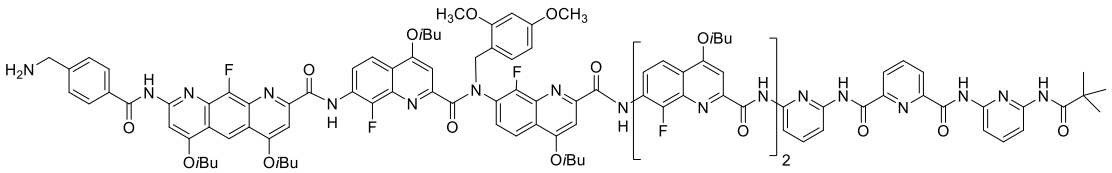

22

oligomer 22: Oligomer **20** (180 mg, 0.080 mmol) was dissolved in dioxane (2 mL), and HCl (4M in dioxane, 5 mL) was added. The mixture was stirred at room temperature for 3h. The solvent was evaporated, and the residue was dissolved in CH_2Cl_2 (20 mL), washed with saturated $NaHCO_3$, dried over Na_2SO_4 and then evaporated to give amine **22** as a yellow solid (171 mg, 97%). It was dried in vacuum and used without further purification. ^{1}H NMR (300

MHz, $CDCl_3$, 298 K) δ 11.14 (s, 1H), 10.96 (s, 1H), 10.78 (s, 1H), 10.74 (s, 1H), 10.64 (s, 1H), 10.12 (s, 1H), 10.00 (s, 1H), 9.14 (s, 1H), 8.85 (s, 2H), 8.66 (s, 1H), 8.51 (s, 1H), 8.37 (d, *J* = 7.2 Hz, 1H), 8.30-8.26 (m, 2H), 8.21-8.14 (m, 2H), 8.08-7.71 (m, 12H), 7.64 (s, 1H), 7.55-7.37 (m, 5H), 7.25 (s, 1H), 7.15 (s, 1H), 6.50 (s, 1H), 6.25 (s, 1H), 5.22 (d, *J* = 14.0 Hz, 1H), 4.97 (d, *J* = 14.0 Hz, 1H), 4.23-3.97 (m, 12H), 3.82-3.60 (m, 6H), 2.47-2.26 (m, 6H), 1.78 (s, 9H), 1.31-1.21 (m, 36H).

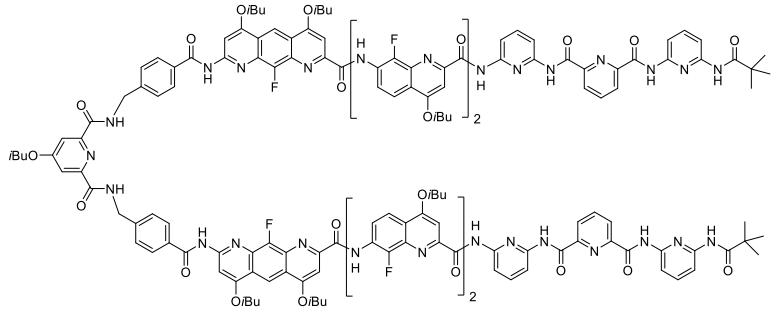

3

Compound 3. Amine **21** (80 mg, 0.054mmol), diacid (6.1 mg, 0.025 mmol) and PyBOP (283 mg, 0.54 mmol) were placed in a 10 mL round-bottom flask filled with argon. Freshly distilled $CHCl_3$ (2 mL) and DIPEA (132 μL, 0.761 mmol) were then successively added. The solution was stirred at 45 °C for two days. The solvent was removed under reduced pressure and the residue was dissolved in dichloromethane, washed with 5% NH_4Cl, distilled water and brine. The organic layer was dried over Na_2SO_4, filtered and concentrated under reduced pressure. The crude product was purified by recycling GPC and compound **3** was obtained as a yellow solid (35 mg, 48% yield). ^{1}H NMR (300 MHz, $CDCl_3$, 298 K) δ 11.11 (s, 1H), 11.08 (s, 1H), 10.81 (s, 1H), 10.67 (s, 1H), 10.60 (s, 1H), 10.51 (s, 1H), 10.43 (s, 1H), 10.33 (s, 1H), 10.21 (s, 1H), 10.14 (s, 1H), 9.93-9.86 (m, 3H), 9.61 (s, 1H), 9.58 (s, 2H), 9.53 (s, 1H), 9.38 (s, 1H), 9.30 (s, 1H), 8.95-8.91 (m, 2H), 8.71-8.60 (m, 2H), 8.56-8.43 (m, 1H), 8.32 (d, *J* = 7.1 Hz, 1H), 8.25-8.11 (m, 3H), 8.07-7.90 (m, 2H), 7.85 (s, 2H), 7.79-7.70 (m, 8H), 7.49-7.29 (m, 6H), 7.19-7.07 (m, 4H), 6.99-6.90 (m, 3H), 6.69-6.58 (m, 2H), 6.50-6.45 (m, 2H), 6.39-6.34 (m, 2H), 4.13-3.91 (m, 12H), 3.75-3.60 (m, 10H), 2.38-2.22 (m, 9H), 1.36-1.08 (m, 72H).

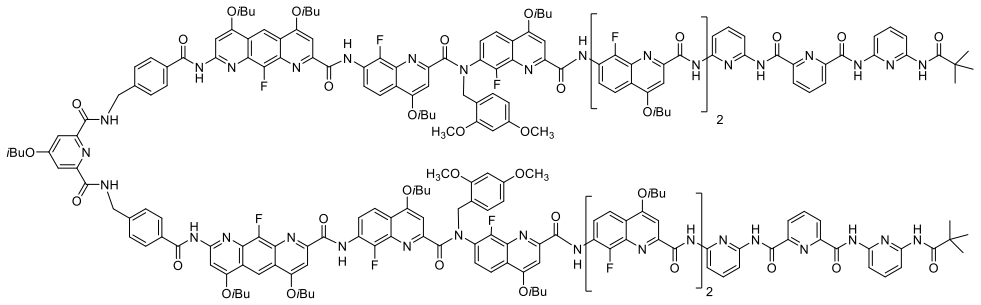

23

Compound 3. Amine **22** (170 mg, 0.079mmol), diacid (9.0 mg, 0.037 mmol) and PyBOP (192 mg, 0.37 mmol) were placed in a 10 mL round-bottom flask filled with argon. Freshly distilled $CHCl_3$ (2 mL) and DIPEA (90 μL, 0.518 mmol) were then successively added. The solution was stirred at 45 °C for two days. The solvent was removed under reduced pressure and the residue was dissolved in dichloromethane, washed with 5% NH_4Cl, distilled water and brine. The organic layer was dried over Na_2SO_4, filtered and concentrated under reduced pressure. The crude product was purified by recycling GPC and compound **3** was obtained as a yellow solid (61 mg, 35% yield). ^{1}H NMR (300 MHz, $CDCl_3$, 298 K) δ 11.04 (s, 1H), 10.97 (s, 1H), 10.90 (s, 1H), 10.53 (s, 3H), 10.41 (s, 1H), 10.31 (s, 2H), 10.18 (s, 2H), 10.08 (s, 1H), 10.04-9.96 (m, 4H), 9.29 (s, 1H), 9.09 (s, 1H), 8.89 (s, 2H), 8.75-8.54 (m, 4H), 8.43-8.38 (m, 2H), 8.32(s, 2H), 8.23 (s, 1H), 8.18-8.16 (m, 2H), 8.13-8.11 (m, 2H), 8.07-7.98 (m, 6H), 7.93-7.78 (m, 8H), 7.73-7.55 (m, 8H), 7.52-7.35 (m, 8H), 7.16 (t, J = 7.6 Hz, 6H), 6.94-6.85 (m, 4H), 6.60 (s, 2H), 6.47 (s, 2H), 6.40 (s, 2H), 6.31 (s, 2H), 6.07 (s, 2H), 5.47 (br, 2H), 5.06 (br, 2H), 4.43-3.88 (m, 30H), 2.47-2.29 (m, 13H), 1.32-1.12 (m, 96H).

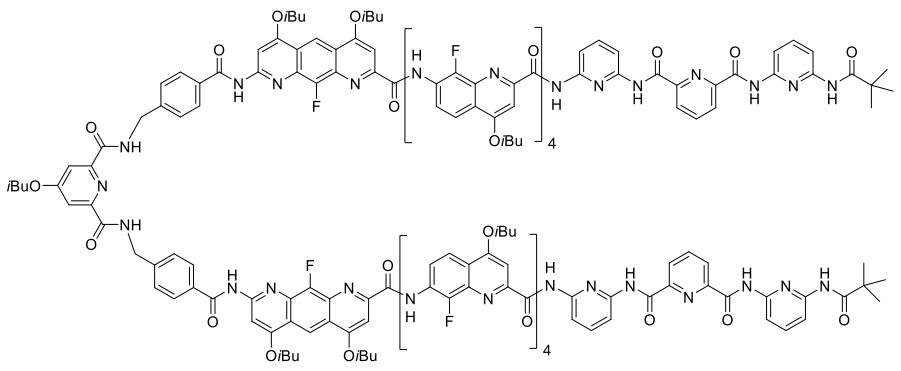

4

Oligomer 4. Dimethoxy benzyl protected oligomer **23** was taken in a 5 mL round bottom flask. To that 1 mL $CHCl_3$ and 1 mL trifluoroacetic acid added subsequently under argon atmosphere.

The mixture was kept for stirring for 12 hours at room temperature. The solution poured into saturated aqueous solution of $NaHCO_3$ to neutralize, extracted with DCM, washed with water and brine respectively. The organic part was dried over anhydrous Na_2SO_4. Evaporation of organic part resulted yellow solid, which was further purified by recycling GPC. Oligomer **4** was obtained as a yellow product (57 mg, 95% yield). ^{1}H NMR (400 MHz, $C_2D_4Cl_2$, 328 K) δ 10.94 (s, 1H), 10.83 (s, 1H), 10.71 (s, 1H), 10.66 (s, 1H), 10.52 (s, 1H), 10.38 (s, 1H), 10.25 (s, 2H), 10.19 (s, 1H), 10.13 (s, 1H), 10.06 (s, 1H), 10.03 (s, 1H), 9.98 (s, 1H), 9.84 (s, 1H), 9.81 (s, 1H), 9.71 (s, 1H), 9.62 (s, 1H), 9.45 (br, 1H), 9.30 (br, 2H), 9.06 (t, *J* = 7.7 Hz, 1H), 8.97 (t, *J* = 7.5 Hz, 1H), 8.70 (t, *J* = 7.5 Hz, 1H), 8.59 (t, *J* = 7.7 Hz, 2H), 8.43 (t, *J* = 7.7 Hz, 1H), 8.15 (s, 1H), 8.13(s, 1H), 8.10 (s, 1H), 8.08 (s, 1H), 8.00 (s, 1H), 7.95-7.73 (m, 8H), 7.64-7.47 (m, 7H), 7.42-7.30 (m, 5H), 7.24-7.04 (m, 8H), 6.98-6.88 (m, 8H), 6.77-6.64 (m, 6H), 6.54-6.33 (m, 6H),6.12 (s, 2H), 5.83 (s, 1H), 4.49-3.66 (m, 26H), 2.62-2.10 (m, 13H), 1.42-1.03 (m, 96H).

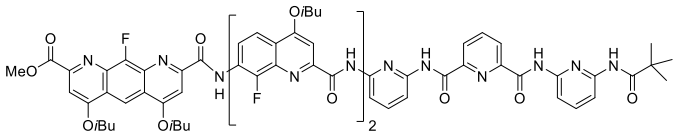

24

Oligomer 24. Acid **9** (61 mg, 0.115 mmol) was suspended in anhydrous $CHCl_3$ (1 mL), then oxalyl chloride (26 µL, 0.31 mmol) was added and the reaction was allowed to stir at room temperature for 2 hours. The solvent and excess oxalyl chloride were removed under reduced pressure and the residue was dried under high vacuum for 3 hours to yield the corresponding acid chloride as a yellow solid. The solution of amine **7** (100 mg, 0.104 mmol) and distilled DIPEA (54 µL, 0.312 mmol) in anhydrous $CHCl_3$ (1 mL) was added dropwise via a syringe to solution of the freshly prepared acid chloride dissolved in anhydrous $CHCl_3$ (0.5 mL). The reaction was allowed to proceed at room temperature for 16 hours. After evaporation of the solvents, the crude product was purified by recycling GPC. Oligomer **14** was obtained as a yellow product (71 mg, 46% yield). ^{1}H NMR (300 MHz, $CDCl_3$, 298 K) δ 10.96 (s, 2H), 10.60 (br, 1H), 10.36 (s, 1H), 10.33 (s, 1H), 8.85-8.75 (m, 3H), 8.04-7.89 (m, 6H), 7.72 (s, 1H), 7.66 (s, 1H), 7.54 (s, 4H), 7.40 (s, 1H), 7.35 (t, *J* = 7.7 Hz, 1H), 7.10 (s, 1H), 4.27 (d, *J* = 6.1 Hz,

2H), 4.19 (t, *J* = 6.5 Hz, 4H), 4.11 (d, *J* = 5.7 Hz, 2H), 4.01 (s, 3H), 2.51-2.36 (m, 4H), 1.31-1.24 (m, 9H).

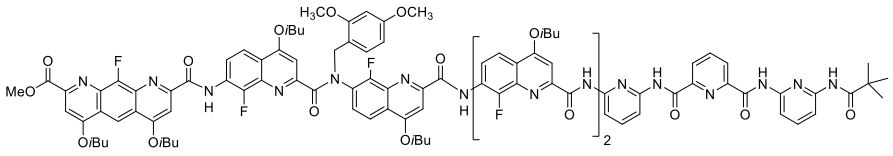

25

Oligomer 25. Acid **9** (65 mg, 0.123 mmol) was suspended in anhydrous $CHCl_3$ (1 mL), then oxalyl chloride (31 μL, 0.36 mmol) was added and the reaction was allowed to stir at room temperature for 2 hours. The solvent and excess oxalyl chloride were removed under reduced pressure and the residue was dried under high vacuum for 3 hours to yield the corresponding acid chloride as a yellow solid. The solution of amine **8** (200 mg, 0.123 mmol) and distilled DIPEA (64 μL, 0.369 mmol) in anhydrous $CHCl_3$ (1 mL) was added dropwise via a syringe to solution of the freshly prepared acid chloride dissolved in anhydrous $CHCl_3$ (0.5 mL). The reaction was allowed to proceed at room temperature for 16 hours. After evaporation of the solvents, the crude product was purified by recycling GPC. Oligomer **14** was obtained as a yellow product (147 mg, 57% yield). ^{1}H NMR (300 MHz, $CDCl_3$, 298 K) δ 10.86 (s, 1H), 10.77 (s, 1H), 10.72 (s, 1H), 10.66 (s, 1H), 10.42 (s, 1H), 10.25 (s, 1H), 9.03 (s, 1H), 8.87 (t, *J* = 7.7 Hz, 1H), 8.75 (t, *J* = 7.7 Hz, 1H), 8.55 (t, *J* = 7.3 Hz, 1H), 8.41 (d, *J* = 7.0 Hz, 1H), 8.30 (d, *J* = 7.7 Hz, 1H), 8.20-7.96 (m, 8H), 7.83-7.47 (m, 11H), 7.23 (s, 1H), 6.50 (d, *J* = 7.7 Hz, 1H), 6.27 (s, 1H), 5.20 (t, *J* = 13.4 Hz, 1H), 4.96 (t, *J* = 12.8 Hz, 1H), 4.30 (s, 3H), 4.14-4.12 (m, 8H), 4.06-3.97 (m, 4H), 3.82 (s, 3H), 3.45 (s, 3H), 2.44-2.38 (m, 6H), 1.37-1.21 (m, 36H), 0.96 (s, 9H).

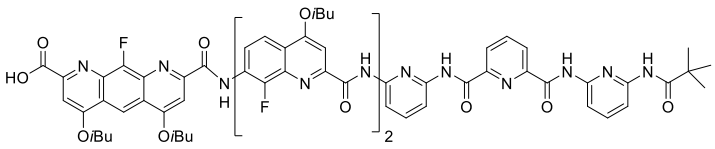

26

Compound **26**: **24** (60 mg, 0.040 mmol) was dissolved in a mixture of THF (2 mL) and H_2O (400 μL). To this solution was added LiOH (17 mg, 0.40 mmol). The solution was stirred at room temperature for 3 h. Then solution was neutralized with 1N HCl to pH = 4~5, and

concentrated under reduced pressure to remove THF. H_2O (30 mL) was added to the residue. The aqueous phase was extracted with CH_2Cl_2 (3×20 mL). The combined organic phases were dried over Na_2SO_4, filtered, then evaporated to give acid **15** as a yellow solid (58 mg, 99%).^{1}H NMR (300 MHz, $CDCl_3$, 298 K) δ 11.79 (br, 1H), 11.33 (s, 1H), 10.68 (s, 1H), 10.06 (s, 2H), 9.21 (s, 1H), 9.02 (s, 1H), 8.76-8.64 (m, 2H), 8.25-8.04 (m, 6H), 7.86 (s, 4H), 7.40 (d, *J* = 7.8 Hz, 1H), 7.33 (s, 1H), 6.77 (s, 2H), 4.31-4.24 (m, 8H), 2.49-2.43 (m, 4H), 1.30-1.22 (m, 24H), 1.05 (s, 9H).

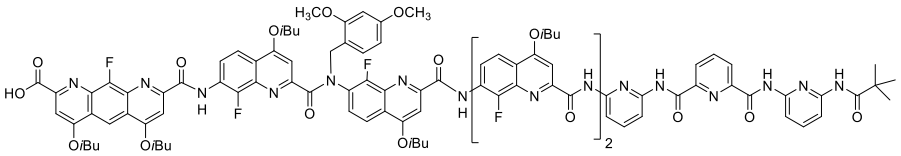

27

Compound **27**: **25** (150 mg, 0.070 mmol) was dissolved in a mixture of THF (2 mL) and H_2O (400 μL). To this solution was added LiOH (30 mg, 0.70 mmol). The solution was stirred at room temperature for 3 h. Then solution was neutralized with 1N HCl to pH = 4~5, and concentrated under reduced pressure to remove THF. H_2O (30 mL) was added to the residue. The aqueous phase was extracted with CH_2Cl_2 (3×20 mL). The combined organic phases were dried over Na_2SO_4, filtered, then evaporated to give acid **15** as a yellow solid (141 mg, 99%).^{1}H NMR (300 MHz, $CDCl_3$, 298 K) δ 10.77 (s, 1H), 10.73 (s, 1H), 10.54 (s, 1H), 10.47 (s, 1H), 10.19 (s, 1H), 8.83 (s, 2H), 8.59 (t, *J* = 7.8 Hz, 1H), 8.46-8.41 (m, 2H), 8.31 (d, *J* = 7.2 Hz, 2H), 8.15 (d, *J* = 9.3 Hz, 2H), 8.02-7.77 (m, 8H), 7.64 (s, 3H), 7.50 (s, 2H), 7.39 (s, 2H), 7.18 (s, 2H), 6.47 (d, *J* = 8.1 Hz, 1H), 6.30 (s, 1H), 5.30 (t, *J* = 14.1 Hz, 1H), 4.93 (t, *J* = 14.2 Hz, 1H), 4.21-4.02 (m, 8H), 3.81 (s, 3H), 3.77-3.07 (m, 4H), 3.51 (s, 3H), 2.79-2.61 (m, 6H), 1.76-1.66 (m, 36H), 1.06 (s, 9H).

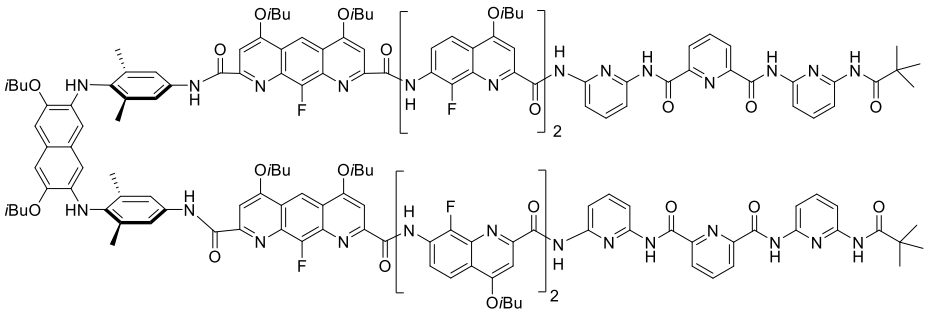

5

Compound 5. Diamine **9** (14 mg, 0.026mmol), acid **26** (70 mg, 0.051 mmol) and PyBOP (133 mg, 0.26 mmol) were placed in a 10 mL round-bottom flask filled with argon. Freshly distilled $CHCl_3$ (2 mL) and DIPEA (44 μL, 0.256 mmol) were then successively added. The solution was stirred at 45 °C for two days. The solvent was removed under reduced pressure and the residue was dissolved in dichloromethane, washed with 5% NH_4Cl, distilled water and brine. The organic layer was dried over Na_2SO_4, filtered and concentrated under reduced pressure. The crude product was purified by recycling GPC and compound **3** was obtained as a yellow solid (32 mg, 41% yield). ^{1}H NMR (300 MHz, $CDCl_3$, 298 K) δ 11.38 (s, 1H), 10.59 (s, 1H), 10.54 (s, 1H), 10.43 (s, 1H), 10.31 (s, 1H), 10.24 (s, 1H), 10.18 (s, 2H), 10.09 (s, 1H), 9.70 (d, *J* = 4.6 Hz, 1H), 9.63 (s, 1H), 9.60 (s, 1H), 9.57 (d, *J* = 2.8 Hz, 1H), 8.84 (t, *J* = 7.7 Hz, 1H), 8.59 (s, 1H), 8.56 (s, 1H), 8.42-8.27 (m, 4H), 8.22-8.11 (m, 7H), 8.07-7.98 (m, 3H), 7.76-7.67 (m, 4H), 7.64-7.61 (m, 4H), 7.56-7.44 (m, 4H), 7.40-7.33 (m, 3H), 7.19-7.06 (m, 5H), 7.04-6.88 (m, 6H), 6.86-6.70 (m, 5H), 6.65-6.52 (m, 3H), 6.25 (s, 1H), 6.18 (s, 1H), 6.15 (s, 1H), 5.77 (s, 1H), 5.45 (s, 1H), 5.33 (s, 2H), 5.30 (s, 1H), 5.24 (s, 1H), 5.22 (s, 1H), 4.56-3.60 (m, 20H), 2.46-2.03 (m, 10H), 2.02 (s, 12H),1.39-1.14 (m, 60H), 1.06 (s, 18H).

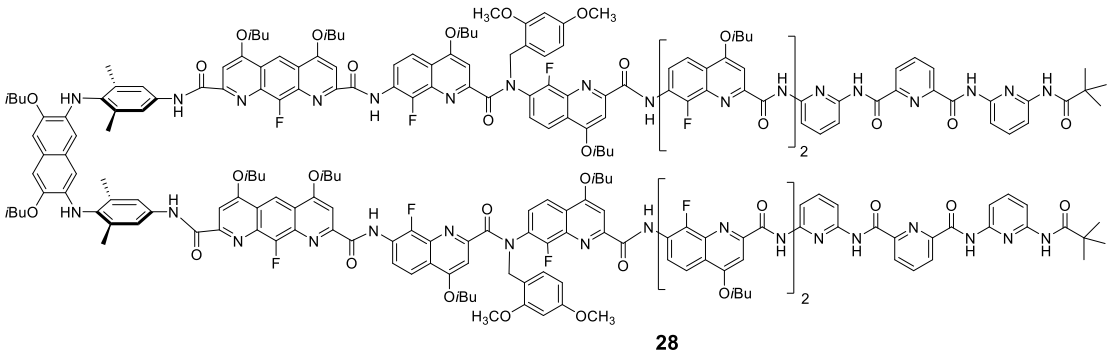

28

Compound 28. Diamine **9** (20 mg, 0.037mmol), acid **27** (150 mg, 0.074 mmol) and PyBOP (191 mg, 0.37 mmol) were placed in a 10 mL round-bottom flask filled with argon. Freshly

distilled $CHCl_3$ (2 mL) and DIPEA (64 μL, 0.368 mmol) were then successively added. The solution was stirred at 45 °C for two days. The solvent was removed under reduced pressure and the residue was dissolved in dichloromethane, washed with 5% NH_4Cl, distilled water and brine. The organic layer was dried over Na_2SO_4, filtered and concentrated under reduced pressure. The crude product was purified by recycling GPC and compound **3** was obtained as a yellow solid (61 mg, 37% yield). ^{1}H NMR (300 MHz, $CDCl_3$, 298 K) δ 11.10-9.76 (m, 14H), 9.15-8.16 (m, 12H), 8.07-7.38 (m, 26H), 7.11-5.73 (m, 28H), 5.23 (br, 1H), 4.92 (br, 2H), 4.30-3.22 (m, 40H), 2.48-1.93 (m, 26H), 1.38-0.84 (m, 96H), 0.55-0.28 (m, 18H).

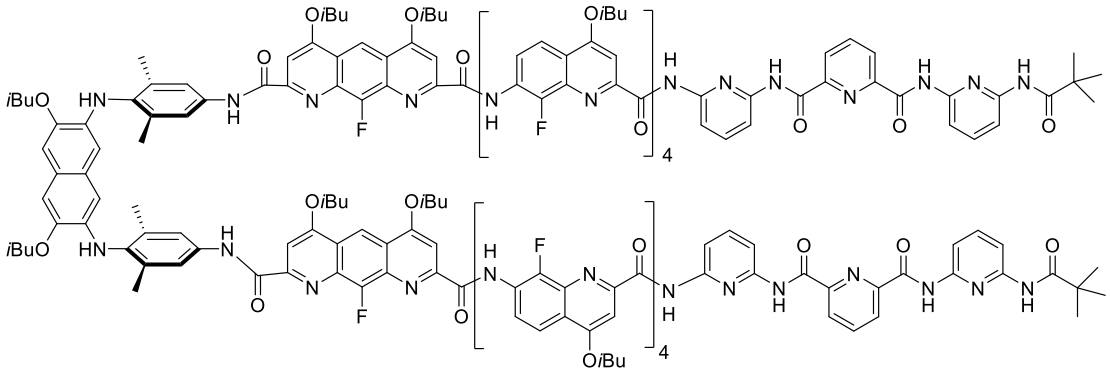

6

Oligomer 6. Dimethoxy benzyl protected oligomer **28** was taken in a 5 mL round bottom flask. To that 1 mL $CHCl_3$ and 1 mL trifluoroacetic acid added subsequently under argon atmosphere. The mixture was kept for stirring for 12 hours at room temperature. The solution poured into saturated aqueous solution of $NaHCO_3$ to neutralize, extracted with DCM, washed with water and brine respectively. The organic part was dried over anhydrous Na_2SO_4. Evaporation of organic part resulted yellow solid, which was further purified by recycling GPC. Oligomer **6** was obtained as a yellow product (52 mg, 92% yield). ^{1}H NMR (300 MHz, $CDCl_3$, 298 K) δ 10.49 (s, 2H), 10.20 (s, 2H), 10.02 (s, 2H), 9.74 (s, 2H), 9.70 (s, 2H), 9.60 (s, 2H), 9.53 (s, 2H), 8.65 ((t, *J* = 7.7 Hz, 2H), 8.46 ((t, *J* = 7.7 Hz, 2H), 8.16 ((t, *J* = 7.7 Hz, 2H), 7.81 (s, 2H), 7.78 (s, 2H),7.74 (s, 2H), 7.74 (s, 2H), 7.65 (s, 2H), 7.63 (s, 2H), 7.55 (s, 2H),7.52 (s, 2H), 7.45 (s, 2H), 7.42-7.33 (m, 4H), 7.21 (s, 2H), 7.19 (s, 2H), 7.13-6.99 (m, 6H), 6.94-6.85 (m, 4H), 6.70 (s, 2H), 6.69 (s, 2H), 6.65 (s, 2H),6.43 (s, 2H), 6.21 (s, 2H), 6.10 (s, 2H), 5.18 (s, 2H), 4.69 (s,

2H), 4.12-3.83 (m, 20H), 3.68-3.44 (m, 8H), 2.40-2.22 (m, 14H), 1.84 (s, 18H), 1.29-0.98 (m, 102H).

Résumé de these en français

1. Introduction

Les foldamères, qui peuvent être définis comme des “architectures moléculaires artificielles repliées”,[1] s’inspirent des structures et fonctions des biopolymères. Les principaux motifs observés au sein des biopolymères (hélices, brins linéaires, coudes et feuillets) sont communement observés dans les foldamères. Ces structures secondaires repliées sont rendues possible grâce à la combinaison d’interactions faibles (e.g. liaisons hydrogène, interactions électrostatiques, empilement aromatique ou liaisons de coordination métal-ligand) et à liaisons covalentes fortes.

Les foldamères représentent une classe prometteuse de mimes de biomoélcules. Les scientifiques cherchent non seulement à mimer les structures secondaires des protéines et des acides nucléiques mais également à mimer leurs fonctions. Par exemple, les foldamères peuvent agir comme inhibiteurs de protéines ou mimer des enzymes pour catalyser des réactions chimiques. De plus, leurs applications dans le domaine des matériaux, telle que la formation de nanofibres ou de cristaux liquides, démontrent leur capacité à posséder des fonctionnalités dépassant le cadre de la Nature.

Notre groupe se focalise sur l’étude des foldamères d’oligoamides aromatiques. Divers monomères codant pour des courbures variées ont été développés conduisant à une large variété de foldamères. Les chaînes latérales (hydrophobes, hydrophiles, anioniques ou cationiques) peuvent être facilement modifiées en fonction des besoins. Les conformations des foldamères peuvent être modulées par l’incorporation de divers monomères au sein de la séquence oligomérique. Selon les monomères utilisés, des hélices simples, doubles ou même quadruples peuvent être obtenues. Des assemblages de foldamères hélicoïdaux, soit par le biais de liaisons covalentes, soit *via* des interactions non covalentes, ont été également investigués.

Les foldamères d’oligoamides aromatiques peuvent se replier sous forme d’hélices stables. Au cours des deux dernières décennies, de nouvelles stuctures ont été explorées : a) structures

1 For a book, see: S. Hecht, and I. Huc, editors. *Foldamers: structure, properties and applications*. John Wiley & Sons, **2007**.

hélicoïdales multiples;[2] b) structures secondaires de type hélice-feuillet-hélice;[3] c) capsules moléculaires possédant une forte sélectivité pour différentes molécules invitées.[4] Dans cette thèse, nous discuterons de topologies moléculaires constituées de foldamères d'oligoamides aromatiques.

2. Introduction des projets

I) Hélicité frustrée: macrocycles basés sur des foldamères d'oligoamides aromatiques hélicoidaux

Les foldamères peuvent se replier en conformations hélicoïdales stables. En raison de ce repliement en forme de croissant, les foldamères peuvent être utilisés comme précurseurs de macrocycles à forme persistante. Les hélices présentent une conformation spatiale définie, dans laquelle les deux extrémités du brin divergent et ne sont pas préorganisées pour effectuer une réaction de macrocyclisation (Figure 1). Pour générer un macrocycle à partir d'une hélice, nous devons surmonter ce problème structural. L'introduction temporaire de « perturbateurs d'hélicité » donne ainsi une chance au brin de cycliser. Après la cyclisation, une étape de déprotection de ces « perturbateurs d'hélicité » peut être effectuée aboutissant à un macrocycle comportant des segments hélicoidaux.

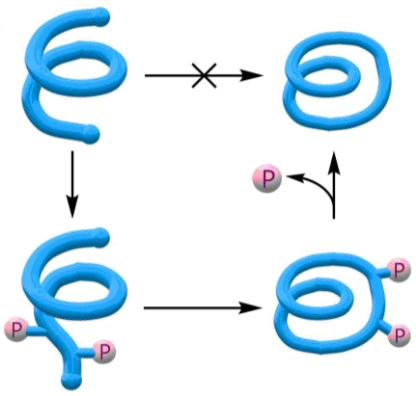

2 Gan, Q.; Ferrand, Y.; Bao, C.; Kauffmann, B.; Grélard, A.; Jiang, H.; Huc, I. *Science* **2011**, *331*, 1172; Ferrand, Y.; Gan, Q.; Kauffmann, B.; Jiang, H.; Huc, I. *Angew. Chem. Int. Ed.* **2011**, *50*, 7572-7575.

3 De, S.; Chi, B.; Granier, T.; Qi, T.; Maurizot, V.; Huc, I. *Nat. Chem.* **2018**, *10*, 51-57; Sebaoun, L.; Maurizot, V.; Granier, T.; Kauffmann, B.; Huc, I. *J. Am. Chem. Soc.* **2014**, *136*, 2168-2174; Lamouroux, A.; Sebaoun, L.; Wicher, B.; Kauffmann, B.; Ferrand, Y.; Maurizot, V.; Huc, I. *J. Am. Chem. Soc.* **2017**, *139*, 14668-14675.

4 Horeau, M.; Lautrette, G.; Wicher, B.; Blot, V.; Lebreton, J.; Pipelier, M.; Dubreuil, D.; Ferrand, Y.; Huc, I. *Angew. Chem. Int. Ed.* **2017**, *56*, 6823-6827; Mateus, P.; Chandramouli, N.; Mackereth, C. D.; Kauffmann, B.; Ferrand, Y.; Huc, I. *Angew. Chem. Int. Ed.* **2020**, *59*, 5797-5805.

Figure 1. Les extrémités d'une hélice longue ne peuvent se rejoindre, cependant l'introduction de « perturbateurs d'hélicité » (groupements P) permet la cyclisation. Un macrocycle contraint est alors obtenu après élimination de ces groupements P.

Il a été montré que les séquences basées sur l'acide 7-amino-8-fluoro-2-quinoléinecarboxylique (noté Q^F) peuvent se replier sous forme d'hélices pouvant s'auto-assembler en hélices multiples. De plus, les foldamères hélicoïdaux à base de fluoroquinoléine Q^F qui incorporent 4 unités par tour d'hélice, génère une cavité suffisamment large pour accueillir une chaîne alkyle en tant qu'invité. La structure d'une hélice simple composée de 4 monomères Q^F a déjà été observée à l'état solide. Ce tétramère s'étend sur un peu plus d'un tour d'hélice et en raison de l'encombrement stérique,[5] deux extrémités de la séquence se chevauchent en une seule hélice avec un pas d'environ 3,5 Å (Figure 2).

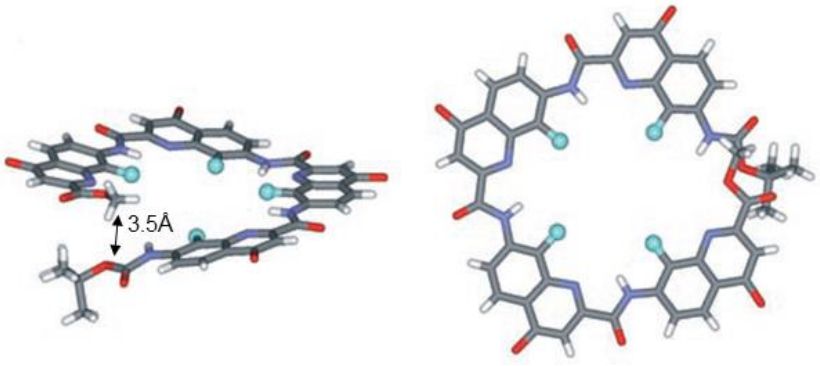

Figure 2. Structure cristallographique de la simple hélice $\mathbf{Q^F_4}$. Les atomes de fluor convergeant vers la cavité centrale de l'hélice sont représentés par des sphères.

Dans cette thèse nous avons produit une séquence octamérique de fluoroquinoléine qui a pu être cyclisé et caractérisé par diffractions des rayons X. Comme présenté sur la Figure 3a, le macrocycle **25** adopte une conformation sous la forme d'un « huit ». Les deux anneaux de **25** ont la même hélicité, soit P, soit M, nous avons donc nommé ces conformations (P,P)-**25** et (M,M)-**25**. Un seul énantiomère est représenté sur la Figure 3.

Bien qu'ayant la même hélicité, les cycles hélicoïdaux présentent une polarité opposée, N→C ou C→N, cela peut également être observé sur la position des atomes de fluor (Figure 3, bleu foncé et bleu clair). Il est intéressant de noter que l'empilement cristallin a révélé un dimère

5 Gan, Q.; Bao, C.; Kauffmann, B.; Grélard, A.; Xiang, J.; Liu, S.; Huc, I.; Jiang, H. *Angew. Chem. Int. Ed.* **2008**, *47*, 1715-1718.

de macrocycles de même hélicité, tous P ou tous M. Ce dimère présente une forme triangulaire. Le dimère [(P,P)-**25**]$_2$, représenté sur la Figure 3b, est composé de deux macrocycles en forme de huit disposés de manière anti-parallèle (tête-bêche).

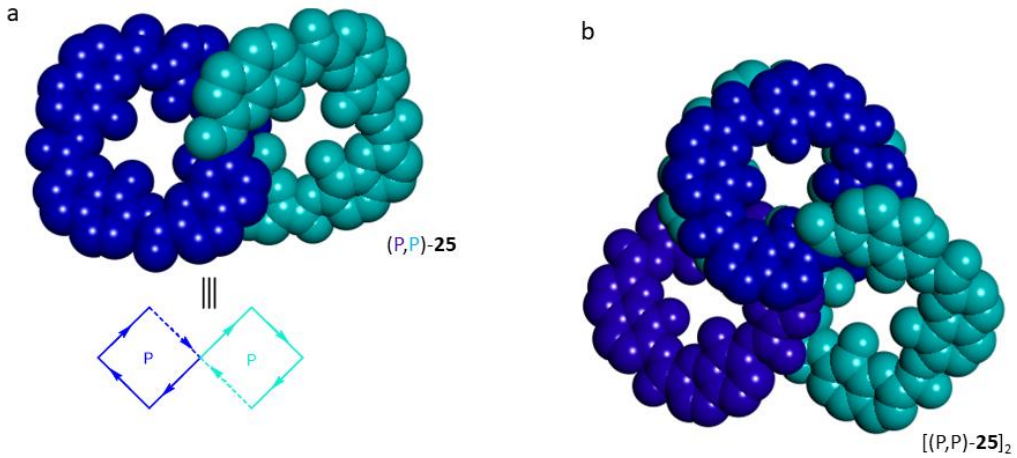

Figure 3. Structure cristallographique de l'octamère macrocyclique **25**. a) Vue du dessus de (P,P)-**25** avec les deux cycles d'hélicité P et b) vue du dessus de l'empilement cristallin présentant une espèce dimérique [(P,P)-**25**]$_2$.

Un dodécamère macrocyclique a également été préparé et la cristallographie aux rayons X a été utilisée pour confirmer sa structure. Comme le montre la Figure 4a, le macrocycle **30** existe sous forme de dimère : deux dodécamères macrocycliques **30** dimérisent pour former le dimère anti-parallèle (tête-à-queue) **(30)$_2$**. Dans l'unité monomérique, des cycles indépendants de chiralité opposée sont liés par deux segments constitués de deux monomères Q^F et qui ressemblent à des feuillets aromatiques légèrement courbés (couleur taupe sur la Figure 4). Les deux segments sont positionnés sur deux couches horizontales différentes. Les deux anneaux bleu et rouge (P et M, respectivement, Figure 4) sont constitués de quatre monomères Q^F bien repliés. Cette conformation de **(30)$_2$** est appelée pseudo-plétonème, du fait de l'abse,ce de torsion dans son arrangement. Les deux segments gris ($2*Q^F$) sont anti-parallèles et disposés en forme d'« escalier » (Figure 4b), ce qui offre l'espace nécessaire au phénomène de dimérisation.

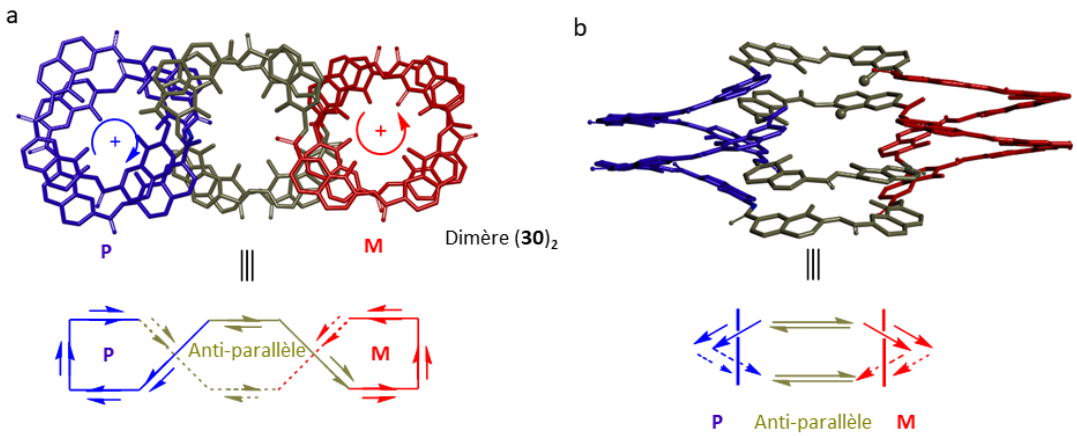

Figure 4. Structure cristallographique du dimère $(\mathbf{30})_2$. a) Vue du dessus de $(\mathbf{30})_2$ avec des cycles d'hélicité opposée, P en bleu et M en rouge. Le cycle du milieu est représenté quant à lui en gris. b) Vue de coté de ce dimère $(\mathbf{30})_2$.

II) Foldaxanes photocommutables

La lumière est un stimulus non invasif et la photochimie présente diverses applications sur les systèmes contrôlables en raison de son efficatcité de sa facilité de mise en place. L'intégration dans un foldamère d'un composant sensible aux stimuli lumineux permet de contrôler sa conformation et ainsi engendrer le relargage d'une molécule invitée localisée au sein de la cavité de ce foldamère. L'un de ces composants est le 1,8-diaza-anthracène qui forme un photodimère stable après irradiation lumineuse.

Au cours de cette thèse, nous avons conçu un nouveau foldamère multibrin qui contient à la fois des portions hélicoïdales, des feuillets aromatiques et des coudes (Figure 5a). Les unités diazaanthracène des feuillets aromatiques s'arrange en configuration parallèle, ce qui définit une ouverture sur le côté du foldamère. Les deux portions hélicoïdales, empilées au-dessus et en-dessous de ces feuillets, possèdent quant à elles la même hélicité. L'architecture hélice-feuillet-hélice résultante permet au foldamère de complexer une molécule invitée en forme de T.

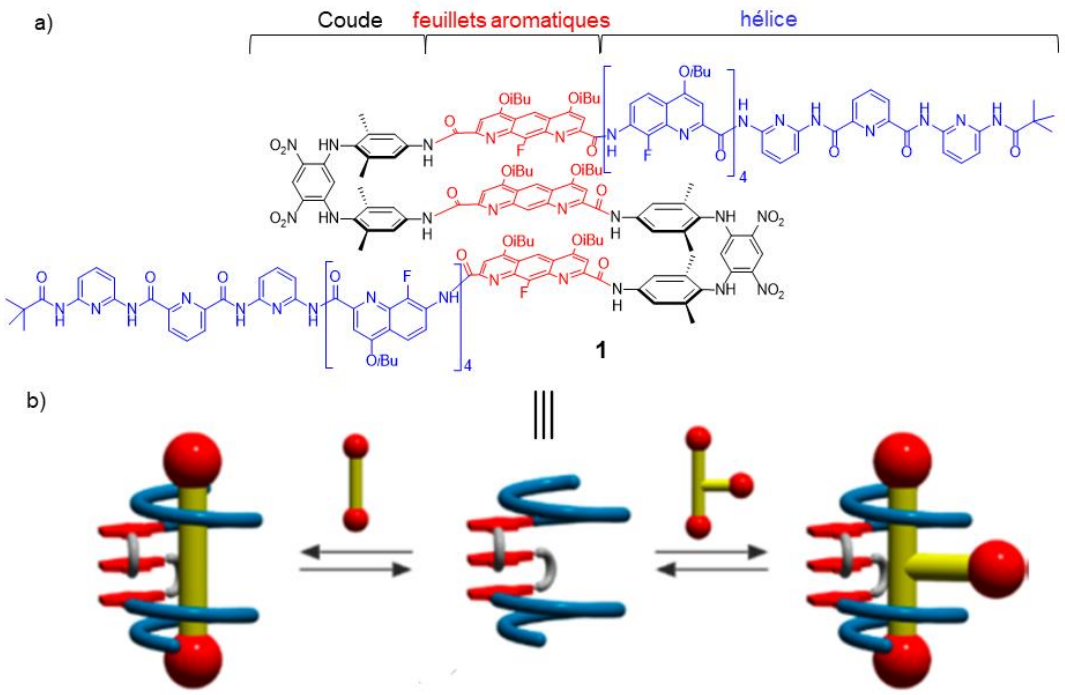

Figure 5. a) Formule du composé **1**, formé de portions hélicoïdales (en bleu), de feuillets aromatiques (en rouge) et de coudes (en noir). b) Représentation schématique de l'encapsulation d'une molécule invitée en forme d'haltère (à gauche) et d'une molécule invitée en forme de T (à droite), au sein du foldamère de type hélice-feuillet-hélice **1**.

Des réactions photochimiques entre les différentes couches de feuillets aromatiques peuvent être réalisées sous irradiation lumineuse. La cycloaddition [4+4] réversible de deux feuillets de diazaanthracène génére le photocycloadduit. La photoréaction modifier la taille et la forme de la cavité induisant la libération de la molécule invitée.

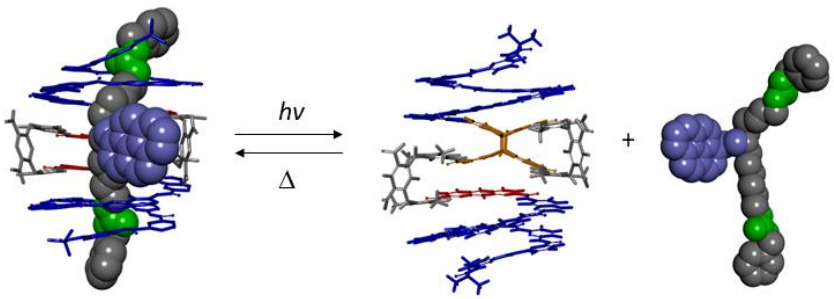

Figure 6. Représentation schématique de l'irradiation lumineuse causant le relargage d'une molécule invitée en forme de T et du traitement thermique réversible.

La réversibilité de cette photoréaction peut être réalisée par chauffage du photoproduit qui retrouve un cavité à même de complexer à nouveau une molécule en forme de T. Pour conclure, l'irradiation lumineuse du foldamère libére une molécule de la cavité de ce dernier alors qu'un traitement thermique engendrera la complexation de cette même molécule. Des cycles irradiation lumineuse/traitement thermique peuvent être répétés. Il est donc possible contrôler l'incorporation et la libération d'une molécule invitée au sein d'un foldamère, par un stimuli externe.

III) Noeud de Prusik: du monde réel au monde moléculaire

Le nœud Prusik est une topologie qui est largement utilisée dans notre vie quotidienne. Dans le monde macroscopique, le nœud Prusik peut être noué par deux boucles, tandis qu'au niveau moléculaire on peut envisager d'utiliser une structure repliée telle qu'un foldamère d'oligoamide aromatique de type hélice-coude-hélice. Pour concevoir un nœud Prusik, nous avons envisagé d'utiliser une architecture hélice-coude-hélice composée de deux portions hélicoïdales de part et d'autre d'un feuillet central aromatique. Le point critique de ce design est que les deux segments hélicoïdaux doivent adopter une hélicité opposée (M, en rouge et P, en bleu, sur la Figure 7b). Le coude aromatique (en gris, Figure 7b) agit comme un centre d'inversion d'hélicité. De plus, l'architecture hélice-feuillet-hélice doit avoir la capacité de lier une tige linéaire. Pour cela, nous pouvons utiliser notre expérience dans la conception de foldaxane. Le positionnement de pinces polaires à chaque extrémité de l'architecture permettrait en théorie de lier une tige dotée de deux groupements carbamates. Le complexe formé entre le foldamère et la tige est nommé foldaxane (Figure 7c). Enfin, pour obtenir un nœud Prusik complet, il est nécessaire de joindre les deux extrémités hélicoïdales par une boucle par exemple en utilisant une chaîne alkyle.

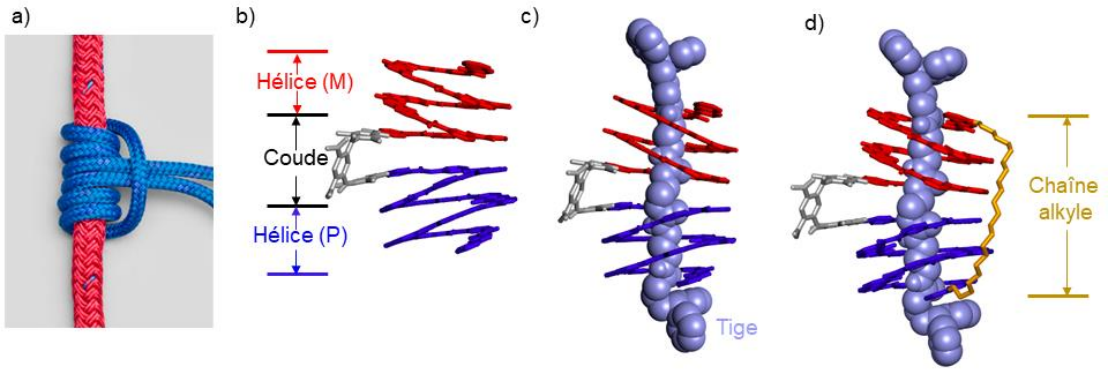

Figure 7. a) Représentation d'un noeud de Prusik dans le monde réel. Modèles moléculaires b) de l'architecture hélice-coude-hélice contenant deux segments hélicoïdaux d'hélicité différente (M et P) de part et d'autre d'un coude (gris), c) du foldaxane correspondant composé d'une architecture hélice-coude-hélice et d'une tige en forme d'haltère (bleu clair et de style CPK), d) du nœud de Prusik moléculaire.

Pour maximiser nos chances d'obtenir un nœud Prusik, nous avons testé trois coudes aromatiques différents (Figure 8a) pour l'architecture hélice-coude-hélice : 2,7-diisobutoxy-3,6-naphtalènediamine (T^N), 4,6-dinitro-1 ,3-phénylènediamine (T^B) et N,N'-dibenzyl-2,6-pyridine-dicarboxamide (T^{py}). Ils peuvent tous adopter une conformation en épingle à cheveux et induire une hélicité opposée pour les deux hélices. Des segments hélicoïdaux de longueur variable, $P_3Q^F_2$ et $P_3Q^F_4$, et les coudes T^N, T^B et T^{py} ont été choisis pour préparer les structures hélice-coude-hélice. Au total, six séquences ont été envisagées (Figure 8b) et dans chacune d'entre elles, les deux hélices sont reliées par un coude central possédant un plan de symétrie.

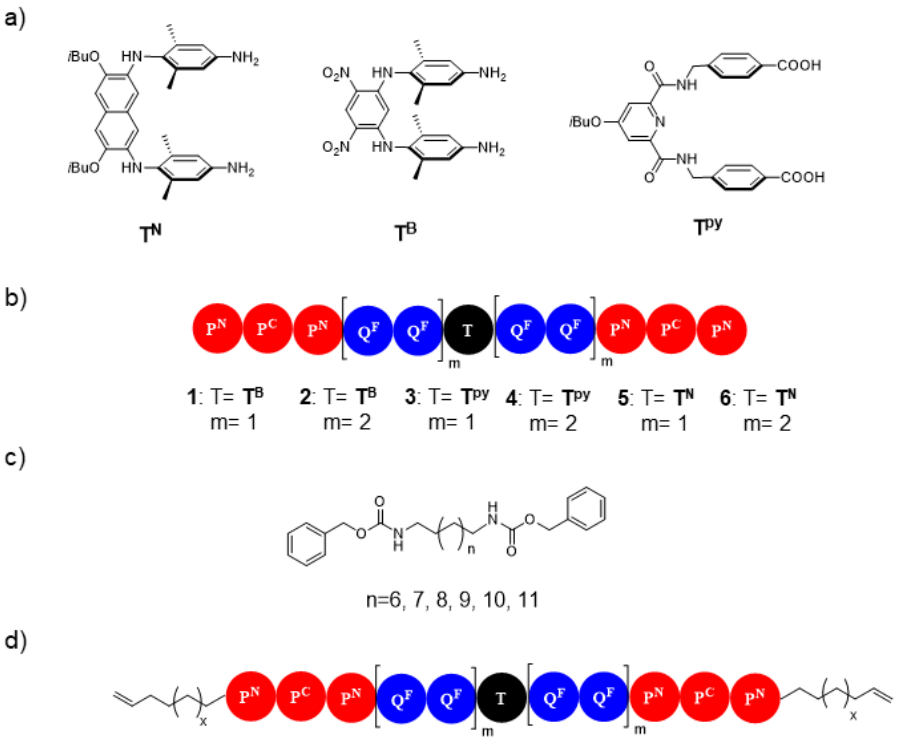

Figure 8. Formules et représentations schématiques a) des coudes T^N, T^B et T^{py}, b) des foldamères **1** à **6**, c) des différentes tiges moléculaires en forme d'haltère composées d'une station dicarbamate et d) du foldamère hélice-coude-hélice possédant des fragments alkyles à chaque extrémité.

Les architectures hélice-feuillet-hélice synthétisées ont été étudiées et plusieurs types de conformation ont été recensés. Le foldamère **1**, composé d'un coude T^B, a montré une conformation en forme de cône, dans laquelle un domaine hélicoïdal (en bleu sur la Figure 9a) a basculé de 180° pour s'intercaler dans l'autre segment hélicoïdal (en rouge, Figure 9a) conduisant à une structure en double hélice parallèle. Les deux segments hélicoïdaux adoptent la même hélicité (P ou M car la structure est centro-symétrique) et sont reliés par le coude aromatique T^B qui stabilise la double hélice.

Dans le foldamère composé du coude T^{py}, une conformation hélicoïdale globale est obtenue (Figure 9c). Les coudes et les feuillets aromatiques jouent un rôle de pont pour relier les deux segments hélicoïdaux. La structure rayons X correspondante présente deux foldamères monomériques **4** auto-assemblés et empilés tête-bêche pour former la double conformation hélicoïdale $\mathbf{(4)_2}$ présentant une symétrique C2 autour de l'axe horizontal (Figure 9c).

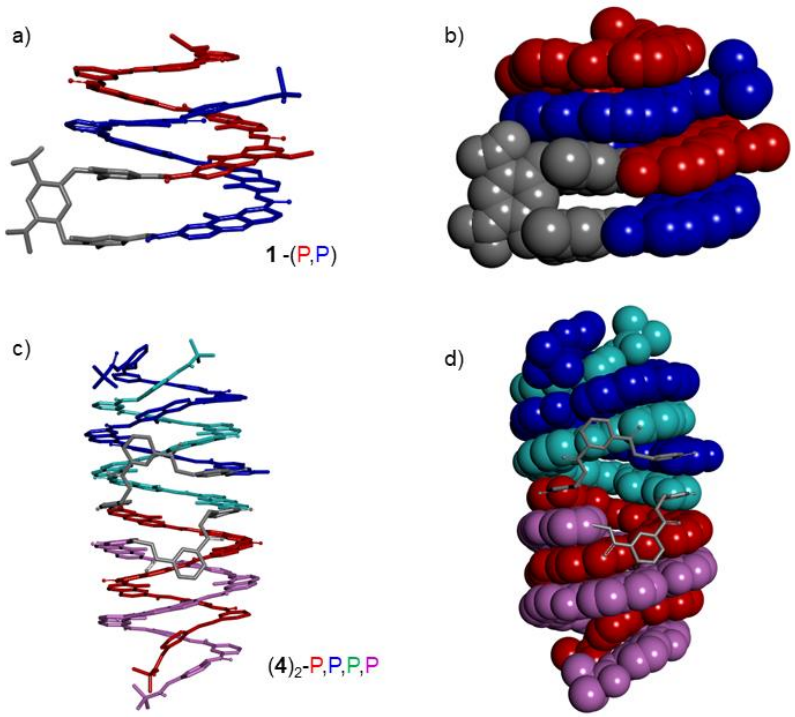

Figure 9. Structure rayons X du foldamère **1**. a) Vue de face de **1** composé de deux segments hélicoïdaux marqués en bleu et rouge. Le coude aromatique est quant à lui marqué en gris, b) vue de face de **1** en représentation CPK, c) vue de face du dimère $\mathbf{(4)_2}$ avec les quatre segments hélicoïdaux marqués en bleu, rouge, vert et rose. Les coudes sont marqués en gris, d) vue de face du dimère $\mathbf{(4)_2}$ en CPK.

Comme le montre la Figure 10a, le foldamère **5** adopte une conformation inattendue. Deux foldamères **5** auto-assemblés sous forme de dimère $\mathbf{(5)_2}$, dans lesquels un segment hélicoïdal de chaque brin **5** (rouge et rose, Figure 10a) se replie en une conformation hélicoïdale complète. Les autres segments (bleu et vert, Figure 10a) se sont retournés du même côté et empilés sous l'hélice rouge et rose précédente, d'hélicité M. Dans l'hélice bleue, les unités Q^F peuvent participer à la structure hélicoïdale avec l'hélice rouge pour former une hélice multiple, tandis que les unités P_3 ont basculé dans une orientation et une hélicité opposées (P).

La conformation de **6** a également été confirmée par cristallographie aux rayons X. Et ce foldamère a montré une conformation symétrique avec deux segement d'hélicité opposées (P et M) et un arrangement parallèle des feuillets aromatiques du feuillet (Figure 10c). Deux hélicité différente résident donc au-dessus et au-dessous du coude, comme prévu. Ce foldamère **6** adopte une conformation à symétrie plane passant par le centre du foldamère.

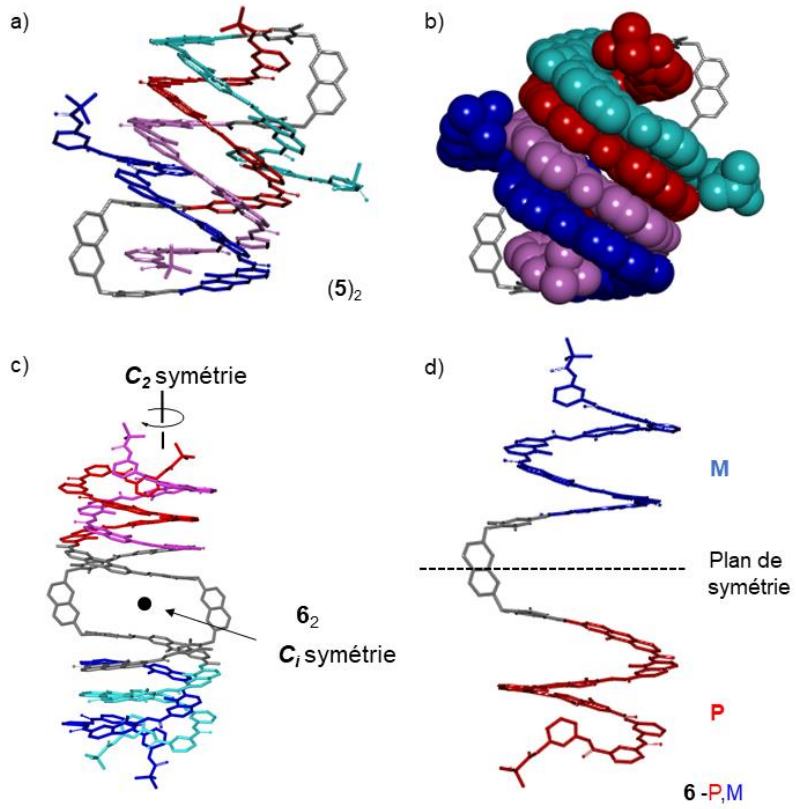

Figure 10. Structure aux rayons X du foldamère **(5)$_2$** a) vue de face avec les quatre segments hélicoïdaux représentés en bleu, rouge, vert, rose et avec les coudes en gris, b) vue de face avec les segments hélicoïdaux en représentation CPK. Structure aux rayons X du foldamère **6** c) Vue de face de **6** composé de deux segments hélicoïdaux; d) vue de face avec les segments hélicoïdaux d'hélicité opposée (M en bleu et P en rouge). Les feuillets aromatiques ont été marqués en gris.

La formation d'un foldaxane est généralement obtenue *via* un mécanisme de dépliement puis de repliement subséquent d'une hélice simple autour d'une tige en forme d'haltère. Or, ce processus peut être entravé par une dimérisation forte des brins. Bien que ce processus soit réversible, la grande stabilité de l'architecture en double hélice ne permet pas sa dissociation en simple hélice et inhibe ainsi la formation du complexe hélice/tige. Dans tous les exemples présentés ci-dessus, lors de l'ajout de tiges en forme d'haltère aux séquences **1** à **6**, aucun foldaxane n'a été observé. Nous supposons que la conception de séquences pouvant adopter une conformation de type hélice-feuillet-hélice monomérique permettrait de former plus facilement le foldaxane.